PADAMOT
Palaeohydrogeological Data Analysis and Model Testing
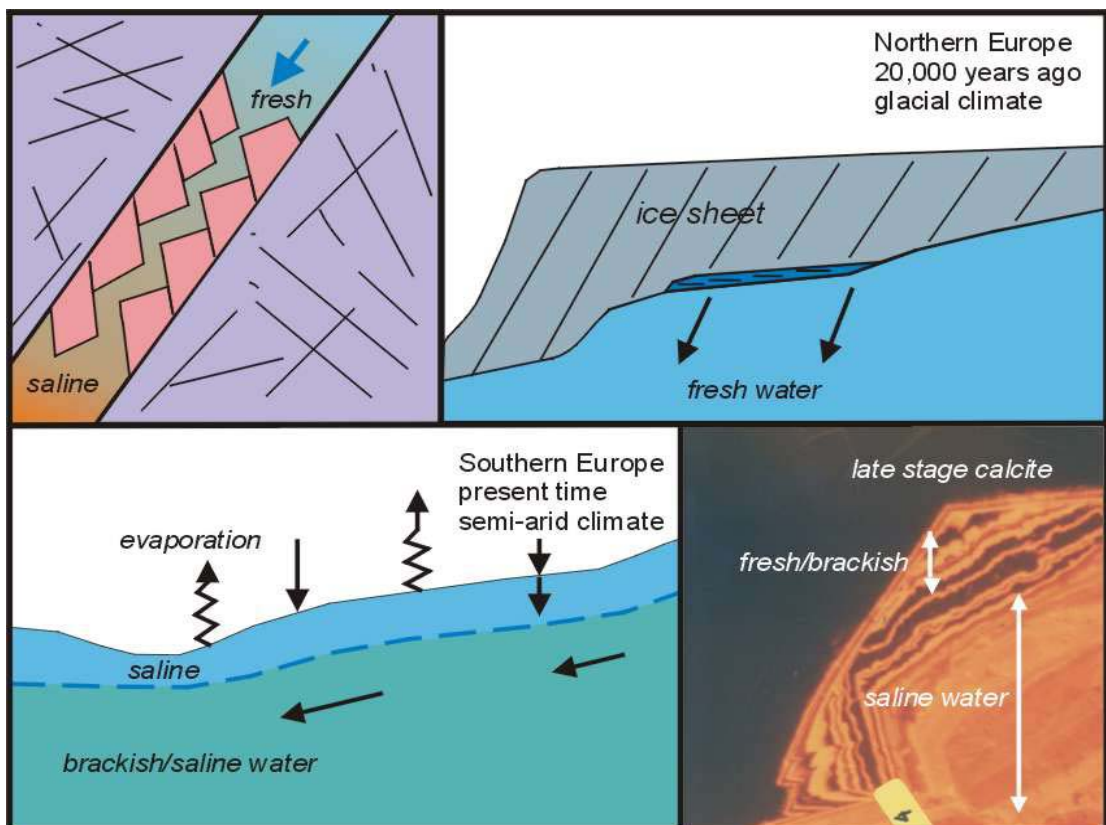
Application of Mineralogical, Petrological and Geochemical Tools for Evaluating the Palaeohydrogeological Evolution of the PADAMOT Study Sites

PADAMOT PROJECT
TECHNICAL REPORT WP2

Application of Mineralogical, Petrological and Geochemical Tools for Evaluating the Palaeohydrogeological Evolution of the PADAMOT Study Sites

A.E. Milodowski[1], E-L. Tullborg[2], B. Buil[3], P. Gómez[3], M-J. Turrero[3], S. Haszeldine[4], G. England[4], M.R. Gillespie[1], T. Torres[5], J.E. Ortiz[5], J. Zachariáš[6], J. Silar[6], M. Chvátal[6], L. Strnad[6], O. Šebek[6], J.E. Bouch[1], S.R. Chenery[1], C. Chenery[1], T.J. Shepherd[1] and J.A. McKervey[1].

[1] British Geological Survey, Keyworth, Nottingham, UK

[2] Terralogica AB, Gråbo, Sweden

[3] CIEMAT, Dept. Impacto Ambiental de la Energia, Avda. Complutense 22, Madrid, Spain

[4] Department of Geology, University of Edinburgh, West Mains Road, Edinburgh, UK

[5] Universidad Politécnica de Madrid, E.T.S.I. Minas, C/ Ríos Rosas 21, Madrid, Spain

[6] Univerzita Karlova v Praze, Ústav Hydrogeologie, Inženýrské Geologie a Užité Geofyziky, Praha, Czech Republic

Harwell   UK Nirex Limited   2005

Foreword

PADAMOT, 'Palaeohydrogeological Data Analysis and Model Testing', is a project within the European Union's 5th Framework RTD programme in nuclear fission safety (Contract Number FIKW-CT-2001-00129). It aims to improve the understanding of past groundwater conditions that supports assessments of future long-term safety of repositories for radioactive wastes. The project began in December 2001 with a duration of 36 months. The consortium of organisations involved in the PADAMOT project comprises:

United Kingdom Nirex Limited (UK)

Svensk Kärnbränslehantering AB (Sweden)

Terralogica AB (Sweden)

Empresa Nacional de Residuos Radioactivos S.A. (Spain)

British Geological Survey (UK)

Centro de Investigaciones Energéticas, Medioambientales y Tecnológicas (Spain)

Intellisci Ltd (UK)

Charles University (Czech Republic)

University of Edinburgh (UK)

Universidad Politecnica de Madrid - School of Mines (Spain)

Safety assessments of proposed repositories for the long-term storage or disposal of radioactive wastes must take into account scenarios for environmental change over the long period of time during which the waste will be a hazard, typically up to one million years into the future. The scientific consensus in a number of countries is that disposing of long-lived and/or higher activity radioactive wastes and spent nuclear fuel deep underground in a 'geological repository' is the preferred option for long-term radioactive waste management. The reasons for preferring this option are that the host rock for a deep repository should provide stable conditions for performance of the engineered barrier system and that the rock mass separating a repository from the surface environment is a further barrier to radionuclide migration.

During the last two million years (the Quaternary Period), global climate has fluctuated between extremes of ice ages and warmer conditions than at present. Over various intervals in the past, large areas of northern Europe were covered by ice sheets and experienced extensive permafrost, whilst southern Europe was sometimes more pluvial (wetter). Consequently, the present-day climate is not representative of the climate that has existed for much of the Quaternary. This natural pattern of climatic fluctuation is expected to continue into the future, albeit modified by the impacts of anthropogenic greenhouse gas emissions Variations in climate and in other environmental factors may affect future movements and compositions of groundwaters in the vicinity of a repository and thus affect the mobility of radionuclides and the rate of their leakage back to the surface. It could be argued, therefore, that present-day groundwater conditions may not be an adequate basis for assessing long-term repository safety. However, if it can be demonstrated that, despite significant environmental change at the surface, groundwater flows and compositions at depth remain stable or change in a way that does not impact significantly on safety, then confidence in repository concepts for disposal will be increased.

PADAMOT has sought to address the following questions. How can such groundwater stability be assessed, with respect to climate-driven environmental change? In particular, what evidence is there that a deep geological repository will eliminate or reduce the effects of extreme changes in environmental conditions in the long term? In seeking to answer these questions, PADAMOT

has investigated geosphere systems at various European sites, using analytical methods and numerical modelling.

PADAMOT comprises five work packages (WPs) with the following tasks:

WP1. Convening a preliminary workshop of PA specialists, PADAMOT researchers and other geoscientists on the use of palaeohydrogeology in PA.

WP2. Making palaeohydrogeological data measurements on mineral samples from sites in Spain, Czech Republic, Sweden and UK, using high resolution and high precision analytical methods, e.g. ion-probe and laser ablation.

WP3. Constructing a relational database and a public domain website to store data from EQUIP and PADAMOT, accessible to project partners and to external researchers via the internet.

WP4. Developing numerical models to test palaeohydrogeological information interpreted from proxy geochemical, mineralogical and isotopic data, based on understanding of the processes that link the proxy data with climate-driven groundwater phenomena.

WP5. Synthesising project outcomes and disseminating an improved approach to the use of palaeohydrogeological information in the description of FEPs and hydrogeological scenarios for PA.

There are final reports from each of the five WPs plus a Summary report:

Technical Report WP1. The Long-Term Stability of Groundwater Conditions at Repository Sites: Proceedings of the PADAMOT Workshop, Brussels 2002.

Technical Report WP2. Application of Mineralogical, Petrological and Geochemical Tools for Evaluating the Palaeohydrogeological Evolution of the PADAMOT Study Sites.

Technical Report WP3. Design and Compilation of Database: Final Report.

Technical Report WP4. Interpretative Modelling of Palaeohydrogeological Data: Final Report.

Technical Report WP5. Dissemination and Use of Palaeohydrogeological Results for Safety Assessment.

Summary Report. PADAMOT: Palaeohydrogeological Data Analysis and Model Testing – Overview.

Conditions of Publication

This report may be freely used for non-commercial purposes. Any commercial use, including copying and re-publication, requires permission from the PADAMOT consortium. All copyright, database rights and other intellectual property rights reside with the members of the PADAMOT consortium. Applications for permission to use the report commercially should be made to each of the respective organisations. Although great care has been taken to ensure the accuracy and completeness of the information contained in this publication, the PADAMOT consortium members cannot assume responsibility for consequences that may arise from its use by other parties who are responsible for interpretation of its contents.

Further Information

Further information on the PADAMOT programme can be obtained from the project website www.bgs.ac.uk/padamot

Abstract

The role of Work Package (WP) 2 of the PADAMOT project – 'Palaeohydrogeological Data Measurements' - has been to study late-stage fracture mineral and water samples from groundwater systems in Spain, Sweden, United Kingdom and the Czech Republic, with the aim of understanding the recent palaeohydrogeological evolution of these groundwater systems. In particular, the project sought to develop and evaluate methods for obtaining information about past groundwater evolution during the Quaternary (about the last 2 million years) by examining how the late-stage mineralization might record mineralogical, petrographical and geochemical evidence of how the groundwater system may have responded to past geological and climatological changes.

Fracture-flow groundwater systems at six European sites were studied:

- Melechov Hill, in the Bohemian Massif of the Czech Republic: a shallow (0-100 m) dilute groundwater flow system within the near-surface weathering zone in fractured granitic rocks;

- Cloud Hill, in the English Midlands: a (~100 m) shallow dilute groundwater flow system in fractured and dolomitized Carboniferous limestone;

- Los Ratones, in southwest Spain: an intermediate depth (0-500 m) dilute groundwater flow system in fractured granitic rocks;

- Laxemar, in southeast Sweden: a deep (0-1000 m) groundwater flow system in fractured granitic rocks. This is a complex groundwater system with potential recharge and flushing by glacial, marine, lacustrine and freshwater during the Quaternary;

- Sellafield, northwest England: a deep (0-2000 m) groundwater flow system in fractured Ordovician low-grade metamorphosed volcaniclastic rocks and discontinuous Carboniferous Limestone, overlain by a Permo-Triassic sedimentary sequence with fracture and matrix porosity. This is a complex coastal groundwater system with deep hypersaline sedimentary basinal brines, and deep saline groundwaters in crystalline basement rocks, overlain by a shallow freshwater aquifer system. The site was glaciated several times during the Quaternary and may have been affected by recharge from glacial meltwater;

- Dounreay, northeast Scotland: a deep (0-1400 m) groundwater flow system in fractured Precambrian crystalline basement overlain by fractured Devonian sedimentary rocks. This is within the coastal discharge area of a complex groundwater system, comprising deep saline groundwater hosted in crystalline basement, overlain by a fracture-controlled freshwater sedimentary aquifer system. Like Sellafield, this area experienced glaciation and may potentially record the impact of glacial meltwater recharge.

In addition, a study has been made of two Quaternary sedimentary sequences in Andalusia in southeastern Spain to provide a basis of estimating the palaeoclimatic history of the region that could be used in any reconstruction of the palaeoclimatic history at the Los Ratones site:

- The Cúllar-Baza lacustrine sequence records information about precipitation and palaeotemperature regimes, derived largely from the analysis of the stable isotope ($\delta^{18}O$ and $\delta^{13}C$) signatures from biogenic calcite (ostracod shells).

- The Padul Peat Bog sequence provided information on past vegetation cover and palaeogroundwater inputs based on the study of fossil pollen and biomarkers as proxies for past climate change.

Following on from the earlier EC 4th Framework EQUIP project, the focus of the PADAMOT studies has been on calcite mineralization. Calcite has been identified as a late stage mineral,

closely associated with hydraulically-conductive fractures in the present-day groundwater systems at the Äspö-Laxemar, Sellafield, Dounreay and Cloud Hill sites. At Los Ratones and Melechov sites late-stage mineralization is either absent or extremely scarce, and both the quantity and fine crystal size of any late-stage fracture mineralization relevant to Quaternary palaeohydrogeological investigations is difficult to work with. The results from the material investigated during the PADAMOT studies indicate that the fracture fillings at these sites are related to hydrothermal activity, and so do not have direct relevance as Quaternary indicators. Neoformed calcite has not been found at these two sites at the present depth of the investigations. Furthermore, the HCO_3^- concentration in all the Los Ratones groundwaters is mainly controlled by complex carbonate dissolution. The carbonate mineral saturation indices do not indicate precipitation conditions, and this is consistent with the fact that neoformed calcite, ankerite or dolomite have not been observed petrographically.

Indicators of palaeo-salinity

Calcite crystal morphology had been found to vary systematically with present-day or palaeo groundwater chemistry at Dounreay and Cloud Hill, confirming earlier observations from Sellafield. At Sellafield the morphological variation is very well defined, and the 'Morphological Transition Zone' (MTZ) between short *c*-axis (fresh water type) and long *c*-axis (saline water type) crystal forms lies just above the interface between freshwater and brackish water of the present groundwater system. Applying calcite morphological observations to the Laxemar site suggests that freshwater may have penetrated to depths of up to 1000 m in the relatively recent past. This is consistent with evidence from $\delta^{18}O$ data that indicates that glacial meltwater is a component of water in the deep groundwater system at this site.

Changes in crystal morphology during the growth of the late-stage calcites are revealed by detailed cathodoluminescence petrography. In the case of the Sellafield site, these observations suggest that the interface between the shallow fresh groundwater and the deeper saline groundwater (STZ) has changed with time. In general across the site the change in calcite growth fabrics indicate that within the MTZ, there has been an overall progressive downward movement of this interface of only 50 to 150 m. However, there is some evidence for deeper penetration of fresh water in the past (revealed by the growth of freshwater morphology calcite on saline water morphology calcite in very localised fracture zones. This might reflect 'fingering' of freshwater along a small number of locally more conductive fracture flow paths that perhaps responded more rapidly to short-lived enhanced freshwater flushing events. In the case of the Dounreay site, similar growth fabrics in the late calcite suggest that freshwater may have penetrated along localised fractures to depths of over 1000 m.

The top of the MTZ occurs at salinities of >300 mg/L chloride, and the base of the MTZ is defined by salinities between 1000-2000 mg/L chloride. This morphology change appears to be a potentially very useful tool for following changes in salinity in dilute groundwater systems.

Ion-microprobe technology was successfully used to investigate trace Cl and Br variations in late calcite from the Sellafield site. The high spatial resolution of the ion-microprobe enabled variation in trace elements such as Br and Cl to be determined for the first time in the individual fine-scale growth zones in the calcite revealed by CL. The ability to record other trace elements and oxygen isotope information from the same calcite zone, using ion microprobe technology, presents the opportunity to examine co-variations between isotopic composition, chemistry and salinity variations.

Indicators of palaeo-redox

Late-stage calcites from Laxemar, Sellafield, Dounreay and Cloud Hill display fine scale growth zone variations in Fe and Mn, which can be potentially attributed to factors influencing redox. These elemental differences are also reflected in variations in the CL characteristics of the calcite. Modern high-resolution ion-microprobe and laser ablation microprobe - inductively-

coupled plasma mass spectrometry analytical techniques have successfully enabled detailed information to be obtained on the variation in trace element chemistry of individual calcite growth zones. This has allowed variations in Fe and Mn to be compared with variations in other redox-sensitive elements. In particular, rare earth element (REE) geochemistry and the presence or absence of anomalous Ce behaviour, provides evidence to corroborate and constrain interpretation of palaeo-redox variations based on data from Fe and Mn, and CL zonation characteristics of the calcite.

Indicators of groundwater origins and palaeoenvironmental impacts

In the Laxemar and Äspö area the integration of stable carbon and oxygen isotope and Sr isotope data and trace element (REE, Sr, Ba, Mn) data obtained on bulk samples of late calcite fracture mineralization, together with observations on calcite morphology and fluid inclusion data, enabled the differentiation of different types of calcite that might be related to different palaeohydrogeological regimes. By integrating these different observations, it has been possible to distinguish and evaluate the distribution of low-temperature calcites, of possible brackish to marine groundwater origin (Type 2 and 3), low-temperature calcite of dilute meteoric origin (Type 1), and calcite possibly precipitated from recharged glacial meltwater (Type 4). However, no evidence of Type 4 calcite has been found during this study at Laxemar. Although some fresh water calcites from Laxemar have an isotopic composition that indicates precipitation from a water slightly lighter in $\delta^{18}O$ than the present groundwater, these calcites are not clearly differentiated from the Type 1 calcites, and are therefore included in this group. Present-day groundwater with various proportions of a glacial meltwater component (isotopically-determined) has however been identified at depth from 100 to 1100 m in the Laxemar area. Two possible explanations for this are:

- The intrusion of glacial meltwater did not result in any calcite production, or;

- The amounts of glacial meltwater component in the present groundwaters are small and Quaternary calcite with a diagnostic isotope signature has not been identified so far.

High spatial resolution studies of growth zone variations in $\delta^{18}O$ and $\delta^{13}C$ in late-stage calcite have been undertaken using modern He-LACE, LAMP-ICP-MS and ion microprobe. These techniques have been successfully used to micro-sample and analyse individual crystals of late-calcite mineralization at Sellafield, in order to evaluate the variation in trace element and stable isotope ($\delta^{18}O$ and $\delta^{13}C$) compositions at different stages of crystal growth. The advantages and disadvantages of these techniques have been evaluated. The ion microprobe was found to have a much better spatial resolution than the laser micro-sampling techniques. This enabled the very fine overgrowths and fine-scale growth zoning to be precisely sampled for both trace element and $\delta^{18}O$ isotope analyses. In contrast, the two laser-based techniques produced much coarser-scale sampling. In particular, the current BGS He-LACE laser system was not able to provide the very fine spatial resolution needed to sub-sample some of the ME9 calcite zones, particularly the later growth zones. Thermal shock and rapid thermal expansion of the calcite under the laser probe can sometimes cause the calcite crystals to shatter, particularly near the edges of crystals. However, advances in laser technology and mass spectrometry development are likely to result in better micro-sampling resolution and analytical sensitivity in the future.

For stable isotope studies, He-LACE analysis has an advantage over the ion microprobe by being able to provide both $\delta^{18}O$ and $\delta^{13}C$ data simultaneously, whereas the ion microprobe is set up to determine the isotopic composition of only one element ($\delta^{18}O$ in this case) at a time. To provide $\delta^{13}C$ data is feasible if adequate analytical standards for the local instrument are developed. The cost of the He-LACE equipment is also substantially lower than ion microprobe facilities. However, the ion microprobe has much better spatial resolution and more controllable sample ablation, whereas with the coarser micro-sampling by He-LACE it proved much more difficult to relate the analytical data to specific growth zones in the calcite

Despite these differences and problems the ion microprobe and the laser techniques provided corroborative results on the samples studied. Oxygen isotope data obtained by ion microprobe and He-LACE data both identified strongly depleted $\delta^{18}O$ values in calcites from both Sellafield and Dounreay, which provide potential evidence for a significant (30-100 %) component of glacially-recharged groundwater at depth in the past. However it is presently not possible to ascribe this influx to a specific glacial episode.

Biomarkers

Biomarkers have been studied in late-stage mineralization from five of the investigation sites (Sellafield, Dounreay, Laxemar, Los Ratones and Cloud Hill). Potentially, biomarkers might provide information on the origin of the groundwater (via identification of the source of the biomarker) and on palaeoclimatic/palaeoenvironmental conditions in the recharge area (i.e. organics derived from the soil zone processes and different types of plants). Although only a limited number of samples have been analysed during the PADAMOT project, the study found evidence at three sites (Sellafield, Dounreay and Laxemar) that biomarkers can be preserved in late calcite mineralization. Unfortunately, the biomarkers are only present in low abundance, and because the amount of fracture calcite that is available for analysis is typically very small, analysis was very close to analytical detection limits of the GC-MS technique used. In this study, only a few organic compounds were detected, many of which have ambiguous origins. In a few cases, biomarkers indicative of possible plant origins were detected (Sellafield, Laxemar), which may have been derived during recharge of the groundwater through the soil zone. Unfortunately, the dataset is too small to make any reliable interpretation. Nevertheless, the work completed in PADAMOT has demonstrated the feasibility of finding biomarkers in the late calcite. As analytical methods improve in sensitivity the study of biomarkers may allow the development of this application in future palaeohydrogeological studies.

Palaeoclimate reconstruction

Palaeoclimatic reconstructions have been successfully carried out for the Cúllar-Baza Basin and the Padul Basin in southern Spain in order to provide a regional understanding of climate change and recharge variations during the Quaternary.

In the Cúllar-Baza Basin study, it was found that the $\delta^{18}O$ signature of ostracod shells provided a good proxy for global climatic variations from 2 Ma to the upper part of the Middle Pleistocene (279 ± 77 ka). The variation in $\delta^{18}O$ reflected changes in the evaporation/inflow ratio of the water bodies and the amount of rainfall. A good correlation was found between the ostracod $\delta^{18}O$ variation and the deep-sea oxygen isotope (OIS) record, and with palaeoclimate proxies in other Quaternary basins in the Mediterranean area.

In the Padul Basin study, it has been shown that the concentration of organic carbon, the atomic H/C and C/N ratios, the $\delta^{13}C_{org}$ and CPI values, and the distribution of organic biomarkers (*n*-alkanes) proved to be excellent palaeoenvironmental proxies for evaluating palaeoclimatological and palaeohydrogeological evolution. Used together, these measurements can be used to provide information on the nature of plant cover, which can be used to infer the palaeoclimatic conditions within the basin region. This in turn can be used in modelling past recharge and water balances.

Flow path evolution

At present, PA models do not generally account for the progressive evolution of site characteristics such as porosity, permeability, and water chemistry, and define these as fixed. However, petrological investigations from the Sellafield site, and to some extent from the Dounreay site and the Äspö-Simpevarp-Laxemar area (cf. earlier EQUIP study observations by Milodowski et al, 1998b) show that the porosity of these groundwater systems has evolved significantly over time, and that secondary porosity is an important component. In the case of Sellafield, most of the present-day fracture porosity in the shallow and deep groundwater system

and a large proportion of the matrix porosity in the shallow sandstone aquifer are the results of dissolution of minerals, primarily anhydrite, gypsum, dolomite-ankerite and, in the near-surface, calcite. Consequently, the shallow and deep groundwater flow paths, and their porosity and permeability distributions, have evolved over time since uplift, weathering and erosion introduced recharge of meteoric water at Sellafield during the Tertiary period. Dissolution of those pre-existing fracture-filling and matrix minerals would have been a major contributor to saturated compositions of groundwaters from which new generations of secondary minerals were precipitated. Therefore permeability on a regional scale has been affected over time by both dissolution and precipitation, with the general pattern being that precipitation would have taken place down-gradient of dissolution. The mass transfer involved in the overall process, and therefore the effect on permeability, decreases with depth because of smaller water fluxes and more equilibrated compositions. Mass transfer via groundwater flux through the system suggests that cumulative dissolution should be slightly greater than precipitation, and this is certainly the case in the shallow system, but it is uncertain for the deeper system as also is the local spatial variability of the processes.

A potential limitation of PA models in their inability to consider the evolution of porosity and permeability, and changes in flow paths due to mineral dissolution (which will also affect factors such as matrix diffusion and changes in surface with which radionuclides transported in the groundwater will interact) may need to be examined more closely in future.

Acknowledgements

Contents

FIGURES

TABLES

APPENDICES (on CD ROM)

1 Introduction

1.1 OVERVIEW OF THE PADAMOT PROJECT

PADAMOT (Palaeohydrogeological Data Analysis and Model Testing) is a project in the 5th Framework R&D Programme of the European Union (EU). The research was undertaken to evaluate the response of deep groundwater systems to climatic change (e.g. glaciation-deglaciation-periglacial-temperate cycles in northern Europe, and arid-humid cycles in southern Europe. This will contribute to our understanding of the long-term safety of placing radioactive wastes in underground repositories.

PADAMOT was funded by the European Commission, United Kingdom Nirex (Nirex) Limited (UK), SKB (Sweden), ENRESA (Spain), RAWRA (Czech Republic) and the British Geological Survey (BGS) (UK). The project was coordinated by Nirex (UK) and the research was undertaken by Terralogica AB (Sweden), CIEMAT (Spain), Universidad Politecnica de Madrid (Spain), Universidad de la Coruña (Spain), Charles University Prague (Czech Republic), University of Edinburgh (UK), Intellisci (UK) and the BGS (UK).

Safety considerations for storing radioactive wastes must take into account the various scenarios for environmental change over the long period of time during which they will pose a hazard. One of the factors potentially affecting safety is therefore changing climate. Putting high-level (HL), intermediate-level (IL), and some low-level (LL) radioactive wastes and spent nuclear fuel deep underground in a 'geological repository' is the generally preferred option for their long-term management. A major reason for preferring this option is that the impacts of changing climate and the consequent increased uncertainty about long-term safety are removed or at least reduced by putting the waste deep underground

During the last two million years or so (the Quaternary Period), global climate has alternated between extremes of ice ages and conditions that are warmer than today. Large areas of northern Europe were covered by ice sheets and experienced extensive permafrost, whilst southern Europe was more pluvial (wetter) in the past. The present-day climate is not representative of the climate that existed for much of the Quaternary, and it could be argued that present-day groundwater conditions are not an adequate basis for assessing long-term repository safety. Variations in climate above a repository could potentially affect groundwater flows and compositions.

Stability of groundwater conditions is one of the most important safety requirements, because the chemical composition of water and the rate of water movement are key factors influencing the reliability of containment in the repository, the mobility of radionuclides, and the rate of their leakage back to the surface. How can this stability be assessed with respect to changes in climate? Key issues raised in connection with this are:

- What evidence is there that 'going underground' eliminates the extreme conditions that storage on the surface would be subjected to in the long term?

- How can the additional stability and safety of the deep geosphere be demonstrated with evidence from the natural system?

PADAMOT has attempted to investigate methods for addressing these questions by looking at what has happened in the past - as recorded by the rock mass and groundwater system (i.e. palaeohydrogeology). In particular, the project has investigated how minerals and groundwater at a number of sites have evolved, and possible relationships between past climate changes and what the mineralogy records about the sensitivity of groundwater conditions in response to climate at various depths.

1.2 OBJECTIVES OF PADAMOT WORK PACKAGE 2

1.2.1 Primary objectives

The primary objective of the PADAMOT project was to investigate the pattern of changes in deep hydrogeological conditions as a result of changing climate within the context of safety assessments. The role of Work Package 2 (WP2) – 'Palaeohydrogeological data measurements' was to study late-stage fracture mineral and water samples from deep groundwater systems in Spain, Sweden, United Kingdom and the Czech Republic, with the aim of understanding the recent palaeohydrogeological evolution of the groundwater systems.

The palaeohydrogeology of the sites at Äspö in southeast Sweden, Sellafield in northwest England, and the Padul and Cúllar-Baza basin in southern Spain were previously studied during the earlier EU 4th Framework EQUIP project (Bath et al., 2000). These sites were examined further during PADAMOT:

- To obtain new data to further evaluate and understand the palaeohydrogeological history of the sites;

- To refine or apply new analytical techniques (e.g. ion microprobe, biomarker analysis) to obtain improved mineral, chemical and isotopic data at a finer (spatial and temporal) resolution to enable better geochemical interpretation of the palaeofluid history recorded by minerals.

In addition, materials have been studied from new sites at Dounreay and Cloud Hill (United Kingdom), Los Ratones (Spain), Laxemar (Sweden) and Melechov Massif (Czech Republic). The principal objectives were:

- Together with observation from the previous sites, to obtain a broader generic understanding of the palaeohydrogeological information that can be recorded by fracture minerals;

- To validate observations on the relationships between mineralogical features and palaeohydrogeology made during the EQUIP project, and to test the applicability of these relationships to other sites.

Much of the effort in EQUIP focussed on the analysis of late-calcite mineralization, which is often characteristic of the deep groundwater systems in the EQUIP study sites (Bath et al., 2000). Calcite/carbonate fracture mineralization remains an important component for the PADAMOT WP2 investigations. Specific objectives in relation to this were:

- To determine whether the occurrence and distribution of fracture calcite is sufficiently consistent and well enough understood that it could reliably be used for characterisation of some or all site types.

- To determine under what geological, hydrogeological and climatic conditions does the growth of calcite and other minerals provide a useful record of groundwater change/stability in the recent past.

1.2.2 National objectives and selection of study sites

1.2.2.1 LOS RATONES SITE, WESTERN SPAIN

ENRESA's interest in studying the Los Ratones Uranium Mine site was to obtain site-specific data on shallow and deep carbonate fracture-fillings in a fractured rock in the southwest of Spain, which could potentially provide a record of the geofluid evolution in this area. The main objective was to try to determine the impact of past environmental conditions at the theoretical depth of a granitic high-level waste repository.

The Albalá granitic pluton was the site selected for the studies. The main reason is that this area has experienced fluctuating aridity and water table elevation in the past.

The strategy followed was:

- To analyse the composition of deep subsurface waters flowing through fractures because of the potential information that it can provide on the geochemical and hydrological evolution of the system. In particular, this could provide an understanding of the major chemical processes which control water composition flowing through fractures in this area.

- To determine the mineralogical and chemical composition of secondary minerals, including fracture-fillings, and to determine their spatial distribution and relationship with groundwaters. Special emphasis has been placed on characterising the carbonate minerals in the system.

All the data acquired have been used for palaeohydrogeological interpretation and modelling.

1.2.2.2 Äspö and Laxemar site, southeast Sweden

One 1000 m borehole (KLX01) was drilled on the mainland west of the Äspö island during the SKB investigations prior to the construction of the Äspö Hard Rock Laboratory. Later on (1992 to 1993) a 1700 m deep borehole was drilled on the Laxemar mainland west of the KLX01 borehole. This borehole was drilled for studying the hydrogeology and hydrogeochemistry in a more regional perspective. During the site investigation processes carried out by SKB since 2002, Laxemar was selected as one of the areas of interest and site investigations are at present being carried out within the area. These site investigations aim to determine/evaluate the site's suitability for hosting a national repository for the disposal of high-level radioactive waste.

For the PADAMOT project, the KLX01 borehole was chosen in 2001 because the Laxemar area is considered to be more of a local recharge area compared with Äspö which was investigated within the previous EQUIP study. The larger drill core diameter (56 mm) of the KLX01 borehole in the upper 670 meters was also considered to be more favourable for providing good fracture fill samples, since one of the aims of WP2 has been to combine and evaluate results from different analytical methods. The study has focused on calcite mineralization because of the potentially wide range of different analytical information (petrographical, morphological, microchemical, stable C and O isotope, Sr isotopes, fluid inclusions) that can be obtained from this mineral. However, a major problem had to be faced in that the amount of calcite present in any given fracture is usually very limited even though it occurs in many of the open fractures.

The strategy for the investigation was to:

- Use the morphology of late-stage calcite (which had been shown in previous EQUIP studies at Sellafield to be a useful indicator of recent groundwater flow and type) for selecting the most recent and potential low temperature calcites.

- Try to combine as many different types of analyses as possible on these potentially late calcites including; $\delta^{18}O$, $\delta^{13}C$, $^{87}Sr/^{86}Sr$, chemical composition (including trace elements) and fluid inclusions, in order to use the different types of information to help interpret the results from individual tests more reliably.

- To interpret possible past hydrogeochemical regimes and input of organic (biogenic?) material to the deeper groundwaters.

1.2.2.3 Sellafield, Dounreay and Cloud Hill sites, UK

Earlier Nirex site investigations and palaeohydrogeological studies for the EQUIP project at the Sellafield site in northwest England, demonstrated a close relationship between the distribution

of late-stage calcite fracture mineralization and present-day groundwater flow in deep (up to 2 km) boreholes at the site (Milodowski et al., 1995; 1998; 2002; Bath et al., 2000). Mineralogical and fluid inclusion evidence suggested that the calcite could have formed from groundwaters similar to those present in the region at the present day. It was also found that the morphology and microchemical characteristics of the calcite varied systematically with groundwater salinity, and could be used to differentiate freshwater and saline calcite precipitation. Furthermore, detailed petrographical analysis of calcite growth zoning characteristics indicated the calcite crystals within the freshwater-saline groundwater mixing zone might have changed morphology during their growth. This could potentially provide an indicator of the evolution and stability of the groundwater system, with respect to the interface between the different water masses.

The PADAMOT studies at the UK sites sought to test whether the relationships observed at Sellafield, between the late-calcite mineralization and groundwater chemistry, could be applied more generically as a palaeohydrogeological tool at other sites. To this end, calcite fracture mineralization was studied from a fully cored deep borehole drilled by Nirex at Dounreay in northern Scotland (as part of the Nirex site characterisation programme for IL/LL radioactive waste disposal in the UK). In addition, late calcite fracture mineralization was examined from a shallower fresh groundwater system in Carboniferous Limestone at Cloud Hill in the English Midlands. The purpose of this was to compare observations from this site, with those calcites from Sellafield and Dounreay, to establish whether freshwater calcites exhibited similar characteristics. A significant amount of supporting information was available from this site, which had originally been studied under a BGS 'Core Programme' project examining the influence of fracturing on the development of porosity in dolomitized limestone aquifer and reservoir systems (Bouch et al., 2004).

Overall the UK objectives for WP2 were:

- Further evaluate the relationships between late-stage calcite mineralization and the evolution of the modern groundwater system at Sellafield;

- Compare relationships observed between late calcite and groundwater relationships at Sellafield with other UK sites, to evaluate their application as a more generic palaeohydrogeological tool in site characterisation.

- To determine whether variations in calcite mineralization associated with the development of the present-day deep groundwater system records the impact of past climatic changes during the Quaternary.

1.2.2.4 MELECHOV SITE, BOHEMIAN MASSIF, CZECH REPUBLIC

The objective of PADAMOT WP2 at the Melechov site in the Bohemian Massif has been to provide a basic insight into the groundwater system, for modelling groundwater flow in the relatively small granite body at Melechov Hill, which is located as a northernmost promontory of the Moldanubian granite pluton in the Bohemian Massif in central Europe. The area is being considered as a testing site for the development of a deep geological repository

The region has a complex system of fractures and fracture porosity, related to its long and complex tectonic history. In addition, Tertiary uplift and erosion have significantly modified the land surface and impacted on drainage patterns. Furthermore, weathering and superficial deposits at the surface affect the permeability of the fissured zones. These features seem to be the controlling factors on groundwater circulation and residence time. The main focus of the studies at this site have been:

- To demonstrate if tectonic zones with deeper groundwater circulation systems exist in the Melechov Massif;

- To compare the groundwater residence time in the fissures of the Melechov Massif with groundwater residence time in granite bodies elsewhere in the Bohemian Massif.

The overall aim has been to clarify and update ideas about the shallow origin and circulation of groundwater in the fractured Melechov granite body, and to provide basic data for hydrogeological modelling.

1.2.2.5 PADUL AND CÚLLAR-BAZA BASIN, SOUTHERN SPAIN

The main objective of the study of these two sedimentary basins was to obtain palaeoenvironmental information to be applied to modelling the palaeohydrogeological behaviour of groundwater systems. The study of the sedimentary record of both sites provides information that can be interpreted in the context of climatic change. The Cúllar-Baza lacustrine record seems to have mainly recorded information about precipitation and palaeotemperature regimes while the Padul peat bog record offers a wide range of information about vegetation and palaeohydrogeological input. The palaeoclimatic data obtained from these two sites would be used to estimate the palaeoclimatic history at the Los Ratones site which is situated in a similar palaeoclimatic belt.

The palaeoclimatic information derived from Cúllar-Baza basin was mainly based on the analysis of the stable isotope ($\delta^{13}C$ and $\delta^{18}O$) signatures from biogenic calcite (ostracod shells). Whereas in Padul Peat Bog, fossil pollen and biomarkers were used as proxies for climatic change. In both areas a significant effort was devoted to the dating of the analysed sequences.

1.3   ANALYTICAL TECHNIQUES

1.3.1   Characterization of fracture mineralization

A wide variety of mineralogical, geochemical and isotopic analytical techniques were used to characterize the fracture mineralization associated with the fracture-flow groundwater systems at the study sites of Los Ratones, Laxemar, Äspö, Sellafield, Dounreay, Cloud Hill and Melechov Hill. Significant background mineralogical and petrographical data existed from earlier investigations at the Laxemar/Äspö and Sellafield sites, Dounreay and Cloud Hill that provided a basis for establishing a paragenetic framework for each of these study areas. Research at these sites therefore focused specifically on furthering the understanding of site palaeohydrogeology. In the case of the Los Ratones and Melechov sites, this background information was not available prior to PADAMOT, and consequently a more general range of mineralogical and geochemical analyses was undertaken as a first step ina comprehensive palaeohydrogeological understanding.

The principal analytical methods used during the PADAMOT project are briefly summarised here.

1.3.1.1 OPTICAL PETROGRAPHICAL ANALYSIS

Petrographical analysis was undertaken in thin sections and polished thin sections of fracture mineralization from all sites. Generally, these were prepared after samples were vacuum-impregnated with epoxy resin to stabilise the delicate fracture fillings. The sections were cut normal to the fracture surface so as to present a profile through the mineralization from the wallrock to the interior of the fracture fillings. Observations were made using an optical petrological microscope in transmitted and reflected light.

1.3.1.2 CATHODOLUMINESCENCE MICROSCOPY

Optical cold cathode cathodoluminescence microscopy (CL) was used to characterise the growth zoning and fabrics of the carbonate mineralization from the Los Ratones, Laxemar, Sellafield, Dounreay and Cloud Hill. In addition CL was also used to study the quartz mineralization fabrics from Los Ratones. CL studies were undertaken by the BGS and CIEMAT. Charles

University also tested CL on samples from Melechov Hill but no late-stage carbonate mineralization was found at this site.

BGS analyses was performed on samples from Sellafield, Dounreay, Cloud Hill, Laxemar and a small sub-set of samples from Los Ratones, using a Technosysn MKII luminoscope stage attached to a Nikon Labophot microscope. The system was run with the vacuum regulated to give an electron beam accelerating voltage of between 15-20 kV, and a beam current of 800-1100 µA. Images were captured using a Nikon Coolpix 995 digital camera.

CIEMAT analyses were performed on samples from Los Ratones using a Citl CL 8200 Mk4 CL system coupled to a Nikon Eclipse E400 POL polarizing microscope. Carbonate minerals were examined using an electron beam accelerating voltage of 12-16 kV and a beam current of 300-500 µA. Quartz mineralization was also examined using an electron beam accelerating voltage of >20 kV, and a beam current of 500-600 µA, beam potential.

1.3.1.3 BACKSCATTERED AND SECONDARY ELECTRON SCANNING ELECTRON MICROSCOPY

Scanning electron microscopy was used to examine both morphological characteristics of the fracture mineralization using secondary electron imaging (SEM), and for high-resolution petrographical analysis of polished thin sections or polished blocks using backscattered electron imaging (BSEM). SEM and BSEM studies were primarily undertaken by the BGS and CIEMAT, although Charles University and University of Edinburgh also undertook some BSEM analyses. Energy-dispersive X-ray microanalyses (EDXA) recorded simultaneously during SEM observations was used to aid mineralogical identifications and descriptions. CIEMAT also used SEM-EDXA to provide semi quantitative major and trace element analysis on the fracture-filling minerals.

BGS SEM analysis was performed on samples from Sellafield, Dounreay, Cloud Hill and Laxemar. Samples were prepared as carbon coated fresh fracture surfaces and polished thin sections of rock chips and fragments of late-stage calcite crystals mounted as centimetre-scale stubs using:

- A LEO 435VP digital variable-pressure SEM instrument running in high vacuum mode. Imaging was performed in secondary electron mode, with an accelerating voltage of 20 kV. EDXA was performed using an Oxford Instruments Pentafet (Si[Li]) detector, running ISIS 300 software;

- A Cambridge-Leica Stereoscan S360 SEM instrument using an accelerating voltage of 20 kV. EDXA was performed using an Oxford Instruments GEM (Ge) detector, running INCA and ISIS 300 software.

CIEMAT SEM analysis was performed on samples from Los Ratones. Samples were carbon-coated and analysed using a ZEISS DSM 960 SEM instrument coupled to a LINK AN eXL EDXA system.

The University of Edinburgh used SEM and BSEM to characterise polished sections of late-calcite samples from Sellafield, Dounreay and Cloud Hill prior to detailed microchemical and isotopic analysis by ion-probe. The Edinburgh analyses were carried out using a Philips XL30CP SEM instrument. Digital photographs were obtained, which were carefully merged to construct composite images, which functioned as sample maps. The different image types were overlain at precisely the same scale using software in Adobe Illustrator and Corel Draw, so that locations could be precisely identified before and after analyses.

1.3.1.4 ELECTRON PROBE MICROANALYSIS

Electron probe microanalysis (EPMA) was used to obtain major and minor element from fracture filling minerals and host rock minerals. EPMA was carried out by CIEMAT, BGS, University of

Edinburgh and Charles University. In addition, BGS used X-ray elemental mapping by EPMA to examine elemental distribution in samples of late-stage calcite.

BGS studies focused only on late-stage calcite mineralization from Sellafield, Dounreay and Cloud Hill. Analyses were performed using a CAMECA CAMEBAX SX50 electron probe microanalysis instrument, and were carried out using wavelength-dispersive X-ray spectrometry. The analyses were made with a 10 kV and 20 nA electron beam, with the beam defocused (to prevent damage to the calcite) to give a spot diameter of 10 µm. (X,Y) co-ordinates of the analysis points were recorded to facilitate the matching of analysis points to CL- zones following analysis.

CIEMAT studies focused on samples from Los Ratones. The objective of the analysis was to provide background compositional data for major elements from both the fracture-filling and granite minerals. CIEMAT analyses were performed using CAMECA CAMEBAX SX50 electron microprobe instruments at Oviedo University and Barcelona University. Typical analyses conditions employed a 20 kV electron beam voltage, 40nA electron beam current, beam diameter 1 µm, and a live time counting time of 40 seconds.

The Edinburgh University Cameca SX100 electron microprobe was used to produce initial data on trace element compositions of samples from Sellafield, Dounreay and Cloud Hill, prior to more detailed analysis by ion-probe.

1.3.1.5 ION PROBE MICROANALYSIS

Ion microprobe analyses were carried out at the University of Edinburgh Ion Microprobe Facility (www.geos.ed.ac.uk/facilities/ionprobe) on a small suite of samples of late-stage calcite from Sellafield, Dounreay and Cloud Hill to provide detailed trace element microchemical data, and to try to provide oxygen isotopic information from individual calcite growth zones.

1.3.1.5.1 *Minor and trace element analyses*

Minor and trace (including rare earth element, REE) element analyses were performed by Secondary Ion Mass Spectrometry (SIMS). A series of spot analyses across individual CL zones, produced a profile across an individual crystal. Elemental analyses were carried out using the CAMECA ims 4f instrument. Techniques and data corrections applied are similar to those developed by Dawson and Hinton, (2003). The elements analysed included Ca, Mn, Fe, Mg, Sr, Na, Y, Li, Ba, La, Ce, Nd, Sm, Eu, Dy, Er and Yb. The analytical conditions during two sessions were 10 nA ^{16}O - measurements of positive secondary ions, with a 120 eV energy offset. Ten cycles were performed (over ~ 25 minutes per analysis). Results from the first two cycles are eliminated, to reduce the possibility of surface contamination. Analyses were also corrected for background instrumental drift, by means of several analyses of a laboratory standard before new data was acquired, and after each 10 new data, and after the completion of a session of work in one day. The ion microprobe spot diameter was 10 to 20 microns enabling analyses to be performed, in most cases, within individual CL zones. The Oka calcite was used as a standard, and statistical counting errors varied, but generally were < 1 % for concentrations above 100 ppm, while concentrations below 10 ppm levels showed errors of 10-15 %. After analyses were performed, then samples were re-examined on the SEM, to locate the precise sites of ion probe plasma pits. These were photographed, and computer manipulation was used to precisely re-locate these sites onto a CL base-map of the sample.

1.3.1.5.2 *Oxygen isotope analyses*

For δ^{18}O analyses in calcite, the Cameca ims-1270 ion microprobe was used. A primary beam of ^{133}Cs$^+$ with a ~6.0 nA current and accelerating voltage of 10kV was used. Charge compensation of the Au-coated samples was accomplished using an electron flood gun. Sputtering with the Cs beam produced ~20 µm pit, 2-3 µm deep. Secondary ions of ^{16}O and ^{18}O were extracted with a

10 kV voltage, at a mass resolution of ~2400, and simultaneously collected on Faraday collectors with average count rate of 2 x 10^9 cps for $^{16}O^-$ and 5.0 x 10^6 cps on $^{18}O^-$. Measurements were divided into 2 blocks consisting of 5 cycles/block (totalling 10 cycles) with a count time of 4 s/cycle resulting in a total count time of 40 seconds. Theoretical estimates of internal precision for ^{18}O range from 0.40 ‰ to 0.10 ‰ based on counting statistics. The total time per analysis averaged approximately 6 minutes. During the analytical session a total of ~200 analyses of Edinburgh University lab standard (from University of Wisconsin) UWC-calcite standard ($\delta^{18}O$ = 23.28 ‰$_{SMOW}$ Valley personal com.) were measured and used for calibration during the three days of analysis. The unknown calcites were always bracketed between 20 analyses of the UWC standard. If no instrumental drift or instrumental changes (e.g. primary beam current) were observed then the average of the day's standard was used, otherwise the average of the 20 neighbouring standard was used.

1.3.1.6 LASER-ABLATION MICROPROBE – INDUCTIVELY-COUPLED PLASMA MASS SPECTROMETRY

Laser-ablation microprobe – inductively-coupled plasma mass spectrometry (LAMP-ICP-MS) analysis was undertaken to provide trace element microchemical information on fracture mineralization and host rock minerals. LAMP-ICP-MS was undertaken by BGS and CIEMAT.

BGS analyses were performed on samples from Sellafield, Dounreay, Cloud Hill, Laxemar and Los Ratones, using a purpose-built laser ablation microprobe system designed and built for the BGS by the Department of Chemistry, Birkbeck College, University of London. The system comprises a Spectron Nd YAG ultraviolet laser linked to a high-quality Leitz optical microscope. The laser-microscope system utilises a BGS custom-designed laser ablation chamber, with an optical quartz window, which is flushed by an argon carrier gas stream. The argon stream transfers ablated material to the plasma source in a VG Plasmaquad 2+ spectrometer ICP-MS instrument, using a modified dual-flow sample introduction system. The LAMP-ICP-MS system has been described in detail by Chenery and Cook (1993). The LAMP-ICP-MS system provides data in terms of relative element (ion mass) ratios. This is converted to absolute concentrations by internal normalisation of the data to an element of known concentration in the mineral, analysed simultaneously during the LAMP-ICP-MS analysis. For the purposes of this study, LAMP-ICP-MS analytical data have been normalised to Ca, and assuming an idealised calcite composition stoichiometry (i.e. Ca ≡ 400,000 ppm for pure $CaCO_3$) in the calculations.

CIEMAT analyses were performed on samples of fracture mineralization and granite wallrock minerals from Los Ratones. The analyses were undertaken at Huelva University, using a CETAC LSX-100LA Microprobe coupled to a Hewlett-Packard HP-500 ICP-MS system. Ablation was made with a Nd YAG Laser, using a wave length 254 nm, and ICP-MS: current of 1350 kV. Analyses were calibrated using the NIST SRM 612 calibration standard.

1.3.1.7 He-FLUSHED LASER-ASSISTED CARBONATE EXTACTION FOR STABLE ISOTOPE ($\delta^{18}O$ AND $\delta^{13}C$) ANALYSIS OF LATE FRACTURE CALCITE GROWTH ZONES

An attempt was made by the BGS to microsample individual growth zones in late-stage calcites from Sellafield, Dounreay, Cloud Hill and Laxemar, using laser micro-sampling to extract very small samples of CO_2 for subsequent analysis by conventional mass spectrometry. This technique, He-flushed laser-assisted carbonate extraction for stable isotope (He-LACE) analysis, has been developed and built at the BGS.

The He-LACE technique involves using an infrared laser (Sinrad laser) to ablate small volumes of sample approximately 70-80 μm diameter, which are located under a specially modified optical microscope. The sample - a polished block or polished section – is placed in a purpose-built stainless steel chamber attached to the microscope stage, fitted with a BaF_2 or ZnSe window which is transparent to the laser. As the laser probe strikes the sample, the sample is heated to 2000° K. CO_2 is evolved from the spot and is swept from the chamber in a He carrier-

gas stream to prevent back-reaction with the residual lime on cooling. The swept CO_2 is then trapped by cooling in a liquid-nitrogen trap and subsequently, is transferred to the mass spectrometer for analysis. The extracted CO_2 samples were analysed using a VG Isotech (MicroMass) Optima dual-inlet mass spectrometer, and the analytical data processed using MicroMass ODI2.47 software.

Because the laser ablation causes heating of the calcite samples, conventional resin-impregnated polished thin sections or polished blocks cannot be used, as the resin evolves CO_2 on heating. Therefore, specialised sample mounts were developed, initially using Plaster-of-Paris, and subsequently, low melting-point Bi-Pb-Sn alloy (MX70) to embed crystals of calcite prior to polishing. It was found that the initial Plaster-of-Paris mounts failed to give a good polished surface finish to the specimens. This prevented the acquisition of good CL images from the samples, which were used as reference maps for the location identification of He-LACE analysis points. Subsequent trials with MX70 alloy proved more successful for providing samples with high-quality polished finishes that could also be examined by CL and BSEM techniques.

1.3.1.8 CONVENTIONAL STABLE ISOTOPE (δ^{18}O AND δ^{13}C) ANALYSIS OF BULK FRACTURE CALCITE

The stable δ^{18}O and δ^{13}C isotope composition was determined for bulk samples of fracture calcite from the Laxemar site by Terralogica AB, using conventional mass spectrometric methodology. The stable carbon and oxygen isotope analyses were carried out on hand-separated bulk fracture calcite. Petrographical analysis showed that these samples often contained intergrowths of different generations of calcite that were too fine to separate and analyse individually. Therefore, the stable isotope analyses will represent mixtures of different generations of mineralization. Nevertheless, this approach has been used to previously (Bath et al., 2000) to examine possible ranges and trends of isotopic composition within the calcite fracture mineralization from the Äspö-Laxemar-Simpevarp area. In the PADAMOT study, the sampling was refined by using morphological information from SEM and CL studies to give a better control on differentiating between the different types of calcite that might be present during sample selection.

Sample preparation for isotopic analysis involved heating 200-300 µg of material, in vacuo for 30 minutes, at 400°C to remove possible organic material and moisture. Thereafter, the samples were analysed using a VG Prism Series II mass spectrometer with a VG Isocarb preparation system on line. In this system each sample was reacted with 100 % phosphoric acid at 90°C for 10 minutes, whereupon the released CO_2 gas was analysed in the mass spectrometer. All isotope results are reported as deviation (δ per mil relative to the Vienna Pee Dee Belemnite (VPDB) standard. The analysing system is calibrated to the PDB scale via the NBS-19 standard reference material.

1.3.1.9 STRONTIUM ISOTOPE (^{86}Sr/ ^{87}Sr) ANALYSIS OF BULK FRACTURE CALCITE

The strontium (^{86}Sr/ ^{87}Sr) isotope compositions of bulk samples of calcite fracture mineralization from Laxemar were determined by Terralogica AB. The analyses were performed using thermal ionization mass spectrometry (TIMS). As discussed in Section 1.3.1.8, the samples analysed represent bulk fracture calcite, and consequently will potentially contain a mixture of different calcite generations. However, the sampling was refined by using morphological information from SEM and CL studies to help differentiate and select calcites on the basis of their crystal morphology.

For the Sr isotope analyses about 30 to 40 mg of the carbonate samples were transferred to 2 ml centrifuge tubes, 200 µl 0.2 M HCl was added and shaken. The samples were allowed to react for 10 minutes while shaken in order to release the CO_2 gas. Then 20 µl 2 M HCl was added once or twice until most of the calcite had been decomposed. The samples were centrifuged for about 4 minutes and the liquids transferred to new clean centrifuge tubes by use of a pipette. The

centrifuge tubes were put on a hotplate and evaporated to dryness. To avoid disturbances in measuring the isotopic composition, strontium had to be separated from other elements present in the sample. After evaporation to dryness the samples were dissolved in 200 μl ultrapure 3M HNO_3, centrifuged and loaded onto ion-exchange columns packed with a Sr-Spec crown-ether resin from EIChrom, which retained Sr and allowed most other elements to pass. After rinsing out the remaining unwanted elements from the columns, strontium was collected with ultrapure water (Millipore). The collected Sr- fractions were then evaporated to dryness and loaded on pre-gassed Re filaments on a turret holding 12 samples and 1 NIST/NBS 987 Sr standard. The isotopic composition of Sr was determined by thermal ionization mass spectrometry (TIMS) on a Finnigan MAT 261 with a precision of about 20 ppm and a Sr blank of 50-100 pg. The $^{87}Sr/^{86}Sr$ ratio of the carbonate analysis were monitored by analysing one NIST/NBS SRM 987 Sr standard, for each turret of 12 samples, and the standard has a recommended $^{87}Sr/^{86}Sr$ value of 0.710248. The presented results are not corrected to the NBS 987 recommended value but given together with the specific measured NBS 987 value for the relevant turret.

1.3.1.10 X-RAY DIFFRACTION ANALYSIS

X-ray diffraction analysis (XRD) was used by Charles University for the identification and characterization of clay minerals from fracture fillings and wallrock alteration. XRD analyses of separated ultra-fine fraction were carried out to discriminate between chlorites and smectites.

X-ray traces were obtained using a PANalytical X´Pert Pro diffractometer system. These were recorded in the step-scanning mode, from an orientated diffractionless silicon monocrystal wafer sample substrate, using CuKα radiation (voltage 40 kV, current 30 mA) and a scanning range of 3–70 °2θ with a step size of 0,05 °2θ and counting time of 150.

Clay mineral separates were sedimented onto the silicon wafer from an ethanol-based suspension, to produce orientated sample mounts for XRD. Clay mineral material was separated from the bulk samples by controlled sedimentation in a water column. Glycolated and un-glycolated oriented samples (sample holder diffractionless silicon) were prepared and analysed. A different scan range of 3–30 °2θ was used for the glycolated samples.

PDF-2 Release 2003 (International Centre for Diffraction Data, Pennsylvania) were used for the interpretation of diffractograms.

1.3.1.11 FOURIER TRANSFORM INFRARED SPECTROMETRY

Fourier transform infrared spectrometry (FTIR) was also used by Charles University to further characterise clay mineral fracture fills. Clay samples were homogenised in steel ball mill and mixed with KBr (1 mg of clay sample and 300 mg of KBr). FTIR was conducted using a NlCOLET 740 FTIR spectrometer and OSP 680 data station (Nicolet Instruments Co., Madison, USA) in transmission mode and recording over a spectral range of 4000-400 cm^{-1} with a resolution of 4 cm^{-1}. Measured FTIR spectra were processed by Omnic (version 3.1) software (Nicolet Instruments Co., Madison, USA). Phases were identified by comparison with standard spectra in spectral libraries available at the Institute of Chemical Technology, Prague.

1.3.1.12 WHOLE ROCK CHEMISTRY BY X-RAY FLUORESCENCE SPECTROMETRY

X-Ray fluorescence spectrometry (XRF) were used by CIEMAT to provide major element chemical analysis of whole rock samples of the granite hoist rocks from the Los Ratones site. Analyses were carried out using a Phillips PX 1480 XRF system at Oviedo University.

1.3.1.13 WHOLE ROCK CHEMISTRY AND LEAD ISOTOPE ANALYSES BY INDUCTIVELY-COUPLED PLASMA MASS SPECTROMETRY

Inductively-coupled plasma – mass spectrometry (ICP-MS) was used by CIEMAT and Charles University to obtain trace element and REE geochemical information from fracture fillings and host rock samples from the Los Ratones and Melechov Hill sites, respectively. ICP-MS analysis was also used by Terralogica AB to determine the trace chemistry of bulk samples of calcites from Laxemar and Äspö.

Samples from Melechov Hill were analysed by ICP-MS at Charles University. The trace elements and Pb isotope ratios in fracture fillings were determined following bulk digestion and dissolution in a mixture of HF and $HClO_4$. 0.1 g of sample was digested in a 1 ml $HClO_4$ and 10 ml HF in PTFE vessels (Savillex®, Minnetonka, USA) heated on a hot plate (150°C) after overnight treatment. The sample was evaporated to ca. 0.5 ml, and subsequently re-dissolved in 2 % HNO_3, and then transferred into a 100 ml volumetric flask. All the acids used in the dissolution procedure were reagent grade (Merck, Germany) and double distilled. MilliQ+ deionised water obtained from a Millipore system was used for all dilutions.

A VG PQ3 (VG Elemental, United Kingdom) ICP-MS instrument was used for the analysis. This was equipped with a water-cooled spray-chamber, fitted with a Meinhard type nebulizer used to analyse trace elements (Li, Be, V, Cr, Mn, Co, Ni, Cu, Zn, Rb, Sr, Ba, Tl, Pb, Th, U, Y, REE, Zr, Hf, Nb and Ta) and Pb isotope ratios. Multi-element stock solution reference standards (Analytika Ltd., Czech Republic and Merck Germany) were used as calibration standards.

The Pb isotope ratios were corrected for the mass discrimination factor by using NIST SRM 981 (common lead; NIST USA). During the analytical procedure, the following isotopes were measured: ^{200}Hg, ^{202}Hg, ^{204}Pb, ^{206}Pb, ^{207}Pb, ^{208}Pb, and ^{209}Bi. The precision of the isotopic measurement of Pb was 0.1 - 0.4 % RSD (1σ) for $^{206}Pb/^{207}Pb$ and $^{208}Pb/^{206}Pb$, while the RSD for the $^{208}Pb/^{204}Pb$, $^{207}Pb/^{204}Pb$ and $^{206}Pb/^{204}Pb$ were somewhat higher (0.3 - 0.7 %) depending on low abundance of ^{204}Pb. The accuracy of the measurements was periodically checked against the AGV-2 standard (andesite; reference material of the US Geological Survey).

Terralogica ICP-MS analyses on calcites from Laxemar and Äspö were carried out using the following procedure. 12 (±0.01) mg of calcite sample was placed in a 50 ml tube, where 47 ml of 5% HNO_3 was added containing 15 ppb of iridium and rhenium respectively, to be used as internal standards. The sample was leached for 1 hour with stirring every 15 minutes. 20 ml of this solution was used for analysis, which was carried out on a Hewlett-Packard ICP-MS, model HP 4500. Certified multi-element standards from Merck (nr VI) and Agilent (nr 1) were used for calibration.

CIEMAT analyses were carried out at Granada University, using a Perkin-Elmer Sciex-Elan 5000 ICP-MS analyser.

1.3.1.14 FLUID INCLUSION ANALYSIS

1.3.1.14.1 Microthermometry

Fluid inclusions microthermometry analyses were undertaken by the BGS to study the palaeofluids in late-stage calcites from Dounreay, Cloud Hill and Laxemar, and quartz and dolomite-ankerite mineralization Los Ratones.

The BGS analyses utilised specialised blue-dye resin impregnated, doubly-polished fluid inclusion wafers (40-50 mm thick), which were prepared in the BGS thin-sectioning facility using standard techniques (Shepherd et al. 1985), and which were bonded to a glass cover slip (which increases sample competency during subsequent handling). The wafers were screened by transmitted light microscopy to identify "regions of interest" on each fluid inclusion wafer which contained fluid inclusions of sufficient size and abundance for microthermometric analysis.

These regions of interest were then extracted from the wafer as circular disks of approximately 2-7 mm diameter using a micro-drill attached to an optical microscope. These disks were then transferred to the heating-freezing stage for analysis.

Fluid inclusion microthermometry was conducted using a Linkam MDS600 heating-freezing stage, attached to a Leitz Ortholux II microscope, controlled by Linksys software and a Linkam TP93 programmer. A temperature calibration check was performed using synthetic fluid inclusion standards. The controller was reprogrammed if the measured temperatures differed from the known values by more than ±0.1 °C.

For the determination of all phase changes a "cycling" protocol, compatible with the general methodology for the study of fluid inclusions in diagenetic cements outlined by Goldstein & Reynolds (1995), was applied. This protocol takes advantage of the fact that nearly all phase changes exhibit some degree of metastability on cooling. The temperature of the end point of a phase change was approached incrementally, followed by rapid cooling of the inclusion. If the end-point of the phase change has not been passed, then the "disappearing" phase (e.g. vapour bubble, ice crystal) typically returns gradually. If the end point has been passed, the "disappearing" phase typically only returns after cooling by several tens of °C. The errors in determination of phase changes are thus controlled by the temperature increment used during the approach to the end point of the phase change being measured. Errors are typically:

·   homogenisation temperatures (T_h): between ±2.5 and ±5 °C,

·   final ice melting (T_{ice}): between ±0.2 and ±0.1 °C,

·   for first ice melting (T_{fm}): ±5 °C,

No pressure corrections have been applied to the homogenisation temperatures. The relatively large error on the T_{fm} data is due to the indistinct nature of first melting observations, rather than any instrumental limitation.

For two-phase (aqueous liquid + vapour) inclusions, T_h was determined on "heating runs" prior to the determination T_{fm} and T_{ice} on "freezing runs". This strategy prevents homogenisation temperatures being artificially elevated due to inclusion "stretching" during freezing. Although attempts were made to measure salt-hydrate melting temperature (T_{hyd}), no such data could be obtained.

Following microthermometry, the analysed fragments of samples, were analysed using CL microscopy and the specific cement zone within which individual inclusions occur was determined.

The significant number of monophase (contain liquid only at room temperature) inclusions that were present in many of the calcite samples, were also studied in detail. The ability of an inclusion to nucleate a vapour phase on cooling is related to the interplay between shrinkage of the fluid on cooling (increases internal tension which tends to form a vapour bubble) and the surface tension of the liquid phase (which tends to collapse the bubble; Roedder 1984). In inclusions where the stable vapour phase is sufficiently small in proportion to the size of the entire inclusion and surface tension is able to overcome the internal tension, fluids may become "stretched". This may occur in small inclusions trapped at high temperature, or in larger inclusions trapped at lower temperature. Therefore, although a large inclusion trapped at high temperature would be anticipated to nucleate a vapour phase on cooling to room temperature (and conversely a large monophase inclusion at room temperature may indicate relatively low trapping temperature conditions), the absence of a vapour phase in an inclusion can not be taken to definitively indicate trapping at low temperature.

In addition, T_{ice} data are only reliable for the calculation of bulk salinities if measured when a vapour phase is present in the inclusion. Therefore, in order to derive ice melting, and hence derive salinities for monophase inclusions, the following strategies were applied:

1.   Heating runs to determine T_h of 2-phase inclusions within a sample commonly required heating of the sample to approximately 200 °C. This sometimes caused sufficient deformation and/or leakage of monophase inclusions that when the sample was cooled to room temperature a vapour phase nucleated, enabling determination of ice melting temperatures.   Freezing runs were then undertaken on any, originally monophase, inclusions that had nucleated a vapour phase due to this process prior to attempting any other strategies.

2.   In the event that strategy 1 failed to generate a vapour phase in the monophase inclusions of interest, an attempt was made to deform or stretch the inclusion walls by freezing the inclusion rapidly to -100°C followed by more gradual warming to room temperature.   Freezing runs were then conducted on those inclusions within which a vapour phase had been induced. However, even following repeated freeze-thaw cycles, this strategy was unable to consistently generate a vapour phase.

In both of the above strategies, following the nucleation of a vapour phase in a stretched (or leaked) inclusion, it was commonly observed that the vapour phase was lost on freezing and failed to re-nucleate before final ice melting.

3.   The final strategy exploits the fact that in minerals such as calcite, inclusions heated to temperatures above their homogenisation temperature commonly undergo deformation and stretching, which may be accompanied by leakage of fluid. In inclusions that do not contain daughter minerals at the point of leakage it is probably safe to assume that any fluid lost will be of the same composition as the bulk inclusion (i.e. the loss is isochemical), and consequently that salinity data derived from ice melting in an inclusions leaked in this manner should reflect the original composition of the inclusion.

The procedure adopted a step-wise strategy with heating in increments of 50°C, followed by cooling to <5°C and inspection of the target inclusions for the development of a vapour phase. Freezing runs were then performed on any inclusions within which vapour phases had been induced, prior to running the next heating increment. The maximum temperature used for this strategy was 300°C, during which total leakage/decrepitation of 2-phase inclusions was commonly observed. Because this strategy carries a risk of causing decrepitation of inclusions within the sample, this was only employed if strategies 1 and 2 failed to yield sufficient numbers of inclusions with vapour phases suitable for T_{ice} determination.

Fluid inclusion salinities were calculated from ice-melting data using "CalcicBrine 1.5" (Naden 1996). This allows calculation of salinities in the binary systems $NaCl-H_2O$, $CaCl_2-H_2O$ and in the ternary system $NaCl-CaCl_2-H_2O$.   Where first melting data were available in order to characterise the components present within the fluid, the appropriate binary or ternary system was employed. However, in order to calculate $NaCl:CaCl_2$ ratios, a measurement of T_{hyd} is required. In the absence of data for a specific inclusion, the salinity was calculated as wt % NaCl equivalent.

CIEMAT also carried out fluid inclusion microthermometric measurements on inclusions in samples of quartz and dolomite-ankerite mineralization from Los Ratones. They used a Linkam fluid inclusion stage, with a heating range of -160ºC to +400 ºC, coupled to an Olympus BX50 optical microscope. Temperatures were calibrated using the freezing point/melting point of trichloromethane (-63.4 ºC), distilled water (0 ºC), Merck 9700 standard (+100 ºC), Merck 9735 standard (+135 ºC), adipidic acid (+151.46 ºC) and potassium dichromate (+398 ºC). Temperatures were determined with an error < 0.4 ºC.

Fluid inclusions have also been evaluated by Charles University, on samples of quartz mineralization from the Melechov site, using microthermometry.   These data are published in Doběs (1995), and the reader is referred to this publication for further analytical details. However, no calcite mineralization could be identified from this site.

1.3.1.14.2 Microchemical analysis of fluid inclusions by laser ablation – ICP-MS

To determine the composition of the palaeogroundwaters, the fluid inclusions were analysed by the BGS with laser ablation inductively coupled plasma mass spectrometry (LA-ICP-MS), using a 'state of the art' facility established at the Department of Earth Sciences, University of Leeds. The inclusions were ablated using a GEOLas Q Plus excimer laser (ArF, 193nm) and the analytes analysed with an Agilent 7500c quadrupole ICP-mass spectrometer. The laser optical system is identical to that described by Gunther et al (1997a). All stages of the ablation process were monitored visually via an in-built LED source and CCD camera. Ablated material was transported from a cylindrical chamber with a height of 5mm and an internal diameter of 57mm (approximately 13 cm^3) in a 0.68L/min flow of He gas via Teflon tubing to a small volume mixer cell where the analyte was premixed with a 0.95 L/min flow of Ar gas before introduction into the plasma. A special feature of the GEOLas is the ability to maintain a constant energy density of the laser beam independently of beam diameter. This provides highly reproducible ablation for a wide range of inclusion sizes. For each element the largest isotope mass was used except for Ca and Fe, where the minor isotopes ^{44}Ca and ^{57}Fe were chosen, to avoid isobaric interference from ^{40}Ar on ^{40}Ca and the ^{40}Ar-^{16}O dimer on ^{56}Fe.

Using small, 3-5 mm diameter micro-discs drilled out of polished wafers (as prepared for microthermometric analysis) and +100 μm thick polished sections mounted on glass, 54 inclusions were selected for analysis. After a low energy clean up of the sample surface using a 100micron diameter laser beam (laser fluence 1 J/cm^2), the beam was adjusted to match the diameter of the inclusion (typically 5-20 μm) and the laser fluence raised to 8 J/cm^2. Firing at a repetition rate of 10Hz, a flat-bottomed hole was drilled down to the inclusion, through it and continued into the carbonate matrix for a further 20 seconds. This provided a continuous signal of the matrix above and below the inclusion and captured the transient signal created during inclusion rupture and vaporization.

Calibration of the equipment was achieved using a combination NIST 610 and 612 reference glasses, and aqueous standard solutions ablated directly through the walls of glass capillaries. Direct liquid ablation has been demonstrated as a valid approach to fluid inclusion calibration in previous LA-ICP-MS studies (Gunther et al., 1997b; Shepherd et al., 2000; Ghazi and Shuttleworth, 2000). The silicate glasses were ablated for 200 pulses over a single 50 micron spot using a repetition rate of 5Hz and a laser fluence of 10J/cm^2. Laser focus on the ablation surface was maintained by raising the ablation cell 1 micron per 10 pulses, in accordance with an approximate ablation rate of 0.1 micron/pulse. Aqueous standards were first spiked with HNO_3 to a final concentration of 2 % to enhance absorption at λ = 193 nm and reduce splattering (Boué-Bigne et al., 1999). Standards were drawn into glass capillaries and sealed at least 10 mm from the end of the aqueous column with a narrow butane flame. The capillaries were then vented with an ablation hole at one end, and then breached over the liquid column with a 50 μm spot. Once the glass was removed, the spot size was reduced to 25 μm to avoid signal contamination from the glass, and the liquid surface ablated at 5 J/cm^2 and 10 Hz. Sodium was used as an internal standard for both glasses and solutions. Standards were run at the start and finish of each day to correct for linear drift.

The ablation signals were treated as time series, thus allowing the matrix and inclusion fluid to be characterised independently. In the case of Sr and Mg, this information was used to correct the fluid inclusion signals for matrix contamination. However, for Ca, Mn and Fe this proved impossible; the matrix signals completely swamped the corresponding fluid inclusion analyte signals. Data for the matrix also allowed the host carbonate to be placed within the mineral paragenesis established from complementary EPMS studies. Peak counts for each mass position (i.e. isotope) were background corrected using the instrumental or matrix background as appropriate. The net counts were then corrected for isotope abundance to give the net counts for each element. Finally the net counts were corrected for elemental sensitivity using the relative sensitivity factors obtained for the calibration standards (i.e. counts per ppm). All sensitivity

factors were normalised to sodium. For the samples, net peak counts were considered significant if they were greater than 3 x standard deviation of background counts.

Detection limits for elements in the aqueous phase are inclusion specific and depend upon the mass of analyte present (i.e. volume of inclusion fluid x concentration of analyte in solution). Data for the aqueous phase (Na, K, Cl, ± Sr, Mg) were obtained as equivalent mole ratios with respect to Na, and as wt % element ratios for Ca, Mg, Mn, Fe, Sr with respect to Ca in the carbonate host matrix. The overall precision for element ratios using the Leeds LA-ICP-MS system is about 15-30 % RSD (being best for the alkali elements) whilst the accuracy is typically within 15 % (Allan et al. in prep.).

1.3.2   Analysis of lacustrine and peat bog sediments from the Padul and Cúllar-Baza sites

Geochemical analyses of lacustrine and peat bog sediments from the Padul and Cúllar-Baza sites, and of biomarkers in samples of calcite fracture mineralization from the Laxemar, Sellafield, Dounreay, Cloud Hill and Los Ratones sites were coordinated and carried out by the Madrid School of Mines.

1.3.2.1 ^{14}C DATING

Radiocarbon dating was undertaken on peat samples. For this purpose e.g. 100 g were analyzed in the Instituto de Química Física Rocasolano (C.S.I.C., Madrid). Materials measured by the radiometric technique were analyzed by synthesizing CO_2 from the sample to benzene, measuring for ^{14}C content in a scintillation spectrometer, and then calculating for radiocarbon age. The ages were calibrated using the program CALIB (Washington University, method B,) with 2-sigma 95.4 % confidence intervals).

1.3.2.2 U/Th DATING

For U/Th dating pure peat was selected and prepared from five horizons using the procedure developed by Vogel and Kronfeld (1980). The procedure used for chemical separation is based on that developed by Bischoff and Fitzpatrick (1991). In this procedure, the sample is totally dissolved in strong mineral acids and a radioisotope with known activity is incorporated in order to determine the efficiency of the isotope separation. The U and Th isotopes were isolated by ion-exchange chromatography and then analyzed in an alpha spectrometer from Ortec with a silica barrier detector. For age calculation the program UDATE from Rosenbauer (1991) was used.

1.3.2.3 AMINO ACID RACEMIZATION DATING

Samples were sieved under running water, dried at room temperature, and studied under a binocular microscope to determine the faunal assemblages. Ostracods and Opercula were carefully ultrasonically-cleaned in water to remove the sediment. Afterwards, at least 10 mg of ostracods (ca. 2,000 single valves) and 15-20 mg of Opercula were hand picked.

The sample preparation protocol is described in Goodfriend (1991) and involves hydrolysis under N_2 atmosphere in HCl (2.9 μl/mg of 12 N HCl and 100 μl of 6 N HCl) for 20 h at 100 ºC, and derivitization in two steps: first esterification with thionyl chloride in isopropanol and acylation with trifluoroacetic acid anhydride in dichloromethane.

1-4 ml aliquots were injected into a Hewlett-Packard 5890 gas chromatograph with a Chirasil-L-Val fused silica column (0.39 mm x 0.25 mm x 25 m) from Chrompack and a NPD detector.

1.3.2.4 PALAEOMAGNETISM

The samples were selected in the laboratory and oriented samples taken in situ with a Pomeroy D-2801 portable drill. After removing the weathered surface material, cylindrical cores were prepared and measured in the Palaeomagnetism Laboratory of the Institut de Physique du Globe de Paris (IPGP), using a vertical cryogenic 2G magnetometre. All the samples were submitted to thermal demagnetization to 600 ºC at steps of 50 ºC in a low thermal gradient PYROX oven.

1.3.2.5 CHN ANALYSIS

The samples (4-5 g) from the sediment core were homogenized with mortar and pestle. Total organic carbon, hydrogen and nitrogen were measured with a LECO CHN-analyser (CHN-600) at 1050 ºC. The inorganic carbon fraction was previously removed by adding HCl so the proportional carbon abundance measured (C) is the organic carbon content (% TOC).

1.3.2.6 ORGANIC MATTER $\delta^{13}C$ VALUES

Carbon isotope ratios of bulk organic matter were determined at the "Estación Experimental El Zaidín". After carbonate removal with 1:1 HCl, the $\delta^{13}C$ values of organic matter were measured in selected samples by means of an EA-IRMS elemental analyser connected to a Finnigan MAT 251 mass spectrometer. Results are expressed in d-notation (0/00), using the international Vienna Pee Dee Belemnite standard. The standard deviations are 0.1 0/00 for $\delta^{13}C$ in organic matter.

1.3.2.7 OSTRACOD CALCITES $\delta^{13}C$ AND $\delta^{18}O$ ANALYSIS

For stable isotope analysis, 30 to 50 *Cyprideis torosa (Jones)* valves were selected, although there were some samples with a lesser number of individuals, in some cases 4 ostracods. For these samples a microline was used for a minimum of 0.15 milligrams of weight.

Once the valves of *Cyprideis torosa (Jones)* were selected and ultrasonically-cleaned under running water, they were heated at 4000 °C under a nitrogen atmosphere for one hour to remove the remaining organic matter.

The carbon and oxygen stable isotope analysis were made in a Finnigan MAT 251 mass-spectrometer at the Estación Experimental del Zaidín (CSIC, Granada). In order to obtain the evolved carbon dioxide (CO_2) of the samples, they were reacted with 100% phosphoric acid in a thermostatic bath at 80 ºC during 30 minutes. The experimental error for carbonates ($\delta^{13}C$ and $\delta^{18}O$) was less than ±0.05 %. Carrara Marble and EEZ-1 were used as internal standards that were previously compared with NBS-18 and NBS-19.

All measurements are expressed in δ (delta) 0/00 notation, as a deviation from an internationally accepted standard (Pee Dee Belemnite carbonate fossil from South Carolina).

1.3.2.8 LIPID EXTRACTION AND ANALYSIS (BIOMARKER ANALYSIS)

About 5-10 g of sediment were first ground and biomarkers extracted following the LEB protocol, which consists of (Lucini et al., 2000): 24 hour Soxhlet extraction with dichloromethane and methanol 2:1 (suprasolv Merck) and concentration of the isolated bitumen using a rotary-evaporation device. Three bitumen fractions were extracted through liquid chromatography in a silica-alumina glass column using solvents of different polarities: hexane, dichloromethane/hexane 80% and methanol. Samples were injected into an HP 6890 gas-chromatograph with selective mass detector HP 5973 and HP-5MS column. The compounds were identified with the Data Analysis program and the Wiley Library. n-alkanes were calculated from the GC/MS chromatograms with mass/charge m/z 57.

2 Geological, Palaeoclimatic and Hydrogeological Setting of the PADAMOT Study Sites

2.1 LOS RATONES

2.1.1 Location and geology

Los Ratones mine is situated in the central southern sector of the Albalá Granitic Pluton (Figure 2-1), located in the southwest section of the Iberian Massif (Julivert et al., 1972), which represents the westernmost segment of the European Variscan Belt (Pérez Estaún et al., 1991). This pluton is a concentric zoned body, elongated in a N-S direction, with biotitic, porphyritic granites in the rim and fine-grained two-mica leucogranites in the core. The Albalá Pluton was emplaced in epizonal rocks of the schist-greywacke complex (Upper Proterozoic to Lower Cambrian). Rb-Sr whole rock dating indicates an intrusion age of 302±4 Ma. Sn, W, P and U mineralizations are present in late-magmatic dykes and are genetically related with the most differentiated leucogranitic host rocks (Reguilón et al., 1996).
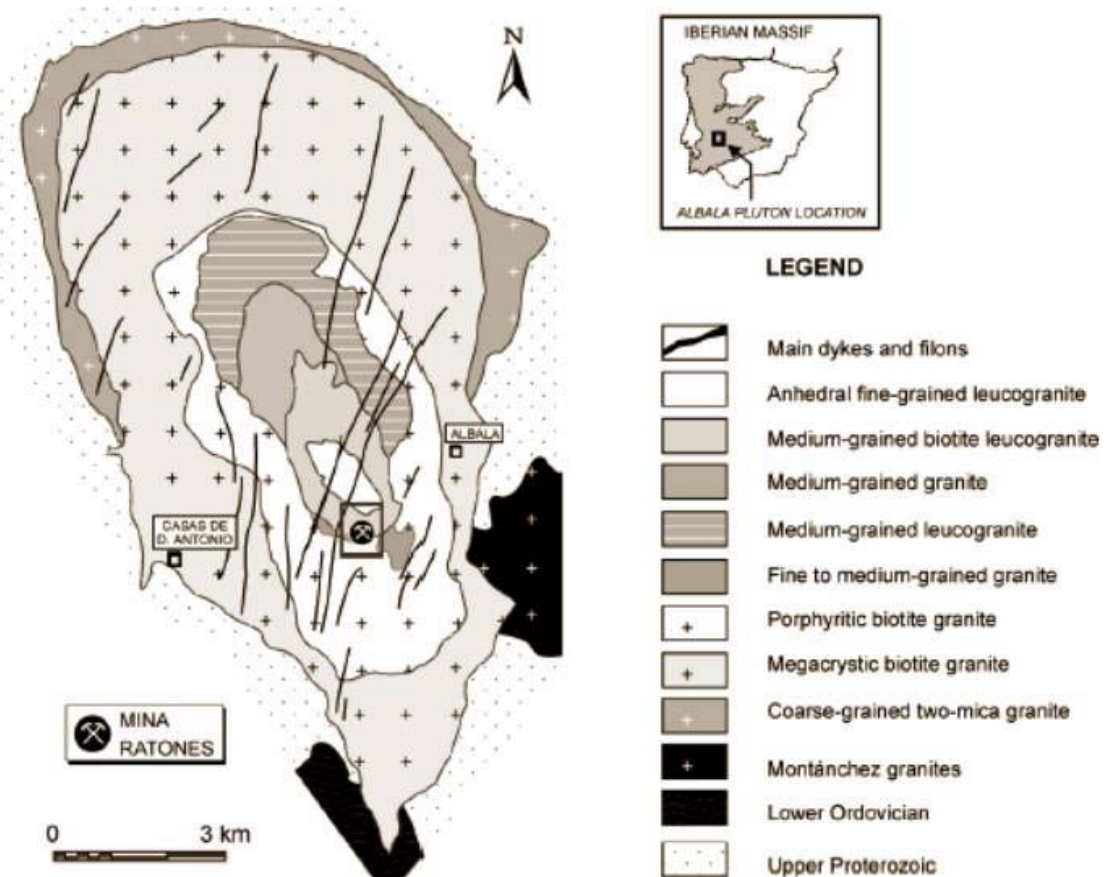
Figure 2-1. Geological map of the Albala Granitic Pluton (ENRESA, 1996, Escuder and Pérez Estaún, 1998).

From a petrological point of view the Albalá Pluton includes a continuous sequence of granitic facies with intrusion ages becoming more modern towards the centre (Escuder, 1999). These units are cut by later dykes, quartz dolerites, aplites hyd aplopegmatites and by granitic porphyrys. In the Mina Ratones area, only four of the ten granitic facies are recognized, and comprise: alkaline feldspar granites and syenogranites, peraluminic and subalkaline granites,

with accessory minerals as monazite, xenotime, apatite, uraninite, cordierite, andalucite and tourmaline. These rock types largely differ in their modal proportion of micas, textural characteristics, grain size and presence or absence of accessory minerals (e.g. cordierite and tourmaline).

2.1.2 Structural setting

Two major deformation events affect the structure of the area. Deformation during the Tertiary generated brittle fractures in the Albalá pluton, which are superimposed on ductile-to-brittle late Variscan structures. These brittle structures are sub vertical and are geometrically grouped in two sets: the sinistral NNE-SSW to ENE-WSW (e.g. the named dykes 27 and 27´) and the conjugate dextral N-S to NW-SE (e.g. the named North Fault and the South Fault) (Escuder Viruete, 1999).

Pérez-Estaún (1999) proposed that within these major deformation events three fracture-generating stages can be identified within the pluton structures. Based on their relation with the pluton emplacement (syn-F3 Hercynian), these can be classified as late and post-emplacement of the pluton. These stages are:

- First fracturing stage: late-magmatic structures;
    - Dykes of porphyritic granites;
    - Tourmaline veins, occasionally mineralized with Sn-W-As;
- Second and third fracturing stages: post-magmatic structures;
    - Second fracturing stage: post-Hercynian deformations;
        - Ductile-brittle shears;
        - Dykes and quartz-apatite fills;
    - Third fracturing stage: post-Hercynian deformations;
        - Basic dykes intrusion;
        - Conjugated brittle structures with local U-mineralizations;
        - Late normal fault. This last stage is related with quartz and carbonate fills.
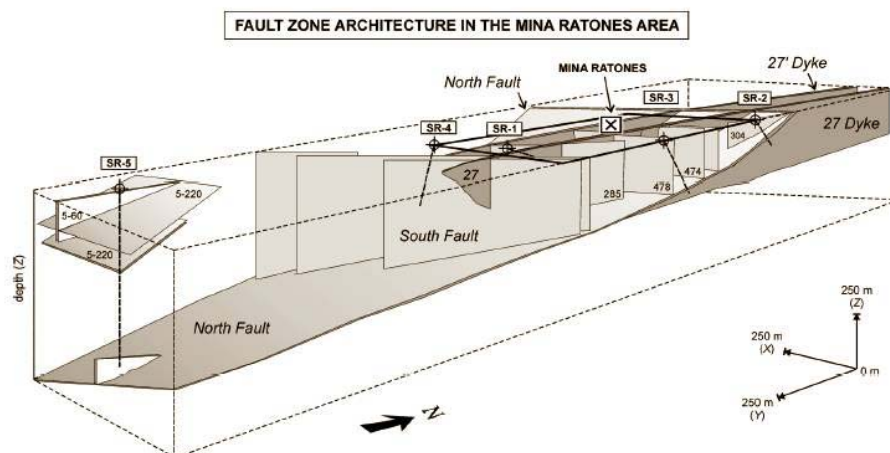
Figure 2-2. Fault architecture of Mina Ratones area (Carbonell et al., 1999; Escuder Viruete and Pérez Estaún, 1998; Escuder Viruete, 1999; Pérez Estaún, 1999, Martí et al., 2002). The main identified structures are the North Fault, the South Fault and the 27 and 27' Dykes.

18

As a result of detailed mapping, the main structures related to fluid flow in the Mina Ratones area are (Figure 2-2):

- Two related subvertical quartz dykes with massive pitchblende and parapitchblende (27 and 27' dykes, which were mined in the past);

- The North Fault. This constitutes the main structure of the Los Ratones mine, and determines the geometry of the deposit;

- The South Fault. This is formed by a set of subvertical and parallel fractures and dykes.

Each structure has been characterized by reflection seismics, seismic tomography, televiewer, geophysical logs, and by borehole examination carried out around the mine (Escuder et al., 1999).

2.1.3 Main hydrogeological and hydrogeochemical features

Five 101 mm diameter boreholes have been drilled around the mine to depths of up to 500 m to investigate the geology, hydrogeology and geochemistry of the area (their location with respect to the main structures is depicted in Figure 2-2). These boreholes were cored using the triple-tube system.

Borehole SR1 is inclined and cuts dyke 27 between 65 and 75 m in depth. Borehole SR-2 (79 m deep) allows for the characterization of waters that circulate through the Northern Fault at a depth of 58-60m, which are considered to represent the recharge waters of the mine. Borehole SR-3 (195 m deep) allows sampling of the waters that flow at a greater depth through the Northern Fault (140-150 m), and enables information to be gained on the chemical evolution of the water as a function of depth, between two hydraulically connected zones. Borehole SR-4 (124 m deep), located at the southern part of the mine, allows the characterization of the waters from the Southern Fault, which according to the conceptual hydrogeological model of the zone, would have been a previous pathway for the water discharge from the mine. Borehole SR-5 (500 m deep) is located to the south of the mine but is far away from the dykes. The excavation of the mine will have influenced the groundwater flow system and hydrochemistry (Gómez, 2002). The chemical composition of the waters from borehole Borehole SR-5 provides an indication of the impact of the mine on the deep granitic groundwater. The hydrogeochemical behaviour of the main shaft, which is 160 m deep, has also been studied.

The Ratones mine is located in a flat area delimited by Cerro Puerquera (537 m a.o.s.l.) towards the North and by the Maderos stream towards the South. Three hydrogeological units can be distinguished (Ortuño et al., 1999):

a)   Areas of superficial covering, of reduced thickness and irregular distribution, characterized by short and shallow flows and seasonal springs, and that can constitute part of the recharge and subterranean discharge of the granites.

b)   Altered and fractured zones (150-200 m depth) characterized by relatively high transmissivities (10^{-4} to 10^{-6} m^2/s). The main structures and the network of minor fracturing connecting with them control the flow.

c)   Fresh relatively intact granite that constitutes a low permeability media, in which the water flows through sparse fractures with a contrasted conductivity with respect to the more densely-fractured granite.

The main structures identified in the area surrounding the mine have been characterized from a hydraulic point of view. The flow is preferentially through the NE-SW fractures and the mineralized dykes (27 and 27'). The flow is controlled by the topography to a depth of at least 200 m. Below this depth the flows are regional and originated away from the influence of the mine.

The recharge of Ratones mine area is due to the infiltration of precipitation through the superficial altered zones, and by the flow of groundwater from the 27 and 27' dykes and the North Fault. At a regional scale the recharge derives mainly from the infiltration of the rainfall in the San Pedro and Montánchez Ranges.

The relation between δ^2H and $\delta^{18}O$ is shown in Figure 2-3 with respect to the global meteoric water line (Craig, 1961). The relationship for local precipitation recorded during several years (Gómez, 2002) is also depicted and it can be shown that it is very similar. Most of groundwaters lie close to this line indicating that they have a meteoric origin. The deepest waters (SR5, 458-469 m) are depleted both in ^2H and ^{18}O indicating an ancient origin, which agrees with the residence time (15000 to 16000 years) determined from ^{14}C measurements. The small variations within the data can be explained by differences in parameters such as temperature, altitude and the degree of continentality (Dansgaard, 1964).

Dating of the groundwater based on ^3H and ^{14}C measurements indicates the existence of groundwaters at the site falling into age groups of: 3 to 5 years (recent); >50 years, around 1000 years; and between 15000 to 16000 years. This heterogeneity in the residence time of the waters is the result of the existence of the distinct flow paths described above.
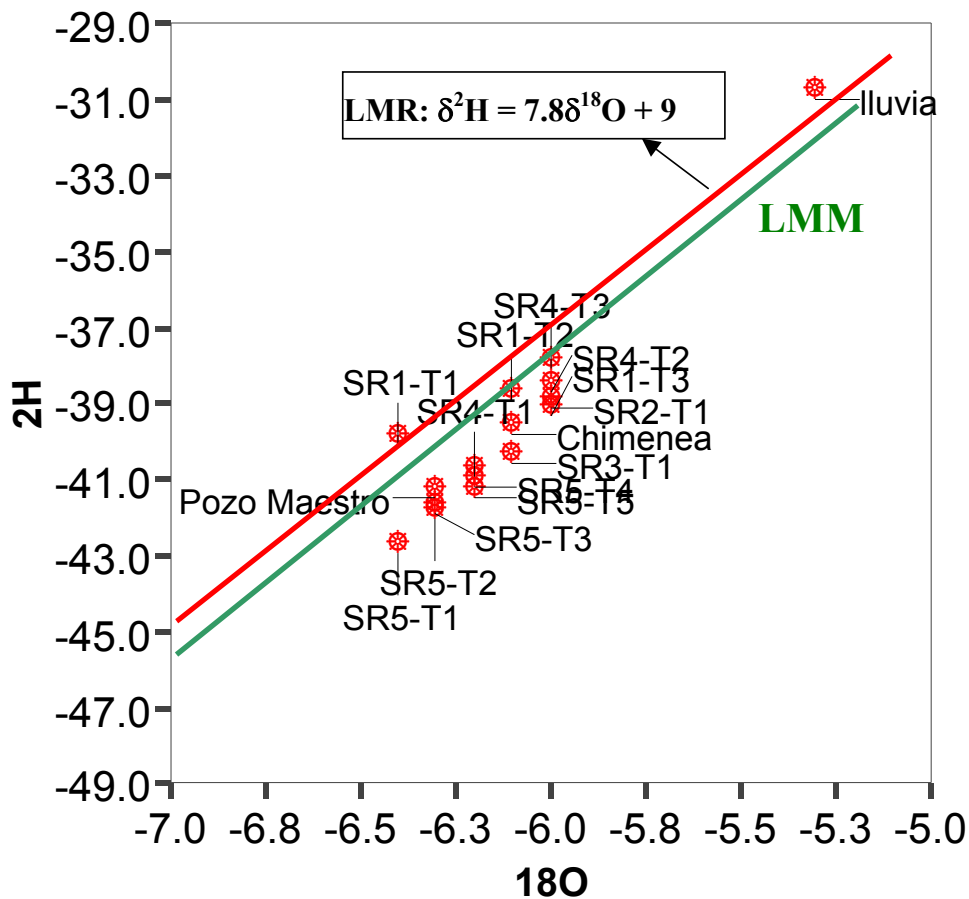
Figure 2-3. Isotopic composition ($^{18}O/^2H$) (‰$_{SMOW}$) measured in groundwater samples from Ratones Mine. The Global Meteoric Water Line (LMM) and Local Meteoric Water Line (LMR) are illustrated.

The discharge from Ratones Mine occurs in the south, through dykes 27 and 27' directed towards the south fault, which acts as a subterranean sink, and through the superficial altered zone towards the Maderos stream (Ortuño et al., 1999). At a regional scale the discharge is towards the nearby streams, through local or intermediate flows.

Groundwaters were sampled and analysed from 13 zones in the 5 boreholes described previously. The boreholes were packered-off, in order to avoid the mixture of waters from different depths due to vertical flows towards the borehole. The chemical integrity of the samples was checked by measuring physico-chemical parameters in situ (Gómez, 2002). The main conclusions that can be drawn about the water composition are described below.

The waters are poorly mineralized, since the electric conductivities are not greater than 740 µS/cm. The mean pH values of the groundwaters are close to neutrality, although the pH range for water associated with the uranium mineralization (SR1 and SR4) is slightly lower than that for the background waters (compare pH values - SR1: 7.1 ± 0.2; SR4: 7.1 ± 0.5; SR2: 7.4 ± 0.5; SR3: 7.8 ± 0.6 and SR5: 7.7 ± 0.2). Only the surface waters from the Maderos stream and the ventilation shaft showed an oxidized redox potential (70-300 mV). The groundwaters, however, showed a slightly to moderately reduced redox potential (from 0 to -300 mV). Dissolved oxygen was almost nil in all the water sampled, in agreement with the redox potentials recorded. Water temperature increases linearly directly with depth as a function of the geothermal gradient (0.03 ºC/m). The waters from the deepest part of borehole SR5 reach a temperature of 29.2 ºC, consistent with the geothermal gradient.

In the present study, groundwater samples were collected from packered-off intervals in order to avoid the mixture of waters from different depths due to vertical flows towards the borehole. Variations of major ions compositions allow the classification of the main groups of water:

- Group A: $Mg-SO_4^{2-}$ type waters represented by the upper sections of boreholes SR1 and SR4; they are found in the surroundings of dyke 27 (SR1) and the South Fault (SR4).

- Group B: $Mg-HCO_3^-$ type waters represented by the deepest sections of boreholes SR1 (dyke 27) and SR4 (South Fault), and the waters from the Main Shaft and old shaft though these two last waters are richer in calcium than in magnesium.

- Group C: $Na-Ca-HCO_3^-$ type waters with 30 % and 25 % of Mg and Ca, respectively. They are represented by boreholes SR2, SR3 and the upper sections of borehole SR5

- Group D: $Na-HCO_3^-$ highly evolved waters represented by lower sections of borehole SR5.

The high sulphate waters of Group A may reflect interaction of the groundwater associated with the oxidation of sulphide-bearing ore minerals, as a result of the mining activities. As the Mg sulphate waters progressively have less contact with the mineralization, they gradually evolve to a composition more typical of the deeper (undisturbed) granitic environment (sodium bicarbonate water) (Gómez, 2002). It must also be pointed out that Cl^- in these waters is very low. The highest Cl^- concentrations are found in borehole SR5 (26mg/L Cl^-) at 417-427 m.

A model for the evolution of the groundwaters has been proposed (Gómez, 2002), in which the main processes are established. The most important water-rock interaction process, with respect to the neutralization of pH in those waters associated with the mineralization, is the dissolution of complex assemblage of carbonate minerals found in the fractures and dykes. Furthermore, the precipitation of siderite has a significant contribution in the regulation of Fe^{2+} and HCO_3^- in the mine waters. Ionic exchange with smectites in the fissure fillings is the main process that controls the cation concentration in the waters.

2.2 ÄSPÖ AND LAXEMAR

2.2.1 Location and geology

Äspö and Laxemar are situated on the Baltic coast of southeast Sweden. The area is characterised by intrusive granitoids belonging to the Transcandinavian Igneous Belt with ages around 1.8 Ga (Kornfält et al., 1997). The compositions range from quartz monzodiorites to

granite. The Swedish Nuclear Fuel and Waste Management Company (SKB) has constructed an underground rock laboratory on the low-lying island of Äspö (Figure 2-4) where it is carrying out a programme of investigations to develop and test methodologies for its programme of research into the storage of spent nuclear fuel.

The Äspö hard rock laboratory (ÄHRL) comprises a spiral tunnel more than 3 km long that reaches a depth of 500 m. Around 20 core boreholes have been drilled from the surface down to various depths (200 to 1700 m) within the area. In the previous EQUIP palaeohydrogeological project, study was made of samples collected mainly from Äspö drill cores. However, the subsequent PADAMOT investigations have focussed on mineralization from the Laxemar borehole KLX01m, which was drilled down to 1070 m depth on the mainland west of Äspö.
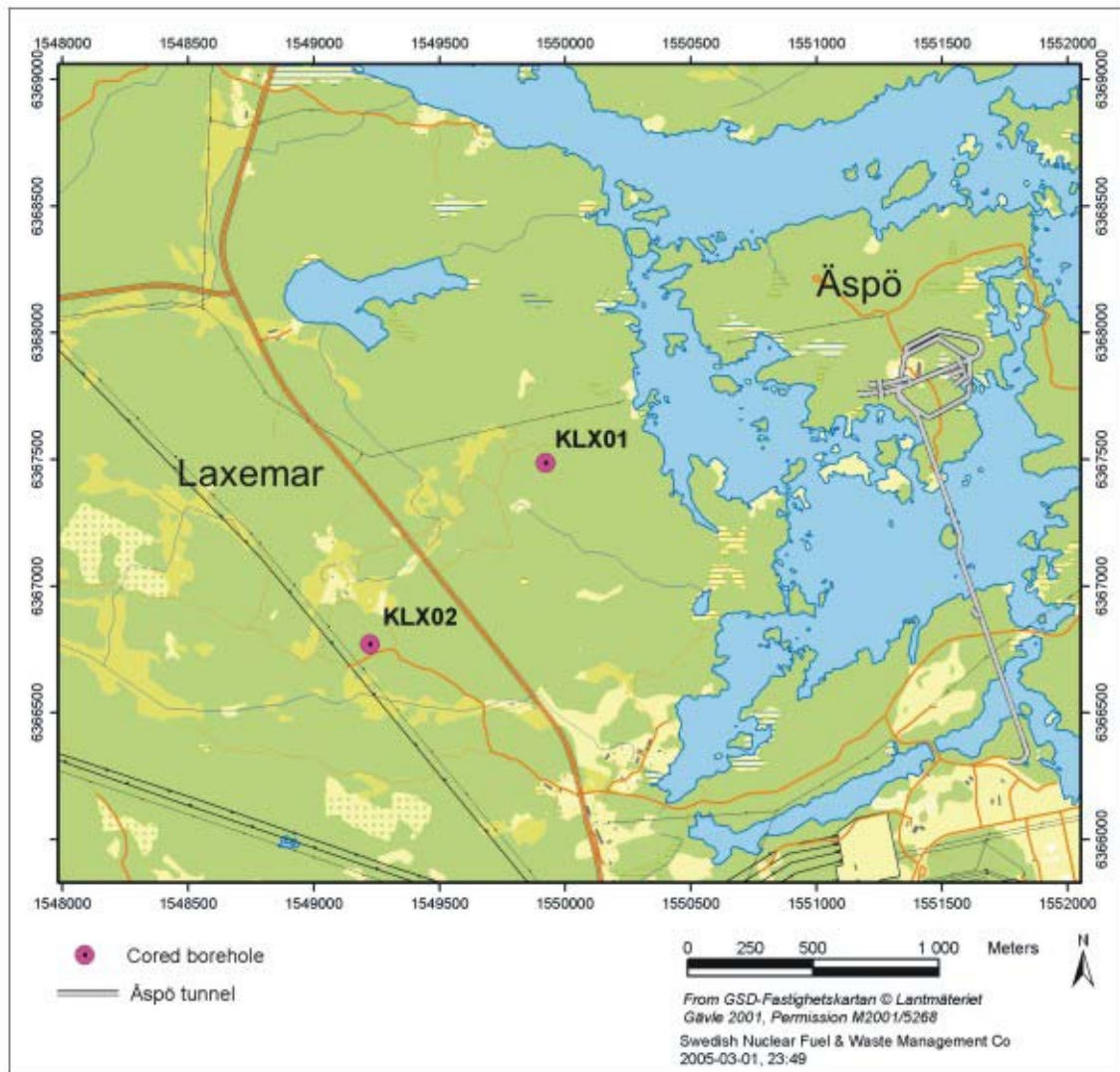
Figure 2-4. Map of the Äspö and Laxemar area showing the location of site investigation boreholes.

2.2.2 Post-glacial hydrogeological evolution and present groundwater chemistry

Since the Äspö/Laxemar area is situated on the low-lying Baltic Sea coast, the postglacial evolution of the area has been strongly influenced by a complex interplay between global sea-level changes, fresh water run-off from the surrounding terrain, and glacio-isostatic fluctuations in the land surface. Consequently, the sites have experienced several different episodes during

22

which either fresh or brackish water environments developed after the last glaciation, and which have had a large influence on the present groundwater chemistry.
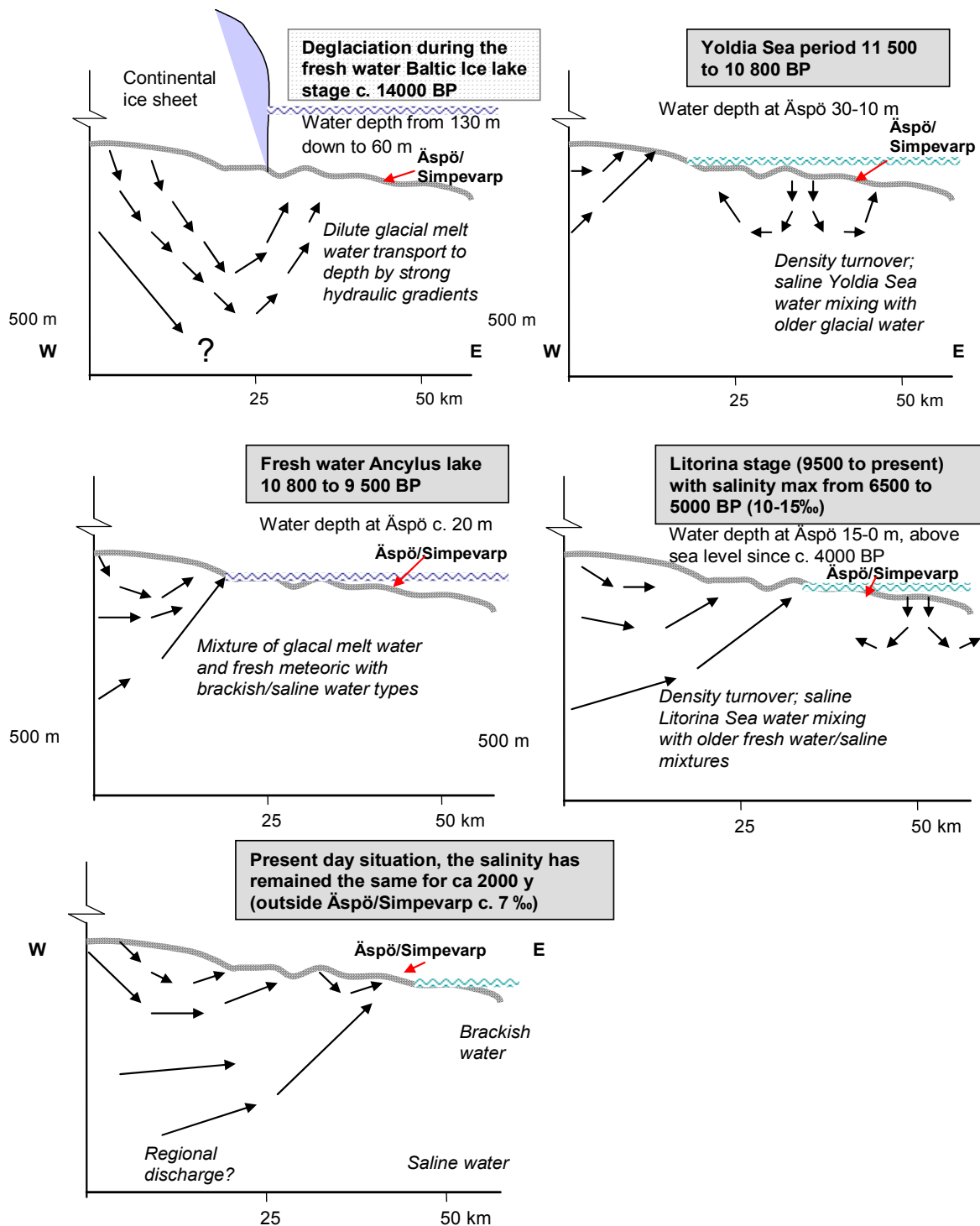
Figure 2-5. **Conceptual postglacial scenario model for the Äspö/Simpevarp area. The figures show possible flow lines, density-driven turnover events, and non-saline, brackish and saline water interfaces. Different stages are: a) Deglaciation, b)Yoldia Sea stage, c) Ancylus Lake stage d) Littorina stage, and e) present day Baltic Sea stage. Based on the shoreline displacement curve by T Påsse (personal communication 2003) and information from Fredén (2002) and (Westman et a., 1999). Modified from Laaksoharju et al. (2004).**

The post-glacial evolution of the area is summarised in Figure 2-5. Deglaciation started about 13,000 to 14,000 years BP during which the Simpevarp/Äspö area was covered by a fresh water ice lake with a water depth of between 60 and 130 m (Baltic Ice Lake stage). This was followed by a period of marine inundation (Yoldia Sea stage) between 11,500 and 10,800 years BP, with water depths at Simpevarp/Äspö of between 10-30 m. A second fresh water lake (Ancylus Lake stage) covered the area between 10,800 to 9,500 years BP. Water depth at Äspö is estimated to have been about 20 m during this stage. The Simpevarp/Äspö was again inundated by marine conditions between 6,500 and 5,000 years BP (Littorina Sea) during which the water depth at Äspö is estimated to have been between 0-15 m, but has risen above sea level since 4,000 years BP. The present-day brackish water conditions of the Baltic Sea were established around 2,000 years BP and have remained constant to the present day.

The brackish marine input of the Baltic Sea stage will have been of less significance in the western Laxemar area compared with Simpevarp/Äspö area, which is close to the present shoreline of the Baltic Sea and which has a low topography (0-20 m).

At Äspö/Laxemar and in the Simpevarp peninsula (which is currently being studied SKB are part of their on-going site investigation programme) groundwater samples have been analysed from cored boreholes drilled to a maximum depth of 1700 m (borehole KLX02), and percussion-drilled boreholes drilled from the surface to about 100 m to 200 m depth. Hydrochemical interpretations (Smellie et al., 1995; Laaksoharju et al., 1997 and Laaksoharju et al., 2005) have distinguished several different groundwater components. Modelling and interpretation of the groundwater chemistry has shown that several events have contributed to the distribution and composition of the present groundwaters:

- Meteoric water of present climate and cool climate (probably glacial melt water)

- Baltic Sea water; present and probably also ancient

- Brine type water with very long residence time

These studies have also shown that mixing of these waters, bacterially mediated reactions (e.g. sulphur, iron and manganese reduction), ion-exchange, and calcite precipitation/dissolution have taken place in the Äspö groundwater.

Thus the following evolution of the groundwater has been outlined (Laaksoharju et al., 1999):

- Deep recharge by glacial melt water (possibly from several glaciations) due to the high hydraulic heads caused by the ice cap, and mixing at considerable depth with a saline water of brine-type.

- Baltic Sea water has later been introduced by density turn-over.

- Subsequently, when Äspö rose above the sea-level, meteoric water has been recharged and mixed with the earlier Baltic Sea- and glacial-brine mixed waters.

The present day groundwater chemistry of the Laxemar/Simpevarp area is summarised in the conceptual model shown in Figure 2-6 (SKB, 2004). In borehole KLX01 which was specifically examined within the PADAMOT project, six sections have been sampled for groundwater chemistry (Table 2-1). The sampled sections correspond closely to true vertical depth as the borehole is sub-vertical. Table 2-1 shows that the salinity of the groundwater generally increases with depth from about 2000 mg/l Cl⁻ at about 275 m, to 12 600 mg/l Cl⁻ below 1000 m, with a inversion to more dilute groundwater (1700 mg/l Cl⁻) between 546 to 461 m.

Table 2-1. Groundwater chemistry (major components and stable isotopes for sampled sections in borehole KLX01 at Laxemar.

KLX01 Section (m)	Na mg/L	Ca mg/L	HCO$_3$ mg/L	Cl mg/L	SO$_4$ mg/L	δ^{18}O ‰ SMOW	δ^{2}H ‰ SMOW
272-277	1040	243	83	2050	48	-11.5	-89.9
546-461	860	223	78	1700	106	-12	-94.5
680-720	1610	1330	24	4680	390	-11.8	-98,8
830-841	2750	3000	6	9180	670	-	-96,9
910-921	3100	3800	6	11200	770	-	-92.9
999-1078	3350	4500	12	12600	695	-	-90.9

Water type A: Dilute 0.5-2 g/L TDS; Na-HCO$_3$; Meteoric dominated; δ^{18}O = -11 to -8 ‰ SMOW
Main reactions: Weathering, ion exchange, dissolution of calcite, redox reactions, microbial reactions
Redox conditions: Oxidising - reducing

Water type B: Brackish 5-10 g/L TDS; Na-Ca-Cl to Ca-Na-Cl; Meteoric (± Marine, e.g. Littorina Sea component at Simpevarp) – Glacial – Deep Saline; δ^{18}O = -14 to -11 ‰ SMOW
Main reactions: Ion exchange, pptn. of calcite, redox and microbial reactions
Redox conditions: Reducing

Water type C: Saline 25-30 g/L TDS; Na-Ca-Cl to Ca-Na-Cl; Glacial – Deep Saline at Laxemar, Glacial – ±Old Marine - Deep Saline at Simpevarp; δ^{18}O = ~-13 ‰ SMOW
Main reactions: Ion exchange, microbial reactions
Redox conditions: Reducing

Water type D: Highly saline, up to 70 g/L TDS; Ca-Na-Cl/Na-Ca-Cl; Deep Saline - Brine mixtures; mixing mainly by diffusion; δ^{18}O = ~-10 ‰ SMOW
Main reactions: Long term water rock interactions
Redox conditions: Reducing

Figure 2-6. Conceptual model of the groundwater chemistry of the Laxemar/Simpevarp area (from SKB, 2004). The situation at Äspö is similar to Simpevarp (cf. Figure 2-4 for location).

2.3 SELLAFIELD, DOUNREAY AND CLOUD HILL

2.3.1 Location and geology

2.3.1.1 SELLAFIELD

The Sellafield study site is located on the Cumbrian coast of northwest England. The site was investigated by United Kingdom Nirex Limited (Nirex) between 1989 and 1997 to determine whether the site would be suitable to host a deep geological repository for intermediate- and low-level radioactive waste. Twenty-nine boreholes (mostly cored) were drilled by Nirex within an area of 8 km by 6.5 km (Figure 2-7), the deepest borehole (Sellafield BH3) reached 1950 m depth. Detailed petrological studies have been made of the fractures and associated mineralization encountered in 23 of these boreholes (Milodowski et al., 1998; 2002). The site was also described as part of the earlier EQUIP palaeohydrogeological investigations (Bath et al., 2000).
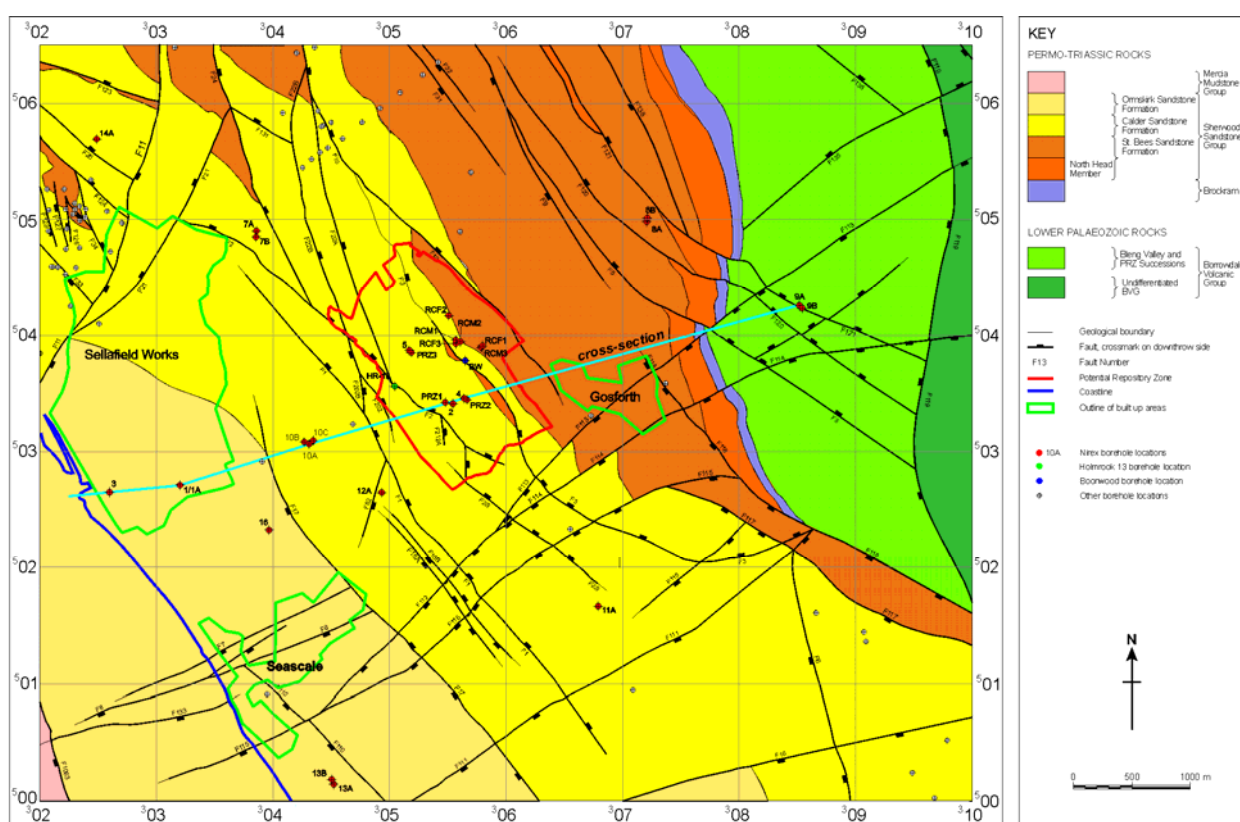
Figure 2-7. Geological map of the Sellafield area showing the locations of deep boreholes.

The geology of the area has been described by Nirex (1993), Michie and Bowden (1994), Michie (1996) and Ackhurst et al. (1997). The Sellafield site lies on a moderately flat coastal plain, about 10 km wide, between the Irish Sea to the west and the Lake District. Much of the Sellafield area is blanketed by a variable thickness of unconsolidated Quaternary lodgement tills and interbedded glaciofluvial and glaciolacustrine deposits, largely attributed to the Devensian. The bedrock geology consists of an eastwards-thinning wedge of Permo-Triassic sedimentary strata, which overlap Carboniferous rocks resting on Lower Palaeozoic rocks of the Lake District Massif (Figure 2-8). This marks the northeastern margin of the large Mesozoic East Irish Sea Basin. The site is bounded to the west by the Irish Sea and to the east by the uplands of the Lake District, from which it is separated by the Lake District Boundary Fault Zone (Ackhurst et al.,

26

1998). The Permo-Triassic sedimentary rocks comprise the sandstone-dominated Triassic Sherwood Sandstone Group (SSG) with a basal conglomeratic or breccia unit (the Brockram), which overly Permian mudstones and evaporites of the St Bees Shales Formation (SBSh) and St Bees Evaporite (SBE) Formation (Figure 2-8). The SSG is about 400 m thick in the centre of the site (Proposed Repository Zone (PRZ) and Rock Characterisation Facility (RCF) areas), although the Permian mudstones and evaporites are absent at this point. However the Permo-Triassic sequence thickens rapidly westwards into East Irish Sea Basin where it attains a thickness of several thousand metres (Figure 2-8). These rocks rest unconformably on the Carboniferous Limestone, which in turn unconformably overlies fractured crystalline basement rocks (low-grade regionally-metamorphosed lavas, pyroclastic and volcaniclastic rocks) of the Lower Palaeozoic Borrowdale Volcanic Group (BVG) (Figure 2-8). These have a proven thickness of over 1000 m.
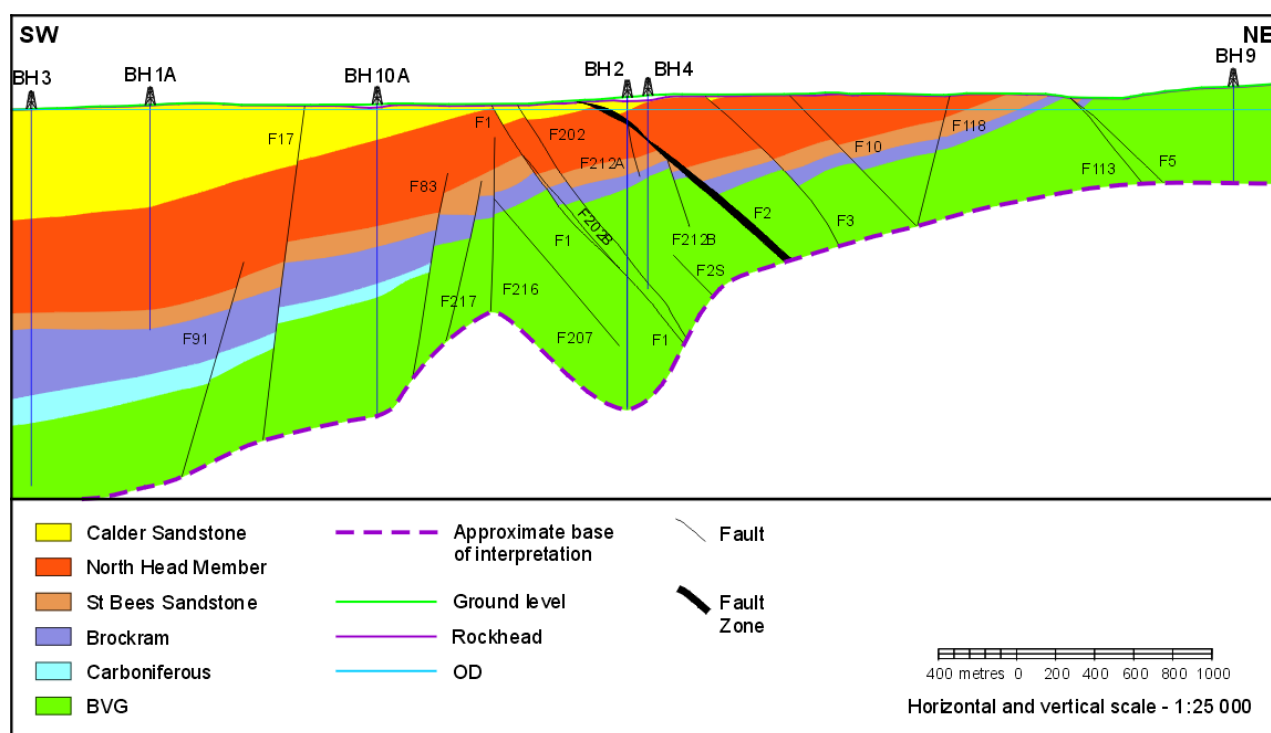
Figure 2-8. Geological NE-SW cross-section of the Sellafield area.

2.3.1.2 DOUNREAY

The Dounreay study site is located on the Caithness coast of northeast Scotland, about 12 km west of the town of Thurso. The site was investigated by Nirex between 1989 and 1991 to determine whether the site would be suitable to host a deep geological repository for intermediate- and low-level radioactive waste. Two boreholes (Dounreay BH1 and Dounreay BH2) were drilled by Nirex (Figure 2-9) the deepest borehole (Dounreay BH1) reached a depth of 1327 m. Investigations during this study have focussed on drill core samples from Dounreay borehole BH1.

The geology and hydrogeology of the Dounreay site are summarised by Nirex (1994). Details of geology, mineralogical and geochemical characteristics of the rocks encountered in Dounreay BH1 are reported elsewhere (Barclay et al., 1992; Hyslop and Milodowski, 1994). The Dounreay site lies on a relatively narrow coastal plain underlain by Devonian sedimentary strata. This extends 2 to 3 km to the south of the site and merges with a series of low peat-covered hills with isolated outcrops of crystalline basement.

The crystalline basement rocks comprise a complex series of Precambrian metasedimentary rocks (dominated by migmatitic psammites) generally correlated with the Moine assemblage (Moine Supergroup). These are cut by two major igneous intrusions, the Strath Halladale Granite and Reay Diorite (Figure 2-9). Structurally, the basement rocks were subjected to intense polyphase deformation and metamorphism during the pre-Devonian Caledonian orogeny. The Moine rocks of the region have been interpreted as a stack of slide-bounded nappes, which are divided into three major thrust units from west to east, the Moine (or Mhoine), Naver and Swordly Nappes (Barr et al., 1986). Caledonian overthrusting towards the west telescoped the pre-existing metamorphic assemblages, which increase in grade from west to east. Caledonian amphibolite-grade metamorphism overprints earlier similar high-grade assemblages in the rocks of east Sutherland (Holdsworth, 1989). Many of these Caledonian thrusts have probably reactivated earlier Precambrian high strain zones. Segments of Lewisian basement occur throughout the Sutherland Moine, both as pre-Caledonian fold cores and along early zones of ductile thrusting (Moorhouse and Moorhouse, 1987).
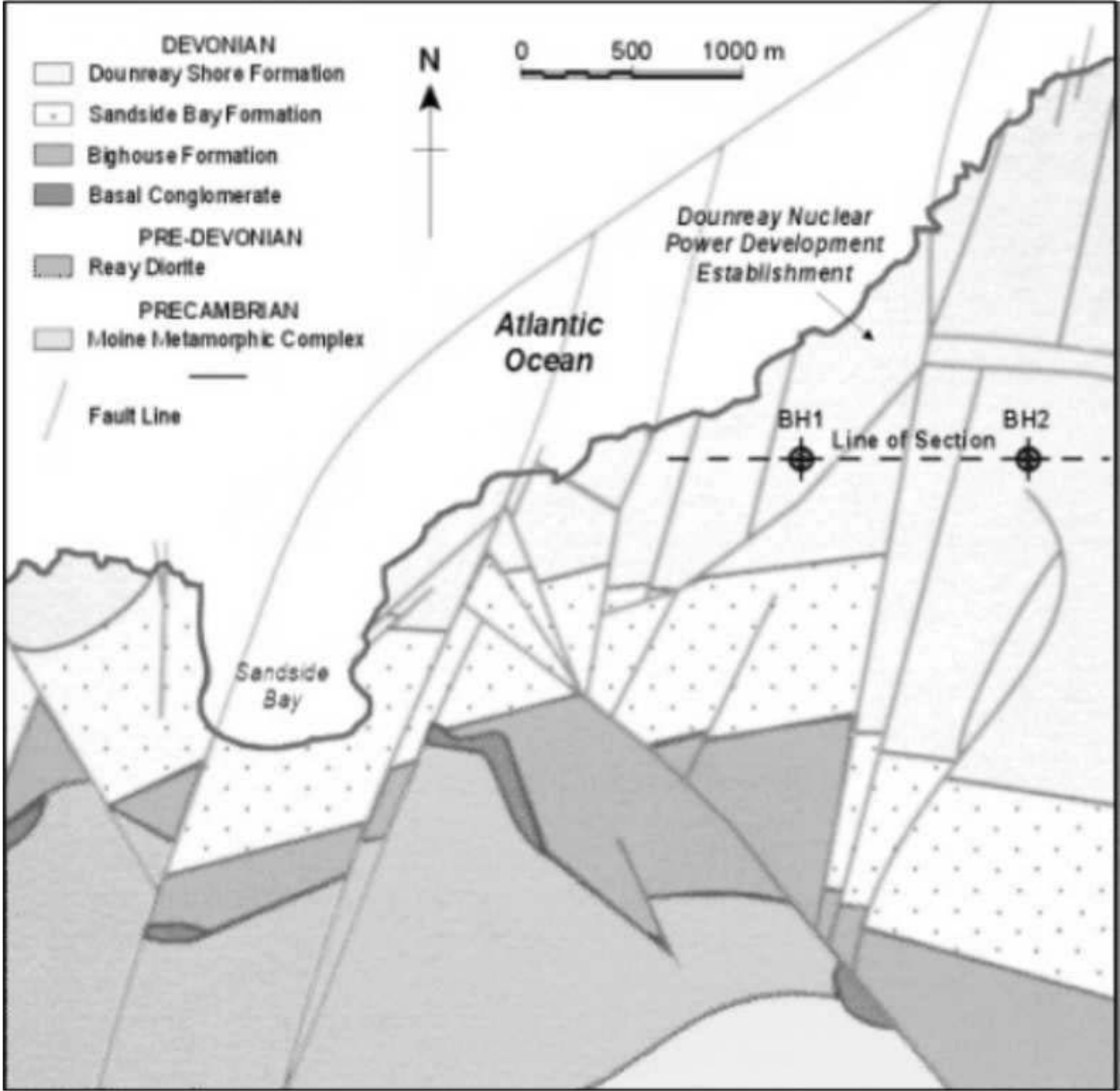
Figure 2-9. Geological Map of the Dounreay area showing the location of deep boreholes (based on Nirex, 1994).

The crystalline basement is unconformably overlain by Devonian sedimentary rocks (Figure 2-10). These were largely deposited in the Devonian Orcadian Basin, formed from a series of northeast-trending continental half-graben sub-basins developed after the Caledonian Orogeny. The strata comprise patchily developed Lower Devonian sandstones, siltstones and conglomerates that are in turn unconformably covered by Middle Devonian sediments, consisting of a thin basal conglomerate (breccia) unit passing upwards through medium to coarse sandstones into finely bedded lacustrine rocks of the Caithness Flagstone Group, which dominate the basin fill. These strata form monotonous series of mainly grey and grey-green, often finely-laminated mudstones, siltstones and fine grained sandstones, which are commonly organic- and carbonate (dolomite-calcite)-rich. Thin, finely laminated deep-water limestones, and shallow-water basin margin limestones and dolomites of algal, stromatolitic and sabkha origin are also present. Facies variations within the Devonian strata are cyclic and reflect lacustrine transgression and regression in response to tectonic and/or climatic drivers within the Orcadian basin. Between 300-600 m of Caithness Flagstone Group strata are present in the Dounreay area, which lies near the southern edge of the Orcadian Basin. However, this sequence attains a total thickness in excess of 4000 m elsewhere in Caithness (Mykura, 1983).
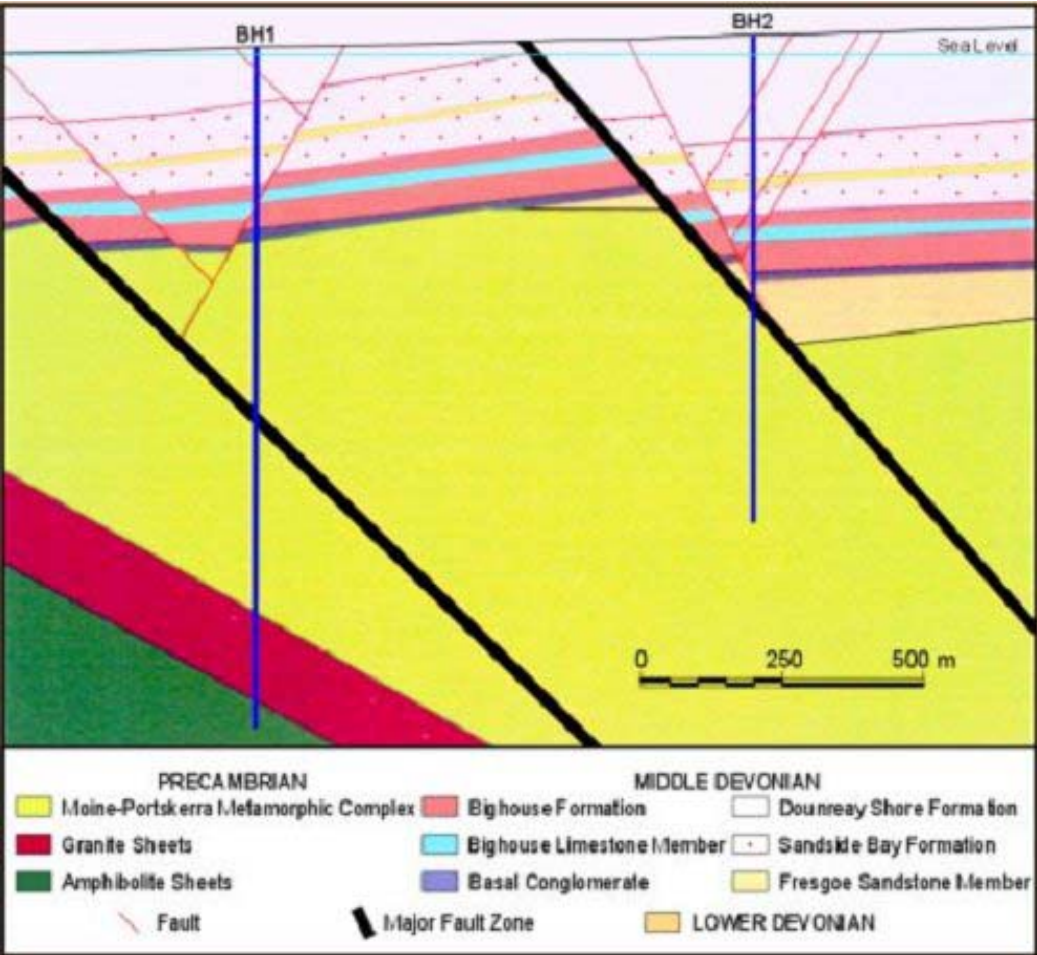
Figure 2-10. Geological E-W cross-section of the Dounreay site (based on Nirex, 1994).

Offshore (to the north) of the Dounreay site, the bedrock is at or close to the seabed and the Devonian strata progressively thicken northwards. Five to ten kilometres offshore, Permo-Triassic sediments cover the Devonian rocks and in turn thicken northwards forming a major regional offshore sedimentary basin, containing sandstones shales and evaporites.

29

Drift deposits, predominantly peat and glacial till, cover much of the surface area where the Devonian sediments are developed.

The Devonian sediments generally dip gently (5° to 15°) away from the basement contact with broad regional flexural folding giving rise to gradual changes in dip and strike. The complete sequence is cut by a network of predominantly extensional NE-SW-trending and NW-SE-trending normal faults, which show a complex sequence of movement and reactivation probably continuing into Tertiary times. Major faults within this system are steeply dipping and form a grid on a scale of 500 m to 700 m (Figure 2-9). No evidence of post-Tertiary tectonic activity is apparent (Nirex, 1994).

Dounreay borehole BH1 penetrated a sequence of approximately 375 m of Devonian sedimentary rocks resting on just over 950 m of crystalline (mainly psammitic) metamorphic and igneous rocks correlated with the Moine Supergroup. The unconformity between the Devonian and the Moine is present at approximately 375.7 m depth. Both the crystalline Moine basement rocks and the Devonian cover rocks are strongly fractured.

2.3.1.3 CLOUD HILL

Cloud Hill is located in northwest Leicestershire, in the East Midlands of England, approximately 25 km southwest of Nottingham. The samples examined in this study were collected from the base of a large quarry (operated by Ennestone Breedon Plc) in fractured dolostone and limestone that is being worked at Cloud Hill for aggregate.

The geology of the Cloud Hill area is described in detail by Ambrose and Carney (1997a, b) and Carney et al (2001a,b). Cloud Hill is one of a number of Dinantian (Carboniferous Limestone) limestone inliers that crop out in Leicestershire and south Derbyshire, within the East Midlands of England (Figure 2-11). These lie on the southern shelf margin (Hathern Shelf) of the Widmerpool Gulf, a Carboniferous half-graben basin bounded to the north by the Normanton Hills (or Hoton) Fault (Carney et al., 2001a; Ebdon et al., 1990). These faults were active during the Dinantian and Namurian until the early Westphalian (Carney et al., 2002a, b). At least 800 m of Namurian and an unknown thickness of Westphalian strata were removed during Variscan inversion. Fault movement also occurred during the Tertiary, with up to 95 m of displacement on the Normanton Hills Fault (Carney et al., 2001a, b; Green et al., 2001).

The Dinantian strata at Cloud Hill are divided into three formations (Ambrose and Carney, 1997a, b; Carney et al., 2001a, b):

- *The Milldale Limestone Formation* (Early Chadian):

    This comprises up to 400 m of strata dominated by dolomitized, well-bedded, fine- to coarse-grained, probably shallow-water platform or shelf-storm carbonate deposits, and deeper-water ramp carbonates, interbedded with thin siliciclastic mudstones and siltstones deposited during quieter periods. Undolomitized rocks are represented by bioclastic and locally oolitic and pelloidal grainstones. Extensive obliterative dolomitization has destroyed much of the original sedimentary fabric, and rendered these rocks largely unfossiliferous. Some fine-medium-grained, locally pebbly dolomitic sandstone and sandy dolostone beds interbedded with dolostone are also present. Massive, structureless, fine-grained dolostone is also present. This is 61 m thick in Cloud Hill but attains a thickness of up to 100 m in the nearby Breedon inlier, and is interpreted as representing mud-mound (Waulsortian) reef on the basis of its occurrence within an otherwise well-bedded sequence, and on the presence of fabrics and textures comparable with mud-mound reefs in the Carboniferous limestones of Derbyshire Dome.

- *The Cloud Hill Dolostone Formation* (Early Asbian)

    This comprises up to 125 m of strata consisting of dolomitized, fossiliferous, bedded shallow-platform or shelf-storm deposits. Mud-mound reef deposits are also present and

include fossiliferous, commonly mouldic pore-rich, finely to coarsely crystalline massive dolostones.

- *The Ticknall Limestone Formation* (Brigantian)

This consists of 14 m of variably dolomitized, muddy to coarse-grained, typically bioclastic, locally oolitic and pelloidal grainstones with muddy and silty interbeds.   These strata represent shallow-water deposits, and periodic emergence and desiccation are recorded by finely crystalline sabkha-peritidal deposits, local rubbly palaeosols and minor karstification.
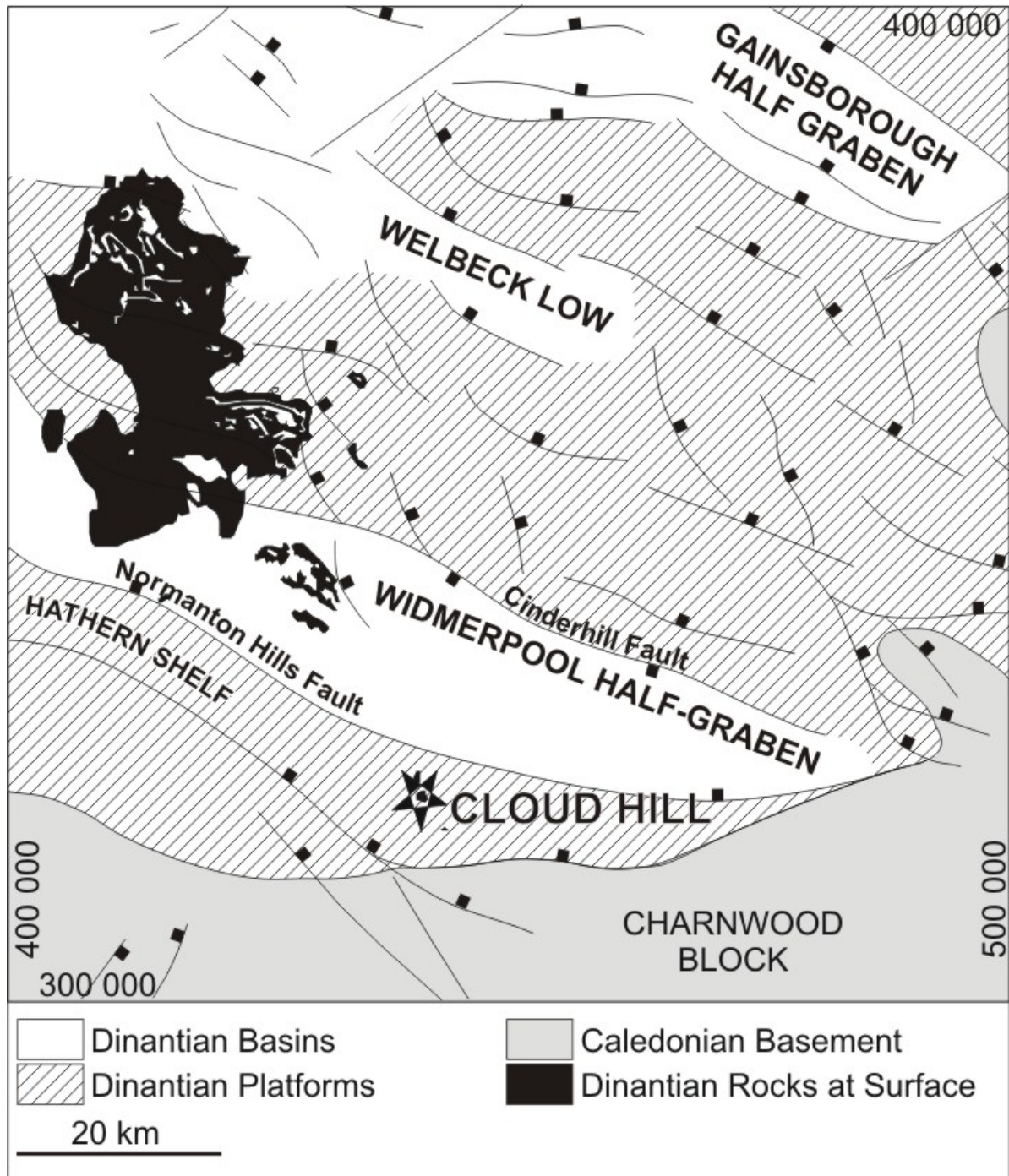
Figure 2-11.   Map showing the geological setting of the Cloud Hill inlier in relation to blocks and basins in Central England during Dinantian times (after Bouch et al., 2004; fault positions from Ebdon et al., 1990).

31

The sequence is highly fractured and extensively dolomitized and Spink (1965) considered that the dolomitization was probably Permian. The sequence is unconformably overlain by red-bed mudstones and siltstones of the Triassic Mercia Mudstone Group. The Carboniferous strata have been affected by karstification beneath the Permo-Triassic unconformity, and the presence of Permo-Triassic sediments filling caves and other karstic solution indicates that some of the karstification is probably of Permo-Triassic age. Detailed petrographical studies (Bouch et al., 2004) show that the dolomitization largely pre-dates the fracturing (Section 3.5).

2.3.2   Palaeoclimatic history

The broad classification of British Quaternary Stages, based on the system proposed by (Mitchell et al., 1973) and augmented by supplementary information from Bowen (1999), Bath et al., (2000), Stuart and Lister (2001) and Lee et al. (2004) is summarised in Table 2-2.

The British Isles were affected by several glacial cycles during the Quaternary, with oscillations between glaciation, periglacial, boreal and temperate climate states. Geological evidence is now largely seen for only two of the glaciations: the Anglian, which was the most extensive; and the Devensian, which was the most recent (Table 2-2). The Anglian is correlated with a European pre-Saalian glaciation (the Elsterian), and the Devensian with the Weichselian glaciation of Scandinavia and the Würm phase in central Europe. Much of the evidence of other glaciations has been obscured or removed by the effects of these two events. However, recent mapping and studies of terrace deposits in lowland eastern England by the BGS and others has provided evidence of an earlier extensive Middle Pleistocene glaciation – the 'Happisburgh Glaciation' (Lee et al., 2004) – considered to have occurred during Oxygen Isotope Stage 16 and to be the equivalent of the Don Glaciation of eastern Europe. Some studies also suggest that Britain was affected by glaciation between the Anglian and the Devensian - during the Wolstonian (Table 2-2). However, the Wolstonian type location is now considered to be pre-Hoxnian and is now correlated with the Anglian 'Lowestoft Formation'. The only lithostratigraphical evidence considered to support a post-Hoxnian, but pre-Ipswichian, glaciation of East Anglia comes from the Nar Valley in Norfolk (cf. ANDRA, 2002).

The location of the PADAMOT study sites in relation to the estimated areal extent of the British Quaternary ice sheets is shown in Figure 2-12. The Anglian Glaciation was the most extensive ice sheet, which is believed to have reached its maximum at around 440,000 years BP, reaching as far south as the Thames and north Devon in southern England (Figure 2-11). Dounreay, Sellafield and Cloud Hill were all covered by the Anglian ice sheet.

The earlier Happisburgh Glaciation (~630,000 years BP) and the later possible Wolstonian Glaciation (sometime between ~130,000 to 270,000 years BP) both reached East Anglia (e.g. ANDRA, 2002, Lee et al., 2004) (Table 2-2). Therefore, all three study sites are likely to have been covered by ice sheets during these two events.

The Devensian glacial phase, which occurred from 110,000 to 10,000 years BP, produced the least extensive ice sheet (Table 2-2). Ice sheets probably covered the Sellafield and Dounreay regions at about 25,000 years BP, and built up to a maximum thickness of rather less than 1000 m (in the case of Sellafield at least) at the glacial maximum between 20,000 to19,000 years BP (Bath el al., 2000). Ice cover at these two sites probably persisted for only 9,000 to 10,000 years at most, becoming ice-free at about 16,000 years BP as the climate warmed during the Windermere interstadial (Table 2-2). The climate again cooled between about 11,000 and 10,000 years BP, at the end of the Devensian (Younger Dryas), giving rise to a period of intense cold associated with the formation of localised corrie glaciers in the British uplands ('Loch Lomond Readvance'). Dounreay, being slightly further north, may be considered to have remained ice-covered for a little longer than Sellafield. However, there is some uncertainty in the extent to which this area was glaciated during the Devensian. Sutherland, (1984) identified the tills occupying the Dounreay area as having been deposited by the earlier 'Wolstonian' glaciation. Hall and Whittington (1989) argued that west of the Dounreay area, these deposits

overlie other tills that were laid down by the Late Devensian ice sheet that covered much of the Scottish Highlands, and must therefore also be of Late Devensian age. If indeed the tills in the Dounreay area are Wolstonian, then their preservation suggests that Dounreay may not have experienced significant ice cover during the Devensian.

Table 2-2. Summary of the Quaternary chronology and climate states of the British Isles

Stage	Age (ka BP)	OIS	Climate State	Stage and Type	Comments
FLANDRIAN	10-0	1	Temperate	Flandrian Interglacial	**Holocene**/postglacial
DEVENSIAN	~11-10	2	Periglacial	Devensian glacial	**Younger Dryas stadial** **Loch Lomond Readvance**
	~14-11		Boreal/ Temperate		**Windermere interstadial**
	~25-14		Glacial		**Late Devensian Dimlington stadial**
	~50-25	3	Periglacial		**Mid Devensian**
	~60-50		Temperate/ Boreal		
	~70-60	4	Glacial		**Early Devensian**
	~110-70	5d-5b	Periglacial/ Boreal		
IPSWICHIAN	~130-70	5e	Temperate/ Warm	Ipswichian interglacial	Central estimate of age ~124. Duration estimated at 10 to 15 ka.
WOLSTONIAN	~270-130	6	?Glacial/ Temperate/ Periglacial	?Wolstonian glacial	The Wolstonian type location is now considered to be pre-Hoxnian and is now correlated with the Anglian 'Lowestoft Formation'. The only lithostratigraphical evidence considered to support a post-Hoxnian, but pre-Ipswichian, glaciation of East Anglia comes from the Nar Valley in Norfolk.
		7			
		8			
HOXNIAN	~319	9	Temperate/ Warm	Hoxonian interglacial	Some authors extend the Wolstonian to cover OIS 10 to 6, but still allow the Hoxnian to relate to OIS 11 to 9.
		10			
	~400	11			
ANGLIAN	~400-460	12	Glacial	Anglian glacial	**Major glaciation and most extensive development of UK ice sheets.** Dating of this major glaciation is disputed.
CROMERIAN	From ~460	15-13	Temperate		Several possible biostratigraphically-defined temperate episodes (Stuart & Lister, 2001)
	~630	16	Glacial		Early pre-Anglian lowland *'Happisburgh Glaciation'* has recently been proposed in eastern England based on recent mapping (Lee et al., 2004).
	To ~880	21-17	Temperate		Several possible biostratigraphically-defined temperate episodes (Stuart & Lister, 2001)
BEESTONIAN	>880	21+	Periglacial		**Early Pleistocene**
PASTONIAN			Warm		
BAVENTIAN			Periglacial		
ANTIAN			Warm		
THURNIAN			Cold		
LUDHAMIAN			Warm/ Temperate		
WALTONIAN			Cool		

Figure 2-12. The location of the PADAMOT study sites in relation to the extent of Quaternary glaciations in the British Isles.

In contrast, to both Sellafield and Dounreay, Cloud Hill lies south of the Devensian glacial maximum and was therefore ice-free during the Devensian (Figure 2-12). The limited re-advances of ice during two subsequent stadials (brief phases of cooler climate) are considered unlikely to have had any significant effects on the deep groundwater at Sellafield (Bath et al., 2000). Similarly, it is thought unlikely that this ice would have affected the deep groundwater systems at Dounreay, or the shallower groundwater system at Cloud Hill.

Periglacial climate conditions prevailed in Britain for about 200,000 of the last 700,000 years (Figure 2-12). Permafrost would possibly have dominated ground conditions during much of this time. All three study sites will have been influenced by periglacial or boreal climate conditions during most of the 100,000 years of the Devensian glacial phase. As well as being cold, conditions may also have been very arid at times during these periods, and recent research suggests significant changes in humidity during the Younger Dryas (Lowe et al., 1994). The coldest and most arid part of this period seems to have been during the interval 10,500 to 10,000 years BP in mainland Britain, Belgium, the Netherlands and parts of southwest Europe. There are also indications of a marked dry period in southwest Europe during the early Holocene. It

34

appears, therefore, that a change to a drier regime began during the Younger Dryas and continued in some regions into the early Holocene. Both the development of permafrost and arid conditions will have been potentially important factors in the palaeohydrogeology of these three areas, both leading to reduced recharge of the groundwater systems.

Both Dounreay and Sellafield are coastal sites and their groundwater systems may have been influenced by eustatic sea-level, and local changes in land elevation in response to ice loading and unloading. Global sea level rose 50 m between 11 and 7 ka BP as a result of melting of the Devensian ice sheet at the end of the last glaciation. However, local isostatic recovery reduced this effect, and in the case of the Sellafield site the position of global sea level relative to the rock mass rose during the Devensian glaciation from -50 m relative to present sea level before 25 ka BP, to a high stand of about +18 m at 23 ka BP, falling again to -28 m below present sea-level at 12 ka BP before rising to a level slightly above present day sea level at 7 ka BP. Overall, it is believed that Sellafield probably experienced nothing more than short-lived period of shallow marine inundation during the late Quaternary (Heathcote et al., 2000). Little information is available for the Dounreay site. However, deposits of calcite-cemented Quaternary gravels, containing well-rounded clasts and that might represent elevated beach deposits, have been found recently in several places near Dounreay (C. Auton, 2004, personal communication). This could indicate periods of marine inundation of the site.

The position of Cloud Hill in the centre of the English Midlands means that the site will not have been influenced by marine inundation during the Quaternary.

2.3.3 Hydrogeology and hydrochemistry

2.3.3.1 SELLAFIELD

The conceptual model of the groundwater system of the Sellafield region (Black and Brightman, 1996, and summarised by Bath et al., 2000, 2005) comprises three discrete regimes:

- A 'Coastal Plain Regime', of fresh to brackish groundwater in which flow is topographically driven and recharged directly in the Sellafield area. The base of this regime coincides approximately with the base of the high permeability Sherwood Sandstone Group aquifer in the east part of the site, and occurs within the sandstone aquifer in the west of the site.

- An 'Irish Sea Basin Regime', dominated by halite-derived basinal brines. This groundwater mass occurs at depth in the western part of the site beneath the present coastline and is essentially stagnant.

- A 'Hills and Basement Regime', in which the groundwater flow is largely topographically driven but other features (e.g. density variations) may be important at depth. The groundwaters are mixtures of fresh water with older saline groundwaters of different compositions.

These three groundwater regimes, and how the boundaries between them may move in response to climatic changes, are illustrated conceptually in Figure 2-13. The movement of the interfaces between these bodies of groundwater is a key issue with respect to the geochemical stability of groundwater system. The interface between the 'Irish Sea Basin' brine and the saline groundwater of the 'Hills and Basement' regime is a very broad salinity transition reflecting diffusive mixing and dispersion associated with the movement of the boundary. In contrast, the interface between the 'Coastal Plain' and 'Hills and Basement' regimes is relatively sharp in the east, where it is controlled by the marked contrast in permeability between the base of Permo-Triassic sandstone aquifer and the underlying Palaeozoic basement rocks.
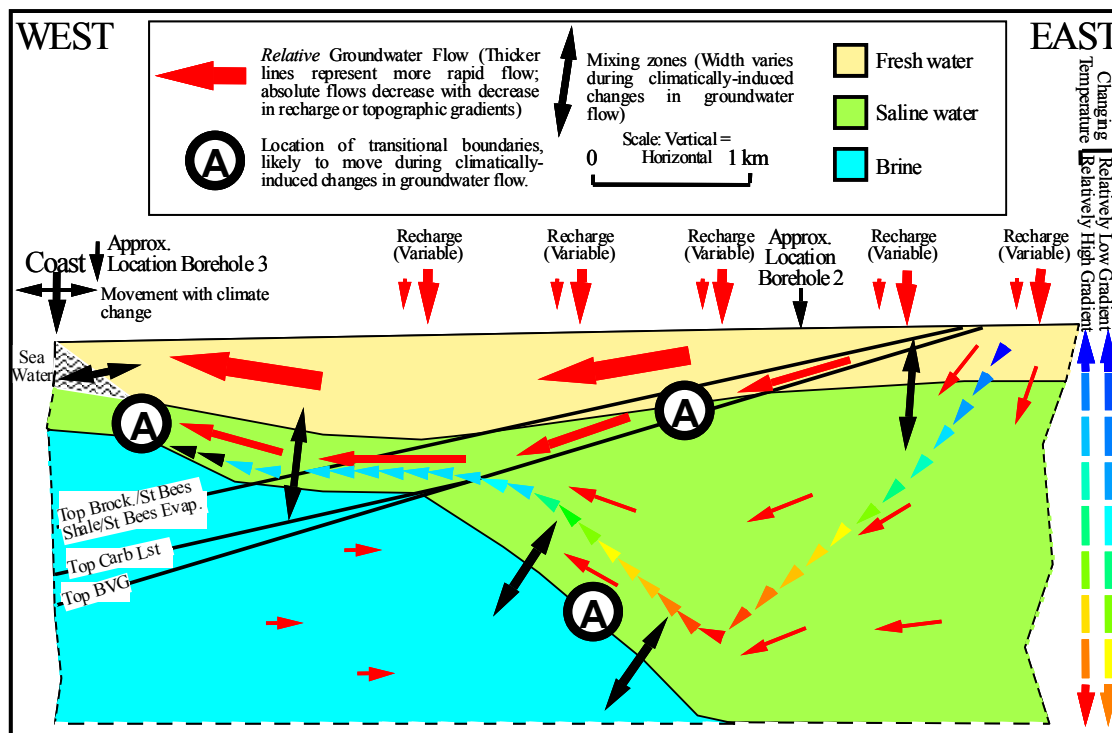
Figure 2-13.Schematic E-W cross-section of the Sellafield site illustrating the features of the groundwater system that could potentially change in response to climatic variations. The black lines dipping to the left of the section are schematic boundaries of the principal geological units: St Bees Sandstone, Brockram/St Bees Shales, Carboniferous Limestone, Borrowdale Volcanic Group.

2.3.3.2 DOUNREAY

The hydrogeology of the Dounreay site is described in Nirex (1994). Only a very thin veneer of Quaternary deposits covers the Dounreay site. There is a shallow and irregular groundwater flow within these deposits and in the underlying regolith and surface weathered rock. Beneath this shallow layer, groundwater flow is predominantly fracture-controlled in both the crystalline Moine basement rocks and in the overlying Devonian sedimentary cover rocks. Thin beds of porous sandstone are present within the Devonian Caithness Flagstone Group, and these may very locally influence groundwater movement. In some cases, these actually contain small accumulations of oil.

The Devonian strata thin rapidly southwards and the crystalline basement rocks form low outcrops rising to 200 to 300 m OD. The principal groundwater flow direction is from south to north, with recharge in the low hills to the south of the site. The groundwater is considered to flow northward and downward, along bedding-related and fault-related fractures, to a zone of discharge and upward flow in the Dounreay coastal plain and possibly offshore. Both basement and sedimentary rocks are cut by a system of faults, spaced 400 to 600 m apart, with a long history of movement and associated processing. The fault system and related fractures provide channels facilitating local deep penetration of active groundwater in the recharge area and upward movement of deeper groundwater in the discharge area near the Dounreay site.

2.3.3.3 CLOUD HILL

The hydrogeology of Cloud Hill has not been studied in detail. The area forms part of the catchment of the middle Trent Valley and lies about 5-6 km south of the River Trent. Cloud Hill Quarry lies on the east side of the valley of a small tributary stream that drains northwards into

the River Trent. Here the ground rises moderately steeply from an elevation of just below 76 maOD in the valley floor to a low incised plateau area of low rolling hills, with an general elevation of about 90 maOD. The highest point of the site, on the eastern face of Cloud Hill Quarry, has an elevation of 111.70 maOD. The bottom of the quarry is at about –10 maOD. The site is most probably within a area of local recharge into the Carboniferous Limestone.

Table 2-3. Chemical and stable isotopic composition of groundwater from Cloud Hill

Sample	TDS	pH	Ca^{2+}	Mg^{2+}	Na^+	K^+	HCO_3^-	Cl^-	SO_4^{2-}	NO_3^-
	mg/L		mg/L	mg/L	mg/L	mg/L	mg/L	mg/L	mg/L	mg/L
CH1	922	8.04	126.77	51.71	37.34	6.56	401	68.5	230.0	0.23
CH2	934	8.05	134.01	53.95	40.07	6.83	402	69.1	228.0	0.27
CH3	1152	7.98	157.18	87.92	14.28	4.75	423	30.4	435.0	0.27

Sample	Cation Total	Anion Total	Balance	S Balance	TIC Balance	Tot. S	Red. S	S Diff.
	meq/l	meq/l	%	%	%	mg/L	mg/L	%
CH1	12.64	13.32	-2.61	-1.05	-3.02	70.1	0.640	-9.5
CH2	13.30	13.31	-0.03	0.64	0.86	73.2	0.710	-4.0
CH3	16.08	16.85	-2.33	0.77	-2.81	128.8	<0.200	-12.8

Sample	Br^-	NO_2-	HPO_4^{2-}	F^-	TOC	TIC	C Diff	Tot. P
	mg/L	mg/L	mg/L	mg/L	mg/L	mg/L	%	mg/L
CH1	0.29	<0.02	<0.01	0.25	<2.00	80.30	1.6	0.01
CH2	0.27	<0.02	<0.01	0.29	<2.00	76.32	-3.7	<0.01
CH3	0.12	<0.02	<0.01	0.12	<2.00	85.14	2.3	<0.01

Sample	NH^{4+}	Si	SiO_2	Ba	Sr	Mn	Tot. Fe	Red. Fe	Oxid Fe
	mg/L	mg/L	mg/L	mg/L	mg/L	mg/L	mg/L	mg/L	mg/L
CH1	2.83	3.48	7.45	0.014	4.484	0.008	0.03	<0.02	0.03
CH2	2.49	3.67	7.86	0.015	4.788	0.008	0.03	<0.02	0.03
CH3	3.48	2.86	6.11	0.051	2.802	0.051	0.06	0.02	0.03

Sample	Al	Co	Ni	Cu	Zn	Cr	Mo	Cd	Pb	V
	mg/L	mg/L	mg/L	mg/L	mg/L	mg/L	mg/L	mg/L	mg/L	mg/L
CH1	<0.010	<0.002	0.012	0.002	0.006	<0.002	<0.015	<0.002	<0.005	<0.010
CH2	<0.010	<0.002	0.011	<0.002	<0.005	0.002	<0.015	<0.002	<0.005	<0.010
CH3	<0.010	<0.002	0.004	<0.002	<0.005	<0.002	<0.015	<0.002	<0.005	<0.010

Sample	B	As	Se	Temp.	$\delta^{18}O$	$\delta^{13}C_{DIC}$
	mg/L	mg/L	mg/L	°C	‰ SMOW	‰ SMOW
CH1	0.069	<0.015	<0.015	10	-7.83	-13.49
CH2	0.077	<0.015	<0.015	10	-7.86	-13.23
CH3	0.065	<0.015	<0.015	10	-7.88	-13.55

The strongly dolomitized Carboniferous Limestone is highly fractured, with locally extensive alteration, which has produced irregular zones with major secondary (diagenetic) vuggy, and sometimes small-scale karstic macroporosity, with channels and cavities up to 1 m diameter within the matrix of dolostones. The fractures are steeply-dipping, and fresh groundwater discharges rapidly from open fractures in the base of the southern end of quarry. Late stage calcite, similar to that found lining conductive fractures in the Sellafield site, was found lining the open fractures associated with active groundwater flow. This mineralization was initially discovered by the BGS during an independent BGS-funded study of the dolomitization and mineralization of the site (Bouch et al., 2004). Samples of this late-stage calcite mineralization, together with groundwater collected from the same fractures, were subsequently collected and analysed as part of the PADAMOT project.

The chemistry and stable isotope compositions of the groundwater from Cloud Hill are presented in Table 2-3. The waters were collected from fracture discharges at the base of the quarry. The groundwater is a dilute (fresh) Ca^{2+}-Mg^{2+}-Na^+-HCO_3^{2-}—SO_4^{2-} type groundwater. The sulphate content is most probably related to the supergene weathering of minor hydrothermal sulphide (galena-chalcopyrite-pyrite) mineralization, which is present within the dolostones and which can be seen to be altering and oxidising to form secondary low-temperature minerals, including goethite, cerussite and malachite. Although Eh was not measured in situ, the reduced Fe (determined on samples preserved for Fe(II) on-site during collection) is low or below detection, indicative of oxidizing conditions.

The $\delta^{18}O$ (SMOW) isotopic signature of the Cloud Hill groundwater (-7.85 ‰) falls within the range of compositions for recent groundwaters English Midlands (-7.5 to -8 ‰), and is similar to the reported composition of annual average of modern rainfall (-7.67 ‰) in the region (Darling et al., 2003).

2.4   MELECHOV MASSIF

2.4.1   Location

The Melechov Massif is a Variscan granite body located about 80 km to the SE from Prague (Figure 2-14). It is situated between the streams Želivka and Sázava, and forms the northernmost promontory of the Moldanubian granite pluton, which stretches from the river Danube in Austria to Bohemia. Because it forms a columnar stock of crystalline rock it was studied as a model area for testing methodologies for the development of a deep geological repository (Mlčoch et al., 2000).

Petrological, mineralogical and hydrogeological information for the Melechov area was obtained from the borehole PDM-1, which was drilled at the southern foot of the Melechov Hill in 2002, close to the village of Rejčkov. The borehole is 100 m deep and has a diameter of 122 mm.

2.4.2   Geology

2.4.2.1 REGIONAL GEOLOGY

The Moldanubian pluton is a part of the Moldanubicum within the Bohemian Massif, which in turn, is a part of the Variscan orogen of Europe. It underlies the major western part of the Czech Republic and extends into the adjoining areas in Austria, Germany and Poland. It submerges below the West Carpathians to the southeast.

The Moldanubicum is the most extensive unit of the Bohemian Massif, occupying its central and southern part, and passing into Bavaria and Austria. It is built up of katametamorphic rocks, penetrated by numerous syn-orogenic as well as post-orogenic plutons. Much of the Moldanubian unit seems to be Precambrian and part may even be Archaean. The Assyntian unit,

which is situated approximately at the northern margin of the Moldanubicum, comprises a Proterozoic (Algonkian) sequence of partially-metamorphosed shales, greywackes, and basic volcanics. In central and western Bohemia, the Algonkian is covered by Cambrian, Ordovician, Silurian and Devonian sequences of the so-called Barrandian basin.
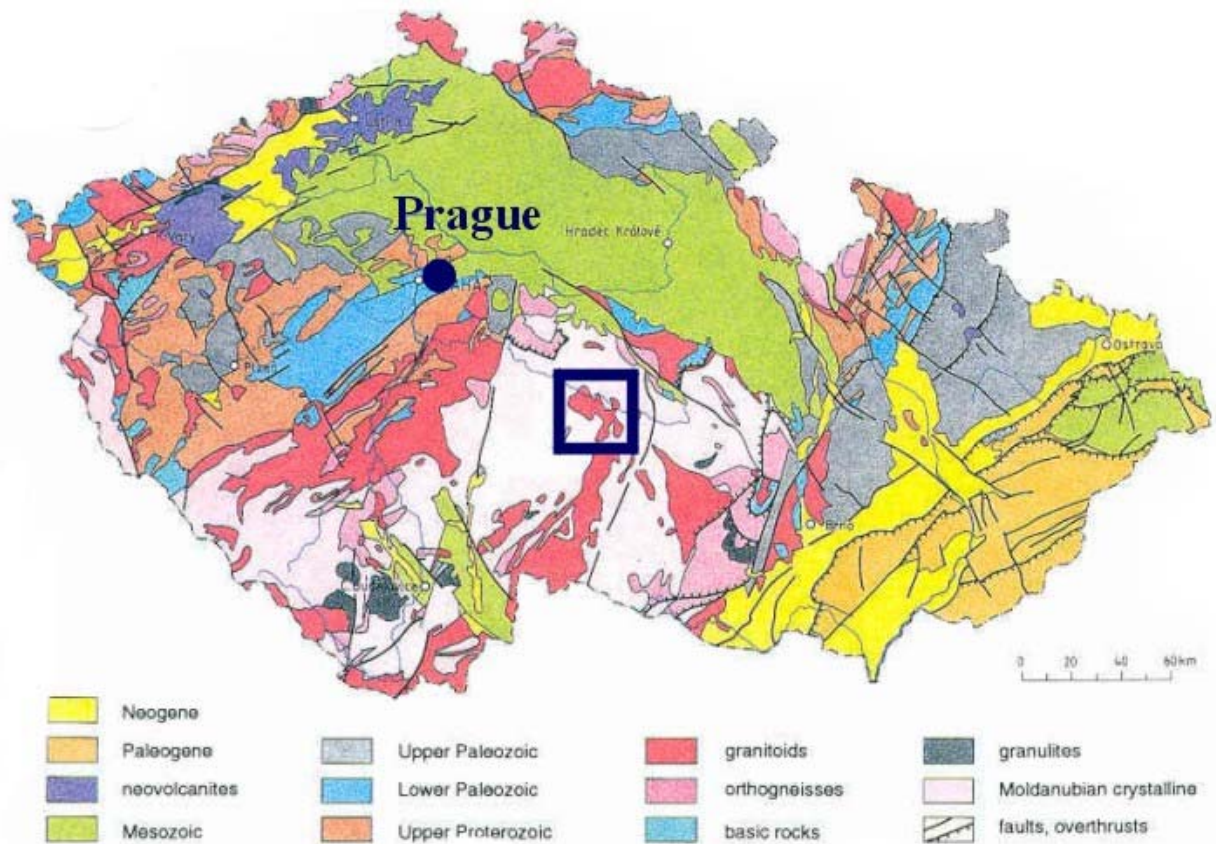
Figure 2-14. Geological map of the Bohemian Massif. The position of the Melechov Massif is highlighted by the thick square.

The tectonic development of the Bohemian Massif (in which the pre-Cambrian, Caledonian and Variscan orogenesis participated) culminated in the formation of the Variscan mountain chain during the Late Palaeozoic. The Bohemian Massif was turned into a cratogen, later covered only by sedimentary rocks deposited in the advancing epicontinental Late Cretaceous sea, or in the unstable areas by large Tertiary lakes. The deposition of these younger sedimentary strata, combined with the effects of long-lasting denudation, led to the peneplanation of the Bohemian Massif, which reached its maximum at the Palaeogene-Neogene time boundary. The true age and geological evolution of the rocks of the Moldanubicum are difficult to determine because of the complexity of the tectonics (Petránek, 1966).

In central and western Bohemia, the metamorphic units pass into non-metamorphosed Proterozoic and Lower Palaeozoic strata. These folded pre-Variscan rocks are covered by later sedimentary sequences of the Upper Palaeozoic, Cretaceous and Tertiary.

Significant hydrothermal systems were associated with Variscan metamorphism, folding and fracturing, and with the fracture systems produced by Tertiary tectonism (which accompanied the Alpino-Carpathian orogeny). The Variscan activity produced metallogenic and quartz veins. Later Tertiary fracturing very often created a systematically-oriented network of open permeable fissures. The development of the Tertiary fissure systems was sometimes controlled by pre-existing Variscan structures.

Neogene tectonic movements (associated with the development of horsts and grabens), together with the general uplift of the Bohemian Massif (which continued into Pleistocene) and Neogene volcanic activity, led to the geomorphological rejuvenation of the Bohemian Massif. Most of the Mesozoic and Tertiary tectonic deformation resulted from the northwards movement and thrusting of the Alpine-Carpathian belt against the rigid foreground of the Bohemian Massif. This rigid block of rock caused the striking bending of the Alpine-Carpathian belt, and at the same time the pressure exerted on the Bohemian Massif led to the development of pronounced radial faulting (associated with horst and graben structures). These radial fault systems may often have rejuvenated older tectonic lines.

The whole region has been uplifted since the Tertiary. The complex tectonic history has created a complex variety of fissure systems. Furthermore, the permeability of the fissured zones is influenced by the nature of the cover of weathering products and unconsolidated sediments at the surface. After the Variscan orogeny, the surface of the folded and fissured crystalline rocks was exposed to a long period of denudation, weathering and peneplanation. This is interrupted to relate to Tertiary fault tectonics, which caused the uplift of large regional blocks. In turn, this changed the morphology of the surface, changed the hydraulic gradients of streams and ground water, and caused deep erosion of streams below the level of the old surface. Depending on the bedrock lithology, the weathering products are either arenaceous and permeable (e.g., the arenaceous eluvia of granitoid rocks), or clayey and less permeable (e.g. the clayey eluvia of cordierite gneisses in the Moldanubian region of Southern Bohemia). These phenomena seem to be the controlling factors of the groundwater circulation and they also affect the ground-water residence time (as demonstrated by isotope groundwater dating).

2.4.2.2 MELECHOV HILL

The background morphological, geological, hydrogeological and hydrochemical details of the Melechov Hill are given in Appendix 1.1 to 1.16.

The Melechov Massif granite belongs to the younger mainly post-orogenic Moldanubian granitoids dated as Upper Carboniferous (Chlupáč et al., 2002). These form the large composite Moldanubian Batholith that is discordant and has sharp contacts with its country rocks. The Melechov granite forms an isolated composite intrusive body that was intruded into the high-grade Moldanubian Unit (biotite paragneisses, migmatites) during the Variscan orogeny (330-300 Ma). The width of the Melechov Massif from SW to NE , and NW to SE, is about 12 km – covering a total area of about 120 km^2. The depth of the intrusion has been estimated by Dudek et al. (1992) to be as much as 15 km in the southern part, not exceeding 10 km in the later intrusions, and only 2 km deep in the northern part.

2.4.2.3 LITHOLOGIES

The Melechov Massif consists of three intrusive units (representing three separate magma pulses) – the Kouty and Lipnice granites and the Melechov stock.

The Lipnice granite (LG) forms an irregular intrusion elongated NE-SW and outcropping in the southern and south-western part of the Melechov Massif. The LG is a fine-grained non-porphyritic peraluminous biotite-muscovite monzogranite. It contains numerous biotite schlieren and small recrystallized xenoliths of gneisses. Compared to the other Melechov Massif granites, the LG exhibits slightly lower content of SiO_2 (69-71 %) but higher contents of other elements (> 0.5-0.6 % TiO_2, >0.6-0.9 % MgO, >2.0-2.5 % Fe_2O_3tot, >1.0-1.3 % CaO, >150 ppm Zr), >40 ppm Th.

The Kouty granite (KG) forms the peripheral parts of the Melechov Massif. Petrographically it corresponds to a two-mica peraluminous alkali-feldspar granite that has a slightly higher content of muscovite than the LG. Its composition is variable, SiO_2 ranges mostly from 71 to 75 wt %.

The Melechov stock in the central part of the Melechov Massif consists of two intrusive phases, arranged in a concentric manner. The coarse grained Melechov granite (MG) forms the outer zone of the stock, and the fine-grained and occasionally porphyritic Stvoridla granite (SG) forms the inner zone (core). Muscovite significantly predominates over the biotite in both granite types. Of the other phases, microclinic K-feldspar and albite are very common. Both MG and SG are significantly depleted in Ti, Mg, Fe, K, Rare Earth Elements (REE), Zr and Th ($_{TiO2}$ ~0.1 %, Fe_2O_3 ~1 %, Zr <50 ppm, Th <5 ppm) but enriched in Al, Na (3.5-4.2 % Na_2O) and P (0.35-0.50 % P_2O_5).

The Melechov Massif is surrounded by metamorphic Moldanubian rocks comprising biotite paragneiss to the west, and cordierite gneiss to the north and south (Biely et al., 1966).

2.4.2.4 FAULT ZONES AND JOINT SYSTEMS

Two sets of joints have been distinguished in the Melechov Massif (Rajlich, 2001): an older system of relatively flat-lying joints, which are inclined at low angles towards the centre of the granite; and a younger system represented mostly by two systems of sub-vertical joints trending NW-SE and NNE-SSW. The younger system affects the whole area of the Melechov Massif without bearing any specific preference/relationship to individual intrusive phases of the granite.

Major fault zones have a similar trend (NW-SE and NNE-SSW to N-S) to that of the joint system. They are also indicated by geophysical surveys. The NNE-SSW to N-S fault system significantly contributed to the development of the present geomorphology of the Melechov area. There is no evidence for the age of the faults, however most were probably reactivated several times.

2.4.3 Geomorphology

Melechov Hill is 709 m high, with an elevation of about 450 m above the valley bottom of the Sázava stream, which is 2.5 km to the north and flows in the direction SE – NW, crossing the granite body. In the west, it is limited by the valley of the Želivka stream (which has been impounded by a dam) and to the east by a shallower valley of a small stream. The land is transitional in a southerly direction towards the Českomoravská vrchovina highlands.

In the NW, the massif is limited by several NE – SW and N – S striking faults. The surface is gently undulating, and is affected by Pleistocene weathering and by erosion from the Sázava and Želivka streams. Two palaeo-surface levels are discernible in the hypsographic curve (Appendix 1.12) at 600 m a.s.l. and about 450 m a.s.l. The natural groundwater drainage is also focused at these levels, and is evident in the frequency of springs.

In the shallow valleys of the Sázava and Želivka tributaries, there are some springs, the discharge of which is around 1 l/s.

2.4.4 The PDM-1 site

The PDM-1 borehole was drilled in fine-grained muscovite-biotite granite of the Lipnice type. The granite encountered in the borehole is highly fractured, and in the upper parts is also intensively weathered. Limited weathering/alteration, however, was also manifested in changes of the granite colour down to the bottom of the borehole. Locally, aplites and pegmatite dykes are present, some of which are several centimetres or tens of centimetres thick. In the lower part of the borehole core small xenoliths, and two larger blocks (2 to 3 metres thick) of migmatitized Moldanubian paragneiss, were found (Figure 2-15).

Four types of fissure fillings were encountered:

- Open fissures with hydrothermal mineralization (quartz) up to 10 mm thick; diagonal to vertical, and inclined to E;

- Chloritized vertical fissures;

- Diagonal fissures with a green clay mineral, inclined to SE;

- Fissures of different orientation, limonitized. Irregularly coated with a black coating (Mn-oxides).

Crystals of pyrite up to 1 mm in size occur on fissure walls of all four types of fracture.
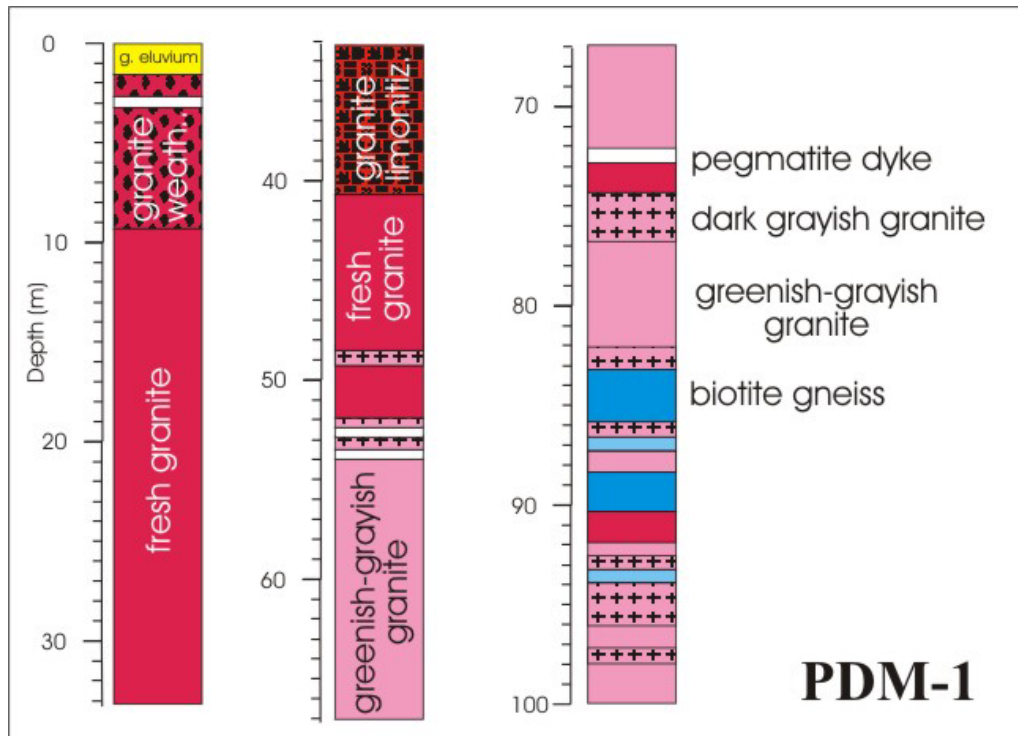
Figure 2-15. Simplified lithological log of the PDM-1 borehole

2.4.5 Hydrogeological and hydrochemical investigations of the Melechov site

A hydrogeological field survey with mapping of hydrogeological phenomena in an area of about 85 square kilometres was done at the scale 1:10,000. The results were transformed into a 1:50 000 digital map, which was used for hydrogeological modelling of the groundwater flow. All springs, wells, one borehole and other hydrographic phenomena were recorded and indicated with their coordinates and basic hydrological data.

Sixty groundwater samples were collected and analysed in the chemical laboratory of the Czech Geological Service. The results are detailed in Appendix 1.6 to 1.11 (the sample identification numbers correspond with those in the map in Appendix 1.4 and are indicated with the prefix "M" in the top line of the table).

2.4.5.1 OBSERVATIONS

The chemical composition of groundwaters have been evaluated and are presented as column graphs in Appendix 1.6 to 1.11 and as a Piper diagram arranged: (a) according to the chemical composition of groundwater, and; (b) according to the geological origin (Appendix 1.16). Trace element analyses for Pb, Rb and Sr are presented in Appendix 1.13 and 1.14.

The groundwaters encountered are mainly dilute, with low dissolved solids and conductivities mainly between 77 and 336 µS/cm, and up to 464 µS/cm as maximum. About 20 per cent of the

water samples contain a relatively high concentration of nitrate (over 50 ppm), indicating a shallow groundwater origin. In general, the groundwater is of Na–Ca–SO$_4$ type, which is common in the granite regions of the Bohemian Massif in wooded and agricultural regions and in grasslands. The SO$_4$ in the shallow groundwater could be related to weathering and oxidation of sulphide minerals in the granite or in the fracture mineralization. There is a striking lack of Ca-Na-HCO$_3$-type groundwater in this area, which in general is the most common type of water in the aquifers of the Bohemian Massif. However, in the Melechov area, this type of groundwater occurs in borehole PDM 1 and in a few springs. It seems that Ca-Na-HCO$_3$-type groundwater is linked with the granitic bedrock the other groundwater types are very heterogeneous, and dispersed over the whole investigated area. The high concentration of the NO$_3^-$ anions indicates a shallow origin of the dissolved solids and reflects the impact of agricultural activities.

So far, no indication of deep reaching tectonic zones and deep groundwater circulation has been encountered in the area investigated neither by hydrogeological mapping nor indicated by any warmer spring discharges.

A striking correlation was found between the depth of the groundwater level and the altitude of the ground, which could be used in considering the flow pattern in groundwater flow modelling.

2.4.5.2 CONCLUSIONS

It is concluded that the groundwater flow is dispersed within the extent of the granite body of the Melechov Massif without any conspicuous concentration of the discharge associated `with tectonic zones and big springs. The springs occur mainly in shallow surface depressions with some exceptions: one of the springs is almost at the top of the Melechov Hill, at an altitude of about 690 m asl. There are no signs of a concentrated discharge from large flow systems at the bottoms of bigger streams.

There is no evidence for any concentrated drainage system, with a concentrated groundwater flow in the granite body of the Melechov Massif, based on the hydrogeological phenomena observed at the surface.

2.5 PADUL AND CÚLLAR-BAZA BASIN

The Cúllar-Baza (Guadix-Baza) Basin is a "basin and range" endorheic depression that covered approximately 4500 km^2. It is located in the central part of the Betic Range, (Figure 2-16) in the northeast extreme of the Granada Province (Andalusia, Southeastern Spain). It has an irregular shape with its maximum length oriented SW-NE and placed 900-1000 m a.s.l. The climate is Mediterranean with a strong continental influence: winters are cold and dry whereas summers are extremely hot, with maximum temperatures reaching over 40 ºC. The rainfall annual average ranges from 300 to 350 mm yr^{-1}, the evapotranspiration is 700-900 mm yr^{-1} and the mean annual temperature is between 12-15 ºC. This semi-arid climate favoured the development of a bad-land landscape, mainly covered by steppe plants finding major trees only along the scarce rivers that run through the basin. Along the basin there are springs characterised by their brackish waters either carbonated or sulphated.

The origin of Cúllar-Baza basin is related to the Alpine Orogeny which affected Mesozoic and Cainozoic rocks within the region. The bedrock comprises mainly Mesozoic limestones, dolostones, marls and gypsum, and marine origin Neogene sediments. Later, during the Upper Tortonian the sedimentary conditions changed to a continental regime.

In brief, the basin can be understood within a centripetal depositional model: consisting of coarse grained alluvial fans at the foot of mountain ranges, which gradually pass into a system of channels that flowed out to a central system of small shallow saline lakes distributed in a mosaic

pattern with sedimentation of gypsiferous lutites, gypsiferous sands, gypsum and, sometimes, decimetrical lutite beds with displacive gypsum crystals (Torres et al., 2003).
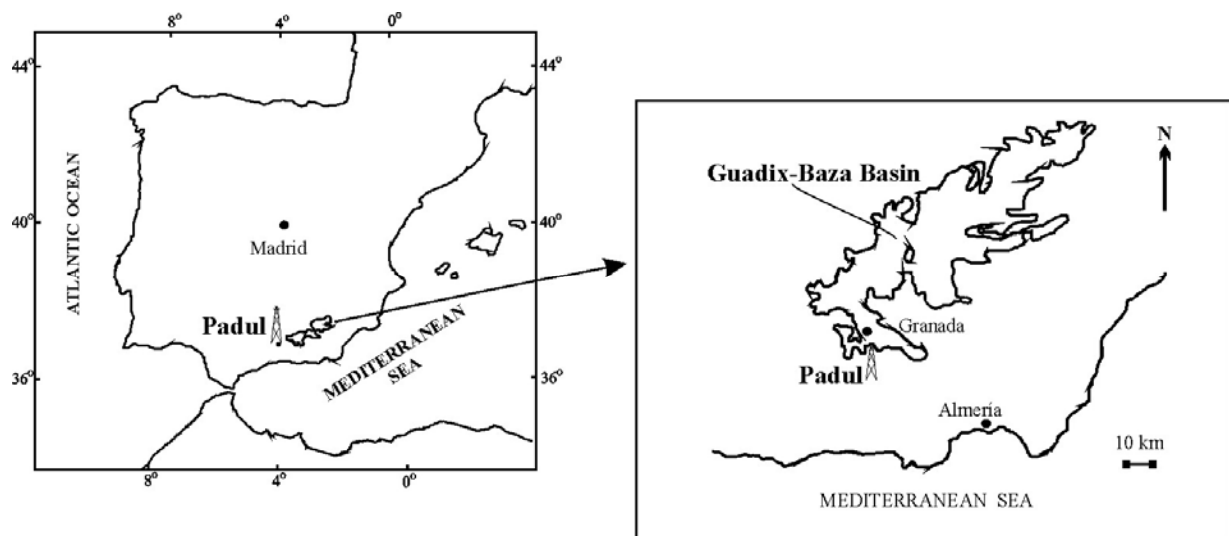
Figure 2-16. Location map of the Padul Peat Bog and the Cúllar-Baza Basin

At the end of Middle Pleistocene, erosional processes began and the current fluvial system was established (Ortiz et al., 2000), producing the typical badland landscape that can be observed nowadays. Likewise the basin drainage was deeply modified, from endorheic to exorheic towards the Atlantic Ocean via the Guadalquivir river.

Three main different depositional settings (facies) are distinguished:

1. Upper alluvial fan gravels and lens-shaped channelled sands;

2. Sand playa deposits and mud flat playa (red lutites);

3. lacustrine sands with abundant ostracod valves and grey lacustrine gypsiferous lutites and sands, carbonate and gypsum beds.

The composite-stratotype-section established for the Pleistocene palaeoenvironmental study in the east domain of Cúllar-Baza Basin is 356 m long,. Its chronostratigraphy was obtained by Ortiz et al. (2004), based on palaeomagnetism and amino acid racemization dating methods (Figure 2-17). It is representative of the depositional history of the basin from nearly the Pliocene-Pleistocene boundary (ca. 2 Ma) to the upper part of the Middle Pleistocene. The detailed lithological and stratigraphical description of the section is given in Section 3.7.

Padul peat bog is located 20 km south of Granada city (Andalusia, southern Spain) (Figure 2-16). It was formed in a depressed fault-bounded tectonic basin at the foot of the Sierra Nevada, and consists of an endorheic basin, surrounded by mountains. It has an elevation of 720 m a.s.l. and some parts are permanently covered by water. Its longitudinal axis is NW-SE oriented, and it has a surface area of 4 km^2 and a maximum depth of 100 m. The bedrock consists mainly of faulted Mesozoic dolostones that caused the basin to sink gradually.

Padul Basin is a discharge area for the groundwater flow from the surrounding aquifers. The flow directions change from sub-horizontal, in the Mesozoic aquifers adjacent to the basin, to essentially upwards discharge inside the peat-containing depression.

Present rainfall in the area is a minor factor in the water balance of the peat deposit, and run-off input of water is estimated to contribute only about 8% of the total (Cañada, 1984). Consequently, changes in the water table in the peat are controlled indirectly by infiltration of water from the surrounding mountains.
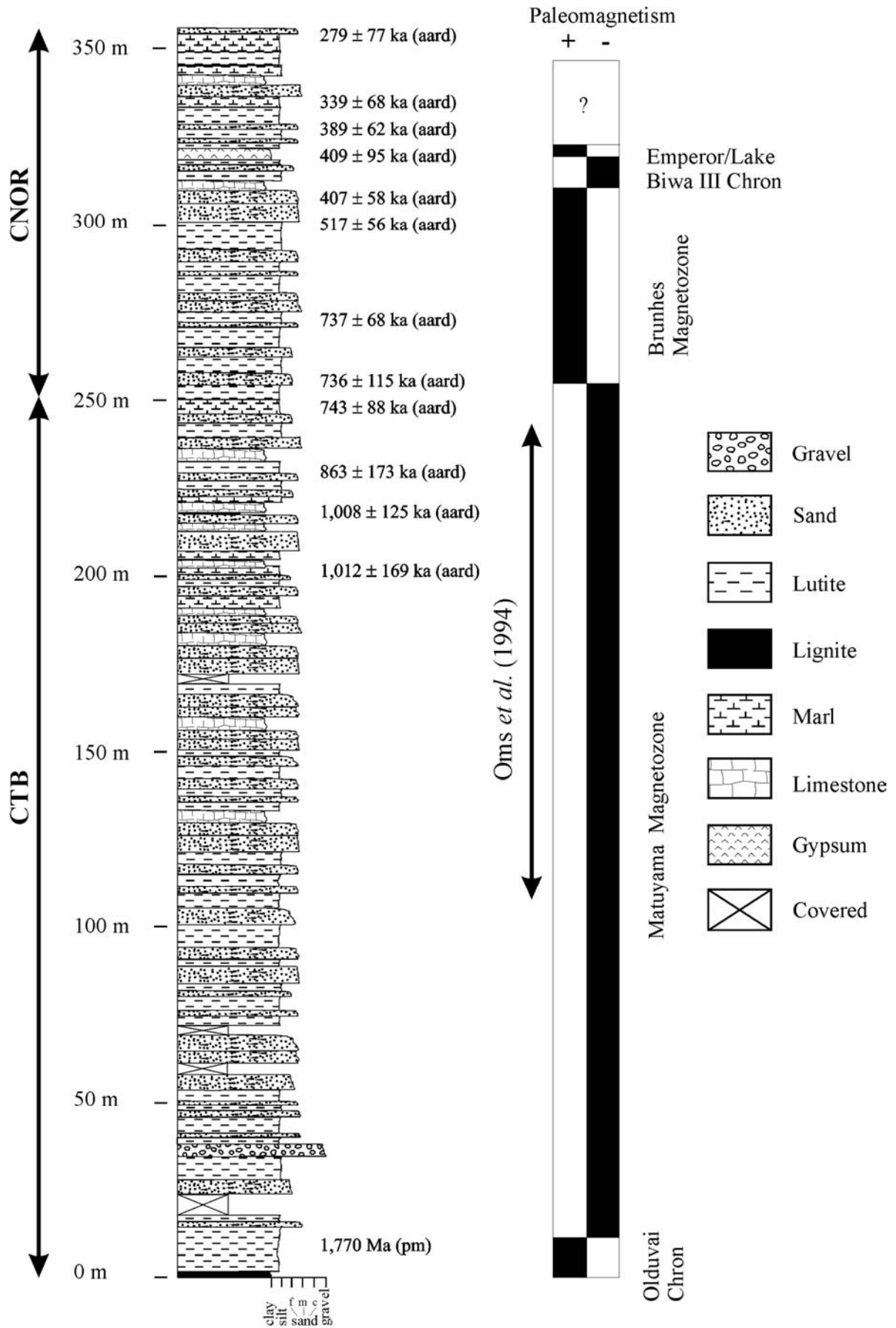
Figure 2-17. Lithostratigraphy and chronostratigraphy of the Cúllar-Baza Basin.

Palaeomagnetism **Datings** **Depth (m)** **Lithology**
+ −

4.4 ± 0.06 ka (^{14}C; P.&R., 1988)
SPD-198: 6.8 ± 0.2 ka (^{14}C)
SPD-300: 8.2 ± 0.1 ka (^{14}C)
SPD-335: 9.8 ± 0.2 ka (^{14}C)
SPD-433: 11.8 ± 0.5 ka (^{14}C)
SPD-533: 17.3 ± 0.5 ka (^{14}C)

SPD-825: 30 ± 1 ka (U/Th)

SPD-1860: 123 ± 9 ka (U/Th)

SPD-2620: 139 ± 9 ka (U/Th)

SPD-3180: 167 ± 17 ka (U/Th)
SPD-3200: 177 ± 10 ka (aard)

SPD-3600: 181 ± 13 ka (aard)

SPD-4135: 252 ± 55 ka (aard)

Brunhes Magnetozone

SPD-5805: > 350 ka (U/Th)

Matuyama M

SPD-9710: 885 ± 150 ka (aard)

Lithology and Fossil Legend

Gravel
Sand
Marl
Lutite
Peaty lutite
Peat
Lost core
Gastropoda
Ostracods
Pelecipoda

clay silt f m c sand gravel

Figure 2-18. Lithostratigraphy and chronostratigraphy of the Padul borehole.

Padul Basin receives an integration of vegetation debris coming from Sierra Nevada, where it is possible to recognize a series of vegetation belts.

The stratigraphical record of the Padul borehole (Latitude: 37º01′01′′ N; Longitude: 3º36′07′′ W; Elevation: 714.20 m a.s.l.) can be divided in two equivalent-in-thickness parts (Figure 2-18). The lowermost part of the record begins with very immature and poorly cemented conglomerates of alluvial origin, followed by lacustrine marls with some sandy/conglomeratic interbeds of fluvial origin as well as peat seams. The marls may or may not be cemented, and their terrigenous content is highly variable. The organic matter content of the marls is also very variable: from scattered phytoclasts, carbonaceous particles or simple specs, to grey organic-rich beds. Lamination, if developed, was not preserved due to bioturbation. The uppermost part of the Padul peat record can be simply described as massive peat with some marly intercalations.

3 Mineralogical and Geochemical Investigations of Fracture Mineralization

3.1 LOS RATONES

3.1.1 Sample selection criteria

The petrological, mineralogical, geochemical and hydrogeochemical characterization of the Ratones mine area was carried out from the study and interpretation of samples from the 5 boreholes described in Section 2.1. Fracture fillings were selected from the same depths as the hydrogeologically-tested packered-off intervals in the boreholes that corresponded to hydraulically active zones.

The Los Ratones fracture fillings can be classified in three types according to size:

- Dykes and sills (centimetre- to metre-scale in thickness);

- Centimetre thickness-scale fracture fillings;

- Very fine, millimetre thickness-scale fracture fillings (millimetre thickness). These are the most frequent features.

The mineralogy of the fracture fillings comprises primary quartz, biotite, muscovite, alkali feldspar, plagioclase, accessory minerals, and secondary minerals consisting mainly of clay minerals (smectite, kaolinite and illite), Fe-oxyhydroxides, secondary sulphides, phosphates, sulphates, uranium minerals, and carbonates.

Most of the fracture samples correspond to very fragile millimetre thick coatings. Only a few are of centimetre thickness-scale. Their mineralogy consists mainly of carbonates (dolomite-ankerite and siderite), apatite and quartz.

Carbonate vein mineralization was mainly selected for mineralogical and chemical analysis, and sample selection was based on various criteria, including: degree of sample consolidation; sufficiency of the mass of material available to meet the analytical requirements; and correlation with groundwater flowing through hydraulically active zones. This type of mineralization coincides with present groundwater flow paths, and it was hoped that it might contain neoformed minerals that record signatures of the most recent palaeohydrogeological events that have influenced the groundwater system. Most samples were taken from boreholes SR3 and SR5, which were characterized by having a greater development of fracture fillings.

Borehole SR5 data have been used in the flow and reactive transport modelling undertaken in PADAMOT Work Package WP4 (Cortez and Bath, 2005). The petrological, mineralogical and geochemical studies on the samples from this borehole have provided the fundamental information used in the multiphase transport model, since the borehole provides representative examples of the hydrogeochemical processes that have occurred outside of the zone of the influence of the mining activities at Los Ratones (Cortez and Bath, 2005).

3.1.2 Fracture mineralogy and its relationship to the groundwater chemistry

Detailed descriptions of representative samples from Los Ratones are given in Appendix 2. An overview of the principal mineralogical and geochemical observations is presented in the following sections.

3.1.2.1 CLAY MINERALS

Smectite is the most extensively developed clay mineral. Kaolinite is much more scarce, and generally occurs in fractures at a relatively shallow level (<82 m). The greater abundance of smectite relative to kaolinite is consistent with the saturation indices of both minerals with respect to the chemistry of the groundwaters, which indicate that most of the groundwater compositions lie in the field of the smectite stability. Figure 3-1 illustrates the composition of the Ratones groundwaters relative to the stability regions of kaolinite and calcium smectite. Most of the groundwater compositions are within the field of calcium smectite stability. The equilibrium lines of chalcedony and calcite are also shown, and some groundwater compositions are close to equilibrium with calcite.
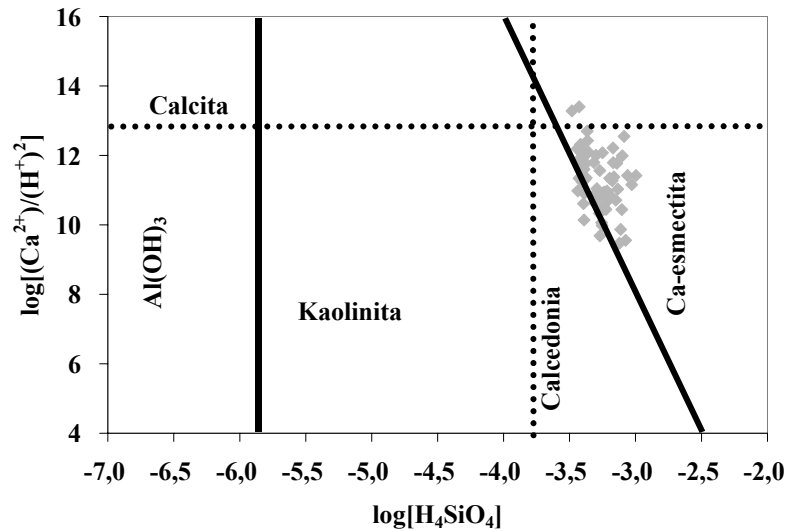
Figure 3-1. **Stability diagram of the CaO-SiO$_2$-Al$_2$O$_3$-H$_2$O-CO$_2$ system for the Ratones mine area. The equilibrium line with chalcedony and calcite is included (dotted line).**

The type of smectite mineralization evolves with depth in boreholes SR-5 and SR-2: calcium smectite prevails in the upper levels; and potassium smectite dominates lower levels. In the other boreholes calcium smectite is dominant throughout.

Corrensite (mixed-layer chlorite-smectite) occurs in the lower and intermediate levels of borehole SR-1, and occasionally in the intermediate zones of borehole SR-4 and in the upper zones of the borehole SR-2.

Illite has been identified in the boreholes SR-1, SR-3 and SR-4, as well as in the upper fillings of the borehole SR-5. Chlorite is developed in the borehole SR-3 and in the intermediate and upper zones of the boreholes SR-1 and SR-2.

3.1.2.2 CARBONATE MINERALIZATION

The carbonate fracture minerals at the Ratones Mine have an important impact on the regional groundwater chemistry, since most of the groundwaters are bicarbonate-type waters and the presence of carbonate minerals in the fracture fillings is a major feature of the fracture flow system. The carbonate minerals have a degree of depth dependence. They mostly occur in the intermediate and deeper zones of the southern part of the studied area (boreholes SR-5 and SR-4) and in the intermediate and upper zones of borehole SR-3. There is a direct relationship between the amount of dissolved carbonate in the waters and the generalized evolution of the composition of groundwater with depth. The origin of the bicarbonate ion in solution in most of the waters is

due to the presence of carbonate minerals in the fracture fillings, except in some waters in which bicarbonate is related to equilibrium with atmospheric CO_2.

Representative descriptions of the carbonate veins are provided in Appendix 2, and mineral chemical data are presented in Appendix 3. Three types of carbonate mineralization in borehole SR-3 have been differentiated on the basis of their mineralogy and chemistry:

Carbonate type 1:

$[Mg_{(0.6-0.9)} Ca_{(0.97-1.09)} Mn_{(0.02-0.04)} Fe_{(0.16-0.34)} Na_{(0.001)}](CO_3)_2$

Carbonate type 2:

$[Mg_{(0.6-0.92)} Ca_{(0.98-1.1)} Mn_{(0.01-0.03)} Fe_{(0.1-0.34)}](CO_3)_2$

Carbonate type 3:

$[Mg_{(0.66-0.77)} Ca_{(1.02-1.08)} Mn_{(0.16-0.033)} Fe_{(0.15-0.23)} Na_{(0.001)}](CO_3)_2$
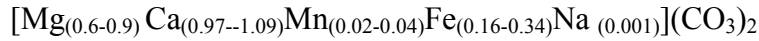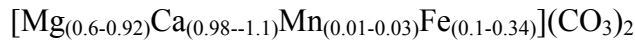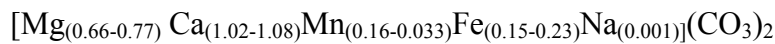
All of the carbonate mineralization in borehole SR-3 corresponds to intermediate compositions of the dolomite-ankerite series. However, the carbonate mineralization in borehole SR-5 lacks the presence of calcium carbonates and is much more ferric in composition, comprising a sideritic end-member of the magnesite-siderite series:

$[Mg_{(0.7-0.82)} Mn_{(0.04-0.06)} Fe_{(1.05-1.24)} Na_{(0.001)}](CO_3)_2$

Both ankerite and siderite are present in borehole SR-4, although the siderite in this borehole also contains significant Ca.

Petrographical observations show that the carbonate vein minerals have suffered corrosion and dissolution to varying degrees. These minerals control the Ca, Mg, Fe and, probably Mn concentration in the groundwater. Figure 3-2 shows a cross-plot of the concentrations of Ca^{2+} and $[Ca^{2+} + Mg^{2+} + Fe^{2+}]$ against bicarbonate in the groundwaters. If these components were derived by the congruent dissolution of calcite, dolomite or ankerite then the compositions of the waters should fit a line whose slope would correspond to the stoichiometric ratios of the ions in the corresponding mineral phases i.e.:

$CaCO_3 + CO_2 + H_2O \Leftrightarrow Ca^{2+} + 2HCO_3^-$ (calcite)

$CaMg(CO_3)_2 + 2CO_2 + 2H_2O \Leftrightarrow Ca^{2+} + Mg^{2+} + 4HCO^{3-}$ (dolomite)

$CaFe_{0.4}Mg0.6(CO_3)_2 + 2CO_2 + 2H_2O \Leftrightarrow Ca^{2+} + 0.6Mg^{2+} + 0.4Fe^{2+} 4HCO^{3-}$ (ankerite)
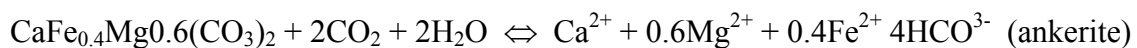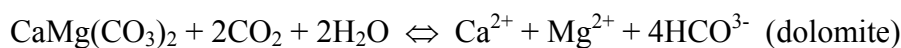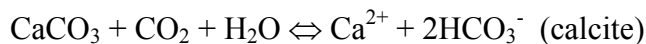
As shown in Figure 3-2, the waters from Group A (Mg^{2+}-SO_4^{2-} waters) display an excess of cations with respect to bicarbonate, if the stoichiometric dissolution of dolomite or ankerite is assumed. However, the composition of the waters would correspond closely to the stoichiometric dissolution of calcite.

Group B (Ca^{2+}-Mg^{2+}-HCO_3^-) waters are generally poor in Ca, and have a certain excess of cations in relation to the stoichiometric dissolution of dolomite and especially of ankerite.

Group C (Na^+-Mg^{2+}-HCO_3^- -type) waters, in general, have a low cation to bicarbonate ratio with respect to the stoichiometric dissolution of all three carbonate minerals considered. However, the waters close to the surface in the North Fault are very close to the dissolution line of ankerite. As the waters of this group flow towards deeper zones, the bicarbonate content increases and the cation deficit becomes more evident and therefore the composition of the groundwater plots further away from the 1:1 bicarbonate:cations line.

Group D (Na^+-HCO_3^- -type) waters are found in deep sections of SR5. These display an even greater deficit of cations with respect to the concentration of bicarbonate than in Group C waters.

In general, the granitic-type waters (Group C and D) show a gradual decrease of the Ca^{2+}, Mg^{2+} and Fe^{2+} with increasing depth and distance from the Los Ratones mine. This would imply that if the dissolution of carbonates is taking place in these waters, Ca, Mg and/or Fe are either

precipitating in new minerals or are being removed from the groundwaters by other geochemical processes. The precipitation of siderite can partially explain the excess of Ca + Mg that is found in the Groups A and B waters associated with the dolomite-ankerite vein mineralization.

The lack of 2:1 stoichiometry between the HCO_3^- and Ca^{2+} concentrations in the groundwater of borehole SR-5, which would imply calcite dissolution, could be related to the lack of any calcium-rich carbonate mineralization in this borehole (Gómez et al., 2001).
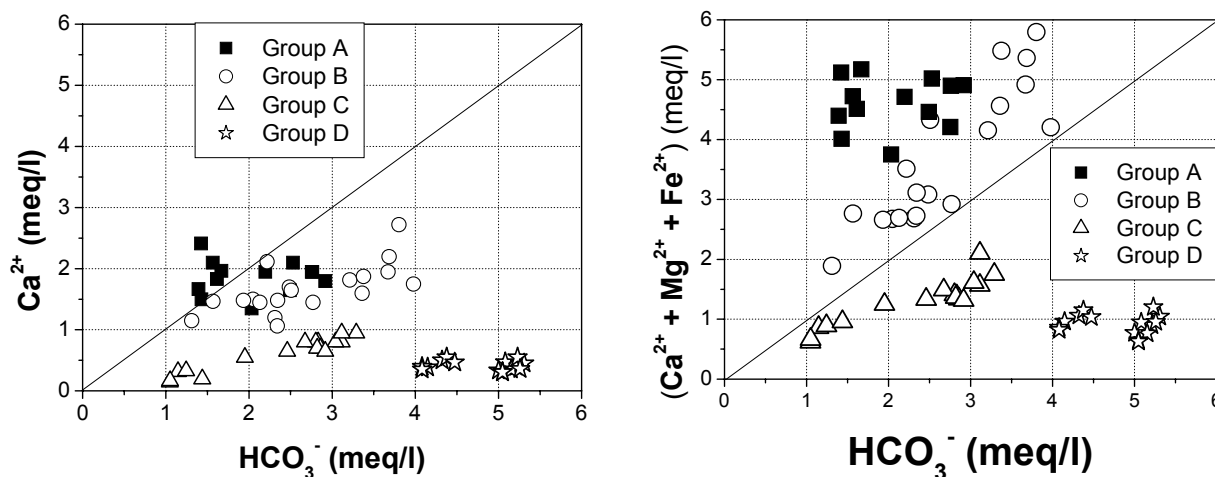
Figure 3-2. Ion-ion diagram of the concentration of bicarbonates versus the concentration of Ca^{2+} and $(Ca^{2+} + Fe^{2+} + Mg^{2+})$ in the four groups of groundwaters.

There is a general correspondence between the concentration of HCO_3^- in the groundwater and the distribution of carbonate fracture mineralization, which both show an increase in concentration and abundance, respectively, with depth and towards the south of the area. In borehole SR-5, high concentrations of HCO_3^- (273-314 mg/L) measured in the waters from the deepest sections correlates with the presence of carbonate fracture mineralization detected in the samples from flowing fractures in boreholes SR3, SR4 and SR5. In contrast, the low concentration HCO_3^- (178-186 mg/l) in the groundwater in shallower sections from the SR5 borehole is consistent with only minor presence of carbonate fracture fillings

Borehole SR-4 is characterised by ankeritic carbonate fracture mineralization in its deepest section (120.44 m). The presence of carbonate mineralization, along with the influence of bicarbonate groundwater that discharge from the mine through the South Fault (which is intersected by this borehole) most probably account for the high carbonate concentration (225 mg/L) in the groundwater in this area. No carbonate fillings have been found in the upper parts of this borehole or in SR-1. Groundwaters in the upper part of the SR-1 and SR-2 connect and mix with those from the upper sections of SR-4, and in SR1 and SR4 are characterized by lower bicarbonate (99-102 mg/L and 168-178 mg/L, respectively) than groundwaters deeper in borehole SR-4. Although no carbonate mineralization has been found in borehole SR-1, the relatively high bicarbonate concentration (243 mg/L) in water observed at its deepest section could be related to the existence of carbonate fillings at the surrounding rock, but more probably, to the influence of the bicarbonate water which discharges from the mine, through 'Dyke-27', in this section. In borehole SR-3, three carbonate veins were observed in both the upper and lower part of the section. The presence of the carbonate mineralization accounts for intermediate concentration values of bicarbonate found in the waters from this borehole (163 mg/L). No carbonate mineralization was found in borehole SR-2. The low concentration of HCO_3^- (64 mg/L) in groundwaters from borehole SR-2 can be explained by the lack of interaction with carbonate minerals.

51

The following conceptual model of the processes related to the precipitation and dissolution of carbonates is proposed:

1. The dissolution of sulphides must be taking place in the shallow zone due to the infiltration of meteoric waters rich in dissolved oxygen. This reaction releases H^+, SO_4^{2-} and Fe^{2+} to the water, as well as other metals derived from the sulphides. Oxidation of pyrite, melnikovite, arsenopyrite etc. are the main reacting minerals in the Ratones groundwaters. Their reaction can account for the concentrations of sulphates, iron and arsenic.

2. The gradual dissolution of ankeritic carbonate fracture mineralization (also present at shallow levels) buffers the acidity produced by sulphide oxidation

3. Subsequently, the dissolved HCO_3^- reacts with Fe^{2+} and down-gradient the groundwater eventually reaches saturation with respect to siderite.

These processes are observed in most of the waters associated with the fracture mineralization at Los Ratones.

Groundwater concentrations of Ca^{2+} and Mg^{2+} decrease with depth, while the Na^+ increases (Figure 3-3). This variation is considered normal, and reflects the more conservative behaviour of Na compared to Ca and Mg, which are involved in irreversible processes (mineral dissolution (near surface) and mineral precipitation including: formation of saleite; neoformation of apatite, Ca silicophosphates, etc) or in "reversible" processes like ion exchange. Geochemical modelling of the groundwaters shows that carbonate minerals are undersaturated with respect to the carbonate minerals and should not precipitate. This is consistent with mineralogical observations in this study, which have found evidence for neither neoformed calcite, ankerite nor dolomite.
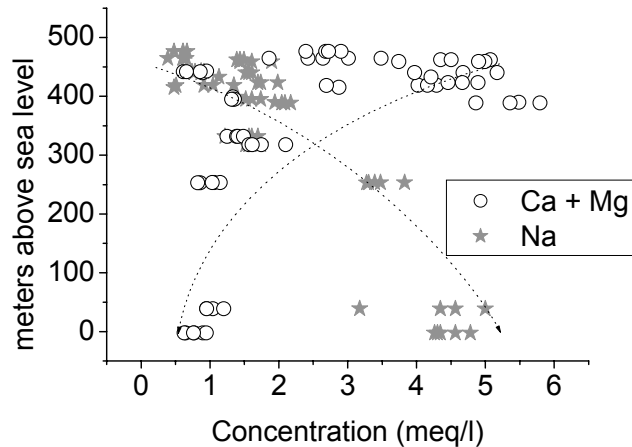
Figure 3-3. Diagram representing the variation of the concentration of Na^+ and Ca^{2+} + Mg^{2+} in the groundwaters as a function depth below surface.

Therefore, it is considered that ion-exchange must be the principal process governing the concentration of cations in solution:

Ca^{2+} + 6Na-montmorillonite $\Leftrightarrow$ 3Ca-montmorillonite + 2Na$^+$

$Na_2X + Mg^{2+} \Leftrightarrow 2Na^+ + MgX$ (X: exchangeable cation)
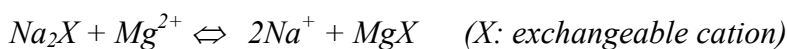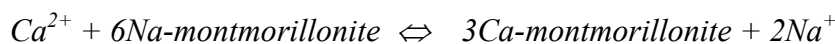
Considering these exchange reactions, the molar concentration of Na in the waters from Group D (the deepest sections of SR5) is approximately equal to the concentration of HCO_3^-, which is consistent with the exchange of Na^+ by Ca^{2+} and/or Mg^{2+} from clay minerals. Previous studies

on the alteration assemblage associated with the uranium mineralization (Arribas, 1962, 1975; Buil, 2002), and the investigations on fracture fillings or dykes intersected by boreholes in this study show that smectite is a frequent and abundant mineral in certain structures, and that Ca and Mg (as indicated by SEM) are present as exchangeable cations.

In contrast to Na, the Ca^{2+}/Mg^{2+} ratio in the waters from the Ratones Mine is <1. However, if both cations are derived from the congruent dissolution of ankeritic vein carbonates then this value should be greater than 1, since the carbonates have higher concentrations of Ca^{2+} than Mg^{2+}. There are a number of possible explanations for the low Ca^{2+}/Mg^{2+} ratios (<1) in the water:

- Additional Mg^{2+} derived from the alteration of biotite to chlorite;

- The dissolution or alteration of chlorite. The almost total disappearance of chlorite and its transformation into sericite or other clay minerals, close to the uranium mineralization (Arribas, 1962), may be significant in regard to this.

- The preference for Ca^{2+} to be exchanged for other cations in the cation exchange sites of clay minerals;

- The tendency for Ca^{2+} to form minerals.

3.1.2.3 URANIUM MINERALIZATION

The Los Ratones uranium mineralization comprises U silicophosphates, phosphates, silicates, and oxides. The greatest abundance of mineralization occurs in 'Dyke 27' and in the South Fault (and its adjacent fractures). Significant autunite, uranotile, coffinite, U-Ca-Zr silicates and U oxide mineralization is present in sampled fracture fillings from intermediate and deep zones in borehole SR-4. In borehole SR5, uranium mineralization is mainly localised in fractures between 140 and 150 m depth, with the development of major amounts of pitchblende, along with secondary uranotile and U-Ca-Zr-silicates formed by pitchblende alteration. This occurs within a large quartz vein or 'dyke' intersected by the borehole (Gómez, 2002). U minerals have been identified only in minor amounts in the upper section of the North Fault area. Overall, the major development of uranium mineralization was encountered in the boreholes situated in the south of the study area (SR-5, SR-4 and SR-1).

Dissolved U in the Ratones Mine groundwaters oscillates between <1 μg/L and 10 μg/L. In general, these concentrations are low due to the reducing conditions. The highest values in the mine waters have all been measured in all packered-off sections from the SR4 borehole, and in the mine ventilation shaft (35 μg/L and 104 μg/L). In the Main Shaft ('Pozo Maestro'), 'Dyke 27' and adjacent fractures, the U concentration is always below 20 μg/L. Waters circulating through the North Fault, and those from the major part of borehole SR5, have U contents of <4 μg/L. The interval between 138 to 149 m in SR5 borehole produces water with high U concentrations (up to 60 μg/L), and coincides with a zone of major U mineralization. Elsewhere in this borehole U mineralization is absent (except for the presence of LREE, Ca and U silicophosphates in a vein at 288,84 m, and between sections 417-427 m and 203-213 m) and the waters have much lower U (0.8-2 μg/L). High concentrations of U are found in waters throughout borehole SR-4 (43-44.7 μg/L). This is explained by the interaction with the significant U mineralization present in this borehole. Borehole SR-1 contains some U mineralization (uranotile, autunite, saleite) at the intersection with Dyke 27, although it is less widely developed than in borehole.SR-4 This fact could explain the intermediate values of U (6-17.7 μg/L) measured in waters sampled from this borehole. U minerals have been found in only two samples from borehole SR-2: one from the hanging wall of the North Fault, where U oxide is present; and the second one with uranotile from below this fault. No U minerals have been found within the North Fault faultrocks themselves. Groundwaters in the North Fault have correspondingly low values of uranium (< 1 μg/L). Overall, the distribution of U minerals present in fracture fillings correlates with high U concentration in groundwater (Gómez et al,

1999), with waters from more southern boreholes (SR-5, SR-4 and SR-1) having a generally greater concentration of dissolved U (up to 46 μg/L U) than in boreholes SR-2 and SR-3 (< 1-1.4 μg/L U).

The conceptual hydrogeological model for the site proposes that the groundwater preferentially flows through the North Fault, within which the main rock-water interaction processes take place. This fault contains little or no U mineralization, and consequently the groundwater discharging from the fault zone contains a very low concentration of U. The contribution to the groundwater chemistry, from any fracture mineralization lying outside of the region of influence of the fault, would be much lower. The dissolved U present in the groundwaters in the southern part of the site is derived from reaction with U minerals in the mineralized zones described above. The phases limiting U solubility in the groundwaters have been predicted from evaluation of mineral saturation indices (Figure 3-4) and from predicted uranium concentrations calculated from chemical equilibrium modelling of pure solid phases (Figure 3-5). Full details of the geochemical modelling at Los Ratones are given in Gómez (2002) and in the WP4 report (Cortez and Bath, 2005).
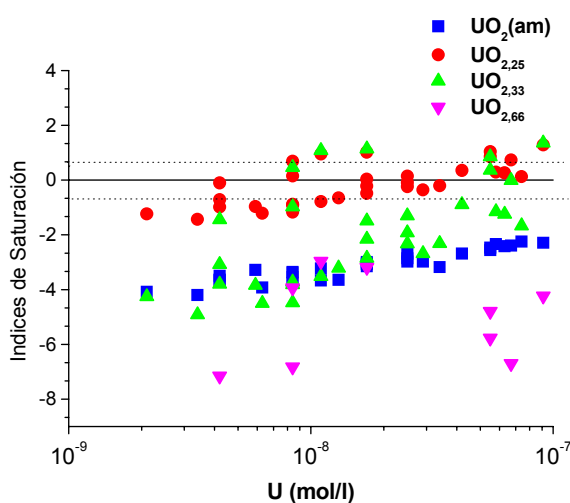
Figure 3-4. Saturation indices for the partially oxidized uranium oxides versus the uranium concentration measured in the groundwaters of the Ratones mine.
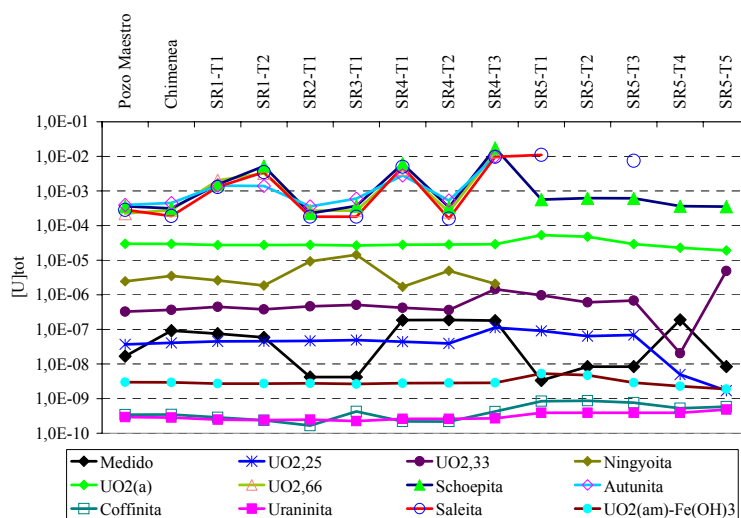
Figure 3-5. Predicted uranium concentrations obtained from chemical equilibrium modelling of pure solid phases, and by applying a co-precipitation model for U-Fe(OH)$_3$. The black line represents the concentration (M) of measured U in waters.

54

U mineral saturation indices predict that amorphous uranium oxides (UO_{2am}) are undersaturated in the groundwaters. However, modelling indicates that the saturation indices for $UO_{2.25}$ (U_4O_9) are quite close to equilibrium with the present groundwaters, and in some cases supersaturation is predicted. $UO_{2.33}$ is also predicted to be close to equilibrium in some of the groundwaters sampled. The more oxidized compound $UO_{2.667}$ is always undersaturated. Modelling suggest that the uranyl phosphates autunite ($Ca(UO_2)_2(PO_4)_2$ and saleite ($Mg(UO_2)_2(PO_4)_2$, which are present as secondary alteration products, are undersaturated and do not appear in equilibrium with the groundwaters. The mineralogical observations suggest that the groundwaters are saturated with regard to uraninite (UO_2) and coffinite ($USiO_4$): Buil (2002) has found evidence of possible neo-formation of coffinite in fracture fillings (described in early studies (Arribas, 1962) as a "black oxide" alteration product of pitchblende). However, the geochemical modelling shows a better fit to equilibrium with the oxides $UO_{2.25}$ and $UO_{2.33}$, which represent slightly more oxidized forms of pitchblende or uraninite (UO_2). These would seem to be the principal minerals controlling U solubility in the system. Although, Gómez (2002) also shows the importance of co-precipitation of U with Fe-oxyhydroxides, in controlling the lowest U concentrations the groundwaters. Fe oxides are also important with regard to scavenging almost all of the U from the waters discharging from the mine to the surface.

3.1.2.4 OTHER SECONDARY MINERALS

The Fe oxides and hydroxides, with varying contents of As, U and Mn, are abundant in fractures from all the boreholes, except for borehole SR5. Phosphates are locally developed in the study area, and in particular: apatite mineralization is found in boreholes SR-5 and SR-3; hamlinite ($SrAl_3(PO_4)_2(OH)_5.H_2O$) is found in boreholes SR-5 (145.55 m) and SR-3 (65.31 m); and tarbuttite ($Zn_2PO_4(OH)$) is found near the surface in borehole SR-1 (9.61 m).

Sulphate mineralization is scarce, and has only been identified in boreholes SR-5 and SR-1. In borehole SR-5 gypsum is formed at 160.99 m depth and barite has been identified in a deeper fracture (288.84 m). In borehole SR-1 gypsum is formed in locally at 20.40 m depth.

Overall, the mineral-groundwater relationships show that the chemistry of the groundwaters in the Ratones Mine are the result of interaction between the groundwaters, and both the granite and the fracture mineralization in the mine area. However, the groundwater flow system characteristic of this area involves: very recent water (3 to 5 years old); modern waters of about 50 years of age; and older waters from about one thousand years to a few tens of thousands (15000 to 16000 years) (cf. Ortuño et al., 1999). These have produced alteration and secondary fracture filling minerals several times in the past, which have acted as sinks and sources of the elements now circulating waters in the system.

%	Oxidos Chimenea		ppm	Oxidos Chimenea
Al_2O_3	1.1		Ba	186.4
FeO	25.3		Ce	3.8
Fe_2O_3	25.0		Co	2.06
CaO	2.6		Cr	4.5
C total	12.7		Cu	10.5
C org	10.5		Li	10.3
C inog	1.89		Mo	3.0
S total	0.04		Ni	4.3
P_2O_5	8.6		Sn	10.8
MgO	0.47		Sr	103.9
MnO	0.25		Rb	20.7
TiO_2	0.03		Th	0.8
Na_2O	0.2		U	396.5
F^-	0.022		V	10.8
Si	2.9		Zn	109.1
As	2.7			
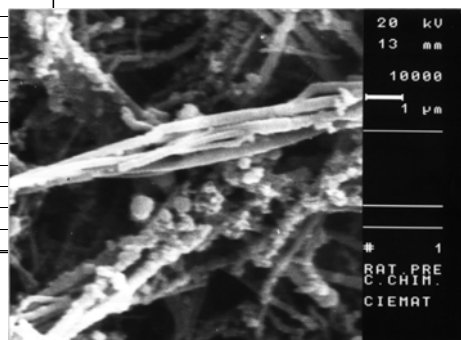
Figure 3-6. (Left) Fe oxyhydroxide composition: major elements have been obtained by XPS and trace elements by ICP-MS; (right) SEM image of secondary Fe oxyhydroxide.

3.1.2.5 FLUID INCLUSION STUDIES

Microthermometric fluid inclusion studies were carried out on materials from Los Ratones by CIEMAT, with a complementary study on a small suite of 5 samples examined at the BGS for comparative purposes (Appendix 4.1 and 4.2). A total of 57 microthermometric measurements were made on fluid inclusions obtained from the hydrothermal quartz and ankerite vein mineralization, and from healed microfractures in the quartz of the granite host rock from boreholes SR3 and SR5.

3.1.2.5.1 Vein quartz

Quartz veining belongs to the third (post-Hercynian) stage of fracturing recognised at Los Ratones (Section 2.1.2). Several generations of quartz may be present, and the veins typically comprise linings of euhedral quartz crystals cemented by later quartz occupying the centre of the veins.

Vein-lining quartz:

Primary inclusions in the vein quartz are scarce, with inclusion sizes ranging from 4 to 19 μm and regular in shape. The CIEMAT studies found that primary inclusion in the earlier vein-lining quartz were mostly two-phases (vapour : total volume ratio $(V_v/V_t) = 0.1-0.2$) Homogenisation temperatures (T_h) are between 113-248 ºC with a modal temperature of 220 ºC, showing that mineralization occurred under moderate to high temperatures. The ice melting temperatures (T_{ice}) are between –0.2 to –3.8 °C indicating a fluid salinity of 0.3 to 6 wt % equivalent NaCl.

Only one sample of quartz mineralization, taken from 463 m depth in borehole SR-5 (sample RT-01, Appendix 4.1 and 4.2) was examined at the BGS. The quartz pre-dates ankerite and ferroan dolomite, which are also present in this sample and rest on top of, and corrode, the early quartz lining. The fluid inclusions are arranged in crystallographically-controlled arrays along concentric growth zones in the quartz crystals. In marked contrast to the CIEMAT results, the BGS studies found only monophase (liquid) primary fluid inclusions in the vein lining quartz from this sample. Because these inclusions are monophase, T_h determinations were not possible. However, the presence of monophase primary fluid inclusions does imply that this quartz mineralization is low temperature (the general consensus amongst fluid inclusion workers is that this indicates formation at temperatures <80 °C (cf. Shepherd et al., 1985), although this interpretation may not always be valid (Roedder 1984, see also discussion in Bouch, 2004). Limited T_{fm} and T_{ice} measurements (c. –30 °C) and melting behaviour are indicative of a NaCl-dominated fluid with salinity of between 16-20 wt % equivalent NaCl.

The marked difference between the CIEMAT and BGS results indicate that the early linings of pre-carbonate quartz veins comprise at least two distinctly different generations of quartz mineralization: a moderate- to high-temperature hydrothermal quartz associated with a dilute to weakly saline fluid; and low-temperature quartz associated with a brine. These fluids appear to have been sampled completely separately in the fluid inclusion studies by the two organisations. Unfortunately, the temporal relationship between the two inclusion types is undetermined.

Later vein-filling quartz cement

Fluid inclusions in the later vein-filling quartz cement were only observed and analysed in the CIEMAT samples, and could not be analysed in the mineralization samples examined by BGS. Inclusions are scarce, and data are restricted to observations from secondary inclusions with sizes <16 μm. The inclusions have regular shapes and most of them are two-phases, with V_v/V_t ratios between 0.1-0.2. Eutectic temperatures between –65 and –64 ºC have been measured, indicating the presence of other cations besides Na. The T_{ice} ranges from –13.5 to –21.7 ºC, showing that the mineralising fluids were brines with salinities are around 17 to 24 wt% equivalent NaCl. T_h values were determined to range from 80 to 144 ºC but these temperatures

are probably not meaningful, since 'necking' and leakage may have occurred during the annealing processes in secondary inclusion arrays (producing erroneous T_h values).

This fluid is distinct from the dilute fluid found in inclusions in the early quartz by CIEMAT. However, it seems likely that the later vein-filling quartz cement may belong to the same generation (or has been deposited from a similar fluid) as the euhedral vein-lining quartz in some fractures, as is shown by the similarity between the fluid inclusion chemistry of this later quartz and that of the vein-lining quartz observed by BGS.

Healed microfractures in quartz in granite

Secondary fluid inclusions in arrays along secondary planes (healed microfractures in the quartz of the granite wallrock adjacent to the veins) were studied by CIEMAT and the BGS. Again, the inclusions are scarce and very small (around 6 to 8 μm in size). Most are two phase with highly variable liquid/volume ratios (V_v/V_t ranges between 0.05 to 0.2) indicating fluid leaking and/or trapping of fluid with variable L/V ratio. T_h is highly variable, as would be anticipated (90 to >240 °C), and should be considered unreliable as an estimate of trapping (mineralizing temperature) conditions. The CIEMAT T_{ice} measurements indicate that the fluids in these secondary inclusions ranges from –1.6 to –2.9 ºC, consistent with the salinities of between 2.7-4.7 wt % equivalent NaCl. The BGS results show a wider range, with T_{ice} values from 1.9 to 4.1 ºC, corresponding to salinities between 3 and 7 %. Inferences on the fluid speciation can not be made from melting behaviour due to the low salinity of fluid.

Overall, there appears to have been several different episodes of quartz mineralization at Los Ratones:

- An early moderate- to high-temperature (113-248 ºC) hydrothermal event associated with a low-salinity (0.3 to 6 wt % equivalent NaCl) fluid. This formed the early vein-lining quartz.

- A later generation of quartz forming some vein linings, and associated with a low-temperature (<80 °C) NaCl-type brine (16-20 wt % equivalent NaCl).

- Later vein-filling quartz cement. No primary fluid inclusion data could be obtained from this mineralization to enable the conditions of formation to be defined. However, the brine (7 to 24 wt% equivalent NaCl) trapped in secondary inclusions in this quartz has a very similar salinity to that associated with the low-temperature generation of vein lining quartz described above. Therefore, it seems likely that the later vein filling quartz observed in some veins is coeval with, or may pre-date, the low-temperature quartz mineralization that forms euhedral linings in other veins.

Secondary fluid inclusion arrays in annealed microfractures in the granite wallrock adjacent to quartz veins show that the wallrock was penetrated in the past by NaCl-type groundwater of low- to moderate-salinity (3-7 % equivalent NaCl). From the broad similarity between the two fluids, this probably occurred during the early hydrothermal stage of quartz mineralization.

3.1.2.5.2 Vein carbonates

Fluid inclusion data were obtained from the dolomite-ankerite vein mineralization associated with the Stage 3 (post-Hercynian) brittle fracturing (Section 2.1.2). The carbonate is seen to be strongly growth zoned under CL and BSEM-EDXA, due to variations in Fe and Mn content (see also Section 3.1.2.6, below). Fluid inclusions are scarce and typically between 10 to 25 μm in size, and most of the inclusions studied exhibit regular shapes and are probably primary.

The inclusions are two-phase inclusions, and in all cases have consistent high liquid vapour ratios with V_v/V_t between 0.5 and 0.1 (i.e. 90 to 95 % liquid) and generally have T_h values of around 85-125 °C, although some T_h values up to 160 °C were found in the CIEMAT studies. Inclusion melting behaviour indicates that the fluids are complex brines with an appreciable

CaCl$_2$ content indicated by low T$_{fm}$ (c. –65 to –50 °C). T$_{ice}$ values of -19 to –25 °C indicate total salinities around 25 wt % NaCl + CaCl$_2$), and hydrohalite and metastable ice melting characteristics suggest NaCl / (NaCl+CaCl$_2$) weight ratios between 0.8 and 0.68.

Overall, the data show that the dolomite-ankerite mineralization was deposited by warm Na-Ca-Cl-type brines. This might indicate a basinal-derived brine rather than a hydrothermal fluid associated with the cooling of the granite.

3.1.2.5.3 *Limitations for palaeofluid reconstruction*

The quartz and carbonate mineralization are the main fluid-inclusion bearing minerals at the Los Ratones site. Quartz (sometimes associated with other silicates) was the earliest mineralization and initially deposited from early moderate- to high-temperature hydrothermal dilute NaCl-type waters; later quartz mineralization was deposited from cooler (probably <80 °C) NaCl brines. These were most probably related to hydrothermal activity associated with the cooling of the granite. Quartz mineralization was subsequently followed by renewed hydrothermal activity associated with warm (85-125 °C) complex Na-Ca-Cl-type brines, which deposited dolomite and ankerite. These fluids are geologically old, and show no relationship to the cool dilute bicarbonate-type groundwater now present in the site. As such, this mineralization would appear to have little direct relevance for Quaternary palaeohydrogeological interpretation at Los Ratones.

At this site, the minerals that are of interest from a palaeohydrogeological perspective are the late-stage Mn- and Fe-oxide and oxyhydroxide alteration products (found in the shallower parts of the groundwater system) and clay minerals (particularly smectite). These are most likely to have formed more recent geochemical interaction (e.g. oxidative weathering) and appear to be in equilibrium with the present waters (3.1.2.1) but unfortunately they are unsuitable for fluid inclusion analyses.

3.1.2.6 MAJOR AND TRACE ELEMENT CHEMISTRY STUDIES

Major and trace elements chemistry was determined on fracture fillings and host rock minerals (mainly carbonate vein mineralization and apatite). The analytical data are presented in Appendix 3. The objectives of these studies were:

- To determine whether different generations of mineralization could be differentiated on the basis of their chemical characteristics;

- To try to use mineral compositional information to help differentiate and evaluate the groundwater geochemical conditions during different mineralization events;

- To use evidence from REE abundance in fracture fillings as an indicator of groundwater environmental changes.

3.1.2.6.1 *Major elements*

The major element compositions of the fracture filling carbonates were determined by electron microprobe analysis (EPMA) at Technic Scientific Services, University of Barcelona). EPMA measurements were made to examine variations within the same carbonate minerals from different fracture samples and to examine compositional growth zoning variations within single crystals.

Two types of carbonate vein mineralization can be distinguished overall:

- Borehole SR-3 and the deeper parts of borehole SR-5 are dominated by dolomite-ankerite solid-solution series vein mineralization of intermediate composition.

$$[Mg_{(0.6-0.92)}Ca_{(0.97--1.09)}Mn_{(0.01-0.04)}Fe_{(0.1-0.34)}Na_{(0-0.001)}](CO_3)_2$$
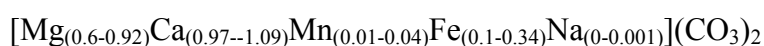
- At intermediate depths in borehole SR-5 the carbonate vein mineralization is dominated by magnesian-rich siderite (magnesite-siderite solid-solution series).

$$[Mg_{(0.7-0.82)} \, Mn_{(0.04-0.06)} Fe_{(1.05-1.24)} Na_{(0.001)}](CO_3)_2$$

The carbonates show minor compositional zoning with respect to Ca, Fe, Mg and Mn. In particular, the dolomite-ankerite displays zoning with higher Mn and Fe in the rims of the crystals, whereas Mg is higher in the core growth zones (Figure 3-7).
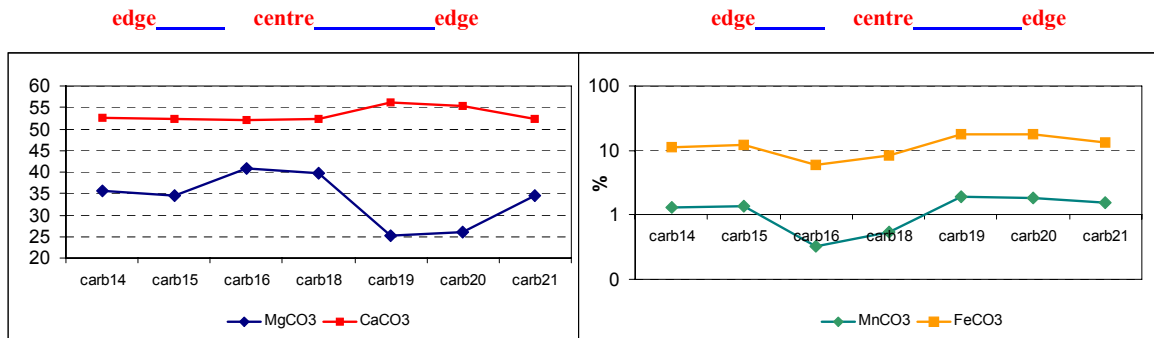
Figure 3-7. Variations of Mg, Ca, Mn, and Fe concentrations (wt %) within a growth-zoned dolomite-ankerite crystal.

3.1.2.6.2 Trace elements

Selected trace elements were determined on bulk vein material because of the difficulty in separating individual minerals. Analyses were performed using ICP-MS at the University of Granada. The variation in the bulk vein trace element chemistry largely reflects the mineralogy of the fracture filling:

- High Sr correlates with the abundance of dolomite-ankerite, and is low in siderite-magnesite;

- U and Th variations mainly reflect the presence or absence of secondary U minerals (e.g. autunite, coffinite etc.), or are enriched in samples containing apatite and monazite. U concentration is also high in secondary Fe oxyhydroxide, where the U is likely to be enriched as a result of adsorption.

The REE patterns of the bulk fracture fills, and individual fracture mineralization, and of REE-rich accessory minerals (apatite, monazite and xenotime) in the granite host, were compared by normalization relative to host Los Ratones granite (Figure 3-8, Figure 3-9, Figure 3-10).

Monazite, xenotime and apatite, which are present as primary accessory minerals in the granite are rich in REEs. All three minerals show a marked depletion in Eu (negative Eu anomaly. However, there is a significant difference in the REE distribution between these minerals. Monazite and apatite both display a preferential enrichment in light REEs (LREE) relative to the bulk granite, whereas xenotime is preferentially enriched in heavy REEs (HREE).

The carbonate fracture mineralization displays enhanced HREE enrichment, suggesting precipitation took place from a fluid rich in HREE. The REE pattern does not obviously mirror the composition of the granite, or of the primary accessory REE minerals in the granite, and therefore would not appear to be derived simply by dissolution of the granite. HREE preferentially form soluble complexes with inorganic ligands, and a HREE-enriched mineralising fluid might be related to the presence of organic complexation. This might be consistent with deposition from a basinal brine-type mineralizing fluid, which could be inferred from the fluid inclusion data (Section 3.1.2.5) that shows the dolomite-ankerite was deposited from a Na-Ca-Cl

type brine. The REE patterns of the carbonate mineralization also vary. Dolomite-ankerite tends to display a positive Eu anomaly, whereas siderite-magnesite displays a negative anomaly. This might be due to the tendency of the Eu to enter in the structural positions of the Ca.
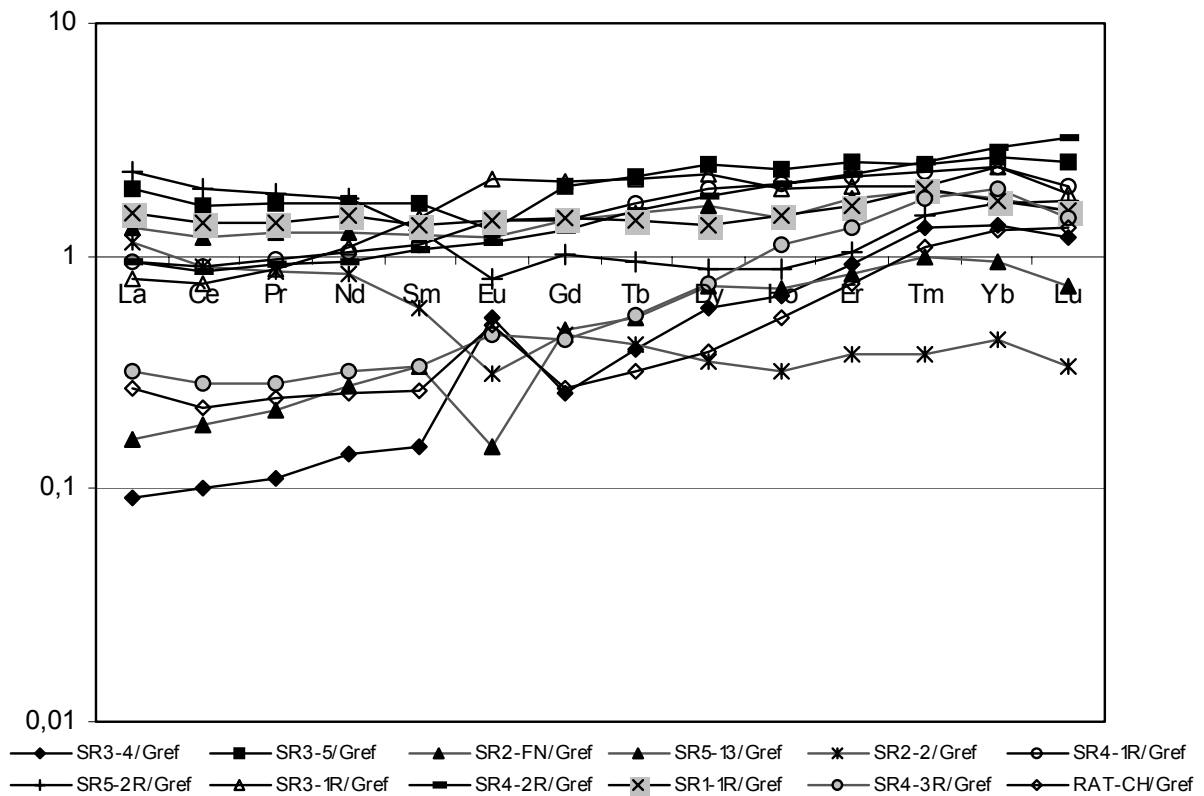
Figure 3-8. REE distribution patterns for the bulk fracture fillings, shown as normalized ratios relative to the REE content in the reference granite.

There is no evidence of differential fractionation of Ce, which behaves either as Ce^{3+} under reducing conditions or Ce^{4+} under oxidising conditions. In this system, Ce appears to behave similarly to the other trivalent LREEs, and therefore it would appear that mineralization did not occur under oxidizing conditions.
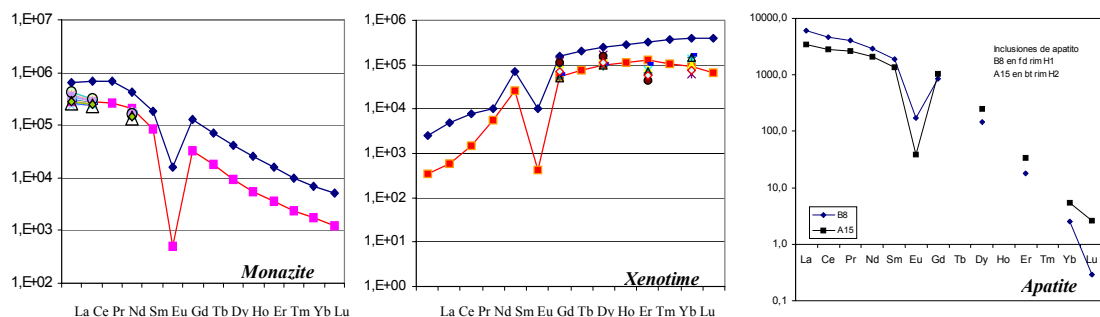
Figure 3-9. REE distribution patterns for granitic monazite, xenotime and apatite of the Ratones Mine normalised relative to the Los Ratones granite.
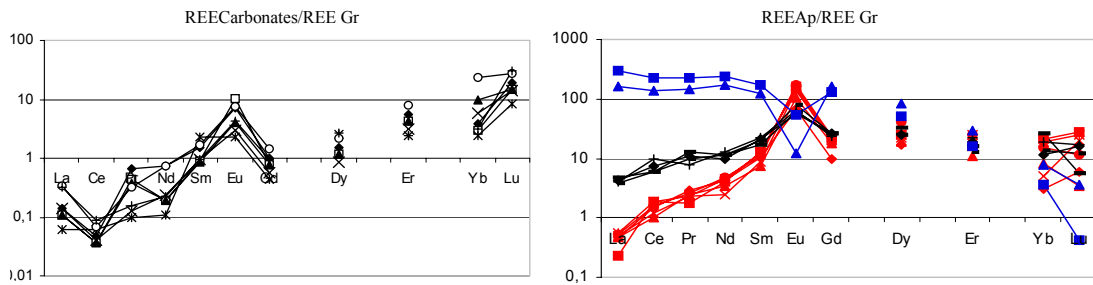
Figure 3-10. REE distribution patterns for dolomite-ankerite (left) and apatite (right) in fractures (red and black) and granitic apatite (blue) normalised relative to the Los Ratones granite. The HREEs and Eu are enrichment in these secondary minerals relative to the to granite. Fracture apatite is enriched in LREE relative to the granite and granitic apatite.
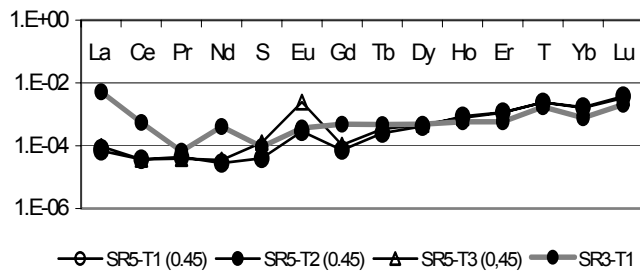
Figure 3-11. REE distribution pattern for the groundwater from boreholes SR3 and normalised relative to the Los Ratones granite.
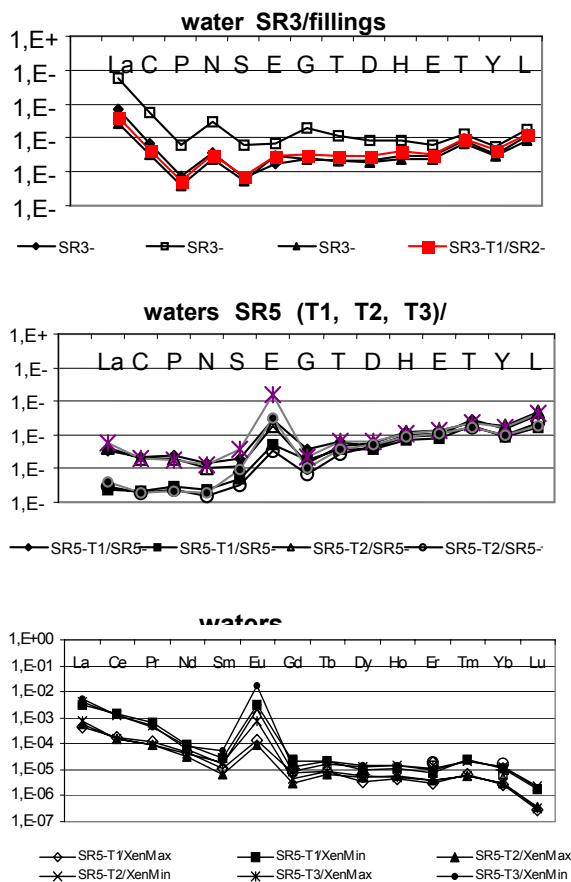
Figure 3-12. REE distribution profiles of the groundwaters for boreholes SR3 and SR5 normalised relative to the fracture fillings with which they interact.
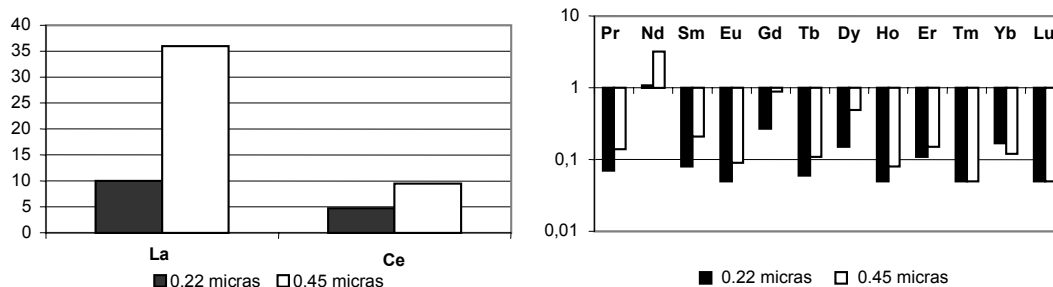
Figure 3-13. Graphic showing the difference in REE concentration (ppm) in groundwaters filtered through 0.45 and 0.22 µm filters.

The REE geochemistry of the fracture fillings and groundwaters have been compared to try to differentiate interactions between the groundwater and either (a) the fracture mineralization, or (b) host rocks, in the Los Ratones mine system (Buil, 2004). Figure 3-11 and Figure 3-12 show the REE distribution patterns for Los Ratones groundwater from boreholes SR3 and SR5 normalised with respect to the host granite and fracture fillings, respectively.

The waters show a moderate enrichment in HREEs relative to the granite, and in some cases, a small positive Eu anomaly is also evident. Therefore, interaction of the groundwater with the host granite alone cannot account for the REE composition the water. The REE profile of the groundwater normalised to the carbonate vein mineralization, displays a very 'flat' profile for the HREE and Eu part of the spectrum, particularly for waters from borehole SR3. This distribution profile suggests that the ankerite-dolomite mineralization may contribute to the HREE content of the water. However, the REE distribution profiles of the groundwaters are enriched in La, Ce and Nd relative to the fracture mineralization. This might be explained if these elements were also transported in the groundwaters in a colloidal form, as indicated by the marked difference in composition of groundwater filtered at 0.45 and 0.22 µm (Figure 3-13). On the other hand, the fracture fillings-normalized REE patterns of waters from the borehole SR5 display a HREE enrichment and positive Eu anomalies. The mineralogy of these fracture fillings (SR5) includes inherited REE minerals of the granitoids (i.e. monazite, apatite and xenotime) and neoformed minerals (mainly phyllosilicates). The waters and fracture fillings, from borehole SR5, present a similar LREE distribution (showing the same 'flat' pattern exhibited by the fracture filling-normalized REE patterns for the waters), which indicates that the LREE-rich minerals present in the fracture fillings (i.e. apatites, monazites) control the LREE content in waters. Xenotime-normalized REE patterns of waters from borehole SR5 tend to 'flatten' in the HREE region (Figure 2-12), for that reason the presence of HREE-rich minerals (i.e. xenotimes) in the fracture fillings, together with competitive action of aqueous complex formation process (increase of stability constants of carbonate complex with REE atomic ratio) and colloid transport of REE, would account for the observed REE distribution of the groundwater from borehole SR5.

Further studies by Buil (2004) have shown that the REE patterns (Figure 28) observed in most of the groundwaters are inherited from a combination of:

- The weathering of easily altered major granite minerals such K-feldspars, plagioclases and their aluminosilicate alteration products, which have REE patterns similar to the bulk granite;

- Leaching of accessory granite minerals - monazite and apatite (enriched in LREE) and xenotime (enriched in HREE);

- Leaching of carbonate and apatite mineralization in water-conducting fractures.

Competing processes such as organic complex formation, the removal of REEs through the precipitation of carbonates, secondary oxyhydroxides of Fe and other metals, sorption on phyllosilicates, and the potential for REE colloidal transport (Figure 3-13) appear to influence the REE geochemistry of the Los Ratones mine waters.

62

The bulk of the carbonate mineralization found at Los Ratones is of hydrothermal origin, and neoformed calcite has not been found at this site. Unlike the situation at the other study sites (Äspö, Sellafield, Dounreay) it has not been possible to sample any late carbonate mineralization that may have preserved evidence of biomarkers. Nevertheless, two samples of largely dolomite-ankerite were taken from a major highly permeable and porous vein ('ankerite dyke') representing major conductive feature 463 m depth in borehole SR-5 (samples RT-00 and RT-01). This was considered to be the most likely material that would contain late carbonate mineralization (if any). The samples were analysed by GC-MS at the Universidad Politecnica de Madrid.

No biomarkers were detected in the carbonate vein mineralization. This is consistent with its hydrothermal origin.

3.1.3   Summary and conclusions

Site-specific studies in the granitic fractured area of the Ratones Mine, in the southwest of Spain, were expected to provide a record of the geofluid evolution of this area. This is a topography-controlled discharge area with flow paths, which occur mainly in the upper 200 m, through the overburden bedrock and through the altered and fractured zones represented by the main structures (dyke 27 and 27', South Fault and North Fault, and the minor fracture network connecting with them). Below 200 m, the fresh granite constitutes a very low permeability media in which the water flows through fractures with a contrasted conductivity with respect to that of the granite host rock (e.g. North Fault).

Hydrochemical data (see Section 2.1.3) indicate that groundwaters are diluted, with Ca-Mg-HCO_3^- type evolving to Na-Mg-HCO_3- and Na-HCO_3- type with depth. The HCO_3^- concentrations in all the groundwaters are mainly controlled by complex carbonate dissolution. The carbonate mineral saturation indices do not indicate precipitation conditions, consistent with the fact that neoformed calcite, ankerite or dolomite have not been observed petrographically. Most groundwaters have a $^2H/^{18}O$ signature close to the global meteoric water line indicating a meteoric origin. The ^3H and ^{14}C contents indicate groundwater residence times of 3-5 years to 10^3 years. The deepest waters (SR5 at 460 m) are depleted in $^2H/^{18}O$ indicating an ancient origin, and probably a colder-climate period, which agree with the residence time determined by ^{14}C measurements, around 15-16 x10^3 years.

Fracture fillings have been sampled and analysed from different boreholes in the Ratones Mine at various depths, up to 500 m. Borehole core examination and detailed studies of thin sections of fracture mineralization have shown that in the upper 300 m the fracture-fillings are characterized by the presence of low-temperature infillings of iron oxyhydroxides (also with Mn) and clay minerals.

Fluid inclusion of the dolomite-ankerite vein mineralization indicate homogenisation temperatures (T_h) of 100-160 ºC, indicating that the vein carbonates are of hydrothermal origin. These probably formed during the last major fracturing event in the area. The absence of biomarkers in the deepest calcites (463 m) also supports the argument that the carbonate mineralization is geologically old. These studies have found no evidence for any young calcite or other carbonate mineralization that is currently forming in the groundwater system.

The REE chemistry may provide a geochemical tracer for water-rock interaction in the Los Ratones groundwater systems. In general, the waters show a moderate enrichment in HREEs relative to the granite, sometimes with a small positive Eu anomaly. Interaction with the major host granite minerals (i.e. weathering of K-feldspars, plagioclases and interactions with their aluminosilicate alteration products,) alone cannot account for the REE composition of the water, and the REE chemistry of the waters is also influenced by interactions with: ankerite-dolomite mineralization (which contribute HREE), and with primary REE-rich igneous phosphate

minerals (apatite, monazite, xenotime) entrained in the fracture mineralization. In addition, competing processes such as organic complex formation, the removal of REEs through the precipitation of carbonates, secondary oxyhydroxides of Fe and other metals, sorption on phyllosilicates, and the potential for REE colloidal transport can also be considered to influence the REE geochemistry of the Los Ratones mine waters.

Unfortunately, no young fracture mineralization (e.g. late-stage calcite) has been identified in the hydraulically-active deep groundwater system at Los Ratones. Consequently, it has not been possible to evaluate variations in the palaeogroundwater geochemical conditions in the last million years from studies of the fracture mineralogy at this site.

3.2 ÄSPÖ AND LAXEMAR

3.2.1 Sample selection criteria

The previous palaeohydrogeological investigations of the Äspö site for the former EU EQUIP Project (Bath et al., 2000) were mainly carried out on samples from Äspö drill cores. In order to avoid any effects of disturbances in the hydrogeological system that may have been caused by the construction of the Äspö URL tunnel samples for the PADAMOT studies from the Äspö-Laxemar area have been selected from a borehole (KLX01) drilled before tunnel construction. Borehole KLX01 was drilled to 1070 m depth on the mainland near Laxemar, to the west of Äspö (Figure 2-4). Borehole KLX01 was drilled conventionally using a single-barrel drilling technique. 56 mm diameter core was recovered from surface down to 670 m, and between 670 and 1070 the core size was reduced to 45 mm diameter. Due to the relatively large diameter the drill core is surprisingly well preserved.

Previous studies indicated that calcite was probably the most suitable fracture mineral for palaeohydrogeological studies within this area (Bath et al., 2000; Tullborg, 2003). Therefore, the sampling for PADAMOT has concentrated entirely on the latest generation of calcite mineralization that can be recognised in core specimens. Sample selection focussed on taking samples of calcite from fractures that could be considered to be hydraulically conductive fractures. These were identified using the following criteria:

- Correspondence of fractures with borehole flow logs produced by hydraulic testing;

- Evidence in core of natural (in situ) open fractures. These were defined on the basis of petrographical criteria as having either intact 'gapped' pore space, or being lined by euhedral calcite indicating crystal growth into open pore space.

Similar criteria were used in the selection of calcite samples from the UK sites at Sellafield, Dounreay and Cloud Hill (Sections 3-5). The primary goal has been to select paragenetically young calcites grown in open space showing euhedral crystal shapes.

With the focus on the modern groundwater flow system and chemical composition in the crystalline environment, it is obvious that a number of problems must be taken into account:

- First of all, low temperature, thin soil cover, and in parts large hydraulic driving forces creates water compositions which lead to dissolution of calcite not only in the soil cover but also in the uppermost part of the bedrock;

- The groundwater flow in a crystalline aquifer is localised within fractures and fracture zones that in large scale can be described as planar structures. However, in detail flow through fractures is better described as a network of channels. Consequently, mineralization deposited from the groundwater is not uniform over the fracture surface.

- Locally extreme environments may be formed at depth by the activity of bacterial colonies on fracture walls, as has been documented at Äspö (Pedersen et al., 1997).

- Carbonate minerals are very reactive in groundwater and small changes in chemistry may produce episodes of dissolution as well as mineralization. Therefore, the relatively high carbonate content of the groundwater does not guarantee that large amounts of calcite precipitation will have been formed continuously over time. Instead, it is possible that dissolution and redistribution may have been extensive in the past.

In conclusion, it is reasonable to assume that fracture coatings do not represent continuous time records of events. Important events may be unrecorded in the growth history of the calcite mineralization, whereas episodic events may be over-represented. A further problem is that he late-stage calcite is usually present only in very small amounts in the drill core samples. It is usually necessary to apply several different analytical techniques to a single sample in order to obtain sufficient and appropriate information about the conditions of calcite growth (e.g. petrographical characteristics, fluid inclusion composition, isotopic information) to enable the palaeohydrogeology to be re-constructed. Therefore, there is a need to optimise and prioritise analyses where there is often conflicting requirements for the analysis of material during site characterization.

In addition to the above-mentioned factors, the core quality has turned out to be a key issue in the PADAMOT investigations. Late-stage calcites (i.e. the generation of interest for palaeohydrogeological studies) grown on top of older coatings in open fractures are very fragile, and are easily destroyed during conventional drilling. In the present sampled drill core KLX01 the degree of preservation is fairly good, probably due to the relatively large diameter of the core. However, the calcite is generally very fine grained and often very sparsely developed, and these factors made sampling and analysis difficult.

3.2.2 Fracture mineralogy and paragenesis

The history of fracture mineralization in the area has been studied both at Äspö (Tullborg 1997 and references therein), and in the nearby Simpevarp area as part of the Swedish radioactive waste management programme site investigations (Drake & Tullborg 2004). A summary of the fracturing history and mineralization paragenesis is presented in Table 3-1.

Table 3-1. Sequence of geological events and fracture mineralization history for Äspö and Laxemar (after Tullborg 1995, 1997).

Event	Effect/Mineralization	Comment
0	Formation of the Äspö Granitoids	c. 1800 Ma (Kornfält et al.,1997)
1	Regional deformation	1660-1450 Ma
2	Mylonitization; formation of fine-grained epidote, muscovite and quartz recrystallization.	Some mylonites probably belong to last phase of event 2.
3	Reactivation of mylonites and formation of idiomorphic epidote and fluorite.	Intrusion of the anorogenic Götemar Intrusion c. 1450 Ma (Åhäll, 2001).
4	Growth of idiomorphic quartz, muscovite, hematite, fluorite, calcite and spherulitic chlorite.	Late-magmatic hydrothermal circulation associated with the Götemar Intrusion.
5	Prehnite, laumontite, calcite, chlorite and fluorite.	Low-temperature burial metamorphism probably Late Proterozoic.
6	Illite-dominated mixed-layer clay, calcite, chlorite.	Low-temperature burial metamorphism and mineralization associated with burial beneath Post-Caledonian sedimentary cover in Sweden.
7	Calcite, Fe-oxyhydroxide, pyrite, clay minerals? (kaolinite, smectite, illite-smectite and corrensite)	Mineralization probably associated with Recent/Quaternary groundwater circulation.

The earliest fracturing event recognised corresponds to mylonite formation and subsequent high temperature hydrothermal mineralization by epidote, quartz, fluorite and pyrite under greenschist facies conditions (Events 2 and 3, Table 3-1). Most of this fracturing is probably older than the intrusion of the anorogenic Götemar granite (ca 1450 Ma), which outcrops within the region a few kilometres from Laxemar.

At least two more high temperature hydrothermal mineralization events can be recognised that correspond to brittle fracturing with prehnite to zeolite facies assemblages (Events 4 and 5, Table 3-1). Most of the fractures in the Laxemar-Simpevarp-Äspö area were formed during these pre-Palaeozoic events, and most of these have been reactivated. Calcite mineralization associated with these fracture events is characterised by hydrothermal stable isotope signatures with relatively high $\delta^{13}C$ values (-7 to -2 ‰ PDB) and low $\delta^{18}O$ values (<-17 ‰ PDB), and with Sr concentrations usually > 200 ppm.

Large parts of the Fennoscandian Shield were covered with marine sediments and subsequent molasse sediments during the Palaeozoic. These are estimated to have attained a thickness of 3 to 4 km in the Äspö/Laxemar area (Tullborg et al 1996; Larson et al., 1999). The sedimentary cover remained for at least 400 Ma, although from the Carboniferous-Permian era and onwards it was successively reduced until finally being removed probably during the late Tertiary or early Quaternary (Lidmar-Bergström, 1996). The ambient temperature of the rocks now at the present surface is estimated to have been between 100 and 150 °C during maximum burial in the Palaeozoic. This facilitated the formation of clay minerals, possibly low-temperature zeolites, and calcite (Event 6, Table 3-1). Pyrite, and possibly some gypsum mineralization (now largely dissolved and removed), was also formed during this period.

Subsequent low temperature mineralization is dominated by calcite (with some pyrite) at depth, and close to the surface by Fe-oxyhydroxide related to the percolation of oxidizing meteoric groundwater alteration (i.e. weathering) (Event 7, Table 3-1). Formation of Al silicates like clay minerals is probably very slow, and although recently formed clay minerals possibly exist in very small amounts (based on observations from previous studies by Bath et al. (2000), and references therein), it has not been possible to document these during this present study. The present groundwater conditions are interpreted to be reducing and calcite-saturated below 50-100 m, based on the presence of late-stage pyrite and calcite in open hydraulically conductive fractures (Tullborg 1997).

Reactivation of fractures is very common in the Äspö-Laxemar area, and the present- water-conducting features usually have a very long history. This started with ductile to semi-ductile deformation, followed by later brittle reactivation events during which hydrothermal activity and subsequent low-temperature mineralization produced a sequence of clay minerals and other low temperature minerals. The outermost (youngest) mineral coatings on the walls of open (potentially hydraulically-conductive) fractures consist mainly of clay minerals, including: illite and mixed layer clays (corrensite – an ordered 1:1 interstratified chlorite-smectite, and randomly interstratified illite-smectite); together with calcite and minor pyrite. It is assumed this mineralization (especially calcite and pyrite formation) is an ongoing process, although the amount of possible recent precipitate is low.

3.2.3 Earlier studies on the origins of the calcite mineralization

Since the hydraulically conductive fractures in the area have been reactivated, and several generations of calcites are commonly found together in the same vein, the separation and characterization of each generation of calcite is one of the critical tasks in the palaeohydrogeological investigations using calcite. Earlier studies (e.g. Tullborg ,1997; Milodowski et al., 1998b; Tullborg et al., 1999; Wallin and Peterman 1999; Bath et al., 2000) showed that compositional and isotopic zoning is very common, and the amount of low temperature calcite present in a given fracture is relatively small compared to the volume of old hydrothermal calcite. Bulk analyses of stable carbon and oxygen isotopes proved useful for the

general differentiation of end-member components within mixtures of different generations of mineralization. Calcites belong to "end-members" of stable carbon and oxygen isotopic ranges were identified, and also analysed for Sr isotope and trace element composition where sufficient material was available. A subset of these samples was then selected for detailed petrographical and microchemical investigation by SEM, cathodoluminescence and electron microprobe techniques, to characterize the calcite growth morphology and its compositional variation and zoning. This integrated approach that was used for the earlier EQUIP study (Bath et al., 2000), and combined with previous calcite analyses (e.g. Tullborg ,1997; Tullborg et al., 1999 and Wallin & Peterman 1999) allowed the differentiation of 6 calcite generations/calcite types precipitated in different environments:

Type 1: Calcite with low Sr content (<100 ppm), high La/Yb ratio, variable content of Mn and Ba, $\delta^{13}C$ values usually between -7 to -15‰, and $\delta^{18}O$ in the range of -7.5 to -10 ‰. This calcite type is most common in the upper 50-100 m of the bedrock but also exists down to 1000 m. The interpretation is that this is low temperature calcite precipitated from fresh water isotopically similar to present-day meteoric water. The few morphological observations made so far indicate that it corresponds to dominantly c-axis-flattened ('nailhead' morphology) type calcite (Milodowski et al., 1998).

Type 2: Calcite with $\delta^{18}O$ in the range of -3 to -6 ‰, usually low to very low $\delta^{13}C$ values (some <-30 ‰) and high Mn, La and Ba contents. This calcite has been interpreted as precipitated at low temperatures from water of Baltic Seawater composition during conditions of high biogenic activity. It is found down to a depth of approximately 500 m and may be partly of postglacial age. This calcite is often associated with pyrite, which may imply that sulphur-reducing bacteria have been active in the bedrock aquifer causing breakdown of organic material to bicarbonate under reduction of sulphate to sulphide.

Type 3: Calcite with $\delta^{18}O$ values close to 0 ‰ and low $\delta^{13}C$ values, (down to -24‰) indicates conditions of biogenic activity and is found down to a depth of 300 m. Its composition is consistent with calcite that may have precipitated from oceanic seawater entering into the bedrock. This calcite may be as young as the Eemian (117,000 to 130,000 years BP), which was the latest time that the Baltic region maintained full oceanic circulation, but it could also be considerably older [Since that time, the waters of the Yoldia Sea stage (11,500 to 10,800 years BP), Littorina Sea stage (6,500 to 5,000 years BP) and Baltic Sea (present) have been much more diluted (brackish), and isotopic composition will have been strongly influenced by waters draining the surrounding landmass].

Type4: Calcite with $\delta^{18}O$-values between -10 to -15 ‰ characterised by low trace element contents and precipitated at low biogenic activity ($\delta^{13}C$ between -5 to -15 ‰). This could be interpreted to represent calcite precipitated from cold climate meteoric water (glacial component?). If so, this calcite must be older than 13 000 years, since the area was deglaciated from that time. This calcite may occur at depths down to 1000 m.

Type 5: Calcite with high Mn content (0.25 to 1.5 %) and enriched in Sr (100 to 250 ppm), and often with c-axis elongated ('scalenohedral' shaped) crystals (indicating precipitation from saline water cf. Milodowski et al., 1998a). $\delta^{18}O$-values typically between -14 to -18 ‰, and $\delta^{13}C$ between -10 and -17 ‰. This calcite is rich in fluid inclusions, and the few microthermometric observations made indicate high salinity and homogenisation temperatures around 100 °C. This calcite is interpreted to be older than Late Mesozoic (>100 Ma) and younger than 1400 Ma, and a possible origin is as a precipitate from warm brine water.

Type 6: Calcite with high Sr content (300 to 900 ppm) and low Ba, Mn and REEs contents. It usually shows intense twinning. The $\delta^{18}O$-values are typically lower than -15 ‰ and the $\delta^{13}C$-values relatively high (-2 to -7 ‰). The high Sr content and low $^{87}Sr/^{86}Sr$ ratio, indicate that the calcite formed early in the geological history of the bedrock, during one or several events that was probably associated with the liberation of Sr during hydrothermal alteration

of plagioclase. This type of calcite is present in less conductive and sealed fractures throughout the sequence from the surface to >1000 m, although it is more common at depth. It is Proterozoic (>700 Ma) in age and probably older than 1400 Ma. This calcite is usually associated with epidote, quartz, adularia and fluorite.

Occurrences of low temperature calcite types 1 to 4 decrease with increasing depth, whereas hydrothermal calcite of type 6 and to some extent calcite of type 5 increase with depth. Calcite generations of type 5 and 6 constitute the thickest precipitates (millimetre-scale coatings), whereas the low temperature calcite constitutes extremely thin coatings or overgrowth rims (sub-millimetre scale thickness) seeded on older hydrothermal calcite precipitates. Reliable definitive age determinations of the low temperature precipitates are therefore very difficult to obtain because of the problem of inheritance of an older age signature from contaminant inclusions of the more dominant host calcite which is often intimately entrained within the later calcite.

It is remarkable that low temperature calcites precipitated from brackish and marine water are only found down to depth of ca 500 m, whereas calcites with meteoric/cold climate recharge signatures can be traced to greater depth, possibly as deep as 1000 m. This might be explained by the differences in hydraulic head when waters were recharged under different environmental conditions. During periods when Äspö and Laxemar were covered by sea (brackish or oceanic environment) the lack of a hydraulic driving force would not have allowed deep penetration of marine water. The penetration by marine water would have been largely determined by the difference in density of the invading water and the background porewater already in the rock. In contrast, when the area was raised above sea level the enhanced hydraulic gradient would encourage recharge to greater depths. The topography (with higher elevations at Laxemar and lower at Äspö) would be expected to influence the hydrogeological environment at these two areas, differently. This is also indicated in the mineralogical data, which show that calcites with meteoric signatures can be traced to greater depth at Laxemar than at Äspö.

3.2.4   Observations from PADAMOT

3.2.4.1 DISTRIBUTION AND MORPHOLOGICAL CHARACTERISTICS OF LATE-STAGE CALCITE

Earlier studies by Milodowski et al. (1997, 1998a, 2002) and research during the EQUIP project (Bath et al., 2000) demonstrated that the distribution of late calcite mineralization coincided closely with present-day groundwater flow paths in much of the site, and could be used to identify flow zones. Furthermore, these studies had indicated that the calcite crystal morphology varied systematically with groundwater salinity. Some limited observations of the morphology of late-stage calcite from the Äspö site were made during the EQUIP project. These identified variations in crystal morphology that might reflect variations in present and/or past groundwater chemistry. Based on the experience from Sellafield, a similar study of fracture mineralization in the Tono Granite in Japan also indicated relationships between the morphology of late calcite mineralization and isotopic composition that suggested that saline groundwater was once present at this site (Iwatsuki et al., 2002). One of the objectives of the Swedish PADAMOT studies in the Äspö-Laxemar area was to further test and validate the applicability of using late calcite morphological and distribution information as a palaeohydrogeological tool for tracing past fluid flow, and as an indicator of groundwater chemistry, in fractured crystalline rocks in Sweden. Therefore, in contrast to the EQUIP project, the PADAMOT investigations based the selection of samples of calcite for isotopic characterization on the identification of late-stage calcite and have evaluated the analytical results by differentiation of these samples by their morphological characteristics. The primary idea has been to use the calcite morphology as a tool to select late calcites that potentially have precipitated from different water types.

3.2.4.1.1 Mapping of potential flowing fractures (PFFs) in Laxemar borehole KLX01.

Potentially open fractures in drill core from Laxemar borehole KLX01 were carefully examined using a binocular microscope. Evidence was sought for coatings of late euhedral calcite, which would indicate growth into open pore space, and therefore indicate that the feature was a potentially flowing fracture (PFF). The occurrence and morphological characteristics of the late calcite were systematically recorded and mapped in the core by Terralogica AB and the BGS, and are detailed in Appendix 5.

A total of 161 PFFs were recorded in the two examined sections, from 0-330 m and 840 to 950 m. No observations were made between 330-840 m due to time constraints. Most of these fractures contain calcite, chlorite and clay as the outermost (i.e. latest) coating, and many also contained minor to trace amounts of very fine-grained pyrite resting on the fracture coating. This suggests that much of the pyrite is relatively late in the paragenesis, and closely associated with the late calcite. In approximately 50 % of the logged fractures it was possible to define the calcite morphology macroscopically or under the binocular microscope. These observations revealed a variety of crystal morphologies, with c-axis flattened ('nailhead'), equant (granular) and c-axis elongated (scalenohedral) crystal forms.

3.2.4.1.2 Morphological characteristics of late calcite

Based on the core-scale logging of PFFs, 39 samples were selected for detailed SEM studies to characterise minerals coating fracture surfaces and to refine the definition of calcite morphology. This work was carried out at BGS, Keyworth. The observations are summarised below

Previous observations from Sellafield (Milodowski et al., 1998a) and limited results from Äspö (Milodowski et al., 1998b) showed a systematic variation in morphology with depth and present-day water chemistry. At this site, c-axis elongated calcites (e.g. 'scalenohedral' or 'dog-tooth' shaped crystal) were correlated with precipitation from saline water; whereas c-axis flattened forms (e.g. 'nailhead' shaped crystals) indicated a fresh water origin. Equant or granular calcite may represent brackish water or a transition zone between fresh and saline. However, observations from the core mapping of borehole KLX01 and subsequent detailed SEM morphological characterization showed an irregular variation in late calcite crystal morphology versus depth (Appendix 5, Table 3-2, Figure 3-14).

The late calcite typically occurs as doubly-terminated euhedral crystals resting directly on the host rock surfaces or on earlier chlorite, quartz or feldspar mineralization. Additionally, it forms syntaxial overgrowths seeded on earlier calcite mineralization. Usually the older vein calcite is re-fractured or sheared and slickensided, and the late calcite overgrowths line the cavities of small 'jogs' created by fracture reactivation. However, there is no evidence that late calcite has been damaged by tectonic movement.

The calcite morphology in the upper part of the borehole is very variable, with alternations between c-axis flattened, equant and c-axis elongated crystal forms. Above about 50 m the late calcite is dominantly c-axis flattened (freshwater-type by analogy with Sellafield). Sub-equant, equant and elongated crystal forms dominated in the interval 60 to 212 m with a few observations of short c-axis type calcites (at around 89 m, 124 m and 152 to 154 m), with the abundance of c-axis elongated calcite reaching maximum towards the base of this interval between 167 to 212 m. This would imply (by analogy with Sellafield) that calcite precipitated from generally more saline groundwater in this interval, but with considerable variation in salinity between different fracture sets.

Within a highly fractured section between 204 and 240 m fresh, brackish and saline water-type calcite morphologies were found in the same zone, although not necessarily in the same fracture. Again, this would suggest that this zone has been water conducting during quite different hydrogeochemical conditions, and also that the fresh and saline groundwater interface may have fluctuated through this zone in the past. Below 240 m the calcite morphology is again dominated

by the c-axis flattened forms, which may indicate a return to precipitation from fresher groundwater conditions.

The interval examined between 840 to 950 m deep intersects a steep fracture zone. The fractures are mainly coated with thin veneers of mostly euhedral calcite. In this zone the crystal morphology is dominated by *c*-axis flattened to equant forms (c:a <1) (cf. (Appendix 5, Table 3-2, Figure 3-14). By analogy with Sellafield (Milodowski et al., 1998a; Bath et al., 2000) this type of calcite is interpreted as providing a strong indication that fresh water penetrated to this depth some time in the past. This contrasts with the saline groundwater now present at this depth (9180 mg/L – 11 200 mg/L Cl), which (by analogy to previous Äspö and Sellafield observations) is expected to produce *c*-axis elongated calcite.

SEM studies revealed that several of the PFFs contain coarse euhedral calcite crystals with later very fine euhedral calcite resting on top of the earlier euhedral calcite, rather than forming a syntaxial overgrowth (e.g. at 42.9, 153.5, 187.36, 255, 910 and 939 m. This suggests that there have been two discrete generations of late-calcite development. In some cases, the morphologies of two generations of calcite are similar (i.e. largely c-axis flattened, Table 3-2). However, changes from short c-axis (coarse calcite) to equant (fine calcite) were observed in features at 153.5 and 939 m, suggesting a very slight increase in salinity between the two generations. Conversely, a change from elongate to equant morphology was observed between the early coarse and later fine calcite at 187.36 and 910 m, implying a decrease in salinity over the time during which late calcite has formed in these fractures. At 187.36 m the calcite was also observed to form the early stages of nailhead shaped overgrowths at the tips of older c-axis elongate calcite (Figure 3-15). In this feature, the earlier generation of calcite is corroded and in places separated from the later calcite by traces of smectite. This suggests that there was a discrete break between the two different stages of late calcite growth, during which the groundwater was undersaturated with respect to calcite (i.e. causing calcite dissolution, associated with very minor clay precipitation).
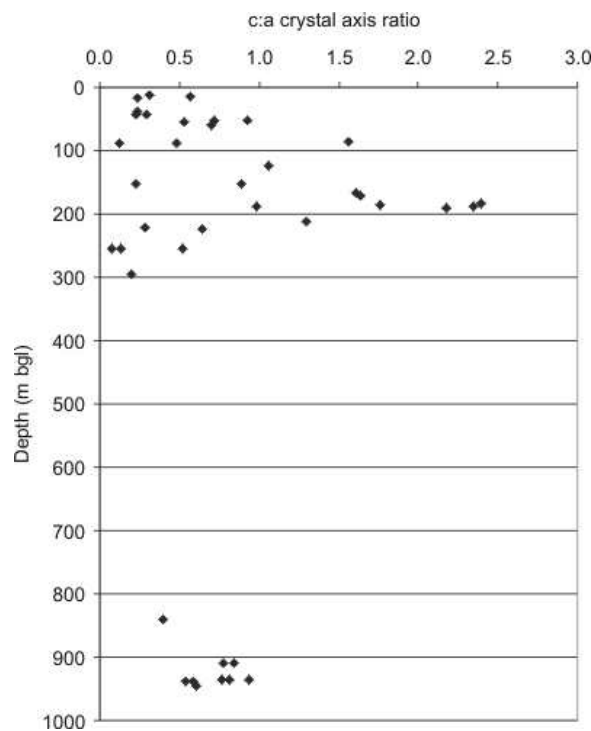
Figure 3-14. Plot of the variation with depth in the crystal morphology of late-stage calcite, observed by SEM, from the Laxemar borehole KLX01.

Table 3-2. Summary of morphological characteristics of late-stage calcites observed by SEM, from Laxemar borehole KLX01.

Sample No	Depth (m)	Mean c:a crystal axis ratio	stand. dev.	Morphology	Comment
MPLJ521	11.80	0.31	0.56	c-axis flattened	
MPLJ522	13.17	0.57	0.39	c-axis flat to sub-equant	2 crystals only measured
MPLJ523	13.95	not det..	-	c-axis flat to sub-equant	Grass pollen inclusions
MPLJ524	17.08	0.24	0.13	c-axis flattened	
MPLJ527	37.35	0.24	0.10	c-axis flattened	
MPLJ528	42.90	0.29	0.12	c-axis flattened	Later, very fine calcite
MPLJ528	42.90	0.23	0.11	c-axis flattened	Earlier very coarse calcite
MPLJ529	51.30	0.72	0.37	c-axis flat to sub-equant	
MPLJ530	52.00	0.93	0.11	equant	Overgrowths on old calcite
MPLJ531	55.00	0.53	0.19	c-axis flattened	
MPLJ532	60.00	0.70	0.08	c-axis flat to sub-equant	
MPLJ535	86.70	1.56	0.41	equant to c-axis elongate	
MPLJ536	87.20	0.48	0.41	equant and c-axis flattened	Very variable morphology
MPLJ553	88.95	0.12	0.04	c-axis flattened	Platy calcite in 'pockets' in slickensides
MPLJ537	123.92	1.06	0.06	equant	
MPLJ538	153.50	0.89	0.10	equant	Later, very fine calcite
MPLJ538	153.50	0.23	0.03	c-axis flattened	Earlier very coarse calcite
MPLJ540	167.03	1.61	0.50	c-axis elongate	
MPLJ541	172.25	1.64	0.41	c-axis elongate	
MPLJ543	182.60	2.39	0.44	c-axis elongate	
MPLJ544	186.25	1.76	0.05	c-axis elongate	Coarse, doubly-terminated crystals associated with harmotome
MPLJ545	187.36	0.98	0.45	equant	Later, finer crystals resting on earlier coarser crystals
MPLJ545	187.36	2.35	0.62	c-axis elongate	Earlier, coarser crystals
MPLJ546	189.90	2.18	0.72	c-axis elongate	
MPLJ547	212.45	1.30	0.31	sub-equant to c-axis elongate	
MPLJ548	220.58	0.28	0.09	c-axis flattened	
MPLJ549	223.90	0.64	0.16	c-axis flat to sub-equant	
MPLJ550	255.00	0.52	0.29	c-axis flat to sub-equant	
MPLJ551	255.00	0.13	0.06	c-axis flattened	Later, very fine calcite
MPLJ551	255.00	0.08	0.01	c-axis flattened	Earlier, platy coarse calcite
MPLJ552	294.35	0.20	0.10	c-axis flattened	
MPLJ554	840.00	0.40	0.14	c-axis flattened	
MPLJ555	910.20	0.78	0.17	c-axis flat to sub-equant	Weak overgrowths on sheared earlier vein calcite
MPLJ555	910.20	0.84	0.09	sub-equant	Fine well-developed doubly terminated crystals
MPLJ556	936.30	0.77	0.15	c-axis flat to sub-equant	Well-developed doubly terminated crystals resting on sheared old calcite
MPLJ556	936.30	0.94	0.10	equant	Overgrowths on sheared old calcite
MPLJ557	936.80	0.81	0.11	c-axis flat to sub-equant	Well-developed, doubly-terminated crystals
MPLJ558	939.00	0.59	0.07	c-axis flat to sub-equant	Coarse, earlier, doubly-terminated crystals
MPLJ558	939.00	0.54	0.05	c-axis flat to sub-equant	Later, overgrowths and fine doubly-terminated 'nailhead' crystals
MPLJ559	945.34	0.61	0.08	c-axis flat to sub-equant	Overgrowths seeded on old calcite
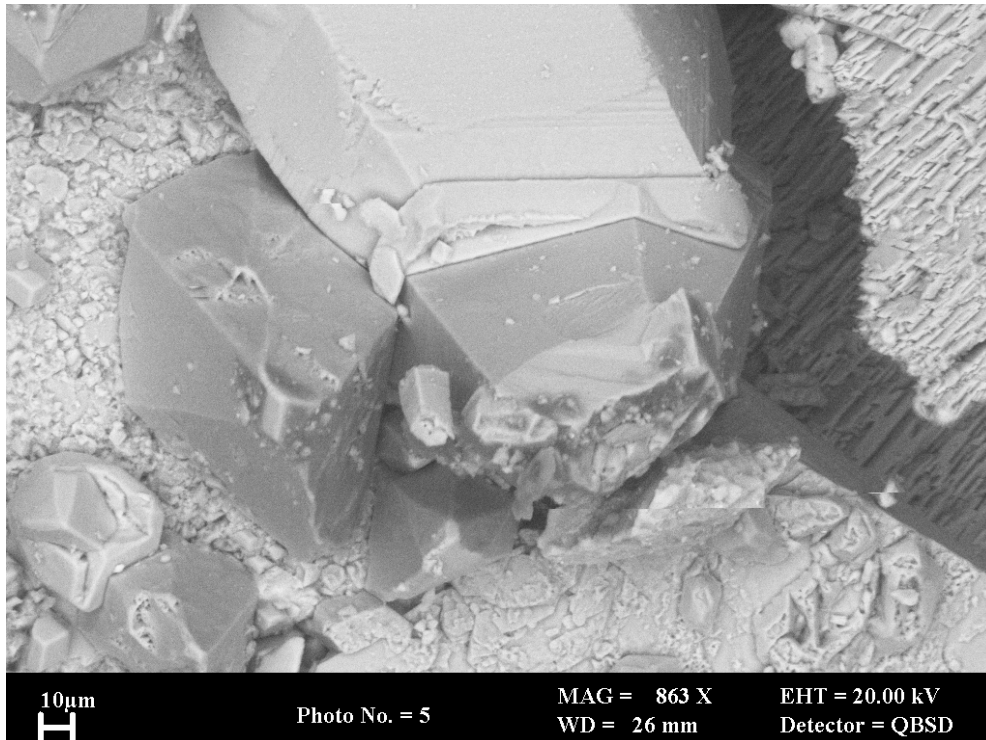
Figure 3-15. SEM image showing overgrowth of short c-axis ('nailhead') calcite developed at the tip of an older generation of c-axis elongated ('scalenohedral') calcite. Late-stage calcite, KLX01, 187.36 m

In some cases, it was not possible to define the morphological characteristics of the late calcite overgrowths due to several factors:

- Where the calcite has grown as a thin film in a very confined fracture space, the calcite virtually fills the space adopting the shape of the fissure. In this case, euhedral faces are limited in development, and are only observed where very minor residual space permits. Consequently, the symmetry and crystallographic forms of the calcite cannot be identified.

- Many of the syntaxial calcite overgrowths are very fine and usually they are volumetrically small compared to the older calcite substrate. Initially, overgrowth calcite tends to adopt the form of the underlying calcite on which it is seeded. If these overgrowths are only weakly developed, their external morphology is inherited from, or dominated by, that of the parent calcite substrate. Often the late overgrowths are manifested simply as limited 'steps' on the faces of parent calcite.

- Core quality and the degree of preservation. Core observations show that many fracture surfaces have suffered abrasion, either as a result of core 'spinning' during drilling or through subsequent movement during core handling. Calcite is soft, and small crystals grown on open fracture surfaces are very delicate and are easily destroyed during drilling and subsequent handling of the drill cores.

The overall impression is that crystal morphology is very variable in the upper part of the borehole but in general shows an overall change from c-axis flattened near the surface, through equant forms, to c-axis elongated crystals by 200 m depth (Figure 3-14). Between 200 and 300 m the morphology rapidly changes back to c-axis flattened calcite.

If the calcite morphology–groundwater chemistry relationship seen at Sellafield is applicable to Laxemar, then these observations would suggest that the late calcite mineralization preserves a palaeosalinity profile showing a general increase in salinity from the surface ('freshwater') to

72

about 200 m depth ('saline/brackish'). The palaeosalinity profile then rapidly changes back to a 'freshwater' character below 200 m. At depth (below 840 m), the palaeosalinity recorded by the calcite morphology has 'freshwater' characteristics. There is some locally-preserved evidence of 'freshwater-type' calcite superseding more 'saline-type' calcite, which may indicate that saline waters have been flushed or displaced by freshwater at this depth in the past.

3.2.4.1.3 Other minerals and features in PFFs

Detailed SEM observations also revealed the presence of barrel-shaped euhedral crystals of the Ba-zeolite harmotome lining the fracture surfaces in discrete intervals, at 20-30 m depth and at 159 m (Figure 3-16).   Harmotome has also been identified in the recent site investigation borehole KSH01A at the nearby Simpevarp peninsula (Drake & Tullborg 2005).   Harmotome has been recorded from fractures about 10 times so far in this area, all from above 300 meters depth but from different boreholes. Harmotome is a low temperature zeolite that forms under warm hydrothermal conditions, and may be related to the "warm brine"-type calcites. As such, the mineralization is probably of Palaeozoic origin (cf. Table 3-1).
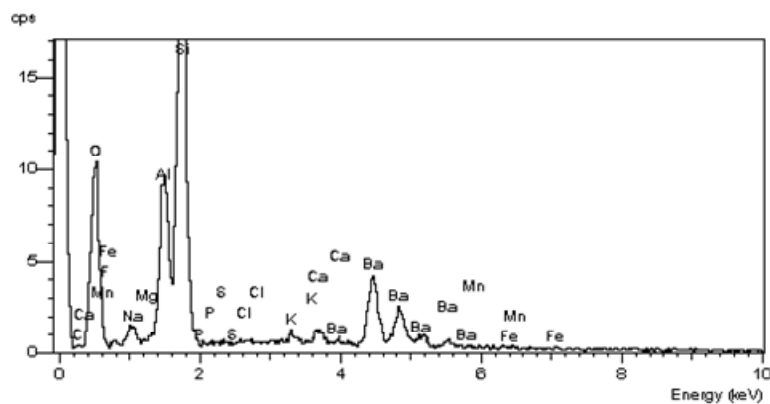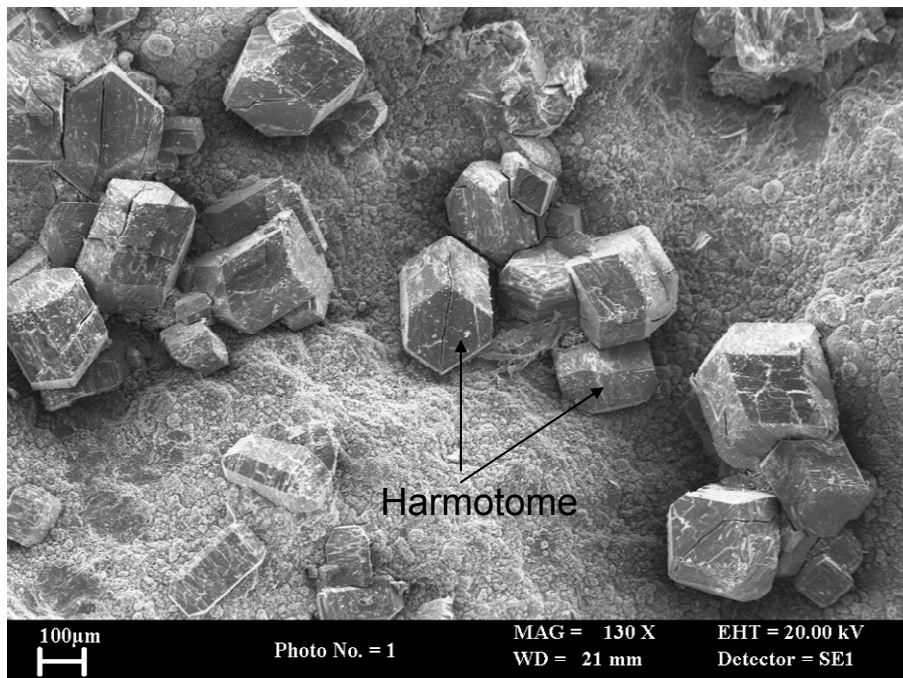
Figure 3-16.   (top) SEM image of euhedral harmotome crystals resting on a fracture surface covered with fine colloform chlorite; (bottom) EDXA spectrum of harmotome showing composition dominated by Ba, Al, and Si with minor Na, K and Ca also present. Sample KLX01, 159.32 m.

73

Both core-scale and SEM observations showed that fine (1-10 μm) octahedral and cubic crystals of pyrite, or more rarely as tiny dendritic 'planar florets' of iron sulphide (possibly marcasite) up to 1 mm diameter, are occasionally present with the late calcite, particularly in fractures between 11-152 m, and 205-327 m. These usually rest on the open fracture surface, either directly on the wallrock or coating substrates of earlier chlorite mineralization, and may be coeval with the late calcite. Pyrite appears to be less common in the deeper section examined in the borehole, but was observed in fractures at 909, 910 and 936 m. Traces of fresh pyrite also occur intergrown with earlier hydrothermal silicate minerals (chlorite, quartz, feldspar) or within the granitic host rock, and in these cases it must be paragenetically old. This earlier pyrite sometimes forms crystals up to 200 μm across.

Minor to trace amounts of smectite (or illite-smectite mixed-later clay) is sometimes associated with the PFFs. It has been observed mainly in fractures between 11 to 90 m deep but traces of smectite were also observed between 250 to 295 m, and 910 to 939 m depth. The smectite forms very thin structureless films, or occurs as clusters of 'cornflake-like' platelets or 'cabbage-like' fine aggregates of clay platelets (containing Mg, Al, Ca, ±Fe, ±K), resting on the host rock or on the reactivated surfaces of earlier chloritic veins. In most cases smectite pre-dates the late calcite, which generally rests on top of the clay coating (where present). However, at 910 m smectite was observed coating corroded crystals of coarse euhedral c-axis elongated calcite, with later fine equant to c-axis flattened calcite resting on the smectite (sample KLX01 910). This suggests that there are at least two separate generations of 'late' euhedral calcite mineralization, separated by an episode of calcite dissolution and very minor clay (smectite or illite-smectite) mineralization. The morphology of the earlier calcite would be consistent with formation from a more saline fluid, whereas the later calcite is more typical of precipitation from freshwater.

Traces of goethite were observed, as a late-stage alteration product in only one fracture, near the top of the borehole at 14.13m.
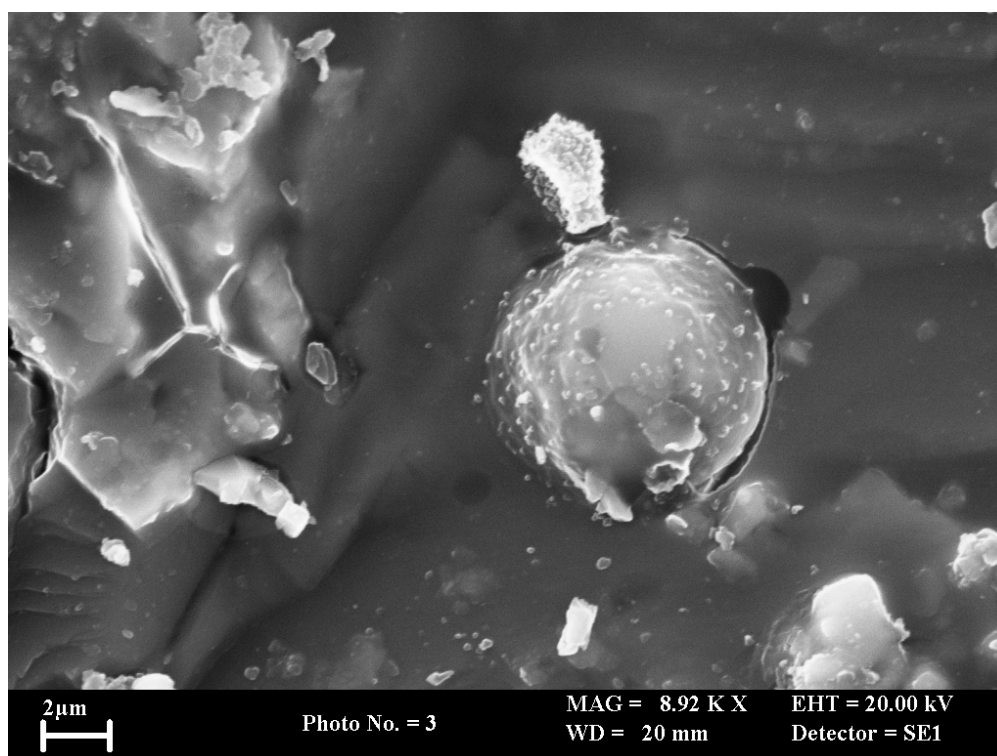
Figure 3-17. SEM image showing a grass pollen grain (ca 5 μm in diameter) enclosed within late-stage fracture calcite at 14 m depth. Sample KLX01: 13.95 m.

74

Rare pollen grains (probably from grass) have been identified as inclusions trapped within the late-calcite in one sample from KLX01 at 13.95 m (Figure 3-15). Although this does not provide an absolute age, it demonstrates that the calcite must be quite young and certainly much younger than the low-temperature hydrothermal mineralization associated with Palaeozoic burial (Event 5, Table 3-1), since grasses did not appear until the Palaeogene (Tertiary). This also clearly indicates that downward transport of organic material from the surface soil zone has occurred, probably during the Quaternary.

3.2.4.2 CATHODOLUMINESCENCE PETROGRAPHY

CL petrography was carried out at the BGS on a subset of 13 samples from the Laxemar borehole KLX01 (Table 3-3), and is described in detail by Bouch (2004). A brief summary of the CL observations is presented here.

The fractures contain calcite whose CL characteristics are largely consistent with those of 'Calcite generations 2 and 3' as described previously by Milodowski et al. (1998b; Table 3-4), with evidence for significant fracture rejuvenation, reworking, brecciation and replacement and cementation by later calcite generations. These correspond with calcite mineralization associated with Fracture Events 6 and 7 (Table 3-1), respectively. Generation 1 of Milodowski et al. (1998b), which corresponds with Fracture Event 5 (Table 3-1) was not encountered and generation 4 (Fracture Event 7, Table 3-1) was only tentatively identified in one sample (KLX01, 13.95 m). The CL observations carried out during the PADAMOT project have enabled a refinement of Milodowski et al.'s (1998b) calcite cement stratigraphy scheme with the recognition of 4 distinct sub-generations within 'generation 3' (Table 3-5; Figure 3-18). These generations are primarily recognised on the basis of their CL responses, supported by evidence from electron microchemical maps (not reported here). It should be noted that the different generations of calcite identified and referred to here in the CL stratigraphy are not the same as the different types of calcite differentiated on the basis of their stable isotope compositions (Section 3.2.4.4).

Table 3-3. Summary details for samples from KLX01 studied by CL and analysed for fluid inclusions.

Sample	Depth (m)	Supporting EPMA Microchemical Maps	Duplicate Standard Polished Thin Section	CL imaging (This Study)	Calcite Generations Present [1]	Fluid Inclusion Prospectivity	Fluid Inclusion Microthermometry	Number of Inclusions in Calcite with Data
MPLJ522	13.10		Y	Y	3	Poor	-	-
MPLJ523	13.95	Y	Y [2]	Y	3b, 3c, 3d, 4?	Good	Y	19
MPLJ527	37.35		Y	Y	2, 3b?, 3d?	Moderate	-	-
MPLJ529	51.30		Y	Y	2, 3b, 3d	Good	Y	20
MPLJ532	60.00	Y	Y [2]	Y	2, 3b?, 3c? 3d	Moderate	-	-
MPLJ538	153.50	Y	Y [2]	Y	3a	Moderate	Y	0
MPLJ546	189.90		Y	Y	2, 3a, 3b, 3d	Good	Y	25
MPLJ549	223.90	Y	Y [2]	Y	2, 3a, 3b	Moderate	Y	6
MPLJ551	255.00		Y	Y	unknown	Poor	-	-
MPLJ554	840.00	Y	Y [2]	Y	3a, 3c, 3d	Good	Y	17
MPLJ557	936.80	Y	Y [2]	Y	2?, 3a?, 3c, 3d	Moderate	-	-
MPLJ558	939.00		Y	Y	2?, 3a, 3b, 3c,3d	Moderate	Y	13
MPLJ559	945.34		Y	Y	2?, 3a, 3b, 3c,3d	Poor	-	-

[1] Calcite generation is a refinement (Table 3-5) of that presented by Milodowski et al. (1998b; Table 3-4).

Table 3-4. Summary of the calcite cement generations recognised under CL by Milodowski et al. (1998b).

CL generation (after Milodowski et al, 1998b)	Description	Timing
1	Bright yellow luminescence. Predates a late phase of quartz, local laumontite mineralization, and is deformed by later fracturing and shearing.	Either related to the later stages of hydrothermal circulation associated with the Götemar Granite (Event 4, Table 3-1) or a 1100 Ma regional low-temperature burial metamorphic event (Event 5, Table 3-1).
2	Moderate- to weak- brown-orange luminescence. Postdates laumontite mineralization and dissolution of earlier-formed epidote. This calcite is commonly deformed, brecciated, disrupted with most pronounced shearing observed in samples from below 800 m in the Laxemar boreholes.	There is evidence for corrosion of Calcite 2, prior to syntaxial overgrowth by Calcite 3. Calcite 2 may relate to fracturing and mineralization during post-Caledonian deep burial (Event 6, Table 3-1).
3	Weakly-luminescent, and forms euhedral overgrowths on earlier calcite with some relationship observed between morphology and present day groundwater chemistry, suggesting this calcite formed as part of Event 7 (Table 3-1).	In many of the samples studies by Milodowski *et al.* (1998a) this is the youngest calcite generation observed. Interpreted to be Quaternary or Recent in age.
4	Bright yellow luminescent, forming euhedral overgrowths on earlier Calcite 2/3, with morphological variations also reflecting the present day groundwater chemistry.	Interpreted to be Quaternary or Recent in age (Event 7 (Table 3-1).

Table 3-5. CL characteristics, distribution and summary fluid inclusion properties for calcite generations 2 and 3 distinguished by CL (PADAMOT project).

CL Generation	Description	Distribution	(n inclusions with data)	Salinities	Homogenisation Temperatures
2	orange luminescent, commonly disrupted by later calcite generations	best preserved in upper part of borehole (<255 m)	(15)	relatively low, high and very high salinity groups populations represented.	57.5-122°C no monophase
3a	moderate orange-luminescence (Figure 3-18A), commonly contains well-developed growth and/or sector zoning. Typically clear with only rare fluid inclusions.	throughout	(26)	high and very high salinities only	87.5-190°C common monophase
3b	similar in appearance to generation 3a commonly with well-developed growth and sector zoning, but has only dull-orange luminescence.	throughout	(40)	relatively low and very high salinity groups	53-195°C common monophase
3c	non- or very-dully luminescent (Figure 3-18B).	lower part of borehole (>840 m)	(8)	predominantly very high salinity	55-95°C no monophase
3d	variably bright orange-luminescence, which may resemble generations 3a or 3b.	throughout	(12)	high salinity only	92.5-145°C, no monophase
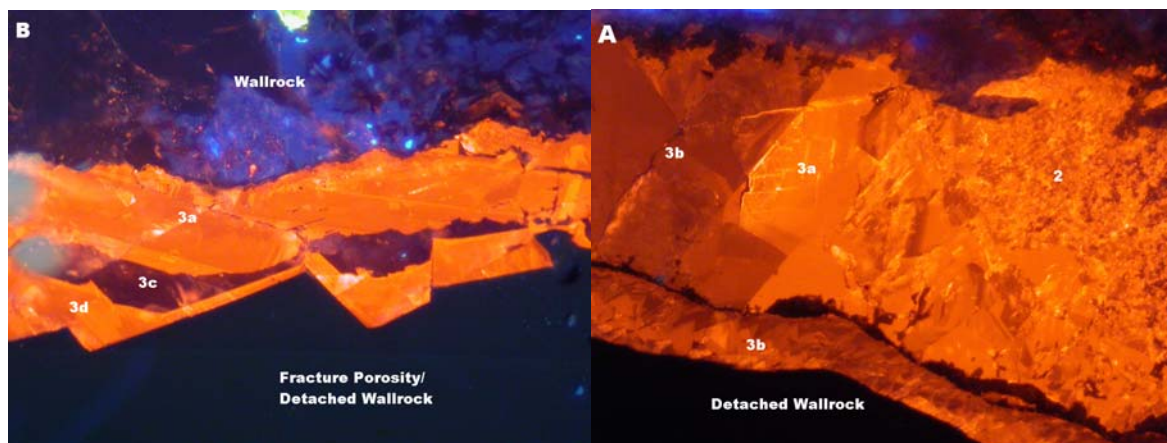
Figure 3-18. CL images showing the relationships between the different calcite generations differentiated under CL.

A) Calcite generation 2 is disrupted, and then overgrown by the moderately orange-luminescent calcite 3a. This is syntaxially overgrown by the less strongly orange-luminescent calcite 3b. Fracture re-activation occurred during the precipitation of calcite generation 3b with the development of a thin fracture parallel to the initial fracture, which is exclusively filled by calcite of generation 3b. Sample KLX01, 223.90 m (MPLJ549), field of view 1 mm.
B) Calcite 3a has an anhedral, fracture-filling morphology, and is interpreted to have completely filled the original fracture. This fracture was then reactivated and calcite generations 3c (non-luminescent) and 3d developed with euhedral morphologies as syntaxial overgrowths into the new porosity.

3.2.4.3 FLUID INCLUSION STUDIES

Fluid inclusion studies were carried out at the BGS on the same sub-set of 13 samples characterised by CL. The aim of this work was to collect fluid inclusion microthermometric data from the youngest generations of calcite in samples from KLX-01, in order to provide more detailed constraints on temperatures and groundwater chemistry during calcite formation than have been available previously. The fluid inclusion studies were limited to microthermometric analysis since no inclusions were found that were suitable for microchemical analysis. A detailed description of the methodology and approach employed is given in Bouch (2004). In summary:

- Following screening to identify workable inclusions, fluid inclusion microthermometry was undertaken on suitable areas ("regions of interest") extracted from doubly-polished fluid inclusion wafers.

- CL analysis prior to fluid inclusion analysis would have been a useful aid in the targeting of specific calcite generations for analysis. However, CL analysis causes significant heating of the sample that may cause inclusions to leak or decrepitate. Consequently, in order to get the best possible thermometric data, microthermometry was performed prior to the CL imaging, meaning that at the time of analysis the cement generation within which an inclusion occurs could not be determined.

- Attempts were made to collect temperatures of homogenisation (T_h for liquid + vapour bearing inclusions only), first ice-melting (T_{fm}), final ice-melting (T_{ice}) and hydrohalite-melting (T_{hyd}).

- CL imaging of the analysed regions of interest was undertaken retrospectively and the calcite generations containing the analysed inclusions were identified (using a refinement

of the paragenetic scheme established by Milodowski et al. (1998b; Table 3-4 and Table 3-5).

CL petrographical descriptions and images of the fracture fills, showing the positions of the analysed inclusions, are presented in Appendix 6, and a complete listing of the fluid inclusion data, including coding of inclusions by calcite generation, is also presented in Appendix 6.

All the analysed inclusions contain aqueous liquid and vapour, or an aqueous liquid phase only. No hydrocarbon-bearing inclusions were identified during screening using ultraviolet light. Individual inclusions are typically small (of the order of 10 μm diameter), and occur in small clusters and in less-common planes. Given the multiple generations of calcite present and the evidence for reactivation, brecciation, replacement and cementation of earlier generations, "resetting" of earlier-formed inclusions, and formation of new "secondary" inclusions in earlier cements would be expected. The fact that this has occurred is proved in situations where inclusions occurring in close physical proximity have different physical characteristics and/or markedly different salinities (Figure 3-19). Clusters (or "assemblages") of inclusions were not typically aligned in any particular orientation relative to crystal faces (where recognisable), and in most cases it proved impossible to definitively identify whether inclusions were of primary (i.e. formed during calcite crystal growth), pseudo-secondary or secondary (i.e. formed at some time after crystal growth, typically in healed microfractures) origin. However, it is considered likely that the majority of the analysed inclusions are pseudo-secondary or secondary in origin, and therefore the interpretation of the microthermometric data, particularly in the earlier cement generations, which may have "seen" later fluids, has to be treated carefully.
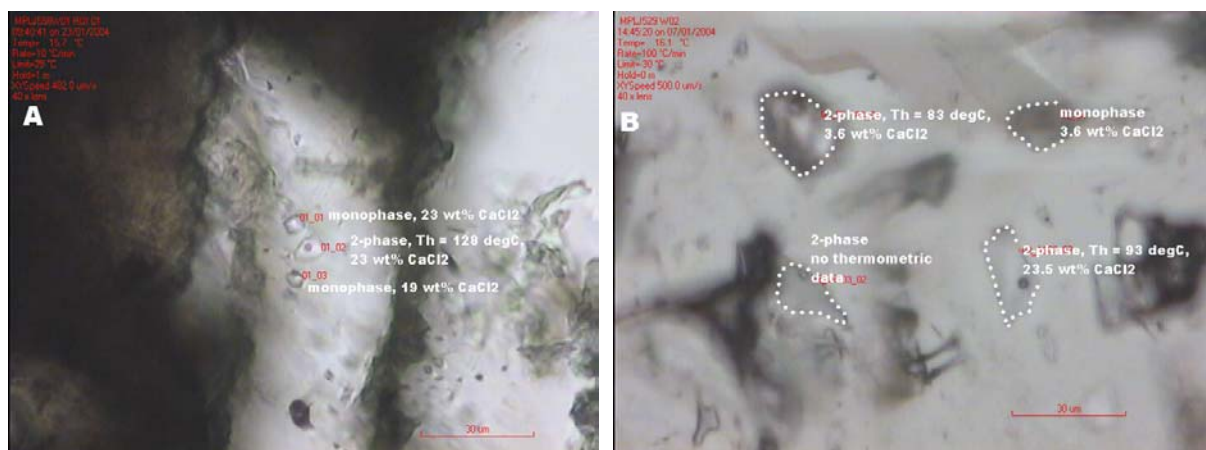
Figure 3-19. Transmitted light photomicrographs of two assemblages of fluid inclusions within which marked differences in physical characteristics and fluid chemistry are observed.
A) Sample KLX01 939.00 m (MPLJ558), inclusion assemblage 1, with a mixture of monophase and 2-phase inclusions and variable salinities (scale bar μm).
B) Sample KLX01 51.30 m (MPLJ529), inclusion assemblage 3, with a mixture of monophase and 2-phase inclusions and highly variable salinity (scale bar μm).

Microthermometric data were collected from 100 inclusions in calcite from six samples, with 84 T_{ice}, and 22 T_{fm} determinations (Bouch, 2004). 33 of the analysed inclusions were monophase at room temperature (no T_h measurement appropriate), and 59 T_h determinations were made on the 2-phase (liquid + vapour) inclusions. It proved impossible to collect any T_{hyd} data.

3.2.4.3.1 Homogenisation temperatures

Aqueous inclusions that are monophase (liquid-only) at room temperature are typically interpreted to indicate that the fluid was trapped at relatively low temperatures although this

interpretation is not always valid (Roedder 1984, see also discussion in Bouch, 2004). In the 2-phase inclusions, homogenisation temperatures are typically between 50-180 °C with a broadly-defined peak between 90-130 °C (Figure 3-20A). No systematic differences in T_h are evident between the samples (or with depth; Figure 3-21) or between the different calcite cement generations (Figure 3-20, Figure 3-21). However, monophase inclusions appear to be restricted to calcite generations 3a and 3b.

3.2.4.3.2 Fluid composition

Due to the low optical contrast between ice and liquid it proved impossible to determine any T_{fm} for the relatively low salinity inclusions and therefore the nature of the dissolved components in these fluids is unknown.

A number of T_{fm} determinations were possible in the more saline (>8wt % $CaCl_2$ equiv.) inclusions in all the calcite generations. These were all in the region -50 to -60 °C, which are probably indicative of mixed $NaCl$-$CaCl_2$-H_2O brine (with a eutectic, and hence T_{fm} expected at -52 °C). In order to estimate $NaCl$ / ($NaCl$+$CaCl_2$) ratios, and hence derive accurate salinity estimates in this system, determinations of T_{hyd} are required, which proved impossible to observe in these inclusions. However, some of the most saline inclusions (> 21 wt % $CaCl_2$ equiv.) have T_{ice} between -29 °C and -25 °C, which implies that $CaCl$ / ($NaCl$ + $CaCl_2$) ratios 0.5 or higher, indicating a predominance of $CaCl_2$ over $NaCl$ in these more saline inclusions.

In the absence of paired T_{hyd} and T_{ice} data, and given the inferred high $CaCl_2$ / ($NaCl$+$CaCl_2$) ratios of some of the most saline inclusions, salinities have been modelled for all inclusions in terms of wt% $CaCl_2$ equivalent, using the freezing point depression data of Oakes et al. (1990) for the system $CaCl_2$-H_2O. This will underestimate the salinity of inclusions with lower $CaCl_2$ / ($NaCl$+$CaCl_2$) ratios at higher salinities (>15 wt % dissolved salt), but is likely to provide reasonable salinity estimates for the lower salinity inclusions, where freezing point suppression is less sensitive to $CaCl_2$ / ($NaCl$+$CaCl_2$) ratios (cf. Bouch, 2004).

3.2.4.3.3 Salinity

Salinities are highly variable (range 0.8-23.9 wt % $CaCl_2$ equiv; Figure 3-20), but this range can be broken down into three components:

- A relatively low salinity (brackish) component (range 0-8 wt%, predominantly < 2 wt % $CaCl_2$ equiv). The dissolved species in this component have not been identified (see above).

- A high salinity component (approximately 16-20 wt % $CaCl_2$ equiv.), considered to be a $NaCl$-$CaCl_2$- H_2O-brine, but of unknown $CaCl_2$ / ($NaCl$+$CaCl_2$) ratio, and

- A very high salinity component (22-24 w % $CaCl_2$ equiv.) considered to be a $NaCl$-$CaCl_2$-H_2O-brine, with $CaCl_2$ / ($NaCl$+$CaCl_2$) ratio of >0.5.

3.2.4.3.4 Summary

In the shallower samples (<225 m), all three fluid components are observed in approximately sub-equal proportions in the fluid inclusion data, whereas in the deeper samples (>840 m) the relatively low salinity component appears to be of minor significance (1 inclusion only; Figure 3-21). There are also some differences in the salinities of inclusions hosted by the different calcite generations, with generations 2 and 3b containing both low and high salinity inclusions, generations 3a and 3c appearing to be dominated by high and very high salinity inclusions, and generation 3d containing high salinity inclusions only. No relationships were observed between inclusion salinity and homogenisation temperature.
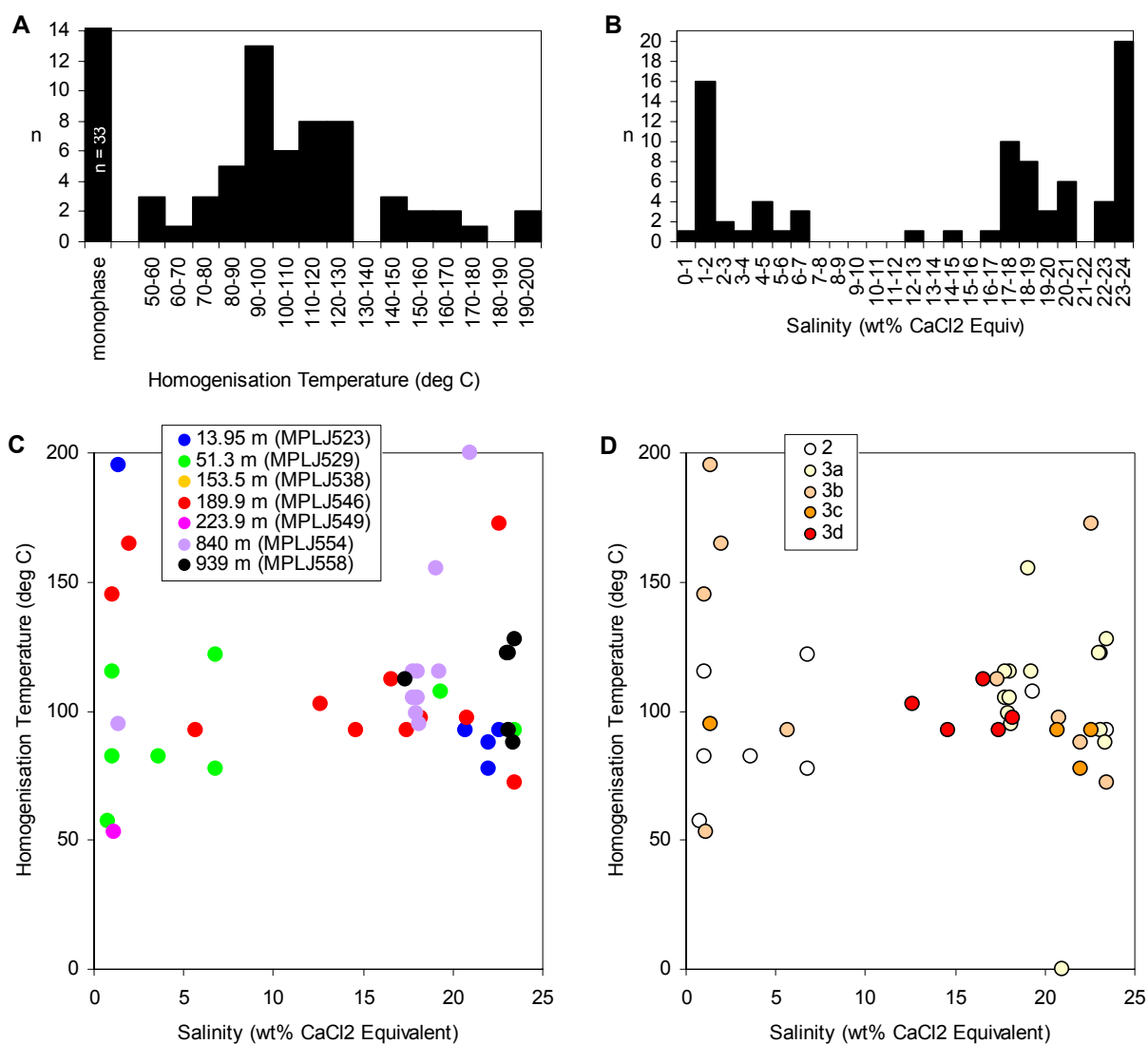
Figure 3-20. Frequency distributions (A and B) and cross plots (C and D) showing the fluid inclusion homogenisation temperatures and salinities for all samples. Note plots C and D do not include monophase inclusions (no T_h data).

One of the main limitations of this study has been the difficulty in assessing whether individual inclusions are of primary or secondary origin. This is particularly significant as the older calcite generations will have "seen" the fluids responsible for the precipitation of the younger generations, and hence, in addition to primary inclusions, these generations may also contain secondary inclusions that reflect the composition of younger fluids. This uncertainty is compounded by the possibility that calcite with similar CL characteristics may have developed in different samples at different times. As a result of these uncertainties, the available data are very noisy. However, some useful inferences can be made:

- Homogenisation temperatures are highly variable (53-195 °C), and significant proportions of monophase inclusions are also present (33 out of the 100 measured inclusions). Monophase inclusions are usually interpreted to represent trapping at relatively low temperatures, which here probably correspond with the lower end of the range of homogenisation temperatures measured for the inclusions containing liquid + vapour. No systematic variations in homogenisation temperature, or in the proportion of monophase vs. liquid + vapour bearing inclusions are observed with depth (note, however, that samples were only available in the intervals <255 m and 840-950 m).

80

- Salinities are highly variable, and three components are recognised:
  - fresh to brackish fluids (predominantly < 2 wt% $CaCl_2$ equiv), of unknown speciation,
  - a high salinity $NaCl$-$CaCl_2$-H_2O brine (approximately 16-20 wt% $CaCl_2$ equiv.), of unknown $CaCl_2$ / ($NaCl$+$CaCl_2$) ratio, and
  - a very high salinity $NaCl$-$CaCl_2$-H_2O brine (22-24 wt% $CaCl_2$ equiv.) with $CaCl_2$ / ($NaCl$+$CaCl_2$) ratio of >0.5.

- Some variations are evident in the character of inclusions from different calcite generations differentiated by CL (Table 3-5).
  - inclusions in CL generation 2 contain fluids of relatively low salinity and also of high salinity. This is perhaps not surprising given the extensive alteration, brecciation, replacement and cementation of this generation by later calcite generations. However, it is impossible to distinguish which, if either, of the saline or fresh inclusions are of primary origin,
  - CL generation 3a contains inclusions of high and very high salinity fluids, with no evidence of a fresh water component. This generation is recognised in samples from below 150 m, and is also characterised by relatively high proportions of monophase inclusions.
  - CL generation 3b contains both relatively fresh and very high salinity fluids, and is characterised by high proportions of monophase inclusions.
  - CL generation 3c contains predominantly very high salinity inclusions.
  - CL generation 3d contains high salinity inclusions only.

  - The presence of two phase inclusions in generations 3a-3d clearly shows that these calcites are of warm hydrothermal origin, and cannot be Quaternary, although they may act as seeds for later calcite overgrowth. The very high salinities measured also favour a "warm brine "origin.

- High and very high salinity brines appear to occur throughout the borehole, whereas the relatively fresh fluids are largely restricted to the shallower interval (only one inclusion containing fresh fluid was measured from below 840 m). In the adjacent Laxemar-2 borehole (KLX02), present day groundwaters are low salinity (<600 mg L^{-1} Cl) down to approximately 1000 m bGL, but below this there is a sharp transition zone with more saline groundwaters (up to 46000 mg L^{-1} Cl; Laaksoharju *et al.* 1999).

  The fact that high salinity fluids are trapped in calcite at relatively shallow depths (<255 m) suggests either that the transition zone between fresh and saline groundwater was shallower than at the present day during calcite precipitation, or the calcites are older than previously recognised and related to deep burial or hydrothermal circulation. There are a number of lines of evidence which support a young age for the calcite, which would suggest a shallower contact between the fresh and saline fluids:

  - the relatively low homogenisation temperatures and abundance of monophase inclusions in all calcite generations would suggest relatively cool conditions during calcite growth, and are inconsistent with hydrothermal conditions.
  - the restriction of relatively low salinity fluids to calcite generations 2 and 3b may indicate that the low salinity inclusions are, in general, recording older events than the high salinity inclusions.
  - Sr-isotope ratios in the youngest calcite generations correspond to the ratios in the present groundwater indicating a possible Quaternary age for these
  - possible grains of grass pollen trapped within the youngest calcite generations in a sample from KLX01 at a depth of 13.95 m (see above) imply that the youngest calcite must be younger than Palaeogene.
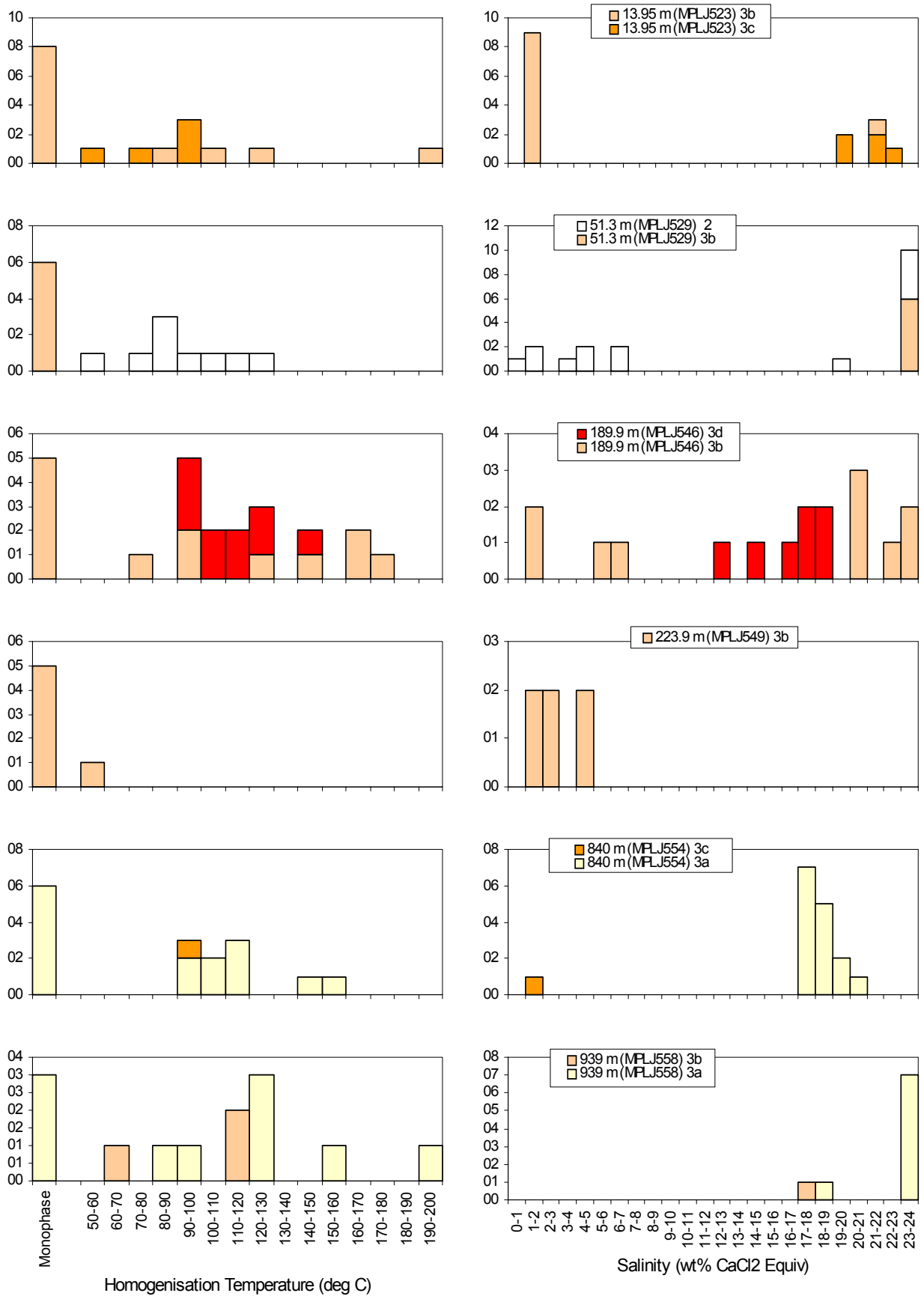
Figure 3-21. **Frequency distributions showing the variations in homogenisation temperature and salinity according to sample and calcite generation.**

Conversely, however, the high Ca:Na ratios inferred for the fluid inclusions are comparable with the Ca:Na ratios of deep saline groundwater at the Laxemar site (Na = 8500 ppm; Ca = 19300 ppm; total salinity ≈ 7 wt % . However, the salinities of these inclusions are much higher than the present deep saline groundwater. It might be possible that the deep saline groundwater at Laxemar represent a mixture between a residual old brine fluid, from which the calcite precipitated, and a much more dilute groundwater. On the basis of chlorine isotope data these deep saline groundwaters have been interpreted to have a minimum residence time of 1.5 Ma (Louvat et al., 1999). However, caution must also be exercised with regard to inferring the timing of the calcite mineralization from this information. If the calcite formed due to changes in environmental conditions such as temperatures, or owing to mixing with another water (e.g. inflow of a small component of meteoric water), it could be much younger than 1.5 Ma, but still carry fluid inclusions reflecting the chemistry of the brines. A possible explanation for this apparent paradox would be that the fracture calcite has been developing over a very long time period, and that the youngest generations, (from which the Sr-isotope data are derived) are not represented by the fluid inclusion analysis because the late calcite is barren of inclusions and inclusion data are derived largely from the old core regions of the calcite crystals.

3.2.4.4 STABLE ISOTOPE STUDIES (δ^{18}O AND δ^{13}C)

Stable isotope analyses (δ^{18}O and δ^{13}C) of small bulk samples of fracture calcite have been used in previous studies at Äspö to try to determine the origin of the mineralizing fluids (Tullborg et al 1991; Tullborg, 1997; Wallin and Peterman, 1999; Bath et al., 2000). This methodology was also used by Terralogica AB in the present study. However, sampling of calcite was refined and constrained by specifically selecting calcite on the basis of its crystal morphology characteristics (cf. Section 3.2.4.1). Where possible, calcite has been sampled from the outermost fracture coating in order to analyse the most recent mineralization rather than older hydrothermal vein mineral. The same approach has now been adopted in the ongoing SKB site investigation programme on Simpevarp peninsula, and the results from these studies have been combined with those from PADAMOT in order to produce a more representative data set. The δ^{18}O data shown in Figures 3-22 and 3-23, for the euhedral calcites examined from 250 m to 800 m, are derived from calcites analysed from the more recent Simpevarp drillcore KSH01 (Drake and Tullborg 2004).

Figure 3-22 presents a plot of the variation of δ^{18}O with depth for all of the analysed calcites from the Äspö/Simpevarp/Laxemar sites. Data from 46 samples of euhedral late stage calcites are included in this plot and are differentiated on the basis of the calcite morphology. These late calcites have δ^{18}O values ranging from -14 to -4 ‰ (PDB). Both scalenohedral and equant shaped crystals show large variations in oxygen isotope composition:

- Long c-axis ('scalenohedral') forms vary between -13.8 to –5.9 ‰ δ^{18}O that may indicate mineralization from a range of different saline waters of various isotopic compositions and/or under different temperature conditions. Alternatively, the data may indicate marked isotopic zoning within the calcite crystals.

- Equant calcite crystals display δ^{18}O values between -10.5 to -4.4 ‰, with eleven out of sixteen samples showing values in the interval -8.2 to -6.5 ‰. These isotopic compositions would be consistent with precipitation from brackish Baltic Sea-type water that could have intruded during some stage in the Quaternary.

Short c-axis ('nailhead') crystals display δ^{18}O values between -10.8 to -8.6 ‰. Their composition is close to equilibrium with the present groundwater (-10 ‰ (SMOW)) at ambient temperature (which would result in calcites around –9.5 to -8 ‰ (PDB)). This does not prove a recent origin for the calcites but is consistent with precipitation from a meteoric water of similar type to the present groundwater, or possibly from a somewhat cooler-climate meteoric water.
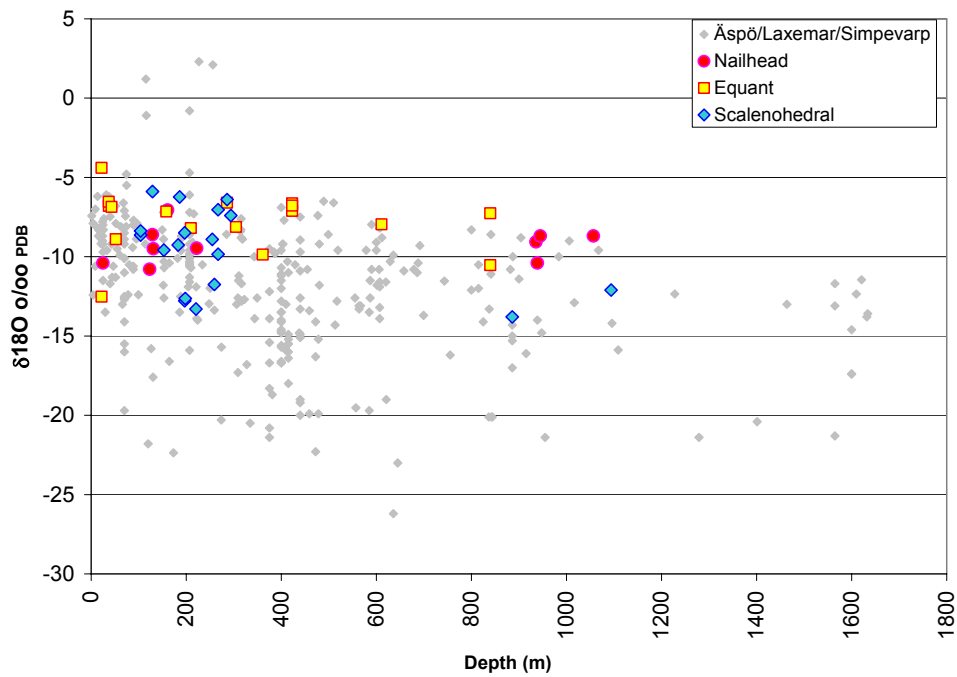
Figure 3-22. Variation of $\delta^{18}O$ with depth for all fracture calcites analysed within the Äspö-Simpevarp-Laxemar area (composite data from Tullborg 1997; Wallin and Peterman 1999, Bath et al., 1990 and present study). Data for euhedral calcites have been differentiated according to morphology.
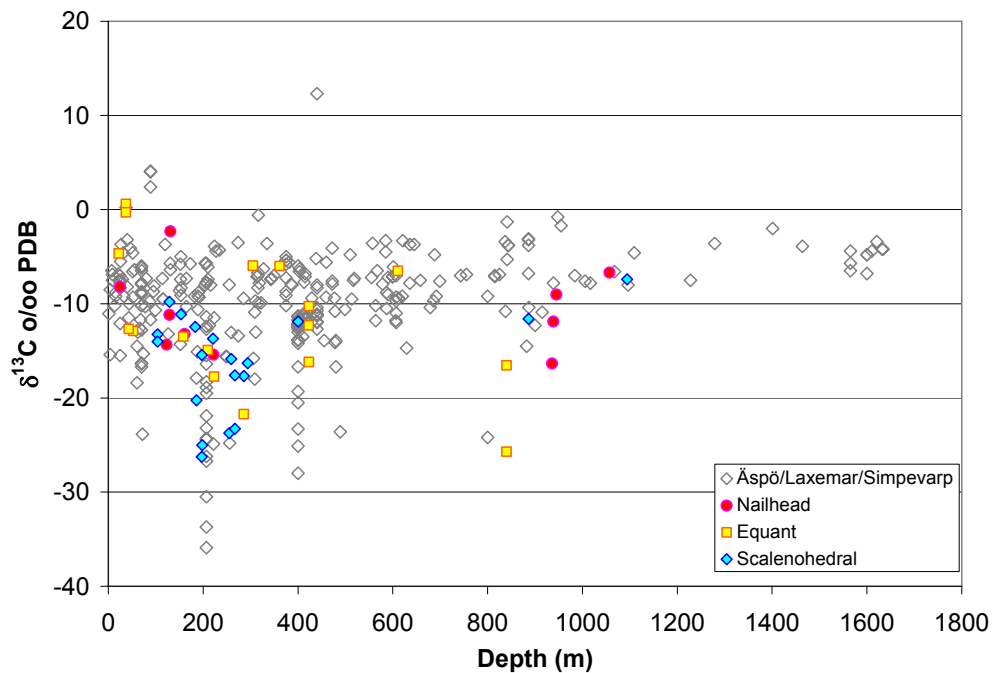
Figure 3-23. Variation of $\delta^{13}C$ with depth for all fracture calcites analysed within the Äspö-Simpevarp-Laxemar area (composite data from Tullborg 1997; Wallin and Peterman 1999, Bath et al., 1990 and present study). Data for euhedral calcites have been differentiated according to morphology. A few values lower than -40 ‰ are not included in the figure but are shown in Figure 3-24.

The depth variation in the stable carbon isotope ($\delta^{13}C$) composition of the calcite mineralization from Äspö-Simpevarp-Laxemar area is illustrated in Figure 3-23. Taking all of the data into account, the following trends can be discerned:

- The $\delta^{13}C$ values in the upper 50 m have values between -15 to 0 ‰ (PDB), indicative of mixing between an atmospheric carbon contribution and biogenic CO_2 in the soil zone ("open conditions").

- At greater depth the range of $\delta^{13}C$ is larger, with both extremely positive (> +13 ‰) as well as extremely negative (< -20 ‰) values. These compositions are interpreted as resulting from CO_2/HCO_3 produced by microbial activity in situ (closed conditions).

- Below 950 m depth, all measured $\delta^{13}C$ values lie between -8 and -2 ‰, indicating the absence of, or only minor contribution from, organically-modified CO_2.

- In general, the different calcite morphologies are not reflected in distinct differences in the carbon isotope composition. However, the fresh water carbonates ('nailhead-type') have a narrower range of $\delta^{13}C$ values (-16 to -3 ‰), whereas some of the equant and long c-axis ('scalenohedral' form) calcites have very low $\delta^{13}C$ values (< -20 ‰).
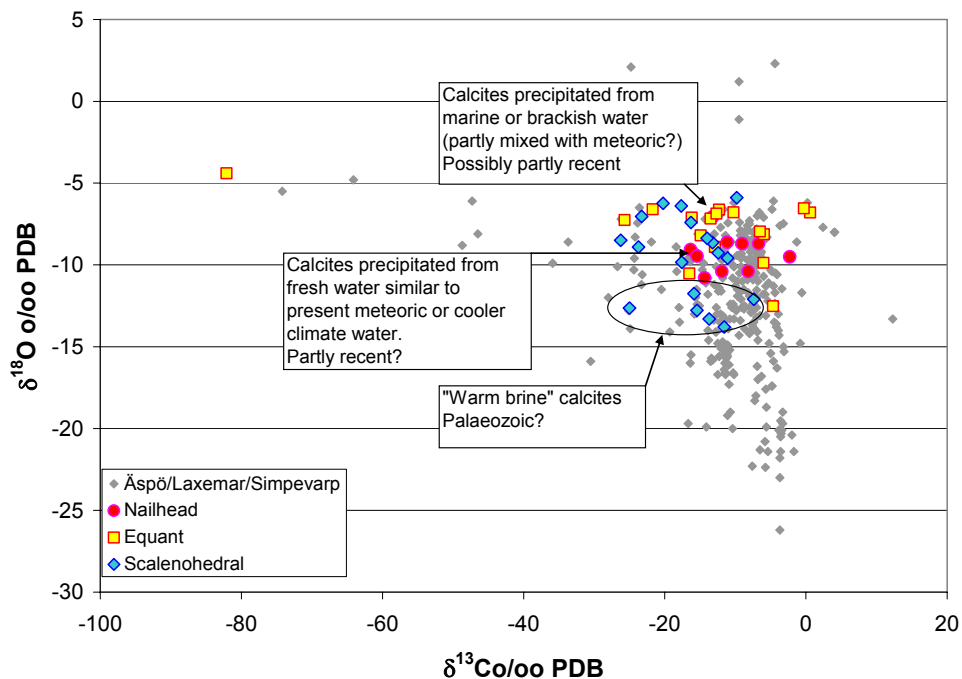
Figure 3-24. Variation of $\delta^{18}O$ versus $\delta^{13}C$ for all fracture calcites analysed within the Äspö-Simpevarp-Laxemar area (composite data from Tullborg, 1997; Wallin and Peterman, 1999, Bath et al., 1990 and present study). Data for euhedral calcites have been differentiated according to morphology.

Figure 3-24 shows a plot of the variation of $\delta^{18}O$ with $\delta^{13}C$. Three main groups of calcite stable isotope compositions can be differentiated on the basis of the morphological characteristics of the late calcite:

- The "warm brine" type calcites showing relatively large scalenohedral crystals (mm in size), with $\delta^{18}O$ varying from -14 to -11 ‰, and $\delta^{13}C$ varying from -25 to -5 ‰.

- Calcites with equant crystal morphology, and some of the elongated and scalenohedral crystals, show higher $\delta^{18}O$ values; mostly between -8 to -6 ‰ with large variations in

δ^{13}C. These compositions could be interpreted as reflecting calcite precipitation from recharged Baltic Sea water of different ages that were mixed to varying extent with meteoric waters.

- Short c-axis ('nailhead-type') calcites. This group shows a rather narrower variation in δ^{18}O and δ^{13}C, and would be consistent with precipitation from meteoric-recharged groundwater.

An attempt was made to use the He-LACE methodology at the BGS, to try to subsample and obtain stable (C and O) isotope data from individual growth zones and generations. However, the complexity of the intergrowth of calcite of different generations proved to be on a scale finer than the current spatial resolution of the laser microsampling technique.

3.2.4.5 STRONTIUM CHEMISTRY AND ISOTOPE (^{87}Sr/^{86}Sr) STUDIES

Although calcite morphology and stable isotope observations give an insight into groundwater origin and conditions during precipitation, they do not provide any indication of the age of the mineralization. Direct dating is very difficult for calcite, and earlier attempts using ^{14}C and ^{230}Th-U have not been successful (Possnert and Tullborg 1989; Tullborg 1997). However, the Sr isotope characteristics can contribute additional information about geochemical equilibria in the present system. Therefore, a number of samples of calcite were selected for Sr isotope analyses (carried out by Göran Åberg at IFE, Norway).
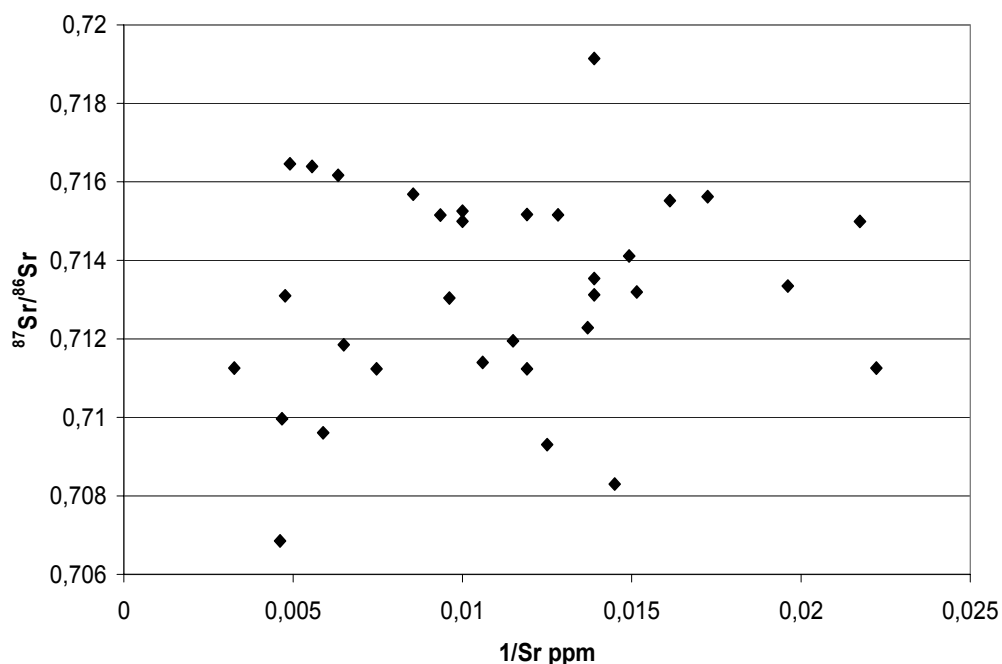
Figure 3-25. Sr content (1/Sr ppm) versus Sr isotope ratio for calcites from Äspö and Laxemar (compiled data from Bath et al., 2000 and the present study) and Simpevarp (Drake and Tullborg 2005).

The strontium geochemical characteristics of the late calcites from the Äspö-Simpevarp-Laxemar groundwater system are summarised in Figure 3-25. Unfortunately, only very limited amounts of calcite are available from individual fractures, making it very difficult to carry out multiple analytical tests and mineralogical characterisation on identical sub-samples. In order to evaluate the strontium geochemistry of the late calcite mineralization, the ideal situation would have been to determine both strontium content and ^{87}Sr/^{86}Sr isotope ratio on the same sample.

Because of the very small sample volumes available this has only been possible for the small set of data shown in Figure 3-25.

Simple mixing trends between two end members usually display a distinct trend when plotting $1/Sr$ versus $^{87}Sr/^{86}Sr$. However, the data for calcites from the Äspö-Simpevarp-Laxemar groundwater system are widely scattered in Figure 3-25. This may indicate that Sr has been variably contributed from several different origins within many of the analysed calcites. The complex picture probably results from a combination of factors, including: redistribution of Sr during the long history of reactivation, dissolution and precipitation processes that have occurred; and the contribution of Sr from inclusion of calcites from more than one generation in the analysed samples. There is also the possibility that in some of the samples Sr has been contributed from leaching of accessory contaminant phases entrained in the calcite samples (e.g. clay minerals).
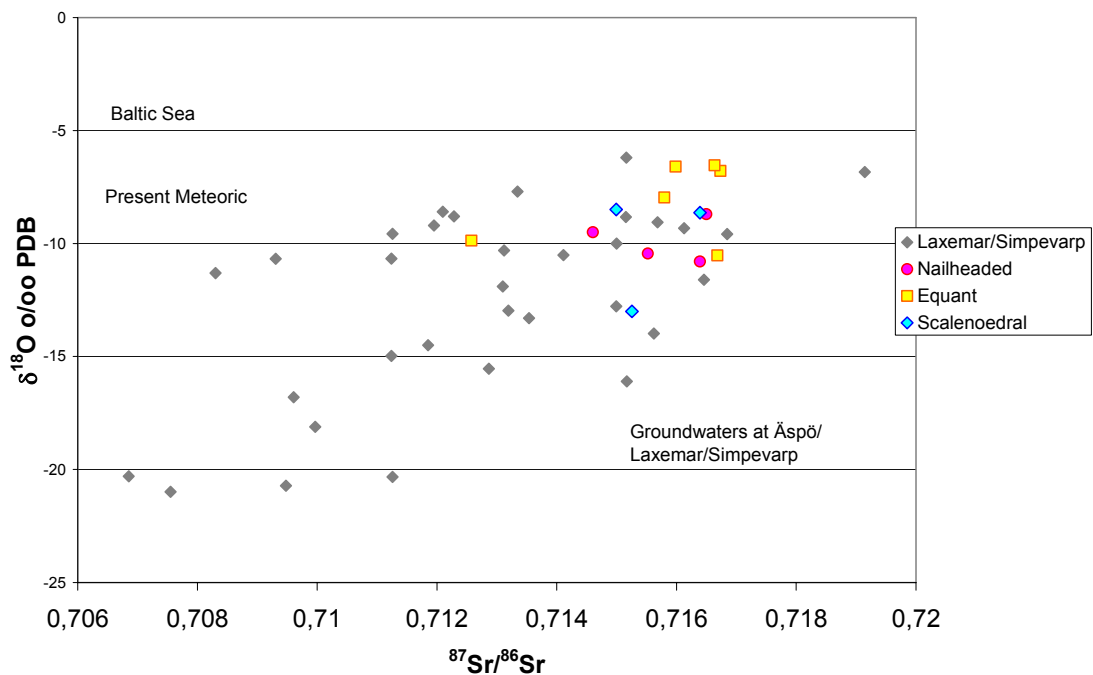
Figure 3-26. $\delta^{18}O$ versus Sr isotope ratio for calcites from Äspö and Laxemar (Bath et al., 2000, and the present study) and Simpevarp (Drake and Tullborg 2005). Crystal morphology of late calcite has been distinguished when possible. The range of $^{87}Sr/^{86}Sr$ ratios for groundwaters is taken from Peterman and Wallin (1999) and from the Simpevarp site investigations (Laaksoharju et al., in press).

Figure 3-26 shows the relationship between $\delta^{18}O$ (PDB) and $^{87}Sr/^{86}Sr$ ratio in all types of fracture calcite (where possible, late calcites with determined morphological characteristics have been distinguished). The range of $^{87}Sr/^{86}Sr$ values found in the present-day groundwaters of the region (vertical shaded interval), and the $\delta^{18}O$ isotope composition of Baltic Sea and present meteoric water (horizontal shaded interval) are also shown for comparison in Figure 3-26. The different types of mineralization can be distinguished in this plot:

- Calcites with very low $\delta^{18}O$ values (< -20 ‰) have generally low $^{87}Sr/^{86}Sr$ values (0.706852 to 0.711258). This group of calcites correspond to early carbonate veins of hydrothermal origin, and are of Proterozoic age.

- The group of calcites with $\delta^{18}O$ between -5 to -11 ‰ show $^{87}Sr/^{86}Sr$ ranging from 0.711238 to 0.716460. This range of compositions would be consistent with part of these

calcites being of recent (Quaternary) origin, whereas others with significantly lower Sr isotope ratios could correspond to the Palaeozoic 'Warm Brine' calcites.

- The majority of the 13 euhedral late-stage calcites (corresponding to the latest mineralization in PFFs in the present groundwater system) that were included within this suite of samples display $^{87}Sr/^{86}Sr$ values within the lower part of the range for that of the present groundwaters in the Laxemar-Simpevarp-Äspö area. This would be consistent with the calcites having grown from the groundwaters similar to those currently present in the region. However this interval is broad, so the uncertainty is large.

In conclusion, the Sr isotope ratio increases with time. The oldest calcite generations show the lowest $^{87}Sr/^{86}Sr$ ratios, and the youngest calcites show the highest $^{87}Sr/^{86}Sr$ ratios (the euhedral late-stage calcite mineralization plots within this group). The few calcites with $\delta^{18}O$ values higher than -7 ‰ are found in the latter group, indicating a possible precipitation from brackish Baltic Sea water from some period during the Quaternary.

The large spread in $^{87}Sr/^{86}Sr$ versus 1/Sr (Figure 3-25) and $^{87}Sr/^{86}Sr$ versus $\delta^{18}O$ (Figure 3-26) underlines the problem of being unable to sub-sample material representing single (end-member) generations of calcite, within these complex, multiply-reactivated and multiply-mineralized fractures. In most cases, the analysed samples contain intimate (and inseparable) intergrowths of calcite belonging to several mineralization events (Table 3-1).

3.2.4.6 MINOR AND TRACE ELEMENT CHEMISTRY STUDIES

3.2.4.6.1 Bulk calcite chemistry

The minor and trace element chemistry of the Laxemar-Äspö fracture calcites has been determined from leaching bulk calcite samples, and these data have been compared with the isotope geochemistry. Contamination was unavoidable in these very small samples because of intimate intergrowth and inclusion of minor aluminosilicate minerals that form part of the vein mineral assemblage (mostly chlorite or clay minerals and in some cases zeolites). The release of sorbed ions from these contaminants, as well as the dissolution of included microscopic mineral grains themselves, will probably have contributed to the leachate chemistry. Because of the difficulty in interpretation of the potentially complex assemblage, only Sr, Mn and La have been considered here, which can be more readily related to other observations on the calcites (Table 3-6).

Earlier studies have shown that calcite fracture mineralization from this area generally has a low concentration of Mg and Fe (e.g. Tullborg, 1995; Milodowski et al., 1998b). Nevertheless, the calcites do display compositional variations, both by syntaxial growth zoning and in sector zones (crystallographically-controlled differential incorporation of trace elements, on different crystal faces and sites), revealed under cathodoluminescence microscopy (CL) (Milodowski et al., 1998b; and cf. Section 3.2.4.2). The variations in CL luminescence shown by calcite are commonly related to Mn and Fe distribution: Mn^{2+} is an activator of luminescence and Fe^{2+} quenches luminescence in carbonate minerals (Pierson, 1981; Walker et al., 1989). However, the luminescence in the Laxemar-Simpevarp-Äspö calcites is controlled largely by Mn, with more brightly-luminescent bands corresponding to higher Mn contents (Milodowski et al., 1998b; and cf. Section 3.2.4.2). Only occasionally does the CL variation reflect Mn:Fe ratio. Earlier studies have also indicated that Mn and La concentrations in calcite can be related to presence of the 'organically-fed' microbial fauna, and that the concentrations decrease with depth (Pedersen et al., 1997; Tullborg et al., 1999; Bath et al., 2000). Mn-reducing bacteria produce Mn^{2+} during the breakdown of organic material, and the Mn^{2+} is then transported in solution in groundwater and subsequently incorporated in calcite precipitates. In contrast, La is probably transported as organic and/or carbonate complexes, and is therefore likely to be less

mobile when the concentrations of complexing agents (derived from the soil zone) decreases with depth.

Table 3-6. Minor and trace element chemistry, stable isotope (C, O) and $^{87}Sr/^{86}Sr$ isotope data for selected (leached) samples of calcite mineralization from Laxemar-Simpevarp-Äspö area.

Sample No. KLX01	Depth (m)	$\delta^{13}C$	$\delta^{18}O$	$^{87}Sr/^{86}Sr$	Sr ppm	Mn ppm	La ppm
7.20	7.2	-6.5	-8				
13.30	13.3	-10.2	-6.2				
15.55	15.55	-8.8	-8.3				
15.51 s	15.51	-9.2	-8.7				
22.10	22.1	-82.1	-4.4				
22.97 E	22	-4.65	-12.52				
23.9	23.9	-7.5	-8.7		50	3736	98
25.6	25.6	-5.5	-8.3				
29.5	29.5	-7.4	-13.5		89	1543	38
37.3 E	37.3	0.6	-6.8				
37.0	37	0.2	-6.2	0.715161	78	13370	115
37.1 E	37.1	-0.3	-6.54	0.716636			
40.01	40.01	-8.2	-11.7				
42.9 E	43	-12.68	-6.86				
51.3	51.3	-6.6	-6.8	0.719145	72	4140	206
51.3 s	51.3	-4.6	-11.3	0.708303	69	653	48
52.0 E	52	-12.9	-8.9	0.712284	73	1587	150
60.4	60.4	-18.4	-8.9				
60.B	60.4	-14.5	-9.9				
79.9	79.9	-7.3	-10.5	0.714114	67	3906	67
87.2	87	-9.76	-9.42				
88.8B	88.8	-11.7	-10.6		79	386	77
88.75	88.75	-43.1	-10.8		144	220	22
96.6	96.6	-8.1	-7.9				
123.92 N	123	-14.35	-10.79	0.716392			
153.5 Sc	153	-11.11	-9.58	0.716848			
160.9 N	161	-13.2	-7.06				
182.6 Scv	183	-12.45	-9.26				
186.2 Scv	186	-20.25	-6.23				
189.9	189.9	-8.8	-8.7				
189.9 Outer	189	-10.61	-9.62				
189.9 Inner	189	-9.18	-9.32	0.716126			
191.15-30	191.25	-9.3	-8.8	0.715156	107	3439	228
204.1	204.1	-5.7	-8.4				
204.2	204.2	-8	-11.9				
210.5	210	-7.4	-10.7	0.711239	84	553	176
213.6A	213.6	-12.3	-9.1	0.715686	117	2940	69
220.58 N	222	-15.41	-9.46				
220.7 Sc	220.7	-13.7	-13.3	0.713538	72	3041	113
223.9 Eq	223	-17.74	-9.47				
255.0	255	-7.99	-7.15				
273.6	273.6	-3.5	-20.3	0.706852	217	174	0.4
306.2	306	-15.8	-13				
327.5-6	327.55	-6.3	-16.8	0.709606	170	1525	157
403.3	403.3	-6.3	-9.2				
403.4	403.3	-6.6	-9.2	0.711948	87	5106	69
405.95	405.95	-12.1	-7.7	0.713345	51	1265	63
499.0	499	-10.6	-8.6				
629	629	-14.7	-10.3	0.713121	72	932	187
699.3	699.3	-7.6	-13.7				
837.4-5	837.4	-10.8	-13.3		54	2399	50
840 Outer E-N	840	-25.7	-7.26				
840 Inner E-N	840	-16.54	-10.53				
915.8	915	-10.9	-16.1	0.715171	84	2636	204

Table 3-6 (continued). Minor and trace element chemistry, stable isotope (C, O) and $^{87}Sr/^{86}Sr$ isotope data for selected (leached) samples of calcite mineralization from Laxemar-Simpevarp-Äspö area.

Sample No. KLX01	Depth (m)	$\delta^{13}C$	$\delta^{18}O$	$^{87}Sr/^{86}Sr$	Sr ppm	Mn ppm	La ppm
936.3 N	936	-16.344	-9.06				
938.7 N	938.7	-11.9	-10.4	0.715521	58	6245	22
938.7	938.7	-7.8	-14	0.715623	62	2829	41
945.3 N	945	-9.03	-8.7	0.716500			
1005.75	1005.75	-7.6	-9				
1016.7	1016.7	-7.8	-12.9				
1056.8 N	1056.8	-6.7	-8.7		71	649	11.0
1067.5	1067.5	-6.6	-9.6				

N = Nailhead crystal (short C-axis);
E= Equant shaped crystals;
Sc= Scalenohedral shaped crystals
Scv= very elongated needle shaped crystals

The variations of total Mn and La concentration in calcite from the KLX01 borehole are plotted as a function of depth in Figure 3-27 (Mn) and Figure 3-29 (La). These elements are also compared with variations in $\delta^{18}O$ in Figure 3-28 (Mn) and Figure 3-30 (La). The data show a general pattern of higher Mn and La contents in calcites with $\delta^{18}O$ values in the range -11 to -7 ‰ (possibly corresponding to a meteoric or brackish sea water origin cf. Figure 3-24 and Figure 3-26). This study has found that the deep calcites from KLX01 (850 to 950 m depth) have higher Mn and La contents than the deep calcites analysed in the earlier EQUIP study (Bath et al. 2000), which were mainly from Äspö with only a few samples from the deep borehole (KLX02).

Two samples from KLX01 with high La contents have $\delta^{18}O$ values of -16 to -15 ‰. This may be the result of a mixture of two or more generations of calcite being present within the samples, or simply contamination by accessory phases.
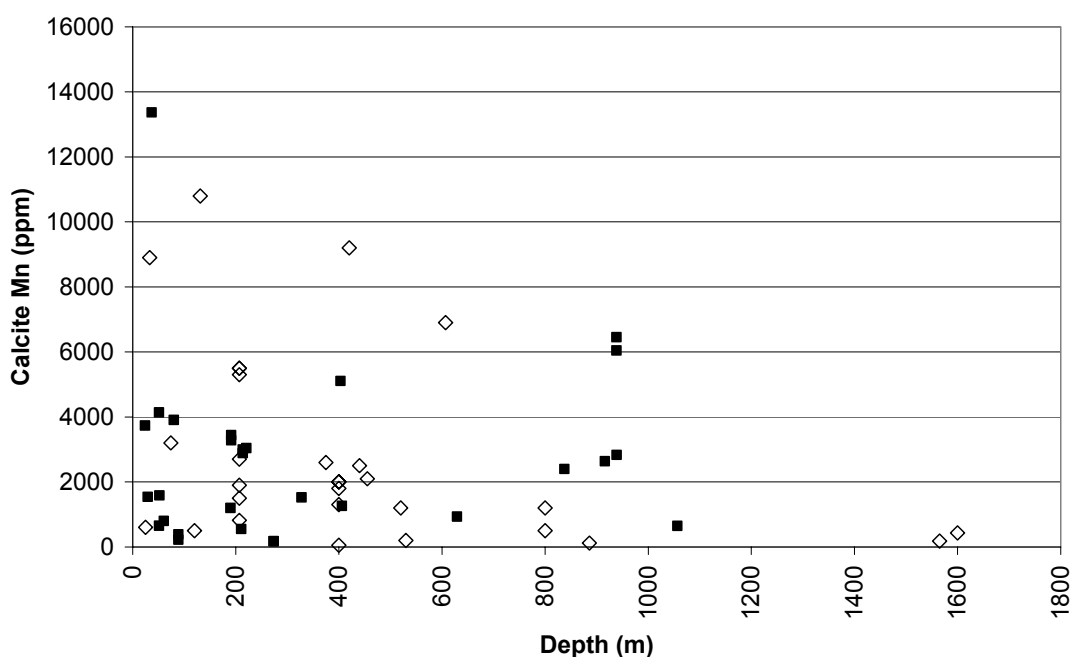
Figure 3-27. Mn concentration in calcites versus depth. Open symbols = results presented in EQUIP (Bath et al., 2000). Closed symbols = this study.
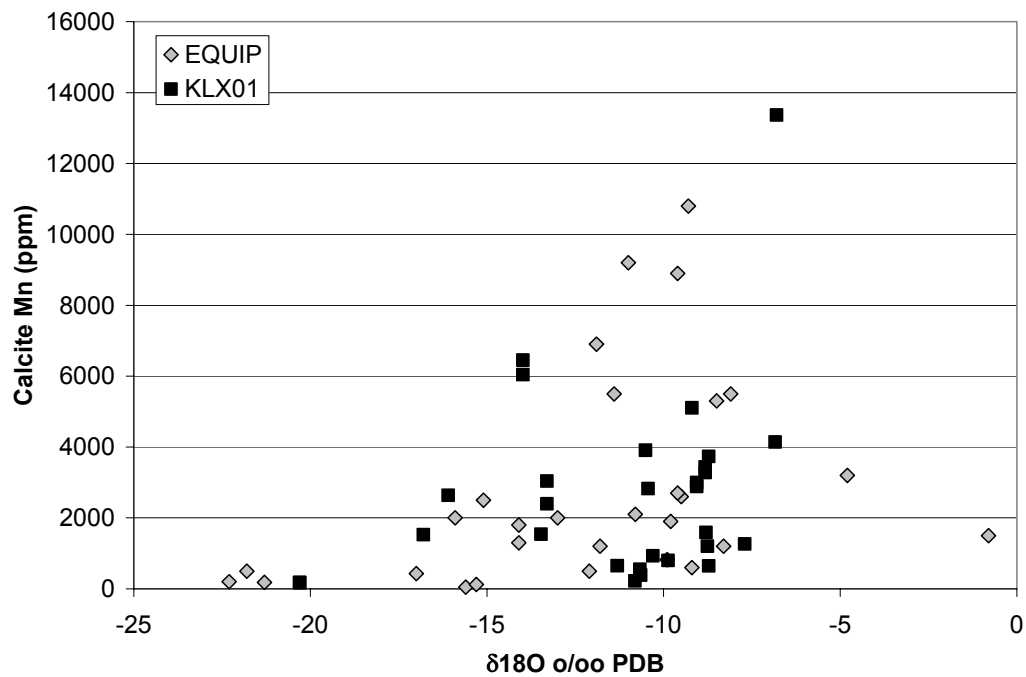
Figure 3-28. Mn concentration versus δ^{18}O values for fracture calcites from Äspö and Laxemar.
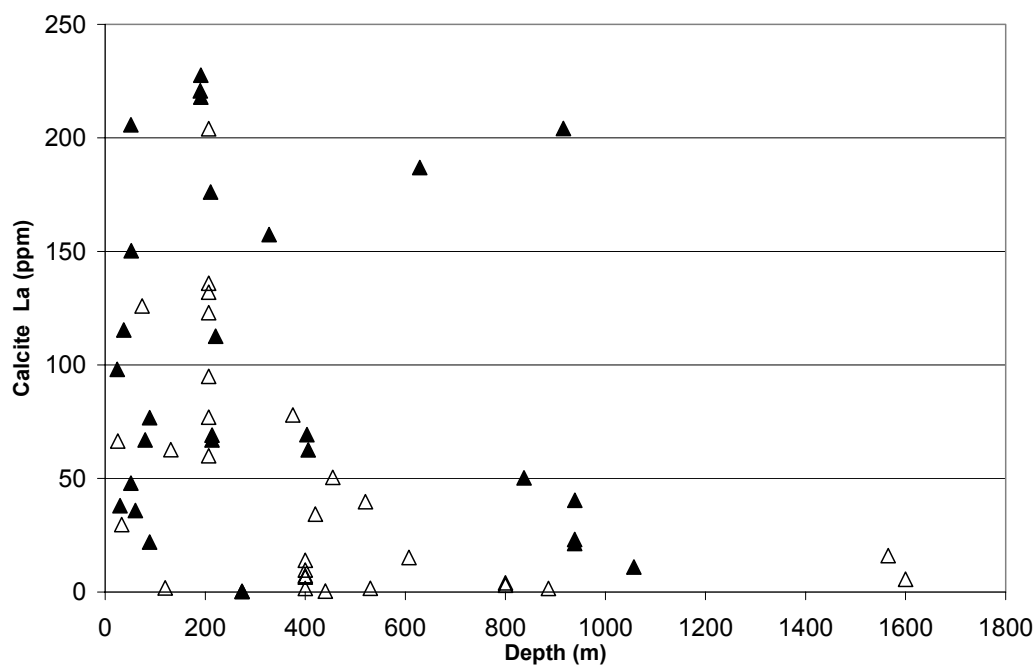
Figure 3-29. La concentration versus depth for fracture calcites from Äspö and Laxemar. Open symbols = results presented in EQUIP (Bath et al., 2000). Closed symbols = this study.

91
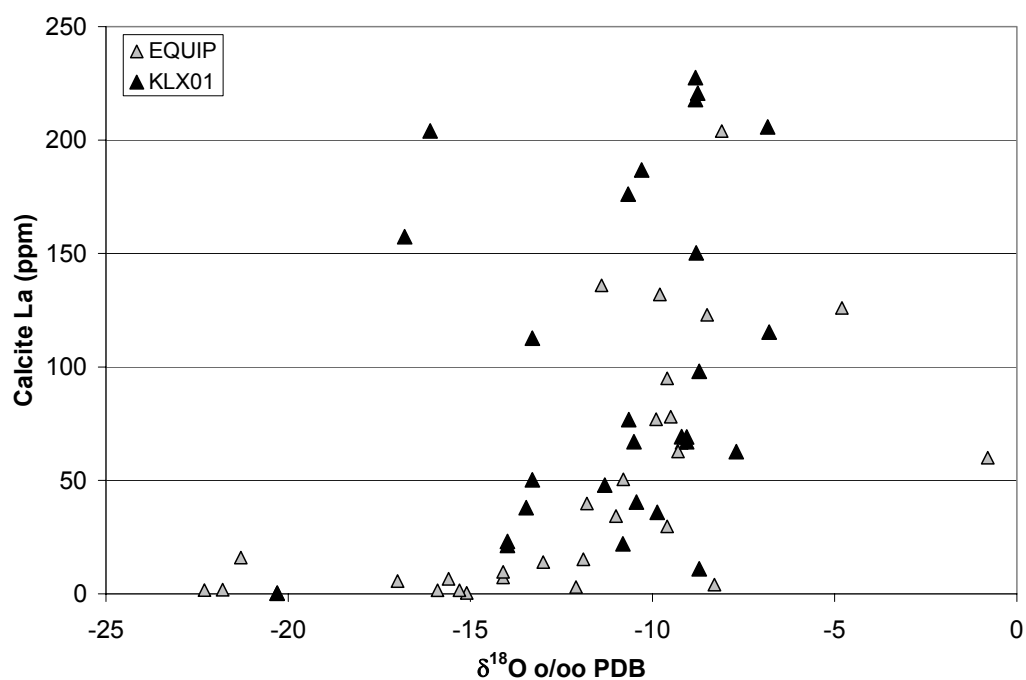
Figure 3-30. **La concentration versus δ^{18}O values for fracture calcites from Äspö and Laxemar.**

3.2.4.7 BIOMARKER STUDIES

Nine samples of late-stage calcite from Laxemar borehole KLX01 were analysed by GC-MS by the Universidad Politecnica de Madrid for the presence of organic biomarker compounds (Table 3-7). These samples were the only ones where sufficient quantity of calcite could be collected for any practical analysis. Biomarkers were found in all but two of the samples (KLX01/13.95 m and KLX01 22.97 m). However, only a few organic compounds were present, and in very low abundances that were close to the detection limits of the technique. The identified compounds include octadecanoic acid, cyclopentane, isoquinoline and 1,2-benzenedicarboxilic acid (Table 3-7, Figure 3-31). As observed in Figure 3-31, other compounds are also present in the GC-MS spectra. However, these are not described further because there are large uncertainties in their identification. The significance of the presence of the biomarker compounds preserved within the late calcite is discussed below.

Table 3-7. Abundances of the different biomarkers found in late-stage calcites from the Laxemar borehole KLX01.

Sample No.	Depth (m bgl)	Sample wt. (mg)	Cyclo-pentane	Hexadeca-noic acid	Octadeca-noic acid	1, 2 benzenedi-carboxilic acid	Isoquino-line	Pyrrolo [3,2-a] dibenzo-furan
KLX01/13.10	13.10	92.8	nd	nd	892085	nd	nd	nd
KLX01/13.95	13.95	42.8	nd	nd	nd	nd	nd	nd
KLX01/22.97	22.97	21.0	nd	nd	nd	nd	nd	nd
KLX01/37.1	37.1-37.2	230.6	nd	nd	1532735	nd	nd	nd
KLX01/189.9	189.9	386.0	298277	nd	nd	7617314	nd	nd
KLX01/223.9	223.9	334.0	301685	nd	1308713	978660	nd	nd
KLX01/840.0	840.0	75.2	nd	nd	2045682	nd	nd	nd
KLX01/936.8	936.8	69.8	nd	nd	1888789	nd	nd	nd
KLX01/939.0	939.0	117.6	nd	nd	1441248	1048348	nd	nd

Notes: 1. nd = not detected

2. Relative concentrations of organic compounds shown as total GC-MS peak counts.

92
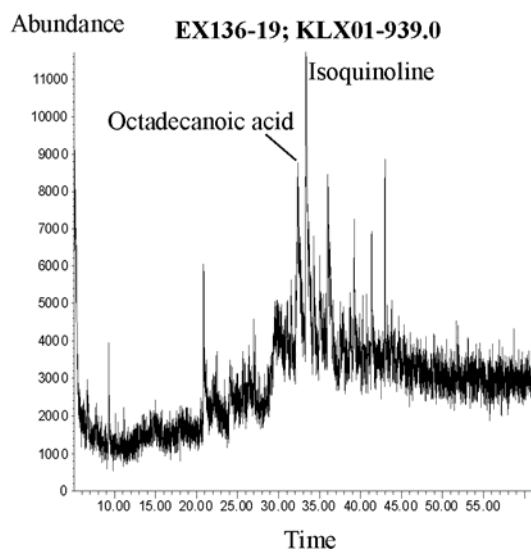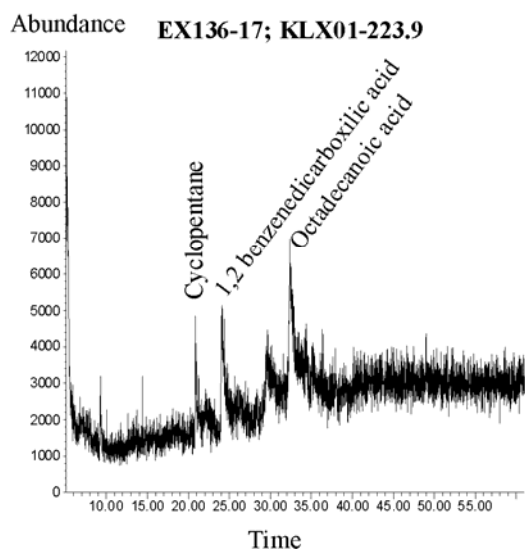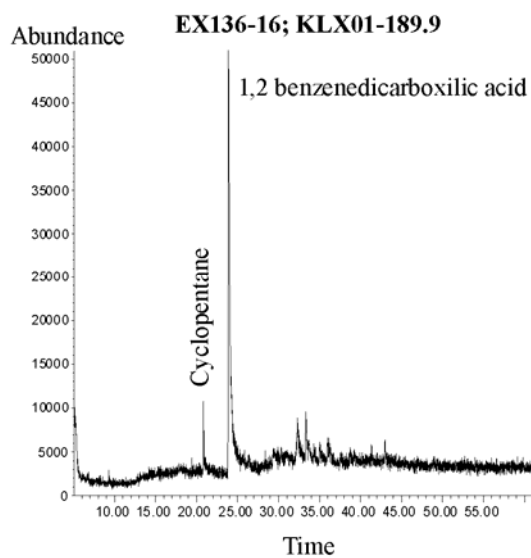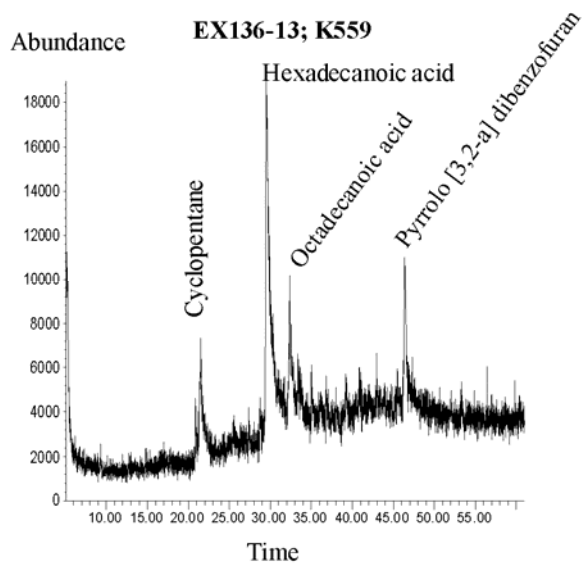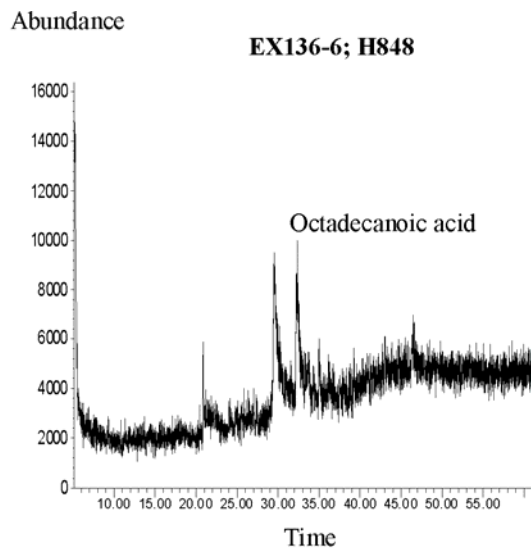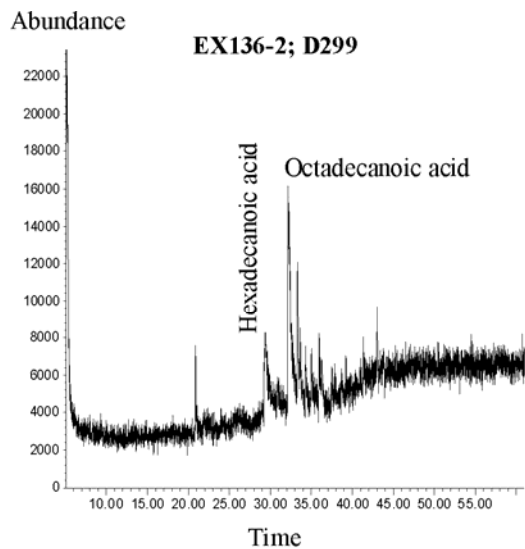
Figure 3-31. Examples of GC-MS spectra of biomarker and other organic compounds extracted from late-stage calcites from Sellafield (spectra 136-2 and 13), Dounreay (spectrum 136-6) and Laxemar (spectra 136-16, 17 and 19).

Hexadecanoic and octadecanoic acid are aliphatic hydrocarbons belonging to the carboxylic acids. Carboxylic acids can be derived from plants, animals and microorganisms. However, long-chain n-alkanoic acids with 24 to 30 carbon atoms (i.e. C24 to C30), and with a predominance of even-chains, are major components of the waxy coatings on land-plant leaves, flowers and pollen, whereas algae and bacteria maximize at shorter-chain C12 to C18 n-acids. Hexadecanoic acid, also known as palmitic acid, and octadecanoic acid, also called stearic acid, are saturated fatty acids. Fatty acids are predominantly un-branched, and those with even numbers of carbon atoms (C12 and C22) react with glycerol to form lipids (fat-soluble components of living cells) in plants, animals, and microorganisms. Hexadecanoic acid and octadecanoic acids are important constituents of most vegetable fats (e.g. 35-45 % of palm oil). Sometimes, diagenetic processes produce a predominance of short-chain n-acids. For example, the microbial synthesis of secondary fatty acids from primary organic matter produces shorter-chain components.

1,2 benzenedicarboxilic acid, also called phthalic acid, is a carboxylic acid. Carboxilic acids can be made by the complete oxidation of primary alcohols.

Quinoline and isoquinoline are alkaloids. They are found in plants from a wide group of genera, including the following: *Argemone* species (prickly poppy), *Chelidonium* species (celandine poppy), *Corydalis* species (fitweed), *Dicentra* species (Dutchman's Breeches), *Papaver* species (poppy) and *Sanguinera* species (bloodroot).

Cyclopentane belongs to the cyclo-alkane group of hydrocarbons, which are one of the most important components of organic matter. The most common cyclo-alkanes are the cyclohexane and cyclopentane series. No more specific details have been found about the origin of these compounds, but they are usually involved in the structure of plant material.

Dibenzofuran is a three-ring polycyclic aromatic furan. It is released to the environment in atmospheric emissions involved with the combustion of coal, biomass, refuse, and diesel fuel. Wastewater emissions can occur from coal tar, coal gasification, and shale oil operations. Dibenzofuran may partition significantly from the water column to sediments and suspended material.

The presence of octadecanoic acid in samples KLX01 13.10, 37.1, 840.0, 936.8 and 939.0 m could indicate the calcite grew from groundwater which had an organic matter input of plant origin, or it may also have been produced in situ through bacterial activity. Cyclopentane, found in two of the calcites (KLX01 189.9 m 223.9 m), is most probably of plant origin. The presence of both cyclopentane and octadecanoic acid would suggest that the groundwater from which these calcites grew had possibly been recharged through a soil cover. It is noticeable that 1,2 benzenedicarboxilic acid was found in three of the samples (KLX01 189.9, 223.9 and 939.0 m). This type of biomarker has been found in Pleistocene and Holocene speleothems from the north of Spain (T. de Torres, unpublished information). Although hexadecanoic acid, isoquinoline and dibenzonfuran have been identified in similarly late-stage calcite from the Sellafield and Dounreay sites (see Sections 3.3 and 3.4), these particular biomarkers have not been found in any of the calcites examined from Laxemar.

3.2.5 Conclusions

3.2.5.1 GENERAL CONCLUSIONS ON THE SAMPLING AND ANALYTICAL METHODOLOGY

3.2.5.1.1 *Core preservation and sample optimization*

One of the conclusions coming out of the EQUIP project (Bath et al., 2000) was the importance of the drilling technique on the preservation of late-stage fracture mineralization relevant to palaeohydrogeological studies. The calcite coatings are soft and delicate, and the latest generations of crystals are often only weakly adhered to the fracture surface. Therefore, they are

easily dislodged, damaged and washed out by drilling fluids during coring. The EQUIP research showed that the best preservation of these delicate calcite fillings was obtained by coring employing triple tube drilling. Mechanical damage induced during subsequent core handling, and conflicting demands for core samples to meet other site investigation/core characterization objectives also have a major impact on the usefulness of core samples for palaeohydrogeological applications. To maximize the potential provision of palaeohydrogeological information that can be obtained from these late-stage calcites, it is necessary to try to sample undisturbed material in sufficient quantity and of an appropriate grain size to meet the requirements and limitations of the mineralogical and geochemical techniques being employed. Therefore the ability to obtain good samples will also be partly dependent on the priority set upon palaeohydrogeological investigations within the site investigation programme.

In the case of the PADAMOT studies at Laxemar-Simpevarp-Äspö, there were no resources within the PADAMOT programme to be able to acquire new deep borehole core recovered using the triple tube technique. Consequently, it was necessary to work with existing core material. To this end, it was decided that core from Laxemar borehole KLX01 would be the best deep borehole material available. Although this borehole had not been cored using triple tube technology, it had been little-studied prior to this project, and consequently the core had suffered very little disturbance from handling or sampling. Nevertheless, it was found that fracture surfaces were generally only sparsely coated with mineralization. In some cases, damage by abrasion of opposing fracture surfaces, as a result of drilling and/or core handling was evident. In other cases, it is likely that significant amounts of loosely adhering surface minerals will have been washed out during the coring processes. This again highlights the importance of using good coring techniques in order to maximise the preservation of material that will be needed in palaeohydrogeological investigations.

In addition to problems with core preservation, the small amount of mineralization present limited the range of analytical techniques that could be applied to a given sample. This highlights a need for prioritization and optimization of the analyses required in such situations.

3.2.5.1.2 *Calcite morphology*

Unlike at Sellafield and Dounreay sites (see Sections 3.3 and 3.4), and previous studies at Äspö, the late calcite in Laxemar borehole KLX01 does not show an overall change in morphology from short c-axis to long c-axis crystal forms, reflecting a simple progressive increase in salinity with depth. The situation at Laxemar appears to be more complex: the late calcite displays very variable morphology in the upper 300 m. Although there is an overall increase in *c:a* crystallographic axial ratio from the surface down to 200 m, below this depth the calcite reverts to short c-axis and equant calcite morphology. This implies a general increase in palaeosalinity from freshwater at the surface to brackish-saline water to 200 m, then a change back to dilute water below this depth. However, within this depth interval different PFFs display quite a wide variation in late calcite morphology, perhaps indicating local variations in salinity/palaeosalinity between different, possibly isolated, fracture flow paths.

Despite the complex depth variation profile, the calcite morphology, together with stable isotope, strontium isotope, and trace element geochemical characteristics has proved very useful in helping to categorize different calcite types and generations. The use of morphology for the selection of small samples for the bulk analysis of stable isotopes and trace elements still does not overcome the problems of sampling and analysing mixed generations (since the calcite is often overgrown on earlier mineralization), nor of contamination from the presence other accessory phases. However, it does provide a possible method to help differentiate the "end member calcites" occurring in the fractures, and integrated with the isotopic information the use of calcite morphology has enabled the identification of calcites precipitated from different groundwaters.

3.2.5.1.3 Absolute age dating

Absolute dating of the late calcite fracture fillings has so far not been possible due to very small volumes of material that can be sampled. Most of the late calcite is also either developed as thin overgrowths on old hydrothermal mineralization, or contains inclusions of older mineralization, and is very finely growth zoned with multiple generations of calcite.   In addition, the U concentration of the calcites is low. This means that large bulk samples of calcite are required to provide sufficient mass of U for mass spectrometric analysis, but these samples will unavoidably contain mixed generations of mineralization.

3.2.5.2 PALAEOHYDROGEOLOGICAL INTERPRETATION

The tentative models of the past and present groundwater circulation proposed in Bath et al., (2000) and Tullborg (2003) are largely supported by the results from the PADAMOT study. A summary of the conceptual model of the distribution of the different types of late-stage calcite, and of the processes influencing calcite precipitation in the Laxemar-Simpevarp-Äspö groundwater system is illustrated in (Figure 3-32). At least three different zones of calcite mineralization are distinguished:

- The upper part of the system is characterised by a dynamic situation involving dissolution and precipitation of new calcite. At times, biogenic activity has been significant and produced reducing conditions, whereas during other periods oxidising conditions may have prevailed. At Äspö this zone is very shallow (0-50 m approx.) but can be extended to greater depth at Laxemar (0-100 m?).

- From 100 m down to between 500-600 m mainly precipitation (or re-crystallisation) of calcite is observed. Several generations of calcite (zoned) are common at these depths. Redox conditions have probably been stable and reducing during the Quaternary, and contributions from biogenically-mediated carbonate precipitation are detected in terms of low carbon isotope values and high contents of Mn and La.

- Between 600 and 1000 m the biogenic carbonate influence decreases drastically but calcite mineralization, consistent with low temperature precipitation from fresh groundwater of meteoric origin, can be traced in the major zones of steep fractures that were intersected at 850 and 950 meters in borehole KLX01. Some of these calcites show bands with weak cathodoluminescence indicating low Mn content, but Mn-rich calcite growth bands are also found.

In contrast to the earlier studies from Äspö, it has not been possible to identify any late calcite in the Laxemar site that has precipitated from water with an isotopic composition consistent a significant glacial component. Groundwater with a glacial meltwater component has however been identified at depths varying from 100 m (in isolated pockets) to 1100 m. One possibility is that the glacial water intrusion did not form any calcite. Alternatively, it could be that calcite precipitated from glacial-recharged groundwater simply has not yet been identified in the specific drill core samples examined to date.

At greater depth (>1000 m) recent calcite precipitation is rare, and the biogenic input seems to be insignificant due to relatively stagnant conditions that pertain at this depth in the system.

The observed distribution pattern of the different calcite generations is the net effect of calcite-fluid interactions (and also of subsurface microbiological activity during long periods) during the entire geological history of the granitoids of the area. The hydrothermal calcite (*Type 6*) is the most widespread fracture calcite precipitation, and probably represents several hydrothermal events. It is probably related to the regional hydrothermal alteration, focussed along fractures and fracture zones that occurred early in the geological history of the granitoids at Äspö. The subsequent dissolution of the hydrothermal calcite, and its replacement by calcite of younger groundwater regimes, has been repeated many times since the initial mineralization in the

Proterozoic. When a thick sedimentary cover on the Fennoscandian shield was present during the Late Palaeozoic, *Type 5* calcite was precipitated from warm brines. It is believed that the present rock surface has been exposed since at least the Late Tertiary, and therefore Type 5 calcites must pre-date this time.

Type 5 calcite precipitated from brine-type water at elevated temperatures. This has been demonstrated by detailed fluid inclusion studies, which show the calcite contains two-phase fluid inclusions with salinities over 1000 ppm Cl (cf. above and Bouch, 2004). Type 5 calcite forms c-axis elongated scalenohedral shaped euhedral crystals, which are also indicative of formation from saline groundwater. Temperature estimates from fluid inclusion homogenization observations, together with $\delta^{18}O$ values mostly in the range of -10 to -17 ‰ SMOW, indicate possible formation temperatures in the range of 60 to 150 °C. This type of calcite is probably older than late Mesozoic (100 Ma) and younger than 1450 Ma, and is interpreted to have precipitated from sedimentary (diagenetic) brines that percolated through the basement when the Scandinavian Shield was covered with sedimentary rocks during the Riphean or Palaeozoic.
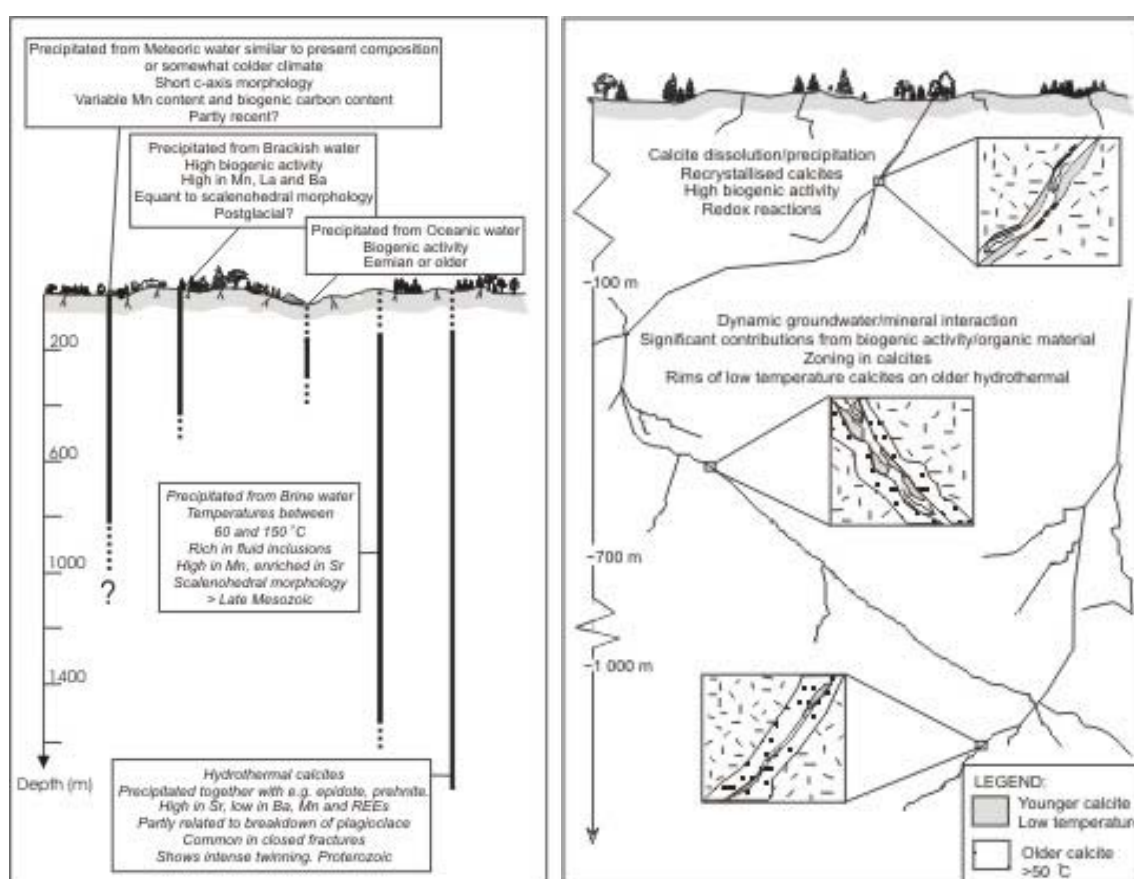
Figure 3-32. (Left) Depth distribution of different calcite types in the Laxemar-Simpevarp-Äspö groundwater system. Solid lines show the main interval over which the calcite is found; the dotted lines indicate the possible range of occurrence. The classification is based on stable isotope data supported by all other available information (trace elements, calcite morphology-groundwater composition relationships, fluid inclusion data, petrography). (Right) Conceptual illustration of processes influencing calcite-groundwater interaction at various depths in the Laxemar-Simpevarp-Äspö groundwater system.

The distribution and abundance of low-temperature calcites (*Types 2 and 3*) of possible marine-brackish water origin ($\delta^{18}O$ > -7 ‰) seems to be more extensive in the Äspö site, where they are found down to 500 m depth. In Laxemar borehole KLX01 these calcites are found only to 200

m. In contrast, low-temperature calcite of dilute meteoric water origin (*Type 1*) are found over a wide depth range from the surface down to at least 950 m, indicating a deeper penetration of fresh groundwater sometime in the past.

Although only limited number of data were acquired, it has been demonstrated that organic biomarker compounds are preserved in trace amounts in the late-stage calcites covering a depth range from the surface to over 900 m depth. The very small amounts of calcite present in the Laxemar fracture mineralization posed a major problem in sampling sufficient mass to be able to detect the presence of biomarkers. Despite their being present in only very small concentrations, it is considered unlikely that their detection is the result of any contamination of the samples, since the organics were extracted from *within* the calcite only after careful acid treatment of the calcite surfaces prior to extraction of biomarkers in order to remove any potential contaminants. The compounds have survived because they have been 'encapsulated' within the calcite and protected from microbial attack. It seems most likely that the organic matter, in some of the calcites containing both cyclopentane and octadecanoic acid, is derived from plants. This would imply that the groundwater from which these calcites precipitated contains a component that was probably recharged through the soil zone. However, microbial activity cannot be ruled out as a potential source of some of these biomarkers (e.g. in samples where octadecanoic acid only is present).

All the results (including: morphology, fluid inclusions, CL, stable C and O isotopes, and Sr isotopes) indicate that most fractures have been multiply-reactivated, and that calcite mineralization has been deposited from fluids of varying salinities and temperature regimes at different times often in the same fracture. The data also show that the position of the fresh water - saline water interface has varied considerably over time.

3.3   SELLAFIELD

3.3.1   Sample selection criteria

Considerable background information regarding fracture mineralization from studies undertaken as part of the Nirex site investigation programme at Sellafield (Milodowski et al., 1998, 2002) provided the basis for a well-defined and well-constrained paragenetic sequence of minerals at this site. These studies, together with the earlier EQUIP investigations (Bath et al. 2000) also demonstrated a close relationship between the modern groundwater flow system and many aspects of the youngest fracture mineralization, which is discussed in more detail in the following sections.

As in the case of the Äspö and Laxemar area (Section 3.2), the PADAMOT investigations have concentrated mainly on the late-stage calcite (which forms part of the youngest mineralization) since previous studies (Milodowski et al., 1997, 2002; Bath et al., 2000) indicated that this mineral probably had the greatest potential to record palaeohydrogeological information for the Sellafield site. However, because the general mineralogical and petrological characteristics of late-calcite from this site had already been well-characterized during the EQUIP project, the emphasis of studies at this site was to:

- Study the variation in stable carbon and oxygen isotope composition during the growth of the calcite. The objective was to use new developments in ion microprobe analysis at the University of Edinburgh, and He-swept laser ablation microsampling technology for the extraction of CO_2 from carbonates (He-LACE) at the BGS, to provide the necessary spatial resolution required to study growth zones in the calcite. The aim was then to use the oxygen stable isotope signature, in particular, as a proxy to follow potential climate/environmental-driven impacts on the groundwater system;

- To further evaluate the microchemical variations during the growth of the calcite, and in particular to study variations in redox-sensitive elements to provide an indication of changes in redox state of the past groundwater system.

- To analyse a small suite of calcite samples at the Universidad Politecnica de Madrid, for the presence of biomarker compounds that might provide palaeoenvironmental information.

Table 3-8. List of samples studied from the Sellafield site with analytical schedule.

Borehole	Sample ID	Top Depth (m bOD)	Bottom Depth (m bOD)	Host rock	Cathodo-luminescence Microscopy	Ion Microprobe Trace Element Analysis	Ion Microprobe Stable Isotope Analysis	Laser Ablation-ICP-MS Trace Element Analysis	LACE-He stable isotope data	Biomarker Analysis
BH2	B946	1527.50		St Bees Sstn.	Y	Y	Y	Y		
BH2*	NSF2/ 1367/P4	5.50		Calder Sstn.				Y		
BH9A	D723	65.22		BVG	Y			Y		Y
BH12A	B877	533.45	534.36	St Bees Sstn	Y			Y	Y	
BH10A	D750	635.00		St Bees Sstn	Y				Y	
RCF1	C719	389.71		St Bees Sstn	Y					
RCF1	C742	690.16		BVG	Y				Y	
RCF1	C755	895.82	896.32	BVG	Y					Y
RCF1	C759	938.00		BVG	Y				Y	
RCF3	MPLK559	863.03		BVG	Y			Y		Y
PRZ2	D280	147.00		St Bees Sstn	Y			Y	Y	
PRZ2	D283	206.35		St Bees Sstn	Y			Y		
PRZ2	D286	236.15		St Bees Sstn	Y	Y	Y	Y		
PRZ2	D299	310.00		Brockram	Y	Y	Y			Y
PRZ2	D311	413.10		BVG	Y	Y	Y	Y	Y	Y
PRZ3	D329	396.31	396.65	BVG	Y			Y	Y	Y
TOTAL					*15*	*4*	*4*	*10*	*7*	*6*

Notes: *This sample is ME8 barium-manganese oxyhydroxide. All other samples are ME9 calcite

The fracture mineralization samples selected for study and their analytical schedule are listed in Table 3-8. These were selected on the following criteria:

- Samples were taken to represent the youngest mineralization differentiated within the paragenetic scheme defined for the Sellafield area (Section 3.3.2). In particular, emphasis was placed on examining well-preserved and well-developed euhedral crystals of late-stage (ME9) calcite, which were considered most likely to furnish sufficient material and with a grain size that was coarse enough to allow detailed microanalysis of growth zones. In addition, the REE chemistry of a well-developed example of late-stage (ME8) manganese oxyhydroxide from the upper part of Sellafield borehole BH2 was determined (sample NSF2/1367/P4) for comparison with that of ME9 calcite;

- Samples were selected from obvious potentially flowing features (PFFs). These were identified on the same basis as at Äspö and Laxemar (Section 3.2.1), and as defined in previous studies (Milodowski et al., 1995; Bath et al., 2000);

- Samples were selected to cover the depth range of Sellafield boreholes;

- Samples were selected to represent ME9 fracture calcites from (a) the freshwater zone; (b) the saline groundwater zone; and (c) the interface between these two groundwater domains, or the 'saline transition zone' (STZ) in both the sedimentary cover rocks and the basement (BVG) formation.

3.3.2 Fracture mineralogy and paragenesis

The fracture mineralogy and paragenesis of the Sellafield site has been studied in detail as part of the Nirex site investigation programme for disposal of low- and intermediate-level radioactive wastes (Milodowski et al., 1995; 1998; 2002, and references therein). Relative age relationships of the fracture mineralization have been established on the basis of:

- Stratigraphical range rocks hosting the mineralization;

- Fracture cross-cutting relationships;

- Vein-filling mineral stratigraphy and mineral replacement fabrics;

- Correlations between fracture mineralization and diagenetic cements in the Permo-Triassic sedimentary strata;

- Limited age dating studies: K-Ar and ^{40}Ar-^{39}Ar dating of ME7 illite mineralization and ME8 K-bearing manganese oxyhydroxide mineralization (ME8); and ^{14}C dating of ME9 calcite (cf. Milodowski et al., 1998; 2002, and references therein).

These studies established that the basement and overlying sedimentary rocks at the Sellafield site have experienced a long and complex history of fracturing and fracture mineralization. Nine broad mineralization episodes (ME1 [the oldest] to ME9 [the youngest]) were originally distinguished (Milodowski et al., 1998; 2002 re). However, in the light of more recent studies (Bouch et al., 2004) a slightly revised paragenetic scheme is summarised in Table 3-9.

3.3.2.1 ME1: LOWER PALAEOZOIC (PRE-ACADIAN) HYDROTHERMAL MINERALIZATION

ME1 is the earliest vein mineralization, comprising quartz, albite, K-feldspar (adularia), chlorite and hematite. It pre-dates the Acadian (mid-Devonian) regional metamorphism and is found only in the BVG strata. ME1 is attributed to early, moderate- to high-temperature hydrothermal (epithermal-mesothermal) activity, possibly associated with a hydrothermal circulation system developed within the BVG pile shortly after its deposition. The veins are generally tightly sealed and play no part in the present-day groundwater circulation.

3.3.2.2 ME2: UPPER PALAEOZOIC (PRE-CARBONIFEROUS) EPITHERMAL SILICATE MINERALIZATION

ME2 is dominated by epithermal quartz mineralization sometimes associated with sericite, epidote, K-feldspar (adularia), albite, chlorite, actinolite, calcite, apatite and hematite. The mineralization was deposited from moderately hot to hot (fluid inclusion T_h 109-300 °C), low- to moderate-salinity (0.2-11.5 wt% eq. NaCl) hydrothermal solutions. ME2 is only found in the Lower Palaeozoic basement rocks, and is attributed to mineralization associated with hydrothermal circulation related to the late Caledonian Lake District Batholith (approximately 390-310 Ma). The veins are generally tightly sealed and play no part in the present-day groundwater circulation.

Table 3-9. Summary of the paragenesis, principal mineral assemblages and stratigraphical range of fracture mineralization in the Sellafield site

Mineralization Episode (ME)	Principal mineral assemblage	Inferred age/origin
Affects the BVG basement strata only		
ME1	Quartz ± albite ± K-feldspar (adularia) ± chlorite ± hematite	*Lower Palaeozoic:* Pre-Acadian (mid-Devonian) regional metamorphism. Related to early moderate-high temperature hydrothermal (epithermal-mesothermal) circulation within BVG.
ME2	Quartz ± epidote ± calcite ± chlorite ± actinolite ± apatite ± K-feldspar ± albite ± sericite ± hematite	*Upper Palaeozoic (pre-Carboniferous):* Moderate to high-temperature (109-300 °C) epithermal mineralization by low-to moderate salinity (0.2-11.5 wt. % eq. NaCl) fluids related to post-emplacement hydrothermal circulation associated with late Caledonian Lake District Batholith. Approx. 390-310 Ma).
ME3	Pyrite ± minor to trace chalcopyrite ± arsenopyrite ± pyrrhotite ± marcasite ± galena	*Upper Palaeozoic (pre-Carboniferous):* Epithermal mineralization closely associated with late stage of ME2
Affects the BVG basement and Carboniferous Limestone strata. Not present in the Permo-Triassic strata		
CME1[1]	Calcite ± siderite ± speccular hematite ± Mn oxides	*Late Carboniferous-Early Permian:* Low temperature hydrothermal mineralization pre-dating the Permian unconformity. In part, possibly related to Permian weathering.
Affects BVG basement to Permo-Triassic strata		
ME4	Major anhydrite ± minor to trace barite ± fluorite ± hematite ± quartz ± siderite (?)	*Post-Permian or syn-Triassic:* Anhydrite derived from remobilization of Permian evaporite sulphate. Equivalent diagenetic cements in the Permo-Triassic strata.
ME5	Kaolinite ± illite ± albite ± K-feldspar ±hematite	*Mid-Triassic to ?Early Jurassic:* Mineralization by warm CO_2/carboxylic acid-enriched, deep-basinal brines evolved during burial diagenesis of Carboniferous and Permo-Triassic strata in the East Irish Sea Basin. Closely associated with ME6. Equivalent late burial diagenetic cements in the Brockram (Permo-Triassic) *[not evident in the Carboniferous Limestone]*
ME6a[2]	Major calcite and colloform-earthy hematite	*Mid-Triassic-?Early Jurassic:* Hydrothermal mineralization associated with expulsion of warm (50-180 °C), Na-Ca-Cl-SO_4-brines (up to 25 wt.% eq. NaCl) from the East Irish Sea Basin during deep burial and diagenesis of the evaporite-bearing Permo-Triassic sedimentary fill. Mixing of two separate fluids; a very saline SO_4-rich fluid and a less saline Cl-rich fluid, is inferred for ME6c barite. Equivalent late burial diagenetic cements in the Permo-Triassic strata.
ME6b	Major dolomite, ferroan dolomite, ankerite, anhydrite ± minor to trace siderite ± quartz	
ME6c	Major calcite ± minor to trace barite ± fluorite ± hematite ± pyrite ± chalcopyrite ± sphalerite ± galena ± Ag-, Ag-Bi, Bi-selenides ± quartz ± rare uranium minerals	
ME7	Illite ± hematite	*Mid-Triassic – Early Cretaceous:* Alteration associated with major fault movements.
ME8[3]	Mn- and Fe oxides/oxyhydroxides.	*?Late-Tertiary to Quaternary:* Oxidative alteration, and dissolution of carbonate and anhydrite mineralization following uplift, weathering and meteoric invasion. Associated with modern shallow groundwater system
ME9[3]	Calcite ± pyrite ± marcasite ± anhydrite ± gypsum ± barite	*?Late-Tertiary – Quaternary:* Mineralization closely associated with modern groundwater system.

Notes:

[1]Originally defined as 'Early ME6a' Permo-Triassic mineralization (Milodowski et al., 1998; 2002) but now recognised as pre-dating the Permian unconformity at Sellafield and revised as 'CME1' (Bouch et al., 2004).

[2]Originally defined by Milodowski et al. (1998, 2002) as 'Late ME6a', now referred to here simply as 'ME6a'.

[3]ME8 and ME9 may be coeval in part, with ME8 occurring near-surface simultaneously with ME9 mineralization in deeper parts of the groundwater system.

3.3.2.3 ME3: Pre-Carboniferous polymetallic sulphide mineralization

ME3 comprises minor polymetallic (Fe-Cu-As-Zn-Pb) sulphide mineralization and is closely associated with ME2. It is poorly preserved in the Sellafield boreholes and is present now only as isolated relicts included within and largely replaced by later (mainlyME6) mineralization. It is considered to correspond to the major regional copper mineralization described from the central and north Lake District (Stanley and Vaughan, 1982).

3.3.2.4 CME1: Late Carboniferous–Early Permian carbonate-hematite mineralization

CME1 was originally classified as the earliest part ('early ME6a') of a complex sequence of fracture-filling minerals defined as 'ME6' mineralization (Milodowski et al.,1998, 2002). However, following more recent studies on the Carboniferous Limestone (Bouch et al., 2004), it is now recognised as an earlier stage of mineralization, that pre-dates the Permian unconformity and is re-designated 'CME1' (Carboniferous Mineralization Episode 1). It comprises fracture-lining euhedral calcite associated with speccular hematite, and sometimes manganese oxide, and is associated with recrystallization and neomorphic calcite cements in the Carboniferous Limestone. There is some evidence to suggest that siderite may have been formed as part of CME1 assemblage in the BVG but was subsequently replaced by calcite and hematite. CME1 is found only in the BVG and Carboniferous strata. Fissures in the Carboniferous Limestone beneath the Permian unconformity contain CME1 fracture-linings beneath a later geopetal fill of sand and silt derived from the overlying Brockram and St Bees Shale formations. Therefore CME1 mineralization may be Late Carboniferous or Early Permian in age, and may in part relate to Permian weathering.

3.3.2.5 ME4: Early post-Permian anhydrite-dominated mineralization

ME4 mineralization is the first veining event that affects both the lower Palaeozoic basement rocks and the overlying Permo-Triassic strata. It is dominated by anhydrite, although minor to trace amounts of hematite and other minerals may accompany the mineralization. This fracture mineralization is correlated with early diagenetic anhydrite cements in the Permo-Triassic strata. Dissolution of the anhydrite mineralization has provided secondary porosity pathways for later mineralizing fluids and present-day groundwater flows. ME4 is best preserved in lithologies in boreholes in the west of the Sellafield site.

3.3.2.6 ME5: Kaolinite-illite-silicate mineralization

ME5 is represented by kaolinite mineralization, which is in part now pseudomorphed by later (probably ME7) illite mineralization. This is associated with the early stages of the major faulting at the site and occurs as a mesodiagenetic cement in the low-matrix, clast-supported Brockram conglomerates. ME5 kaolinite was formed by the interaction of porewaters with host-rock aluminosilicate minerals. Its distribution is lithologically controlled and therefore its absence in the Carboniferous Limestone reflects the scarcity of reactive primary aluminosilicates in the host rock. The kaolinite mineralization is closely associated with, and occurred immediately prior to, ME6a mineralization, which is associated with deep burial cements in the Permo-Triassic strata. Consequently, it is considered to be related to alteration of the aluminosilicate-rich BVG and Brockram by porewaters enriched in CO_2 and/or carboxylic acids (produced during the maturation of organic material in the Carboniferous strata beneath the East Irish Sea Basin). ME5 and ME6 may be closely related: the ME6a calcite could possibly be precipitated as a consequence of the interaction of the high-CO_2 water and/or carboxylic acid-rich waters with the silicate mineral assemblage that gave rise to the kaolinite-illite mineralization.

3.3.2.7 ME6: MAJOR CARBONATE-SULPHATE DOMINATED MINERALIZATION

ME6 is the dominant fracture mineralization affecting the whole sequence of Lower Palaeozoic to Triassic strata in the Sellafield boreholes. It is closely associated with fracture damage envelopes around most of the faults in the area. It can be subdivided into three mineralogically-distinctive sub-episodes:

- ME6a: calcite-hematite dominated mineralization, characterised by veins with alternations of calcite and colloform or earthy hematite. This was originally classified as 'Late ME6a' by Milodowski et al. (1998, 2002) but subsequently revised as 'ME6a' by Bouch et al. (2004);

- ME6b: dolomite-ferroan-dolomite-ankerite-anhydrite-dominated mineralization, with occasional hematite;

- ME6c: predominantly ferromanganoan calcite mineralization with subordinate to trace amounts of barite, fluorite, hematite, pyrite, chalcopyrite, sphalerite, galena, Ag-selenides, Ag-Bi-selenides, Bi-selenides, quartz and rare uranium minerals.

ME6 minerals were deposited from warm (fluid inclusion T_h = 53-180 °C), highly saline (approximately 25 wt% eq. NaCl) basinal brines, most probably derived from the East Irish Sea Basin area during Mesozoic deep burial. It is correlated with the major regional economic hematite mineralization.

The dissolution of ME6b anhydrite and dolomite-ferroan dolomite-ankerite mineralization has produced significant secondary fracture porosity. Secondary porosity produced by the dissolution of similar cements in the matrix of the sandstones is also an important feature of the Permo-Triassic sandstone aquifer. Many of the present groundwater flows in the Sellafield boreholes are closely associated with this dissolution porosity. Dissolution is greatest in the shallow sandstone aquifer and in the east of the site. ME6b anhydrite is relatively rarely preserved in the east of the site but preservation increases with depth and to the west of the PRZ/RCF area. This is consistent with meteoric invasion in the recharge area and leaching of the ME6b mineralization progressively from east of the site.

3.3.2.8 ME7: ILLITE MINERALIZATION

ME7 is closely associated with faults, and is dominated by illite (± hematite) mineralization. This fracture illite can be correlated with diagenetic illite cements in the adjacent sandstone matrix. ^{40}Ar-^{39}Ar and K-Ar ages obtained from ME7 illite indicate that faulting and associated ME6 to ME7 mineralization probably took place between 170-115 Ma (cf. Milodowski et al., 1998, 2002).

3.3.2.9 ME8: TELODIAGENETIC OXIDATIVE GROUNDWATER ALTERATION

ME8 and ME9 are closely related to the development of the present groundwater system. ME8 comprises poorly crystalline to amorphous iron oxyhydroxides and complex K-Ba-Ca-rich manganese oxyhydroxides formed by the oxidative alteration and dissolution of ME6 ferromanganoan carbonates and sulphides. Limited ^{40}Ar-^{39}Ar dating (one sample of K-rich manganese oxyhydroxide, using the method of Vasconcelos et al., 1994) suggests that ME8 mineralization may have been initiated following regional Miocene uplift and subsequent meteoric invasion (Milodowski et al., 1998, 2002).

3.3.2.10 ME9: LATE-STAGE CALCITE-SULPHIDE-SULPHATE MINERALIZATION ASSOCIATED WITH RECENT GROUNDWATERS

ME9 mineralization is the youngest mineralization recognised at Sellafield and is at least partly diachronous with ME8, representing mineralization occurring in the deeper groundwaters

simultaneously with ME8 iron and manganese oxyhydroxides forming at shallow levels. It is dominated by calcite, sometimes associated (in the deeper groundwater system) with pyrite, marcasite, barite, anhydrite and gypsum. In the shallow groundwater system ME9 calcite may enclose or contain inclusions of ME8 oxide. Similar calcite is also recognised as a late cement in the matrix of the Sherwood Sandstone Group rocks.

The distribution of ME9 mineralization corresponds closely with present-day groundwater flow in the boreholes (Milodowski et al., 1995, 2002). Attempts at isotopic dating have been inconclusive but suggest precipitation during the Quaternary (Milodowski et al., 1998). Measurement of ^{230}Th/^{234}U on seven samples indicated apparent ages ranging from 17 to >300 ka but with large uncertainties (Bailey, 2002). ME8 and ME9 mineralizations characteristically line open fracture surfaces, and both occur in close association with zones of groundwater inflow (PFFs) into the Sellafield boreholes. This lends support to a close relationship between the current groundwater regimes and ME8 and ME9 mineralization.

3.3.3 Distribution and morphological characteristics of late calcite mineralization

The distribution and morphological characteristics of the late (ME9) calcite mineralization were studied in detail during the Nirex site investigations at Sellafield (Milodowski et al., 1995, 1998, 2002) and during the previous EQUIP palaeohydrogeology project (Bath et al., 2000).

Milodowski et al. (1995, 2002) demonstrated that there was a very close correspondence between the distribution of ME9 calcite and groundwater inflows in the Sellafield boreholes. ME9 calcite characteristically forms euhedral crystals lining open fractures (Figure 3-33), where it forms either syntaxial overgrowths on reactivated surfaces or corroded cores of older (ME2, CME1, ME6a and ME6c) vein calcite, or it occurs as doubly-terminated crystals resting loosely on hematite-coated and clay-coated fractures and on fresh wallrock surfaces. The calcite crystals range in size from less than 50 μm up to 25 mm in size. The euhedral crystal form of the ME9 calcite clearly demonstrates growth in open fracture space, indicating that these fractures are naturally 'gapped' with in situ open fracture porosity. 'Blind tests' carried out at Sellafield demonstrated that the distribution of groundwater inflows (flow-zones) in the boreholes could be confidently predicted by systematic recording of the occurrence of fractures (PFFs) mineralized by ME9 calcite or ME8 oxyhydroxide mineralization (Milodowski et al. 1995). Furthermore, these tests showed that the logging of ME9 calcite identified many more PFFs with very fine apertures that were not detectable from borehole flow logs, and was a more sensitive tool for identifying potential small flows.

Much of the fracture porosity in the Sellafield site is secondary after the dissolution of ME4 anhydrite and ME6 anhydrite and dolomite-ankerite mineralization, rather than of primary tectonic origin. In many cases, the ME9 calcite lines dissolution cavities in older ME4 features, or in early ME6 veins, where it is evident that the calcite has nucleated on (or rests on) the residual ME6a and ME6c calcite (often present as skeletal frameworks) remaining after the dissolution of ME6b anhydrite and dolomite-ankerite. There is an inverse relationship between the preservation of ME4 and ME6b anhydrite and the occurrence of ME9 calcite. ME9 calcite is most extensively developed in PFFs in boreholes in the east of the site (BH8A, BH8B, BH9A) and in the PRZ/RCF area (Figure 2.7). Further west, in the Fleming Hall Fault Zone (boreholes BH10A, BH12A) ME9 calcite is most extensively developed in fractures in the Sherwood Sandstone Group, Carboniferous Limestone and BVG but is absent in fractures where ME4 and ME6b anhydrite were still present (mainly in the St Bees Shales, St Bees Evaporite and parts of the Brockram). In the west of the site (BH3), PFFs are much less developed and anhydrite mineralization is often well-preserved. Here ME9 is relatively rare or of very limited development (except parts of the Carboniferous Limestone where extensive dissolution porosity is present), and ME9 anhydrite appears to have formed in place of ME9 calcite.
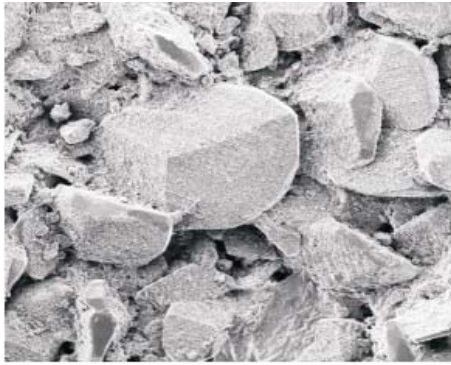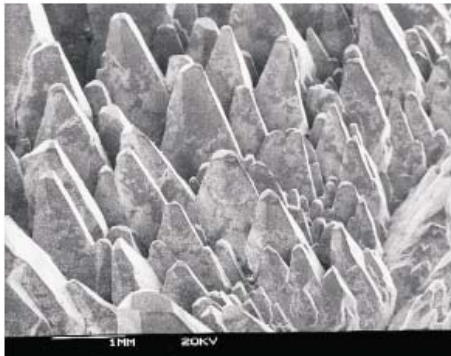
Figure 3-33. SEM images illustrating the different morphological characteristics of late (ME9) calcite at Sellafield: top – short *c*-axis or 'nailhead' crystal form characteristic of the shallow freshwater zone; middle – equant crystal form characteristic of the deeper freshwater zone; bottom *c*-axis elongated 'scalenohedral' or 'dog-tooth' crystal form characteristic of the deeper saline groundwater zone.

ME9 calcite also displays a systematic variation in crystal morphology that closely mirrors the transition from freshwater to saline water with depth. Calcite from the shallow freshwater zone forms short-*c*-axis calcite ('nailhead') crystals (Figure 3-33). In contrast, calcite from the deeper, saline groundwater zone displays the growth of *c*-axis elongated ('dog-tooth' or 'scalenohedral') crystals (Figure 3-33). Intermediate equant calcite crystal forms (Figure 3-33) characterise the lower part of the freshwater zone. The same systematic calcite morphological variation is observed in all the boreholes examined across the site from BH9A in the east, through the PRZ/RCF area boreholes, to the Fleming Hall Fault Zone area (boreholes BH10A, BH12A) further west (Figure 3-34).

The interval within which intermediate forms between short *c*-axis and *c*-axis elongated crystal forms occur is referred to as the Morphological Transition Zone (MTZ). The change between intermediate and *c*-axis elongated crystal forms is generally sharp and appears to occur at a salinity between 1000 and 2000 mg/L chloride (Figure 3-34). The salinity corresponding to the morphological change between short *c*-axis and equant crystal forms is less well defined but appears to coincide with salinities >300 mg/L chloride (Figure 3-34).
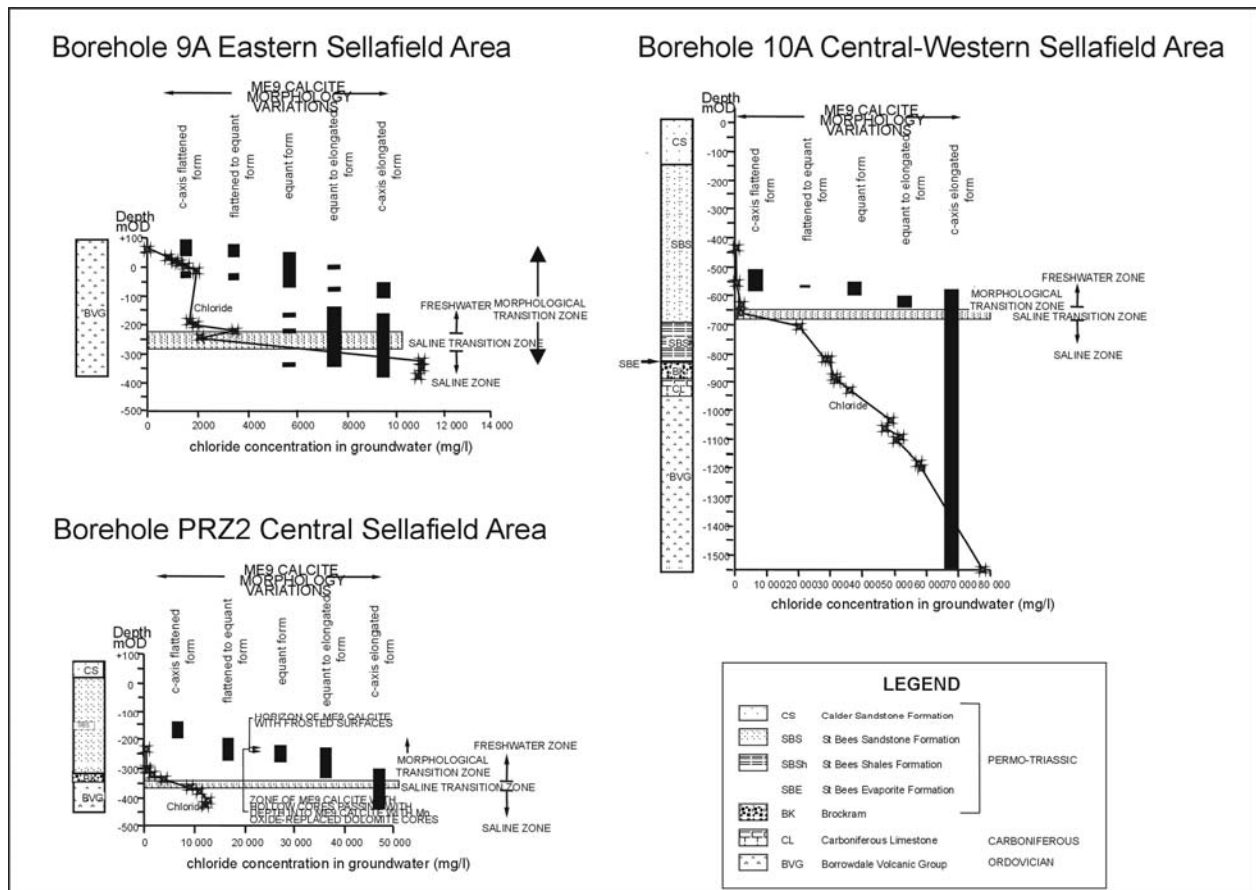
Figure 3-34. Distribution of morphological types of late (ME9) calcite compared to variations in present-day groundwater chemistry for Sellafield Boreholes 9A, 10A and PRZ2.

The position and width of the MTZ varies across the Sellafield site but is independent of lithology. There is some degree of overlap between the distribution of different calcite morphological types. However, the base of the MTZ generally lies 50-150 m above the top of the Saline Transition Zone (STZ) (Nirex, 1997), which has been arbitrarily defined (on the basis of electrical conductivity logs) to represent an interval of approximately 3500-6000 mg/L chloride. In the eastern area of the site (e.g. Sellafield borehole BH9A) the MTZ is much thicker, and intermediate morphological forms are occasionally observed in the saline zone. This thickening of the MTZ mirrors the thickening of the STZ in this part of the site. In contrast, both the MTZ and STZ are much thinner in the west of the site (e.g. Sellafield borehole BH10A).

Morphological observations of the ME9 calcite indicate some movement of the MTZ (and by implication, the STZ) in the past. The general pattern of movement of the STZ/MTZ that is indicated by the calcite morphology and crystal growth fabrics is of an overall downward movement of this interface. In particular, in the upper part of the MTZ, detailed cathodoluminescence petrography studies reveal that the ME9 calcite crystals have cores of *c*-axis elongated (saline type) calcite overgrown by short *c*-axis (freshwater-type) calcite. This indicates that salinity has decreased with time during the growth of the ME9 calcite in the MTZ/STZ. Locally, however, some evidence of upward movement of the STZ interface can also be found in the central and eastern areas of the Sellafield site. Here, the late growth of fine-grained equant calcite nucleated on cores of (older) short *c*-axis calcite is occasionally observed in fractures at around 25 m bOD in borehole BH9A, and between 200-300 m bOD in borehole PRZ3. Similarly, *c*-axis elongated calcite enclosing corroded cores of (older) equant calcite were

106

also observed at around 170 m bOD in PRZ3. These observations suggest that, in these particular fracture flow paths, the salinity has been lower in the past but rose during the later stages of ME9 calcite precipitation. However, evidence for this past upward movement of the MTZ/STZ is rare and may reflect very localised flow-path conditions.

3.3.4 Petrographical and growth zoning characteristics of ME9 calcite mineralization

The growth zoning fabrics of the ME9 calcite were studied in detail during the previous EQUIP investigations (Bath et al., 2000), using CL petrography, with supporting information from BSEM-EDXA and EPMA. CL revealed marked differences in the zoning characteristics between calcites from above the MTZ, and calcites from below the MTZ. These are illustrated diagrammatically in Figure 3-35 to Figure 3-37 and this information formed the starting point for the detailed trace element and isotopic analyses undertaken in PADAMOT.

3.3.4.1 ABOVE MTZ-TYPE CALCITE

Calcite from above the MTZ is characterized by strikingly-zoned crystals with concentric growth zones consisting of alternations of very weakly- to non-luminescent, non-ferroan and non-manganoan calcite and brightly yellow-luminescent, manganoan non-ferroan calcite (Figure 3-35). This late-stage mineralization is often nucleated on a corroded relict core of ME6c or earlier calcite. In addition to variations of Fe and Mn, the calcite also shows zoning with regard to Mg and Sr. However, Mg and Sr distribution is controlled by crystallographic sector zoning rather than within the simpler concentric growth zones.
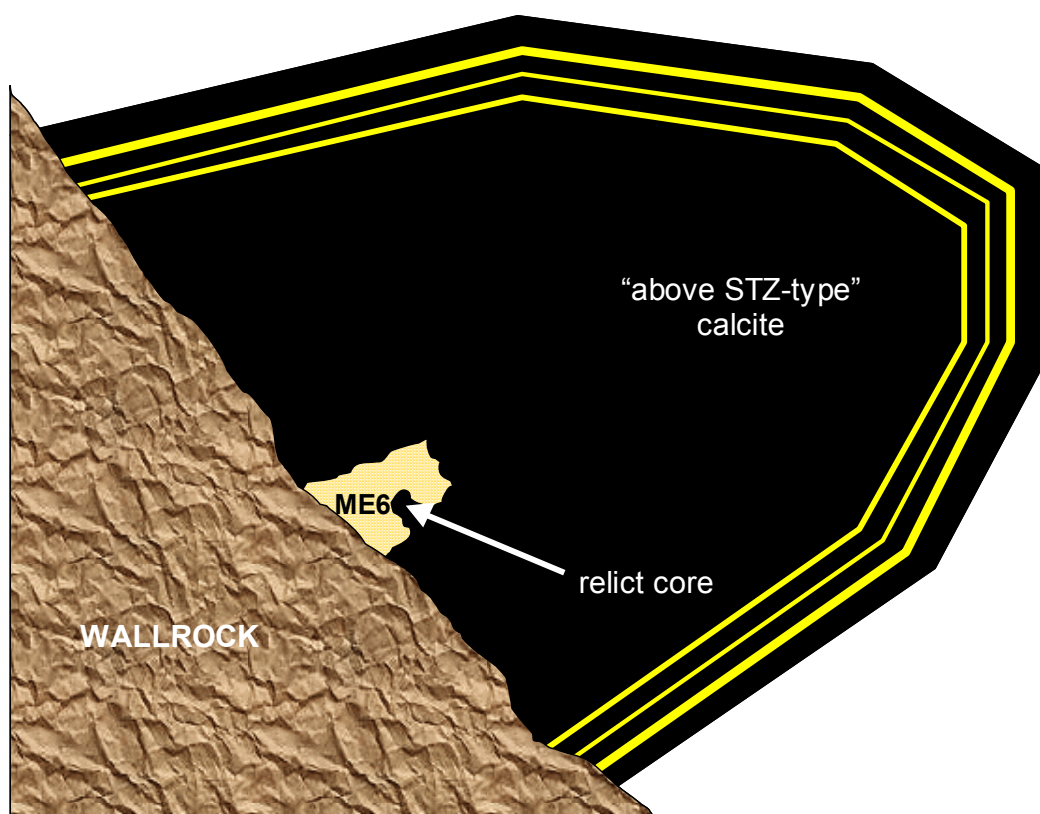
Figure 3-35. Schematic illustration of cathodoluminescence characteristics of calcite from above the morphological transition zone ('Above MTZ-type' calcite), which is typically mainly non-luminescent with fine brightly luminescent zones. The numbers and distribution of bright and dark zones shown are figurative only and vary from sample to sample. Shallow fresh groundwater zone.

The outer (later) regions of the ME9 calcite are typically dominated by the non-luminescent calcite, which typically contains only very thin alternations of brightly luminescent calcite, as shown in Figure 3-40 and shown schematically in Figure 3-35. The brightly luminescent manganoan non-ferroan calcite forms a much greater proportion of mass of the calcite in the earlier inner region of the crystals, where it may be volumetrically the most significant calcite (Figure 3-40). The earlier growth stages with abundant luminescent manganoan non-ferroan calcite are absent in many samples of 'above-MTZ type' ME9 calcite, and the late-stage calcite fracture mineralization is dominated by the later growth stages of non-ferroan and non-manganoan, non-luminescent calcite.

In contrast to calcite from below the MTZ/STZ, individual growth zones cannot be correlated with confidence between different fractures. The fine detail of the zoning appears to be a record of very localised variations in the geochemical environment. However, the overall evolution of the zoning characteristics towards dominantly non-ferroan, non-manganoan calcite suggests that the groundwater may have become generally more oxidizing (i.e. less Fe^{2+} and Mn^{2+} in solution) with time during the growth of the ME9 calcite.

3.3.4.2 BELOW MTZ-TYPE CALCITE

Calcites from below the MTZ and STZ typically display well-developed concentric growth zoning consisting of moderately-to-brightly, yellow- to orange-luminescent bands oscillating with intermediate orange-luminescent and dull, dark-orange to reddish luminescent bands. The ME9 calcite is often nucleated on a corroded relict core of ME6c or older calcite mineralization. Up to 8 distinct CL zones (referred to as Zones 1 [oldest] to 8 [youngest]; summarised schematically in Figure 3-36) can be recognised and can be successfully correlated between different samples and between boreholes. Examples of the zoning characteristics are shown in Figure 3-43 and Figure 3-44.
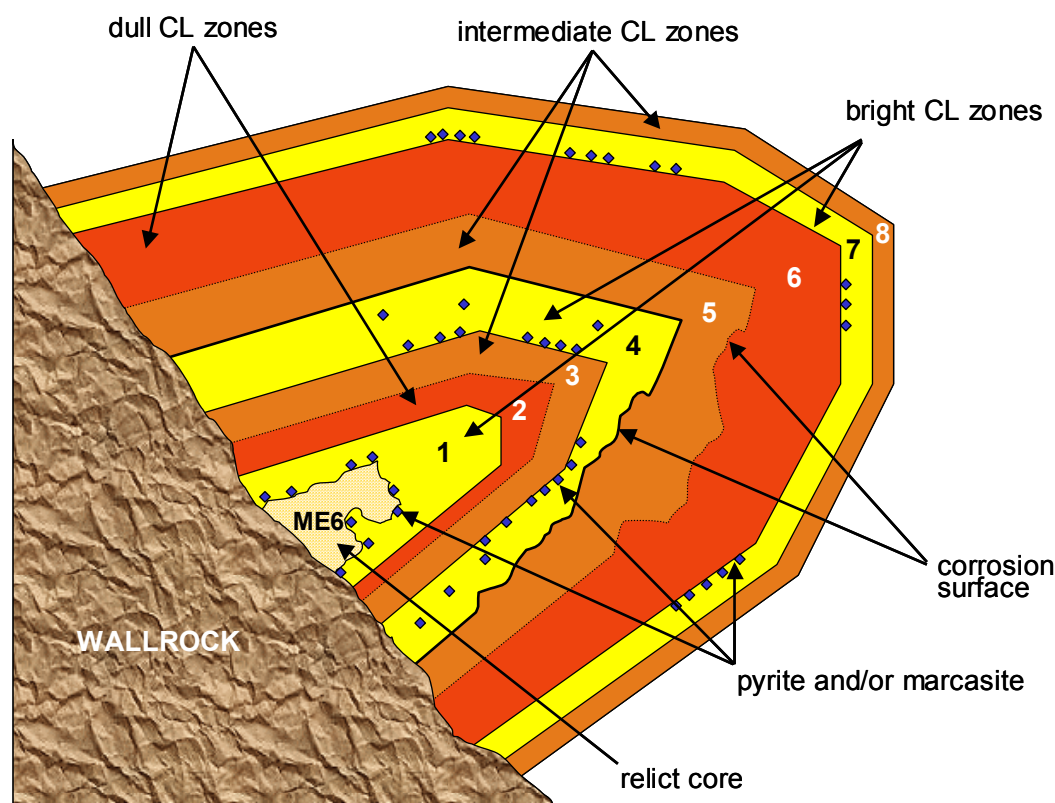
Figure 3-36. Schematic illustration of cathodoluminescence characteristics of calcite from below the morphological transition zone ('Below MTZ-type' calcite).

The variation in luminescence in the calcite is controlled largely by variations in Mn^{2+}, which activates luminescence and Fe^{2+}, which quenches luminescence (Marshall, 1988). Brightly luminescence zones represent calcite with relatively high Mn:Fe ratios, whereas the dull luminescent calcite zones have a lower Mn:Fe ratio. Zones 1, 4 and 7 comprise Mn-rich and low-Fe calcite. Zones 2, 3, 5, 6 and 8 comprise generally dull-luminescent calcite with a relatively low Mn:Fe ratio, with Zones 3, 5 and 8 having a slightly higher Mn:Fe and tending to be brighter than Zones 2 and 6.

Previous studies showed that the more brightly-luminescent high Mn:Fe calcite zones sometimes contained very fine inclusions of pyrite or marcasite (Bath et al., 2000). This suggests that the variations in luminescence in the calcite do not necessarily reflect significant differences in the redox state of the groundwater with regard to the iron and manganese redox couples but that the zones of low-Fe calcite (Zones 1, 4 and 7) were formed during discrete episodes of sulphate reduction, when any Fe^{2+} in solution would preferentially have precipitated as iron sulphide in the presence of S^{2-}. Since these calcites formed at low temperature, below 80 °C (cf. Bath et al., 2000), this implies that sulphide reduction was most probably microbially-mediated, and that these zones correspond to periods of enhance activity by sulphate-reducing bacteria.

Mg and Sr are concentrated in the cores of the ME9 calcite and may show distribution controlled along radial sector zones. The concentration of Mg and Sr in the core region of the ME9 calcite most probably reflects enrichment of Mg and Sr in porewaters associated with the dissolution of ME6b dolomite and anhydrite during the early stages of calcite growth. Corrosion surfaces are also particularly evident at the interface between ME6 calcite and ME9 calcite, Zones 3 and 4, and Zones 5 and 6, indicating periods of calcite instability and dissolution during the evolution of ME9.

Bath et al. (2000) also found that the development of the growth zone sequence in the 'below-MTZ type' calcite varies systematically from east to west across the Sellafield site. The most complete sequence of zones (i.e. Zones 1-8) is found in the boreholes from the east of the site (BH8A/8B and BH9A). Most calcites from the central (PRZ/RCF) area boreholes typically show the development of Zones 1-6 or Zones 1-7. Further west, in BH10A and BH12A the below-MTZ calcite displays a much-reduced sequence of growth zones, with the development of only Zones 1-4 just beneath the MTZ, reducing still further to only Zones 1-3 at greater depths within the STZ. ME9 sulphide mineralization also decreases in abundance from east to west, and is absent in the westernmost borehole (BH3). The dissolution of old (ME4 and ME6b) anhydrite mineralization could provide the sulphur source for pyrite formation, and the antithetic relationship in the distribution of ME9 pyrite (in the east) and ME9 anhydrite (in the west) could reflect a control on sulphate to sulphide reduction by microbial activity (or nutrient supply for microbial activity) introduced by recharge of the groundwater system in the east.

This progressive decrease in complexity or 'maturity' of growth zoning from east to west, and with increasing depth would be consistent with a model whereby the flow system has evolved as meteoric invasion in the recharge area in the east, progressively displacing older groundwaters and creating new flow paths as it dissolves pre-existing anhydrite and carbonate mineralization, as it moves westward and down-gradient. The eastern (recharge) area will have experienced a longer period of meteoric invasion and porosity rejuvenation than the west of the site. Consequently, ME9 calcite in the east of the site potentially records the effects of a more complex history of phenomena that may have impacted on recharge, groundwater flow and changes in groundwater chemistry, than ME9 calcite in the western area or from deeper in the rock sequence and that formed later in the evolution of the Sellafield groundwater flow system.

3.3.4.3 CALCITE WITHIN THE MTZ

ME9 calcite within the upper part of the MTZ displays similar CL zoning characteristics to 'above-STZ type' calcite. Further into, and towards the base of, the MTZ the ME9 calcite

displays a complex hybridization of 'above-MTZ type' overgrowths nucleated on 'below-MTZ type' growth fabrics. This is illustrated schematically in Figure 3-37.

The early core-zones of the ME9 calcite are characterized by calcite typical of the 'below-MTZ type'. In the PRZ/RCF area and further east, the cores show an attenuated sequence of growth zones from Zone 1 up to Zone 5. The outer surface of this 'below-MTZ type' calcite is usually etched or corroded before being enclosed beneath later largely non-luminescent calcite characteristic of 'above-MTZ type' calcite (Figure 3-37). Furthermore, CL reveals that the morphology of the calcite has also changed from a *c*-axis elongated to an equant or short *c*-axis crystal form, during the transition from 'below-MTZ' to 'above-MTZ' luminescence type calcite.
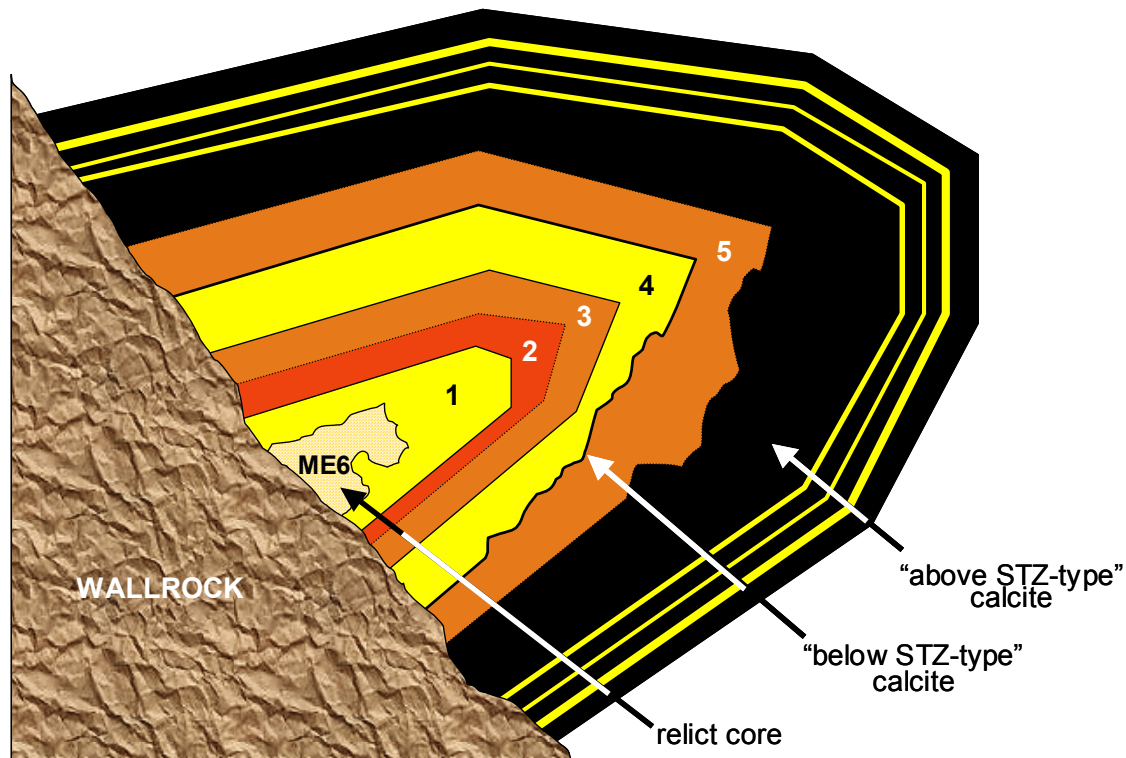
Figure 3-37. Schematic illustration of cathodoluminescence characteristics of calcite from the lower part of the MTZ (just above the STZ). The oldest part of the crystal is formed of calcite typical of below-STZ type. This is terminated by a dissolution unconformity, and overgrown by calcite of above MTZ-type. The calcite growth shape also changes from 'deeper' *c*-axis elongate to a more *c*-axis flattened form characteristic of the shallower freshwater zone.

The change in growth fabric within ME9 calcite in the MTZ is very sharp, and it implies that the calcite has responded to a relatively rapid change in both the salinity and the redox condition of the groundwater within this region of the groundwater system. The observations indicate that the STZ boundary between the freshwater zone and the saline groundwater zone was originally at a higher elevation but has moved downwards as the groundwater system has evolved. There is no evidence preserved in the ME9 calcite, from either the morphological variation or the growth zoning fabrics revealed by CL, to indicate that the STZ has moved downwards by more than 50-150 m.

3.3.5 Trace element characteristics of the late calcite mineralization

Trace element data were obtained for the ME9 calcite mineralization using both the ion microprobe (Edinburgh University) and LAMP-ICP-MS (at the BGS) techniques. Four samples were examined in detail by ion microprobe and 10 samples were examined, but in less detail, using LAMP-ICP-MS (Table 3-8). The samples were selected to cover the range of calcite types identified within the different groundwater types, including calcite from above the STZ, calcite within the STZ, and calcite from below the STZ. The objective was to examine trace element variations during calcite crystal growth that might reflect the geochemical evolution of the palaeo-groundwater system. A suite of elements was analysed with each instrument, ranging from major and minor elements (Mn, Fe, Mg) to trace elements (REE suite).

The sub-samples examined by LAMP-ICP-MS were initially prepared as polished blocks mounted in Plaster of Paris, so that they also could be analysed for oxygen and carbon stable isotope ($\delta^{18}O$ and $\delta^{13}C$) composition using He-LACE microsampling (Section 3.3.7), without contamination from the mounting media. However, this mounting technique was unable to produce good quality polished surfaces that could be readily observed and characterised by CL microscopy. Subsequently, an improved mounting technique was developed by embedding the calcite crystals in M70 low-melting point (70 °C) Bi-Pb-Sn alloy. This did improve the quality of the polished section surface but the polished finish was still substantially poorer than for conventional polished section preparation using epoxy-resin impregnation. In addition, some calcite crystals were lost during preparation because the calcite did not bond to the metal and was readily plucked out during polishing. Furthermore, because the metal mounts are opaque, it sometimes proved quite difficult to locate the position of the laser analysis points under the LAMP-ICP-MS and He-LACE targeting microscopes, relative to the growth zones identified by CL microscopy. In general, the ion microprobe produced analyses with a spatial resolution ('spot size') of 15-20 μm diameter. LAMP-ICP-MS has a comparable but slightly coarser spatial resolution, producing ablation pits typically about 30 μm diameter. Both techniques have similar limits of detection of a few ppm for most of the trace elements determined. Despite these differences, the LAMP-ICP-MS technique provided results that corroborate the ion microprobe data, and these are tabulated in Appendix 7.

3.3.5.1 Fe AND Mn

Both ion microprobe and LAMP-ICP-MS analyses show that the Fe and Mn abundances fluctuate according to the degree of luminescence of individual growth zones, confirming the BSEM-EDXA and EPMA observations, and is consistent with earlier findings (Milodowski et al., 1998; 2002; Bath et al., 2000).

A cross-plot of the data for Fe and Mn from the very limited suite of samples (3 calcites from 236-413 m bOD in borehole PRZ2 and 1 calcite from 1527 mbOD in borehole BH2) analysed by ion-microprobe is illustrated in Figure 3-38. The data appear to show a covariance between Fe and Mn, and an apparent increase in concentration of both Fe and Mn with depth. This could be taken to be evidence of either a decrease in calcite precipitation rate at deeper burial, an increase in water/rock interaction, or an increase in temperature (Myers, 1991). However, analysis of the larger population of samples from a wider range of boreholes by LAMP-ICP-MS (Figure 3-39) shows that there is not a simple relationship between depth and concentration of Fe and Mn, and that the apparent depth-related trend of the data shown in Figure 3-38 is not uniformly consistent across the Sellafield site. If the LAMP-ICP-MS data from the RCF/PRZ area samples are considered separately, the data in Figure 3-39 are better considered as forming two discrete populations, with trends of Fe + Mn co-variance within each sample:

- Samples D280, D283 and D286 form a tight cluster of analyses with most analyses characterised by low Fe (0-700 ppm) and low to moderate Mn (0-2500 ppm). These correspond to the strikingly zoned 'above MTZ type' ME9 calcite;

- Samples B946, D329, D311 and MPLK559 form a broader region of data characterized by high Mn (6000-20000 ppm) and moderate to high Fe (1500-8000). These calcites represent calcites from below the MTZ - from the base of the freshwater zone, the STZ and the deeper saline groundwater zone.

Most of the variation observed in the 'above MTZ' calcite population is for Mn (Figure 3-39). Occasional analysis points with high Fe are probably attributable to included particles of iron oxides. Individual samples of calcite from below the MTZ display a wide range of Mn and Fe concentrations that reflect the CL zoning and with no obvious depth related-trend. This may reflect significant local differences in the degree of rock-water interaction at different locations across the site. The ion-microprobe data (Figure 3-38) could readily be re-interpreted to fall into these two discrete calcite populations.
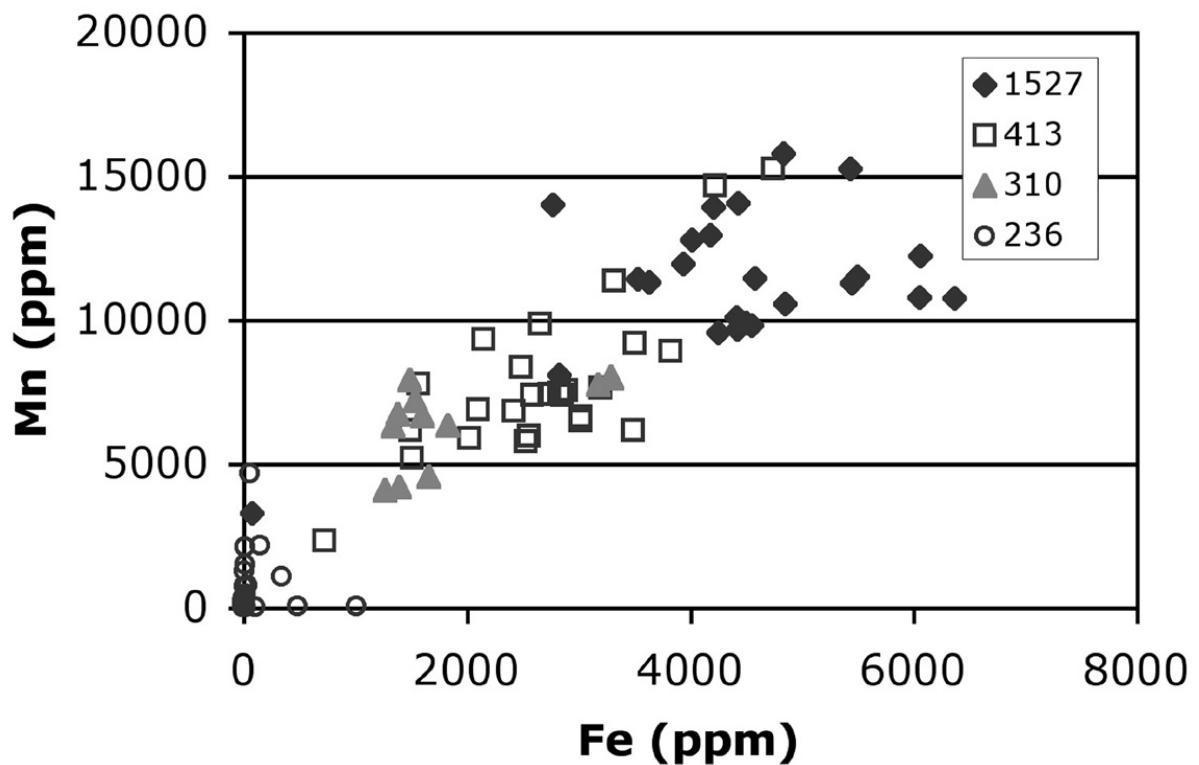
Figure 3-38. Analysis of Fe and Mn content in ME9 calcite (from PRZ/RCF area boreholes, PRZ2 and BH2) by ion microprobe shows a systematic increased content with deeper calcites (sample depths in mbOD indicated by different symbols).

Also shown on Figure 3-39 are data for one sample of 'below MTZ type' ME9 calcite, from boreholes BH9A (sample D723), and one sample of ME9 calcite from the top of the MTZ in borehole BH12A (sample B877). The BH9A sample is consistent with the data from the PRZ/RCF area. However, the calcite from BH12A shows a different trend, and although Fe and Mn co-vary, it does so with much lower Mn and a considerably larger range of Fe concentrations compared to other MTZ/'below-MTZ' calcites. This may reflect redox variations affecting Fe and Mn but in the absence of any sulphate reduction (to remove Fe by sulphide precipitation) in this part of the site. Alternatively, this may reflect differences in rock-water interaction and residence time related to this borehole being situated within a major conductive fault zone – the Fleming Hall Fault Zone.

As observed in previous studies of calcite at Sellafield (e.g. Milodowski et al., 1998; Milodowski et al., 2000), the compositional fluctuation of Mn:Fe within the growth zones appears to generally decrease with depth (e.g. Figure 3-40, Figure 3-43 and Figure 3-44), which may also

be indicative of an increasing groundwater geochemical stability, particularly relating to redox conditions (Milodowski et al., 1998). Alternatively, these less marked variations in Mn:Fe might result from redox changes of similar size to that in the shallower system but within an overall lower Eh.
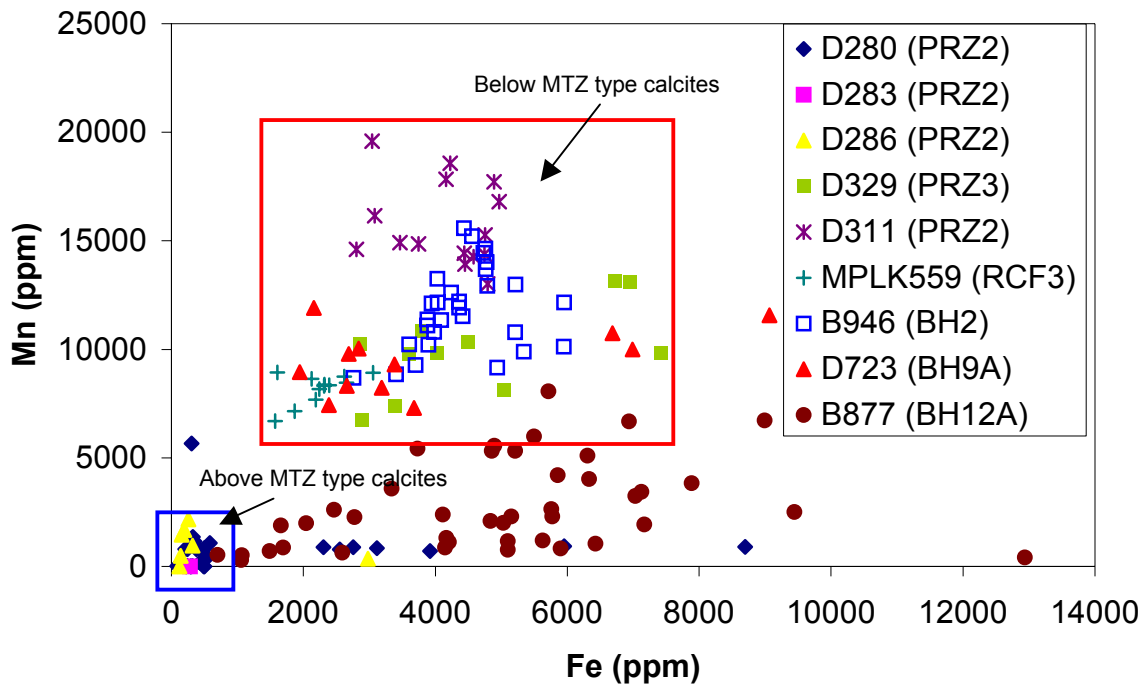
Figure 3-39. Analysis of Fe and Mn content in ME9 calcite by LAMP-ICP-MS. Analyses by each sample, with RCF/PRZ area (PRZ2, PRZ3, RCF3 and BH2) samples listed in increasing depth. Blue box = field of compositions of most 'above-MTZ type calcites; red box = field of compositions of most 'below-MTZ type' calcites (RCF/PRZ area).

3.3.5.2 REE ELEMENTS

Unlike Mn and Fe concentrations, total REE concentration (ΣREE) distribution in calcite does not vary greatly with depth. The main change in ΣREE observed in the samples analysed by ion microprobe is that the inner-most parts of sample B946 (borehole BH2, 1527 m bOD) and sample D311 (borehole PRZ2, 413 m bOD) have lower ΣREE than the outer zones, by a factor of 15, and lower ΣREE than the inner zones of shallower samples by a factor of 100. Individual crystal samples vary internally in ΣREE from 1-2 ppm to 350 ppm. In some cases, ΣREE fluctuates according to luminescent zonation, in other cases, the cause for changes in ΣREE is less apparent.

There is a very marked difference in the distribution characteristics of chondrite-normalised (e.g. Anders and Grevasse, 1989) REE compositions, between the non-luminescent and brightly luminescent zones of the nailhead and equant ME9 calcites in the shallow freshwater zone above the MTZ. This is shown both by the ion-microprobe data (Figure 3-40) and in the more extensive dataset obtained from LAMP-ICP-MS (Figure 3-41). The luminescent (Mn-rich, low-Fe) calcite zone profiles are characterised by a humped REE pattern, associated with Medium (M) REE enrichment, compared to Light (L) REE or Heavy (H) REE (Figure 3-41). In contrast, the non-luminescent calcite zones display a flatter chondrite-normalised REE profile with a very strong negative Ce anomaly (factor of 100) in the LREE (Figure 3-41). This confirms the more limited observations recorded during earlier studies (Bath et al., 2000).
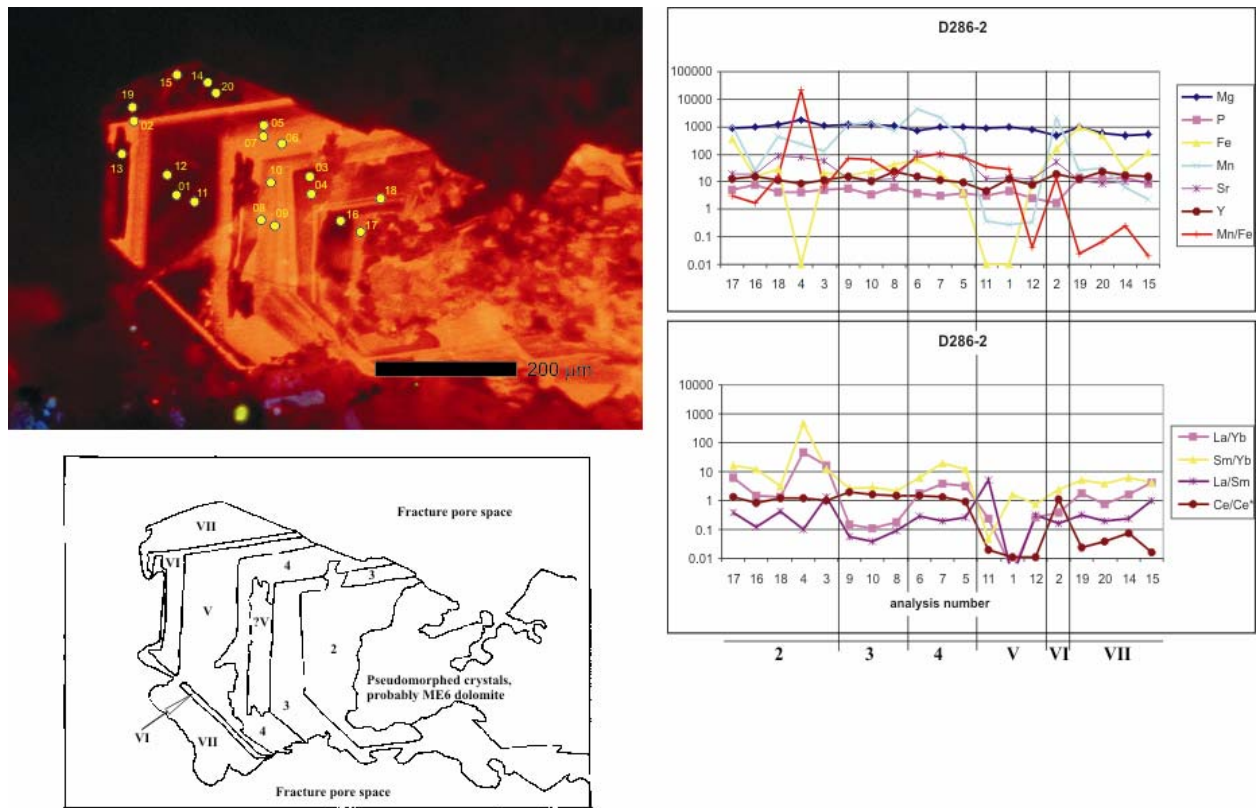
Figure 3-40. Cathodoluminescence characteristics, ion microprobe analysis locations, and compositional characteristics of 'above-MTZ-type' (shallow freshwater zone) late-stage calcite from the St Bees Sandstone Formation, sample D286, Sellafield borehole PRZ2, 236.15 m bOD.

ME8 manganese and iron oxyhydroxide mineralization is often closely associated with ME9 calcite in the shallow fresh groundwater zone, and the carbonate and oxide mineralization are at least partly contemporary: manganese and iron oxyhydroxides forming in the shallowest (i.e. more leaching weathering) environment, simultaneously with calcite precipitation at greater depth; and the calcite may include, and/or be intergrown with, the oxyhydroxides where the ranges of the two phases overlap (cf. Milodowski et al., 1995; 1998a, 2002). LAMP-ICP-MS analyses were also made of one sample of ME8 barium-manganese oxyhydroxide, closely associated with an interval of ME9 calcite from borehole BH2. Chondrite normalised REE profiles of the ME8 oxide mineralization also display a very strong negative Ce anomaly (Figure 3-42) similar to the profiles for non-luminescent ME9 calcite (Figure 3-41).

Cerium is the only one of the REEs that can exist in either the Ce(III) or Ce(IV) oxidation state within the normal range of shallow groundwater geochemical conditions. Ce(IV) is considerably less soluble and less mobile than Ce(III), and Ce anomalies in marine carbonates have for a long time been recognised as sensitive indicators of variations in oxic conditions in the Earth's near-surface chemical cycles (Humphris, 1984; Fleet, 1984; McLennan, 1989; Braun et al., 1990; Leybourne et al., 2000). The location of the Ce anomaly correlates well with colours of CL zones which record Mn:Fe content, and hence together point to a record of relative changes in palaeogroundwater oxidation in the shallow freshwater system. Ce-depleted anomalies are observed in both non-luminescent and luminescent zones of fracture filling calcites in the 'Upper Unsaturated Zone' at Yucca Mountain (Vaniman and Chipera, 1996; Denniston et al., 1997). This is interpreted as Ce^{4+} present in the groundwater being preferentially scavenged by pre-existing and co-precipitating manganese oxide phases. However, the presence of a strong negative Ce anomaly within the ME8 manganese oxyhydroxide as well as in the non-luminescent ME9 calcite clearly indicates that the oxide phases have not sequestered the missing

114

Ce in the shallow fresh groundwater system at Sellafield. The most probable explanation for the observed negative Ce anomaly is that Ce^{4+} was actually depleted (i.e. oxidizing groundwater conditions prevailed) in the palaeo-groundwaters from which both ME8 manganese oxyhydroxide and the non-luminescent low-Mn, low-Fe ME9 calcite growth zones precipitated.
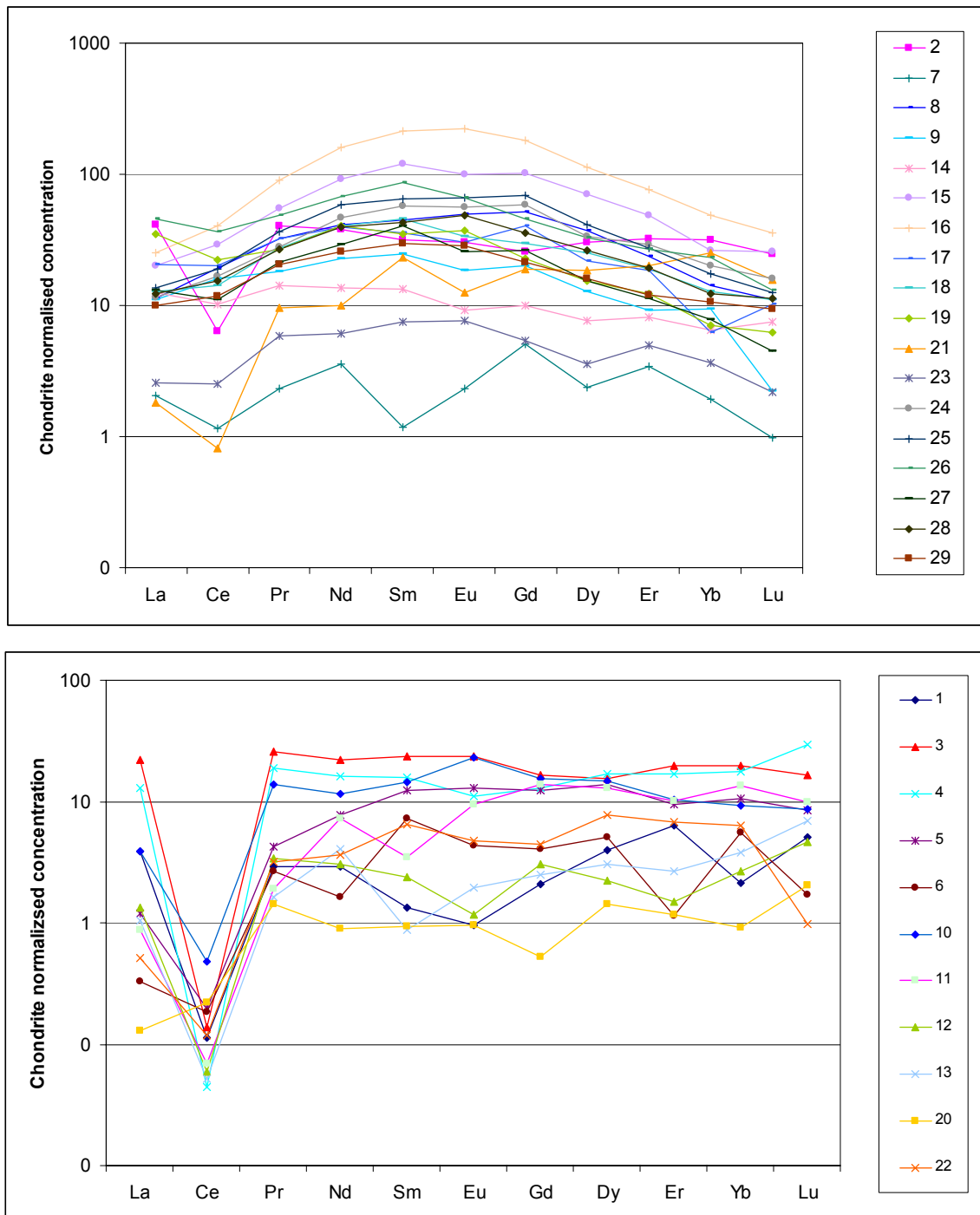
Figure 3-41. Chondrite-normalized REE distribution patterns (determined by LAMP-ICP-MS) for above-MTZ–type (shallow freshwater zone) late-stage (ME9) calcite. Top: brightly luminescent calcite bands (analyses 7-9, 14-19, 23-29); analysis 2 represents intermediate luminescent calcite; and analysis 21 is mixed finely luminescent and non-luminescent calcite. Bottom: non-luminescent calcite zones (analyses 1, 3-6, 10-13, 20 and 22). Short c-axis morphology, St Bees Sandstone Formation, borehole PRZ2, sample D280, 147 m bOD.
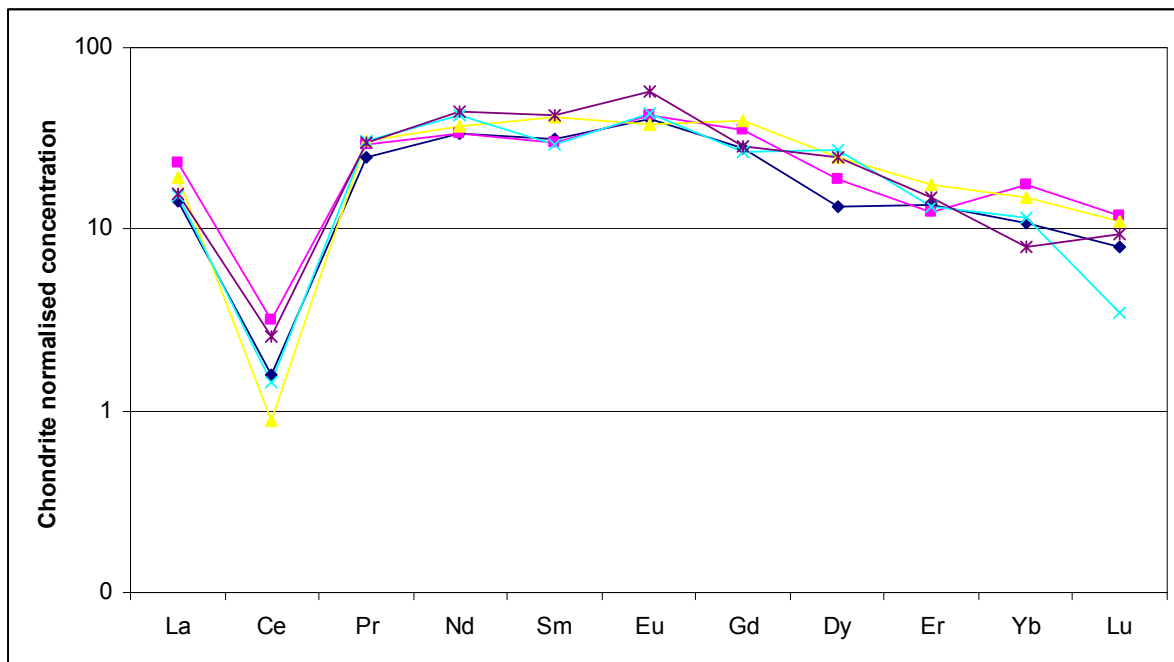
Figure 3-42. Chondrite-normalised REE distribution (determined by LAMP-ICP-MS for ME8 barium-manganese oxyhydroxide fracture mineralization (shallow freshwater zone). Sample NSF2/1367/P4, Calder Sandstone Formation, Sellafield borehole BH2.
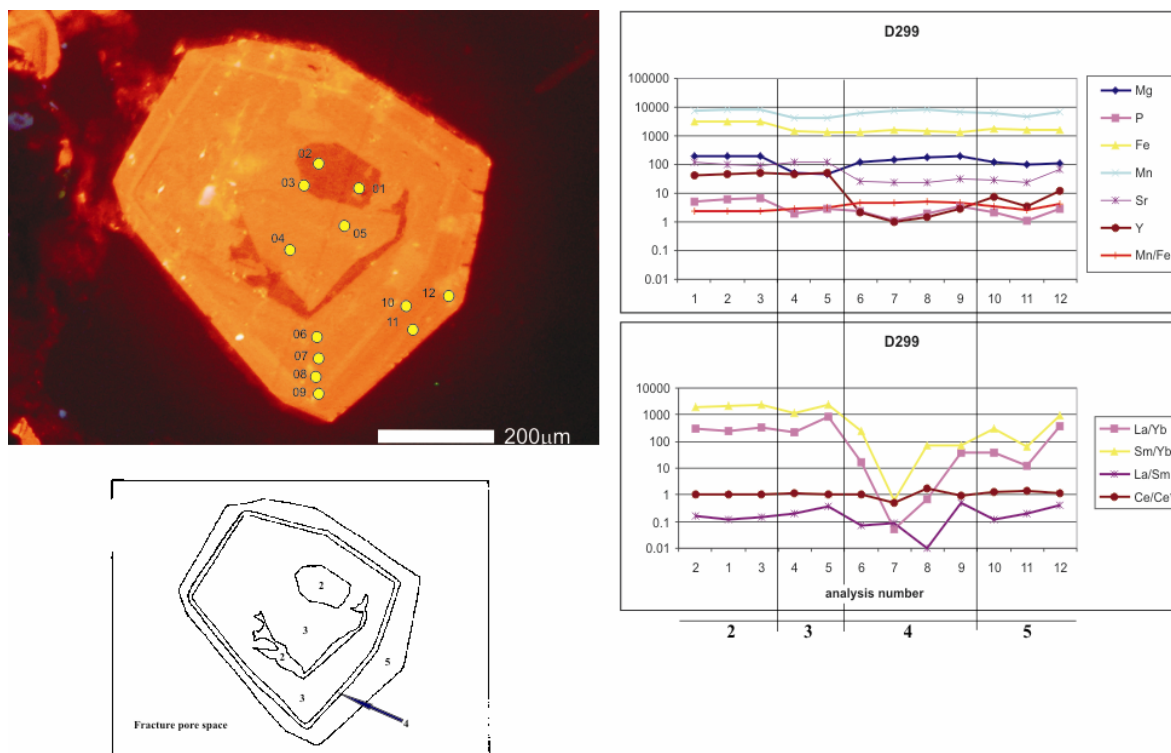
Figure 3-43. Cathodoluminescence characteristics, ion microprobe analysis locations, and compositional characteristics of late-stage (ME9) calcite within the MTZ (deeper freshwater zone) in sample D299, Sellafield borehole PRZ2.
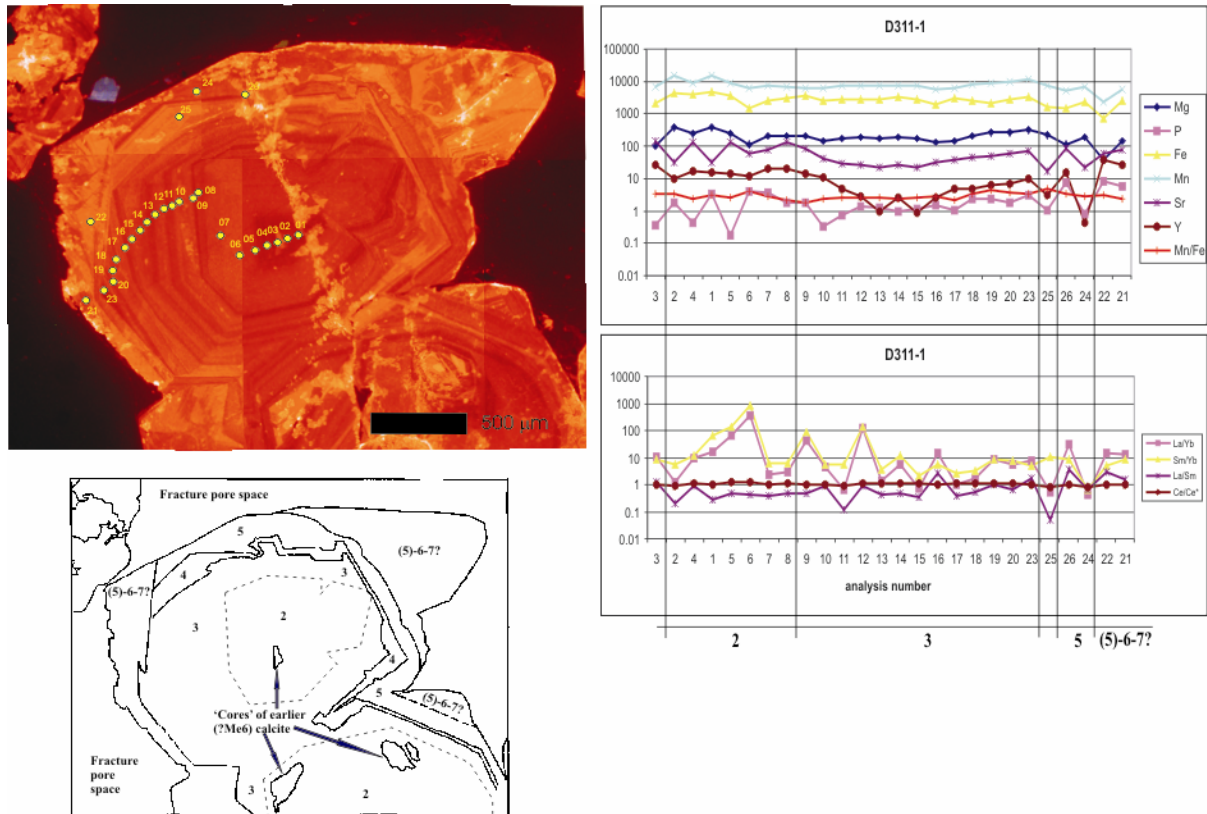
Figure 3-44. Cathodoluminescence characteristics, ion microprobe analysis locations, and compositional characteristics of 'below MTZ-type' (saline groundwater zone) late-stage (ME9) calcite in sample D311, Sellafield borehole PRZ2.

In the site under investigation, we know that groundwater today (Nirex, 1998) has measured pH values of 6.2 to 7.8, and that Ce above the STZ is <0.3 μg/l (2 x 10^{-9} Molar), and groundwater below the STZ has Ce <15 to 20 μg/l (1.8 x 10^{-7} Molar). Consideration of the Eh versus pH diagram for Ce(III) and Ce(IV) speciation (Figure 3-45) indicates that, assuming constant groundwater pH between 7-8, a substantial Ce depletion by two orders of magnitude (i.e. from 10^{-9} to 10^{-11} molar) corresponds to an increase of Eh by about 100 m volts. Thus, Ce depletion within the shallow ME9 calcite records an ancient change of oxidation state from less-oxidising to more-oxidising. At pH 7.0 this would be Eh +40 mV to +160 mV, whereas at pH 8.0 this would be Eh –220 mV to -100 mV. The good coincidence of analysed Ce depletion with dark CL colours is striking in these samples. However, a correspondence between the CL and the Fe and Mn is not so obvious in Figure 3-40, although there is good correspondence in the larger dataset analysed by LAMP-ICP-MS (Appendix 7). This is the first time that such a correlation has been demonstrated for palaeogroundwater, at a fine scale relating to individual growth zones within a crystal. This shows that detailed analyses using ion beam or laser microsampling technology can provide a fine-scale of resolution on ancient groundwater conditions.

ME9 calcites from close to the STZ (MTZ) and in the deep saline groundwater zone below the STZ are characterised by hump-like chondrite-normalised REE profiles, associated with MREE enrichment, compared to LREE or HREE. This is very similar to that for the luminescent zones in 'above-MTZ type' calcite. However, there is very little variation in the normalised REE pattern between different zones of calcite.

Detailed profiles recorded by ion-microprobe show that within dogtooth crystals of the deepest sample studied (B946, 1527 m bOD, borehole BH2), the core displays a depleted, irregular chondrite-distribution of REE. As the crystal becomes younger, LREE and MREE become more enriched, but HREE concentrations remain relatively low. A negative Eu anomaly is evident in

117

the outer rim, strongest at the core / rim contact, and becoming weaker as the crystal becomes younger. The Eu anomaly may be inherited from interaction of the groundwater with the BVG (which also has a Eu anomaly). The progressive reduction in this anomaly, in younger calcite growth zones probably records the reducing influence of the local host-rock REE signature as the growing calcite increasingly seals off the host rock from contact with porewater as mineralization progresses.
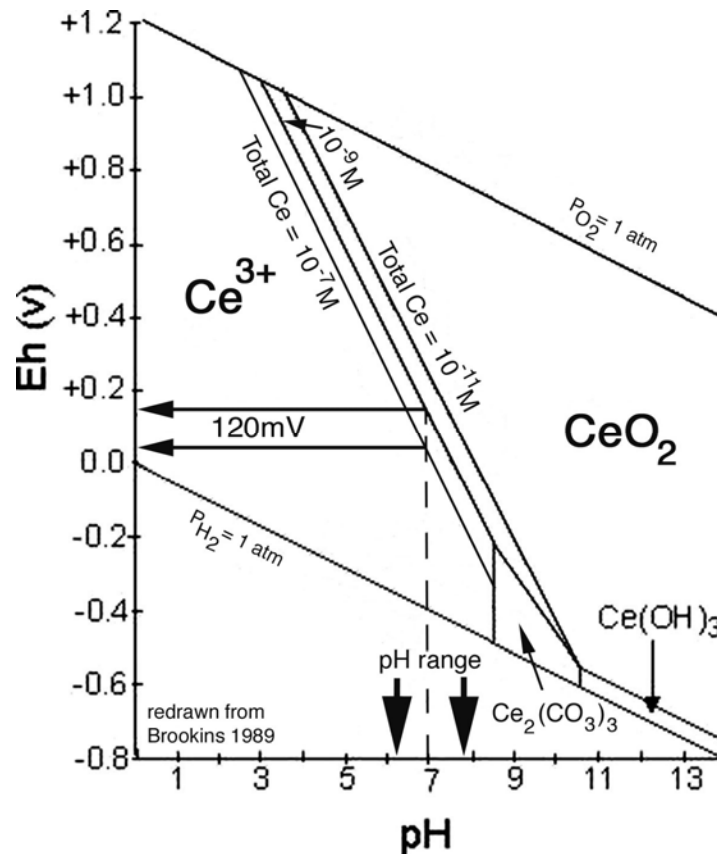
Figure 3-45. Plot of Eh against pH for cerium. For pH around 7.0, which is as measured in Sellafield, then the two oxidation states co-exist at +100mV, being the boundary between Ce^{4+} concentrations 10^{-11} Molar, and Ce^{3+} concentrations 10^{-9} Molar. Ce depletion in calcite crystals can be interpreted to indicate a relative increase of oxidation by +120 mV.

3.3.5.3 HALOGENS

Modern groundwaters contain different mixtures of halogen elements (Cl, Br), and these can sometimes be used to diagnose water origins. Analyses of present-day groundwaters at Sellafield (Bath et al., 1996; Nirex, 1997) have shown that ratios of Br/Cl x 10^{-3} can be discriminatory, when plotted against δ^{18}O or Cl concentration. The Hills and Basement regime groundwaters beneath Derwentwater have Br:Cl x 10^{-3} of 3.8, whereas the STZ has 1.5-1.8, and the Irish Sea brines are less than 1.2.

However no means has yet been found to access similar information about halogen ratios in palaeowaters, to determine the past interfaces and water sources. Fluid inclusions record the compositions of palaeogroundwaters, however these are difficult to access even with laser-beam instruments, because large inclusions (more than 15 μm diameter) are needed to provide sufficient mass of material for analysis. In this project it was attempted, for the first time, to analyse the halogen content on a scale on tens of microns - held either within microscopic fluid inclusions or within the ME9 calcite lattice. Samples examined included 'above-MTZ type'

ME9 calcite (sample D286, 236 m bOD in borehole PRZ2), and ME9 calcite from the deep saline groundwater (sample B946, 1527 m bOD in borehole BH2). The ion microprobe has enabled the first analyses to be gained from halogens in normal growth zones of the calcite crystals.
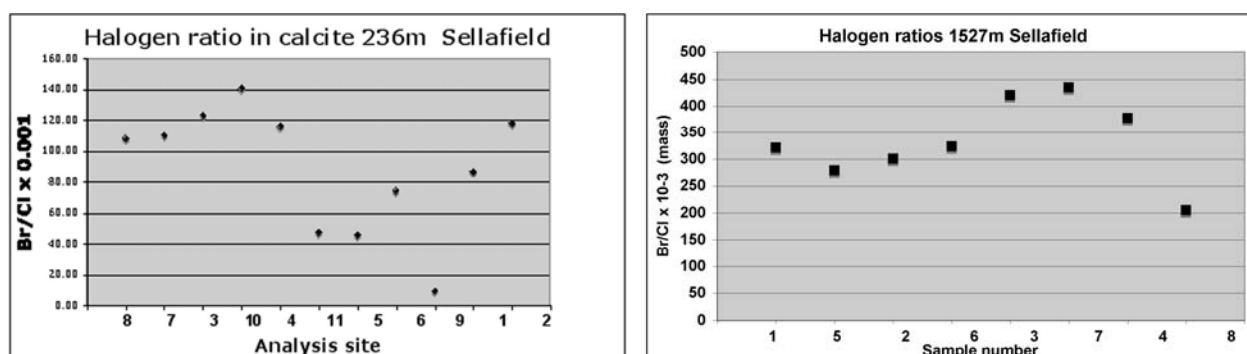
Figure 3-46. Halogen data for two samples of ME9 calcite from Sellafield.

A plot of the ratio $Br/Cl \times 10^{-3}$, as used by Bath et al (1996), shows a coherent pattern for the calcite from the shallow freshwater zone (Figure 3-46), suggestive of varying cycles of salinity. Two cycles of salinity appear to be recorded from inner bright CL zones, to outer dark CL zones. In contrast, a similar plot from the calcite sample in the deep saline groundwater zone (1527m) shows less varying salinity, with much higher Br (Figure 3-46) suggestive of a more continuous history of Hills and Basement water.

The ion microprobe data obtained from these two samples appears to show the potential signatures of ancient groundwater salinity. The Br:Cl ratio can potentially be used to track water origins, and compare directly with modern water analyses. However the ratio values from either sample are unlike those from present-day waters reported by Bath et al (1996), implying that a selective fractionation may have occurred. The possibility that ion-microprobe halogen data from the calcite have been influenced by analysis of entrained microscopic inclusions of halogen-bearing silicate minerals (e.g. illite) is unlikely, since no evidence of such inclusions has been found during detailed petrographical observations by BSEM.

3.3.6 Fluid inclusion studies

Microthermometric and microchemical fluid inclusion studies of ME9 calcite were undertaken during the EQUIP project (Bath et al. (2000). The fluid inclusions displayed salinities of between 3,000 and 120,000 ppm TDS, similar to the overall range of present-day groundwater salinity through the Sellafield site (<200 to 135,000 ppm TDS). Some inclusions with higher salinities in ME9 calcite (up to 252,000 ppm TDS) were observed in boreholes close to the coastline in the southwest part of the study area. Microthermometric data for the lower salinity fluids have T_{fm} and T_{ice} values that are characteristic of alkali-bicarbonate compositions whilst the higher salinity fluids have T_{fm} values that indicate Na-Cl groundwater characteristics.

Microchemical analyses of fluid inclusions by LAMP-ICP-MS was limited by the analytical detection limits. In practical terms this meant that the technique was limited to the analysis of the brackish and more saline inclusions, whereas analyses of freshwater inclusions were at or below detection limits (see below). The results showed that the ME9 calcite-hosted inclusions were chemically similar to the present-day deep groundwaters (Figure 3-47). They have Na-Mg-Sr-Li variations that lie on a mixing line between the average compositions for brines in the 'East Irish Sea Basin Groundwater Regime' and saline groundwaters of the 'Hills and Basement Regime' (Bath et al., 2000).

119
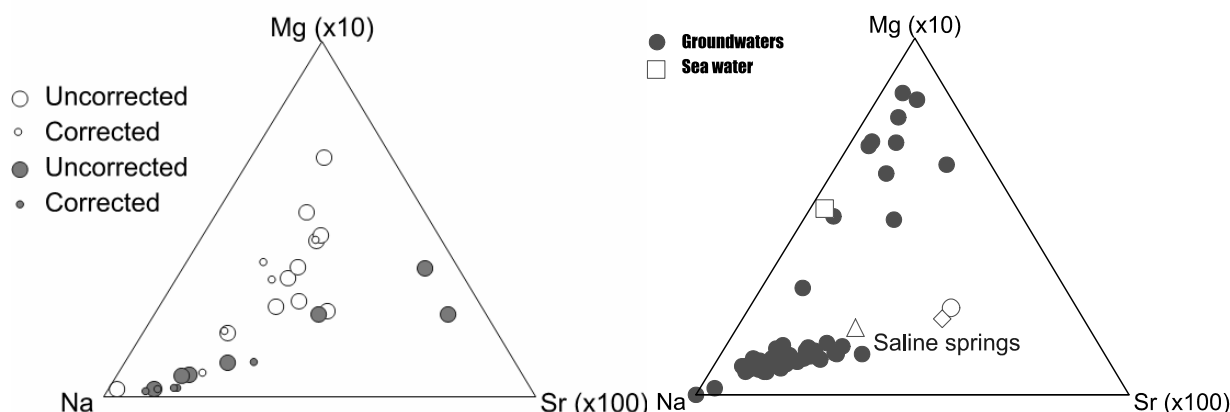
Figure 3-47. Comparison of microchemical data for Mg, Sr and Na from fluid inclusions analysed by LAMP-ICP-MS (left) with groundwaters from the Sellafield boreholes and natural saline springs in the Lake District (right). Fluid inclusion data are shown for uncorrected and corrected for matrix contribution from the host calcite.

Bath et al. (2000) demonstrated that the fluid inclusions show an overall increase in salinity with depth in the PRZ/RCF area. However, a high proportion of the inclusions have salinities that are substantially higher (>50,000 ppm TDS) than those of the present groundwaters at the same depth (up to 25,000 ppm TDS). This indicates that the groundwaters were more saline than at present at some stage(s) during the formation of these calcites.

Both the earlier EQUIP studies (Bath et al., 2000) and re-examination of material during PADAMOT showed that fluid inclusions in ME9 calcite are very sparsely distributed. In some cases, only one or two inclusions per inclusion wafer sample could be found. This means that the acquisition of a representative inclusion dataset requires the preparation of large numbers of replicate fluid inclusion wafer samples. This had major implications on analytical costs and was outside of the resources available within the PADAMOT project, and therefore no new fluid inclusion analyses could be undertaken during PADAMOT. Another aspect is that the majority of the fluid inclusions are preserved within the central region of the ME9 calcite crystals. In particular, inclusions tend to be concentrated along the boundary between the corroded older ME6 calcite mineralization core and the enclosing ME9 calcite. Few, if any, inclusions were observed within the outer, more recent growth zones of the calcite. Consequently, the fluid inclusion data largely represents the early stages of ME9 mineralization and provides very little information on the more recent palaeohydrogeological evolution.

The analytical detection limits also present some problems in the application of fluid inclusion studies to the Sellafield site. The detection limit for fluid inclusion palaeosalinity determination is limited by the precision of the measurement of temperature. Modern fluid inclusion analysis equipment can measure temperatures to a precision of ±0.1 °C, which translates into a precision of 0.2 wt% NaCl (i.e. 2000 ppm NaCl). Therefore, for dilute palaeofluids, this places an effective detection limit for fluid inclusion analysis at 0 ±0.1°C which equates to a salinity of 2000 ppm NaCl. (1213 ppm Cl). In the case of the Sellafield site, this means that it is difficult to reliably differentiate the more dilute brackish waters that would characterise the upper part of the STZ from freshwater.

3.3.7 Stable isotope (δ^{18}O and δ^{13}C) characteristics of late calcite mineralization

Four samples of ME9 calcite were examined for oxygen (δ^{18}O) stable isotope composition using the ion microprobe at Edinburgh University (Table 3-8). Carbon and oxygen stable (δ^{18}O and

$\delta^{13}C$) isotope characteristics of ME9 were also studied by He-LACE at the BGS (7 samples). The samples were selected to span the different types of calcite morphology, from shallow nailhead to deep *c*-axis elongated crystal forms. In addition, 6 samples were also analysed using conventional analysis following microsampling of the calcite using a micro-drill. The objective was to use the microsampling techniques to examine the variation in the isotopic composition (particularly $\delta^{18}O$ signature) across calcite crystals that might reflect the evolution of the palaeogroundwater. Results are summarized in Figure 3-48 and Figure 3-49. Reproducibility between the different methods was good, and well within the range of natural variation, giving confidence that good data has been obtained.

A cross-plot of $\delta^{13}C$ against $\delta^{18}O$ (Figure 3-48) shows a systematic relationship at Sellafield. This suggests co-variation, due to advection and replacement of different groundwater types.
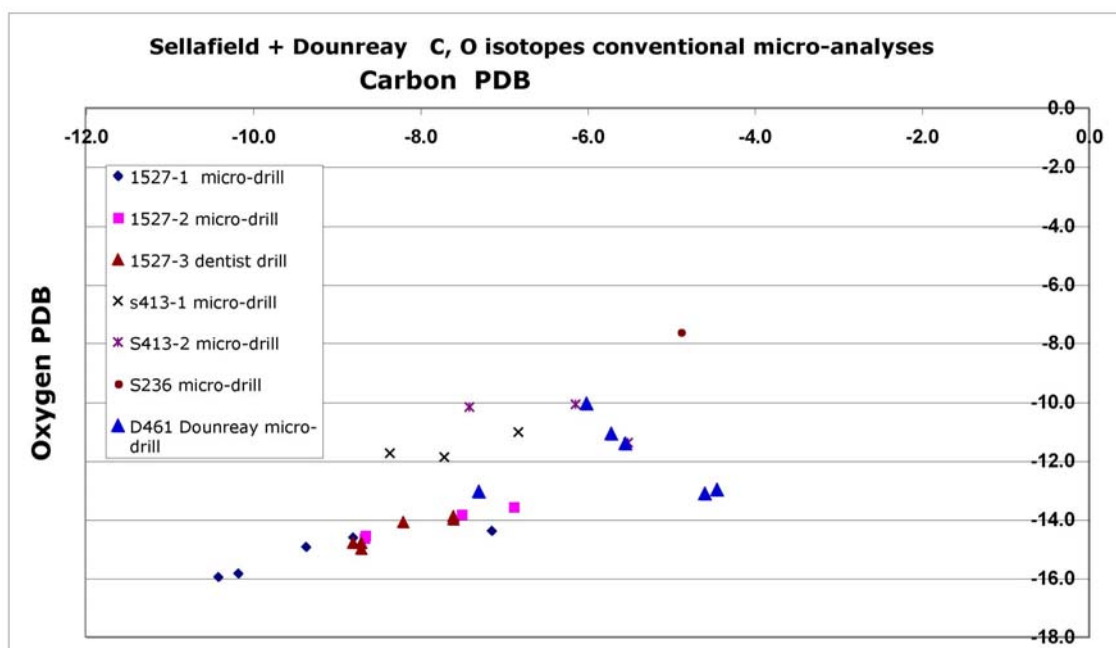
Figure 3-48. Oxygen and carbon isotope data measured conventionally on micro-drilled samples of ME9 calcite crystals at Sellafield (results for a single sample analysed by this method from Dounreay are also included).

The ion microprobe gives much greater sampling resolution of micro-zones within the calcites (20 μm spot size, with no analytical halo), than either He-LACE (which samples from ablation craters about 80 μm diameter) or conventional micro-drilling (sampling pits about 100 μm diameter), especially for the finely zoned 'above-MTZ type' calcite. The ion microprobe data was able to show that the dark (predominantly later) CL zones had notably less depleted $\delta^{18}O$ isotope values than the brighter (predominantly earlier) CL zones. Significant difficulty was experienced with the He-LACE analysis in precisely correlating the laser ablation pit uniquely with a specific calcite growth zone because of the much larger depth and width of the extracted sampling volume. Due to the thinning of the calcite crystals towards their edges in the sample mounts, the outermost growth zones of the ME9 calcite could not be reliably analysed by He-LACE because the extracted sample volume was usually too small. Nevertheless, the two techniques provide complementary and corroborative results.

Figure 3-49 displays the isotope results obtained from the Sellafield ME9 calcites using both ion microprobe and He-LACE techniques. For all ^{18}O data the equation of Friedman and O'Neil (1977) has been used to construct lines that predict the calcite values in equilibrium with present-day water, or other modelled waters. This equation can also be used to explore interpretation of

121

water or temperature variations. For example, the range δ¹⁸O for ME9 calcite at Sellafield at 1527m, could indicate either a change in water temperature of 10 °C, or a change of 2.0 ‰ in the oxygen isotopic composition of the recharged groundwater (which is more than the observed depth variation in present-day water oxygen isotope composition).
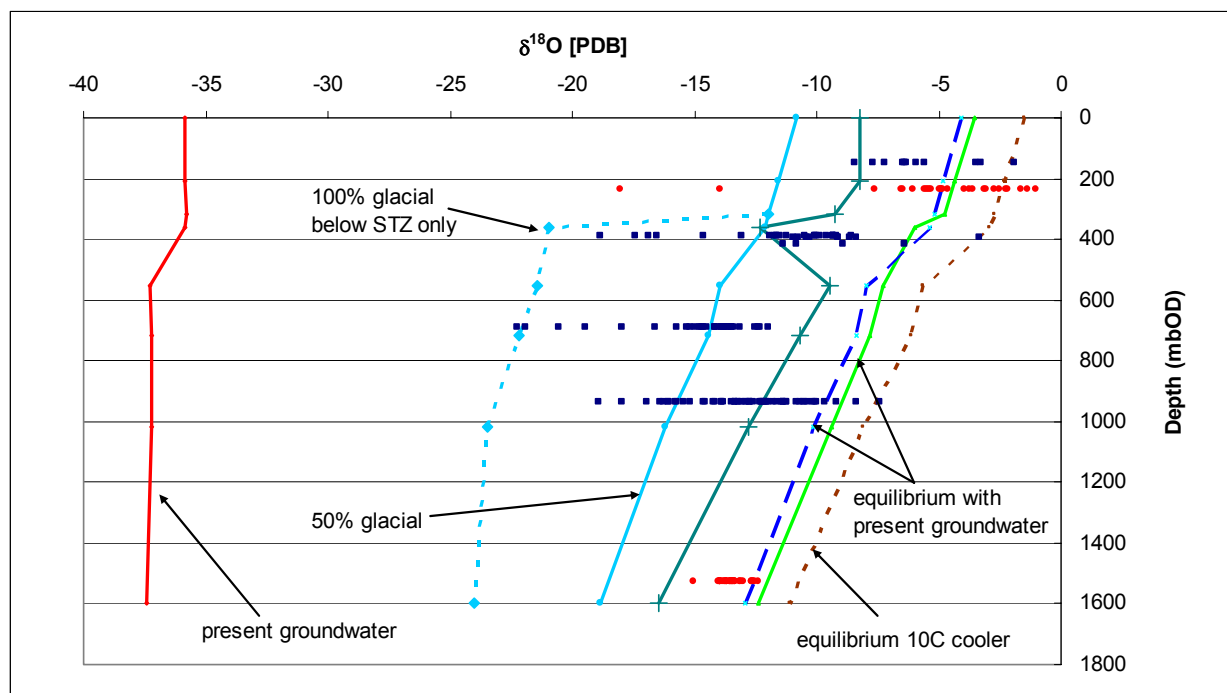
Figure 3-49. Oxygen isotope data for micro sampled Sellafield late calcites. Data are plotted relative to PDB standard. Ion microprobe data (Edinburgh University) are shown in red dots; He-LACE and micro drilled data (BGS) are shown in dark blue dots. Micro drill data from the University of Edinburgh for the sample at 413 m are also shown in blue dots. The present-day groundwater composition is shown by the red curve. The predicted calcite compositions in equilibrium with the present-day groundwater are shown by the green (using the equations of Craig, 1965) and broken blue (using the equations of Friedman and O'Neil, 1977) curves. Modelled calcite composition based on 10 °C cooler water is shown by the brown (broken curve). Modelled calcite composition assuming a 50 % (solid light blue), and 100% glacial meltwater with an assumed composition of δ¹⁸O_SMOW = -20 ‰ (broken light blue line for below the STZ only) are also shown. The dark green central line represents the calcite composition predicted by the model discussed in the text. Present-day water data derived from Nirex (1997).

Comparison of the isotope values of the three samples examined by ion microprobe reveals that more enriched δ¹⁸O values occur on the inner zones and outermost growth zones of crystals at both shallow and deep levels. The middle zones analysed are relatively more depleted in ¹⁸O. Oxygen fractionation is affected by both temperature and porewater composition. A change to enriched (heavier) ¹⁸O values could be produced by colder temperature (e.g. permafrost), and/or by heavier ¹⁸O in porewater (e.g. meteoric, not deglacial, water). Consequently, such a 3-fold zonation could be produced by a period of warming from cold temperature followed by warming, which could equate to a glacial-interglacial-glacial sequence. Or the more ¹⁸O-depleted central growth zones could be produced by an influx of isotopically depleted glacial water, which could equate to crystal growth during glacial meltwater influx. It is noted that dissolution 'unconformities' occur within crystals at all depths. These could equate to several

factors including: changes of advected groundwater; pressure-induced changes (ice loading changes) of CO_2 content; or mixing of different groundwaters and consequent calcite solubility.

The large-scale trends in oxygen isotopes (for both ion microprobe and He-LACE results) with depth and temperature (Figure 3-49) show an overall depletion of $\delta^{18}O$ increasing with depth. The results for the shallowest sample ('above-STZ type' calcite in sample D286) examined by ion microprobe are also the most enriched in $\delta^{18}O$, with ion microprobe analyses taken from the dark CL zones (potentially indicating the youngest growth in most oxidised groundwater).

Figure 3-49 also shows present day water $\delta^{18}O$ profile and temperature data together with the calculated isotopic values for calcite in equilibrium with present day conditions, using two standard equations. It can be seen that much of the ME9 calcite is not in equilibrium with present-day conditions. If calcites had grown in present-day water 10 °C cooler, then analysed values would follow the modelled curve shown in Figure 3-49 for this condition; only the least depleted values for samples above 1000 m bOD are close to this, and many values are substantially more depleted. If calcites had grown in a porewater modified from present day by addition of 50% volume glacial meltwater (assumed $\delta^{18}O_{SMOW}$ -20 ‰), then analysed values would be more depleted, and follow the modelled line illustrated for this condition (Figure 3-49; most of the data from calcites below 390 m bOD would straddle this line. Interpretation of the ancient calcite growth conditions requires variation of both temperature (at shallow depths) and water (at deeper depths).

An example interpretation is shown by the dull-green central line, which plots the most extreme volumes of glacially derived water:

- At 236 m bOD, this models the most depleted $\delta^{18}O$ values by addition of 50% volume glacial water. The least depleted values are close to 0% glacial water (present day water), at 10 °C cooler temperature, however the least depleted values would require to be 13 °C cooler than today, i.e. at 0 °C. This ^{18}O signature would also fit to growth from shallow porewater with a marine isotopic signature, although no additional evidence is known to support a post-glacial shoreline this far inland.

- At 413 m bOD (above STZ), most of the calcite $\delta^{18}O$ values are not in equilibrium with present day water, but require 50-70 % volume glacial water and 8 °C cooler temperature.

- Below the STZ, a uniform 30% volume glacial water has been modelled, with temperature linearly approaching present day values with depth.

- At 1527 m bOD, the calcites require 2 °C cooler temperature with 30 % volume influx of glacial water, through to present-day water with zero glacial water influx.

This outline interpretation makes it clear that conditions above the STZ have been greatly influenced by both glacial cooling, and by glacial water influx of up to 70% by pore volume. At 236 m bOD, the outermost zones of calcites grew either in very cold sub-permafrost water, becoming flushed by glacial meltwater, then warming to the present-day. Or, less likely, in an excursion from 70% glacial water, to marine-derived water, and back to present-day meteoric water. An additional modelled line illustrating the predicted calcite composition for 100 % glacial water component in groundwater below the STZ is also shown in Figure 3-49 (broken light blue line). This better brackets the more depleted end of the $\delta^{18}O$ range of ME9 calcite compositions between 390-1000 m bOD than the model predicted by the green line, when the wider ranging He-LACE data are included. It is inferred that porewaters below the STZ have experienced less temperature fluctuation, but the results suggest that porewaters have possibly been subject to glacial water influx typically of up to 30% pore volume, but with He-LACE analyses suggesting the sporadic occurrence of 100 % glacial water. At all depths, the very wide range of isotope values suggest that the calcites could have grown during greatly changing water

composition. This could be interpreted as a decline of glacial meltwater influx, possibly lasting 1,000–5,000 years, leading to the establishment of the present-day water profile.

3.3.8 Biomarker studies

Six samples of late-stage calcite from the Sellafield site were analysed by GC-MS by the Universidad Politecnica de Madrid for the presence of organic biomarker compounds during the course of the PADAMOT project (listed in Table 3-10). The occurrence of biomarkers in the late calcites from Sellafield appears to be very sporadic and apparently unrelated to depth or location. They were found in only two of the samples (D299 - from above the freshwater zone (310 m bOD) in borehole PRZ2; and MPLK559 - from the deep saline groundwater (863.03 m bOD) in borehole RCF3). As in the Laxemar calcites (see Section 3.2.4.7) only a few organic compounds were present. Identified compounds include cyclopentane, hexadecanoic acid, octadecanoic acid and pyrrolo[3,2-a]dibenzo-furan (Table 3-10, Figure 3-31). As observed in Figure 3-31, other compounds are also present in the GC-MS spectra. However, these are not described further because there are large uncertainties in their identification. The significance of these different biomarker compounds has been discussed earlier in Section 3.2.4.7.

Table 3-10. Abundances of the different biomarkers found in late-stage calcites from the Sellafield site

Bore hole	Sample No	Depth (m bOD)	Sample wt. (mg)	Cyclo-pentane	Hexadec-anoic acid	Octadeca-noic acid	1, 2 benzenedi-carboxilic acid	Isoquin-oline	Pyrrolo [3,2-a] dibenzo-furan
BH9A	D723	65.22	65.22	nd	nd	nd	nd	nd	nd
PRZ2	D299	310.00	81.4	nd	1140392	675743	nd	nd	nd
PRZ3	D329	396.48	120.0	nd	nd	nd	nd	nd	nd
PRZ2	D311	413.13	102.8	nd	nd	nd	nd	nd	nd
RCF3	MPLK559	863.03	182.0	1033229	5754306	1564670	nd	nd	1486919
RCF1	C755	896.07	94.8	nd	nd	nd	nd	nd	nd

Notes: 1. nd = not detected
2. Relative concentrations of organic compounds shown as total GC-MS peak counts.

The presence of octadecanoic and hexadecanoic acids in samples D299 (PRZ2, 310 .00 m bOD) and MPLK559 (RCF3, 863.03 m bOD) could indicate that the calcite grew from groundwater which had an organic matter input of plant origin, but these compounds may also have been produced in situ through bacterial activity. Cyclopentane, found only in sample MPLK559 (RCF3, 863.03 m bOD) is most probably of plant origin. The presence of both cyclopentane and octadecanoic acid would be consistent with the groundwater, from which these calcites grew, having derived these organic compounds from a soil cover in the recharge area.

The presence of pyrrolo[3,2-a]dibenzo-furan within the late calcite sample MPLK559 (RCF3, 863.03 m bOD) is indicative of an input of highly-mature organic matter (coal or oil). Sellafield sits at the margin of the East Irish Sea Basin, which contains major oil and gas resources (e.g. the Morecambe Gas Field). Furthermore, large deposits of coal are also present within Carboniferous rocks both offshore and immediately to the north of the Sellafield site (Ackhurst et al., 1997). These would appear to be the most obvious potential sources of this particular biomarker.

Three samples of ME9 calcite from Sellafield were also analysed by Universidad Politecnica de Madrid in a trial test prior to the PADAMOT project. These included calcite from:

- Sellafield BH2, 1527.50 m bOD (sample B946), *c*-axis elongated calcite;

- Sellafield BH10A, 623.61-623.83 m bOD (sample D749), *c*-axis shortened calcite;

- Sellafield BH9A, 65.22 m bOD, (sample D723, which was also re-analysed during PADAMOT), equant to *c*-axis elongated calcite.

A much more restricted suite of organic compounds was sought in this trial test compared to the more detailed organic analysis undertaken during PADAMOT. The trial test identified the presence of a range of aliphatic hydrocarbons (*n*-alkanes) with moderate-to-high molecular weights (C_{14}-C_{31}), centred on C_{22} but with a distribution showing little predominance of odd-over-even numbers of carbon atoms. The concentration of biomarkers in the calcites is very low, but the two relatively shallow samples D749 (BH10A, c.623.5 m bOD) and D723 (BH9A, 65.22 m bOD), which are located within the freshwater zone in BH9A and BH10A, respectively, showed the greatest concentration. Sample B946 (BH2, 1527.5 m bOD), which is located within the deep basement saline groundwater zone in BH2, showed a broadly similar pattern of *n*-alkane distribution but with a very much lower abundance (close to analytical detection limits). The origin of these organic compounds is unknown but this *n*-alkane distribution pattern is not characteristic of plant-derived waxes. Similar *n*-alkane distribution has been described previously from fluid inclusions and may result from natural distillation processes (C. Vane, BGS, personal communication).

The presence of these biomarker compounds unfortunately does not provide any constraint on the age of the calcite mineralization. Fatty acids, *n*-alkanes and other biomarkers can be preserved for tens of millions of years and, for example, have been found preserved in early diagenetic sparry calcite cements in Jurassic rocks (Pearson et al., 2005). However, their presence does suggest that the calcite mineralization has probably not experienced temperatures above 40-60 °C. This would be consistent with the low temperature (<80° C) indicated by the fluid inclusion observations on ME9 calcite (Milodowski et al., 1998a; 2002; Bath et al., 2000).

3.3.9 Conclusions

3.3.9.1 GENERAL CONCLUSIONS ON THE SAMPLING AND ANALYTICAL METHODOLOGY

3.3.9.1.1 Core preservation and sampling

The impact of drilling methodology and core handling on the preservation and recovery of late stage fracture mineralization has been discussed in relation to the Swedish studies (Section 3.2.5.1.1). The Sellafield boreholes were drilled using triple-tube coring methodology with either 95 mm or 75 mm diameter cores; the triple-barrel drilling technique appeared to limit the 'washing-out' of loose and soft mineral fills. Experience with the Sellafield samples shows that it is important that subsequent core disturbances due to handling and sub-sampling are minimised and that acid testing as a preliminary core logging tool is avoided.

In contrast to late-stage mineralization at Los Ratones, Äspö-Laxemar and Dounreay, late-stage calcite mineralization in Sellafield fractures is relatively abundant and the size of the calcite crystals is relatively coarse. This made sampling and mineralogical-geochemical observation on this material much easier than at the other sites. Nevertheless it was a technical challenge to obtain sufficient material for some types of analyses (e.g. biomarker studies, radiometric dating). Much of the late-stage calcite forms overgrowths on older calcite mineralization, requiring it to be separated and sub-sampled for bulk analyses.

3.3.9.1.2 Calcite morphology

Previous studies had demonstrated a strong relationship between the crystal morphology of the late-stage (ME9) calcite mineralization and groundwater chemistry at the Sellafield site (Milodowski et al., 1995; 1997, 1998a, 2002; Bath et al., 2000). It was also found that the occurrence of ME9 calcite in fractures in core could be used to identify and predict the location of potential flowing features in the boreholes. The studies showed that calcite in the freshwater

zone characteristically formed short *c*-axis crystals ('nailhead' calcite), whereas in the saline groundwaters the ME9 calcite was characterized by *c*-axis elongated crystal forms ('dog-tooth' or 'scalenohedral' calcite). A systematic pattern of crystal morphology variation was observed in all of the boreholes examined, showing a progressive change from short *c*-axis crystals, through equant crystals to elongated *c*-axis crystals as present groundwater salinity increases with depth. The interval over which the crystal morphology changes, the 'Morphological Transition Zone' (MTZ), occurs just above the Saline Transition Zone (STZ) between the shallow freshwater zone and the deeper saline groundwater (arbitrarily defined on the basis of electrical logs at approximately 3500 to 6000 mg/L chloride). The spatial relationship between the MTZ and the STZ is maintained across the site. The base of the MTZ, marked by the transition from equant to *c*-axis elongated calcite, occurs where groundwater salinity is between 1000-2000 mg/L chloride. The top of the MTZ, marked by the transition from short *c*-axis to equant calcite, is less well defined but appears to occur where salinity is >300 mg/L chloride.

No new studies on the calcite morphology were undertaken during the PADAMOT project.

3.3.9.1.3 *Fluid inclusion studies*

Microthermometric and microchemical analyses of fluid inclusions were performed on samples of ME9 calcite studied during the previous EQUIP investigations. These studies found that the inclusions have close chemical affinities to present-day groundwaters in the region. However, a number of factors constrain the use of fluid inclusions for palaeohydrogeological reconstruction:

- Size of inclusions;
- TDS of inclusion fluids;
- Analytical detection limits

Fluid inclusions in ME9 calcite are rare and are typically very small (<5 μm), making it difficult to obtain microthermometric measurements of the subtle phase changes that are used to determine salinity characteristics. Most inclusions are located within the cores of the ME9 calcite, often concentrated along the interface between corroded ME6 'seed' crystals and the early stages of ME9 calcite. Inclusions within later, outer growth zones of the calcite are very rare. The small size of the inclusions also restricts the ability to undertake microchemical analysis using LAMP-ICP-MS techniques, because the inclusions furnish a very low mass of material, which is often below detection limits.

The detection limit for fluid inclusion salinity determination places constraints on the application of the technique to monitor potential changes in the STZ at Sellafield. Salinity determination is limited by the precision of the measurement of temperature. Modern fluid inclusion analysis equipment can measure temperatures to a limit of precision of ±0.1 °C. This translates into precision of 0.2 wt. % NaCl eq. (i.e. 2000 ppm NaCl eq.). Therefore, for dilute palaeofluids, this places an effective detection limit for fluid inclusion analysis at 0 °C ±0.1°C which equates to a salinity of 2000 ppm NaCl eq. (or 1213 ppm Cl eq.). This makes it very difficult to distinguish between brackish water and freshwater at the STZ.

A petrographical review of ME9 calcite samples and background information was carried out to assess the potential for undertaking further fluid inclusion studies at this site. This concluded that because of the very low abundance of inclusions, it would be necessary to prepare and examine multiple fluid inclusion wafers in order to provide sufficient inclusions for representative analysis. Unless this was done, it was considered unlikely that any significant new information could be obtained. Unfortunately, the budget limitations precluded this; the resources for fluid inclusion studies was concentrated on providing potentially more valuable new information for the Los Ratones, Laxemar, Dounreay and Cloud Hill sites.

Further aspects of the application and limitations of fluid inclusion studies are discussed in Section 3.4.9.1.

3.3.9.1.4 He-LACE, LAMP-ICP-MS versus ion microprobe techniques

He-LACE, LAMP-ICP-MS and ion microprobe techniques have been used to try to micro-sample and analyse discrete growth zones within individual crystals of late-calcite mineralization at Sellafield, in order to evaluate the variation in trace element and stable isotope ($\delta^{18}O$ and $\delta^{13}C$) compositions at different stages of crystal growth. Several advantages and disadvantages of these techniques were encountered.

The sample preparation methodology used for the different techniques had a significant impact on the application of the analytical methods. Initial trials during the PADAMOT study showed that conventional epoxy-resin-impregnated polished sections could not be used for He-LACE studies because the epoxy-resin decomposes and evolves some CO_2 as it gets hot during laser ablation. Consequently, crystals of calcite for analysis were embedded and polished in blocks of Plaster of Paris. This overcame the problem of isotope contamination but resulted in surfaces that were too poorly polished to be of use for CL characterisation. The BGS subsequently developed a method of mounting the calcite in M70 low melting point Bi-Pb-Sn alloy. In most of the Sellafield samples, individual calcite crystals could be separated and mounted. However, some samples had to be prepared with calcite crystals still attached to fragments of wallrock, and differences in the hardness of these materials caused significant problems with polishing. As a result, the quality of surface finish of some of the polished mounts was poor, and this had a major impact on the quality of CL images that could be obtained from the mounts. In contrast, the ion microprobe employed polished thin sections prepared from material mounted conventionally in epoxy-resin. This facilitated the preparation of a high-quality surface polish, and allowed high-quality CL images to be acquired from the samples. Good quality CL images are essential for precisely locating analysis points, and for discriminating and correlating the different growth zones. Furthermore, the use of polished thin sections has a major advantage in that the samples can be examined and analysis points located using optical transmitted light microscopy. This is not possible using the M70 polished metal blocks. However, for efficiency and budgetary constraints, the BGS LAMP-ICP-MS studies had to utilise the same M70 mount prepared for He-LACE analysis. However, M70 mounts are not a requirement for LAMP-ICP-MS analysis, and the application of this analytical method would be improved in any future study by the use of conventional polished sections.

The ion microprobe has a much better spatial resolution than the two laser microsampling techniques. This enabled the very fine overgrowths and fine-scale growth zoning to be precisely sampled for both trace element and $\delta^{18}O$ isotope analyses. In contrast, the two laser-based techniques produced much coarser-scale sampling. In particular, the current He-LACE laser system was not readily able to provide the very fine spatial resolution needed to sub-sample some of the ME9 calcite zones, particularly the later growth zones. The LAMP-ICP-MS laser can be reduced to a spot size of about 5 μm, which provides a resolution similar to the ion microprobe but analytical sensitivity is reduced. Thermal shock and rapid thermal expansion of the calcite under the laser probe can sometimes cause the calcite crystals to shatter, particularly near the edges of crystals. Advances in laser technology and ICP-MS development are likely to result in better microsampling resolution and analytical sensitivity in the future.

For stable isotope studies, He-LACE analysis has an advantage of being able to provide both $\delta^{18}O$ and $\delta^{13}C$ information simultaneously, whereas the ion microprobe is set up to determine the isotopic signature of only one element ($\delta^{18}O$ in this case) at a time. However, it proved much more difficult to relate the He-LACE data to specific growth zones in the calcite for the reasons described above.

LAMP-ICP-MS and ion microprobe techniques have comparable sensitivity for trace element analysis of calcites. LAMP-ICP-MS analysis is significantly less expensive but ion microprobe has the advantage of better spatial resolution and more controllable sample ablation.

Despite these differences and problems the ion microprobe and the laser techniques provided corroborative results for the Sellafield site. In addition, the ion-microprobe studies on ME9

calcite have successfully demonstrated for the first time that variations in trace amounts of Cl and Br can be studied in the growth fabric of the calcite. This raises the possibility that this can be used in future to record variations in palaeosalinity.

3.3.9.1.5 Biomarker studies

As in the study of the Laxemar borehole (Section 3.2), the PADAMOT study has demonstrated that organic biomarker compounds are occasionally preserved within the late-stage (ME9) calcite crystals. However, the biomarkers are present only in trace amounts and their analysis is very close to the detection limits using the small amounts of calcite that could be sampled.

3.3.9.2 PALAEOHYDROGEOLOGICAL INTEPRETATION

The mineralogical and geochemical studies of late-stage (ME9) calcite fracture mineralization from the PADAMOT project largely confirm observations from earlier investigations at Sellafield (Bath et al., 2000).

Petrological observations show that the shallow and deep groundwater flow paths have evolved over time. Much of the fracture porosity is secondary in origin, having been re-juvenated by the dissolution of geologically old vein minerals; principally anhydrite and dolomite-ankerite (and also calcite at shallow levels) belonging to ME4 and ME6 mineralization (cf. also Milodowski et al., 1998, 2002). In this respect, the fracture porosity has a similar origin to a large proportion of the intergranular matrix porosity of the Permo-Triassic (St Bees Sandstone and Calder Sandstone formations) sandstone aquifer, which has been rejuvenated by the dissolution of diagenetic anhydrite, dolomite and calcite cements (Strong et al., 1994). Secondary porosity has long been recognised as an important factor in controlling the hydrogeological properties of sandstone aquifers and hydrocarbon reservoirs (Schmidt and McDonald, 1979). However, its role in studies of fractured groundwater systems is seldom considered, and the distribution of fracture porosity is typically modelled as being related solely to tectonic structure.

The PADAMOT and earlier studies show that both the palaeo, and modern, groundwater flow system evolve from east to west across the site. ME4 and ME6 anhydrite, and to a lesser extent ME6 dolomite–ankerite, have leached from fracture fillings, in the BVG basement and Permo-Triassic cover rocks, the east of the site as a result of invasion by dilute meteoric water (with more dissolution) in the recharge area. Similarly, anhydrite and carbonate cements are dissolving in the shallow Permo-Triassic aquifer. The enhancement of secondary porosity is progressively developing westwards and down-gradient from the recharge area as dissolution proceeds. As a result of this process, the porosity/flow pathways in the east of the site are older and more evolved, and they progressively become younger and less evolved westwards. This evolution is reflected in the growth fabric of the late-stage ME9 calcite mineralization, which precipitated from the groundwater as it became supersaturated with respect to calcite down-gradient, or as invading meteoric water mixed with background water in the host rock. Calcites in the east of the site display the most complex sequence of up to 8 clear growth zones, representing a more fluctuating and possibly longer evolutionary history. By contrast, at the west of the site, the borehole BH10A/BH12A area has up to only 4 growth zones, representing a shorter or less complex evolutionary history. Ion-microprobe and LAMP-ICP-MS trace element studies provide evidence to support a close relationship between the evolution of the fracture system and ME9 calcite precipitation. Early growth zones in the calcite are often enriched in Mg, which would be consistent with the dissolution of ME6b dolomite-ankerite mineralization. This is particularly notable in the shallow system where the effects of dolomite-ankerite dissolution are greatest.

Overall, this rock-water interaction process is potentially increasing the porosity in parts of the groundwater system; the void space created by the dissolution of geologically-old hydrothermal fracture mineralization (and the diagenetic cement in the Permo-Triassic strata) is generally

greater than the loss of pore space due to the precipitation of new ME8 and ME9 minerals. However, localised fracture sealing by late-stage minerals is evident in the BVG, with hairline fractures becoming healed by scaly ME9 calcite. Clearly, any predictive hydrogeological modelling of the site for risk assessments for long-term storage/disposal of radioactive wastes must consider in greater detail the possible implications of:

- The progressive evolution with time of the fracture porosity in the BVG, and matrix porosity in the sandstone;

- The relative significance of increased system porosity as old mineralization is dissolved versus reduction of porosity through the sealing of fractures (at least locally) by new minerals;

- The corresponding increase in permeability through time, which will be most apparent in the fracture-flow conductivity. In general terms, an increase of BVG conductivity upwards and eastwards can be explained by this 'deep weathering' dissolution process;

- The distribution of fracture porosity in the rock mass will not simply be related to the location of tectonic features (i.e. faults) but also to the distribution of ME4 and ME6 anhydrite and dolomite-anhydrite mineralization, and the geochemical processes controlling the dissolution of these reactive fracture filling minerals;

- The enhancement and evolution of porosity is driven by recharge in the east. Changes in climate state (e.g. glaciation, permafrost, higher rainfall, lower rainfall) that affect recharge will influence the development of these secondary porosity flow paths.

At present, PA models do not generally account for the progressive evolution of site characteristics (e.g. porosity, permeability, water chemistry etc) and have fixed boundary conditions. This limitation follows from the requirement for simulations to be carried out in reasonably short times, particularly where large numbers of realisations are undertaken to explore uncertainties/ranges in parameter values. Thus, it is probably not feasible to incorporate the observed progressive evolution of porosity identified at Sellafield into PA simulations directly. Instead, the observations made during PADAMOT and EQUIP are presently more relevant for specifying conceptual models and scenarios on which the PA simulations are based.

As discussed above (Section 3.3.9.1) ME9 calcite morphology varies systematically with present-day groundwater composition. The present-day depth of this transition mirrors, but does not coincide exactly, with the present-day STZ as defined by electrical logs; the base of the MTZ being located just above the top of the STZ. This implies that ancient freshwater was generally less deeply penetrating across the site, particularly in the RCF/PRZ area and further east, where the MTZ is thicker. ME9 calcite growth and morphological studies indicate that there has been some movement in the position of the MTZ/STZ over time. A common feature of the ME9 calcite fabric is the growth of later freshwater type crystals on cores of more saline type calcite within the MTZ, indicating a progressive downward movement (between 50 to 150 m) of the MTZ/STZ during the more recent palaeohydrogeological history of the Sellafield site. Although this is the general picture of the palaeohydrogeological movement of the STZ recorded by the ME9 calcite, there is some evidence for the position of the STZ having moved in the opposite direction along localised fractures/fracture zones in some parts of the site. Very rare observations of more *c*-axis elongated (saline-type) calcite crystals nucleated on top of (younger than) equant or short *c*-axis (freshwater-type) crystal forms suggest deeper penetration of freshwater in the past, and that this saline water-freshwater interface may been depressed by between 100-200 m in the east of the site (borehole BH9A – PRZ/RCF area). This might reflect 'fingering' of freshwater penetration along a small number of very localised, more conductive, fracture flow paths that perhaps responded more rapidly than the bulk of the flow system, to short-lived enhanced freshwater flushing events in the past.

The distribution and relationships of ME8 and ME9 mineralization also suggest that locally

deeper penetration of more oxidizing palaeo-waters has occurred than at present. ME8 iron and manganese oxyhydroxides occur to maximum depths, which increase from east to west, from about 25 m in borehole 9A, 170 m in borehole BH8B, 270-400 m in the PRZ/RCF area, and up to 660 m in boreholes in the Fleming Hall Fault Zone area (boreholes BH10A and BH12A) (Milodowski et al., 1995, 1998, 2002). The maximum depth of ME8 oxide mineralization coincides closely with the top of the MTZ in the eastern part of the site (PRZ/RCF area boreholes and boreholes further east) but in the Fleming Hall Fault Zone area, ME8 mineralization extends virtually to the base of the MTZ (which is also much thinner in this area). ME9 calcite rests on, and contains inclusions of, this ME8 mineralization, with 'below-MTZ type' ferromanganoan calcite (containing reduced iron and manganese) now present above these depths. The greater depth of development of ME8 mineralization in the Fleming Hall Fault Zone may reflect deeper penetration by fresh, oxidizing palaeogroundwaters in this area as a result of this fault zone being locally more conductive. However, in all cases this possible indication of intrusion occurs in sedimentary strata. Furthermore, limited age dating (Milodowski et al., 1997) suggests that some of the ME8 mineralization may be late Miocene, and therefore this penetration of oxidizing alteration may represent deep Tertiary weathering following regional uplift at this time.

Significant oxidizing conditions (Eh exceeding +160 mV), as indicated by marked Ce depletion in the ME9 calcite, is only observed episodically in the later stages of calcite growth (non-luminescent, non-ferroan non-manganoan calcite) above the MTZ. There is no mineralogical evidence of strongly oxidizing groundwaters ever having penetrated below the current STZ during the Quaternary. The very limited ion microprobe study of trace halides (Cl and Br) in ME9 calcite also suggests that palaeosalinity may have fluctuated above the MTZ but was more static below the STZ during the recent palaeohydrogeological evolution of the site.

Oxygen isotope (δ^{18}O) variations in ME9 calcite (determined by ion microprobe and He-LACE analysis) suggest the possibility that a significant component of isotopically-depleted glacial water has penetrated to depths of up to 1527 m. Modelling of the δ^{18}O data suggests that glacial water could have replaced between 30 to 100 % of the groundwater from which ME9 calcite grew in the fractures. The impact of potential glacial influx is strongest above about 700 m bOD and in sedimentary formations, but decreases below this to about 30 % by about 1527 m bOD in the BVG of the PRZ/RCF area. Ion microprobe data suggest calcite with these depleted (?glacial) δ^{18}O isotopic signatures characterizes the earlier stages of calcite crystal growth. Later stages are less depleted, and at shallow depths above the MTZ the δ^{18}O signature of the calcite suggests growth under conditions up to 10-13 °C colder than present - possibly this could relate to the establishment of permafrost or periglacial conditions. Alternatively, the calcite composition could be explained by growth in an excursion from water with a significant glacial component, to marine-derived water, back to present-day meteoric water.

It is very important to note that the calcite with potential glacial δ^{18}O signatures does not correspond to calcite grown under oxidizing conditions as indicated by Ce anomalies or Fe and Mn distribution. In contrast, calcite above the MTZ, which shows marked depletion of Ce, correspondingly has heavier δ^{18}O composition. This implies that penetration by glacial meltwater does not necessarily give rise to oxidizing groundwater compositions. In the case of Sellafield, observations seem to suggest that ME9 calcite characteristic of oxidizing conditions in the shallow fresh groundwater system may relate more closely to the impact of post-glacial processes.

There are no age data associated with this preliminary interpretation of glacially derived groundwaters undergoing downward movement to depth. In the UK, Quaternary glaciations have occurred over the past 2 million years. The mechanism associated with such movement is similarly uncertain at the present time. Downward movement to depth may represent discrete events. However a "piston-push" mechanism is possible, which would mean that groundwaters need to be "pumped" over several glacial phases to reach significant depths. The turnover of the

displaced groundwater is an important consideration, both in terms of the timing and with regards to the fluxes. More work remains to be done to investigate the strength of the evidence and the precise nature of the mechanisms involved.

As in the study of the late calcites from Laxemar, organic biomarkers are occasionally preserved within the ME9 calcite crystals from Sellafield. Only a small suite of samples could be examined in PADAMOT and trace biomarkers were identified in only a few of these samples; there does not seem to be any obvious pattern to the occurrence. The biomarkers could be derived from soil cover during recharge, or they may have been produced in situ in the groundwater by bacterial activity, or they might provide tentative evidence for the former presence of deeper basinal brines from either the hydrocarbon-bearing East Irish Sea Basin or older Carboniferous basins. Unfortunately the data cannot be interpreted unambiguously.

3.4 DOUNREAY

3.4.1 Sample selection criteria

Dounreay borehole NDN1 was drilled to produce large (95 mm) diameter core, using the triple barrel coring technique and employing a polymer-based drilling-mud, similar to the drilling operations at Sellafield (Bath et al., 2000). The entire length of the drill core from the Dounreay NDN1 borehole was visually inspected, and fracture surfaces carefully examined with a binocular microscope. Fractures that might be potentially flowing features (PFFs) were systematically logged (Figure 3-50), along with details of any mineral cements and their crystal morphologies, where it was possible to determine this. PFFs were recognised using similar criteria to those for the Sellafield site:

- *Evidence of natural, intact fracture porosity*.

  Fractures, which could be demonstrated to be open and porous in situ, and not opened as a result of drilling disturbance, were considered to be potentially conductive. In particular, evidence was sought for mineralization with euhedral crystals lining the fracture surfaces as these indicate that the minerals grew into open pore spaces, and provide strong evidence of naturally open fracture porosity;

- *Spatial association of fractures with groundwater flow*

  Available hydrogeological flow logs for Dounreay NDN1 were much less detailed than for the Sellafield boreholes. However, summary data identifying the position of flow zones in Dounreay borehole NDN1 and Discrete Extraction Test data (Nirex 1994a,b) were used to help locate the position of PFFs;

- *Presence of the youngest generation of mineralization*.

  Fractures, which contain crystal representing the paragenetically youngest mineralization, recorded at this site, are considered most likely to record the most recent evidence of the groundwater history.

Samples of calcite were selected for analysis on the following basis:

- Samples were taken to represent the youngest mineralization differentiated within the paragenetic scheme defined for the Dounreay area (Section 3.4.2);

- Samples were selected from obvious PFFs;

- Samples were selected to represent the entire depth range of Dounreay borehole NDN1;

- Samples were selected to include intervals covering the different range of groundwater chemistries.
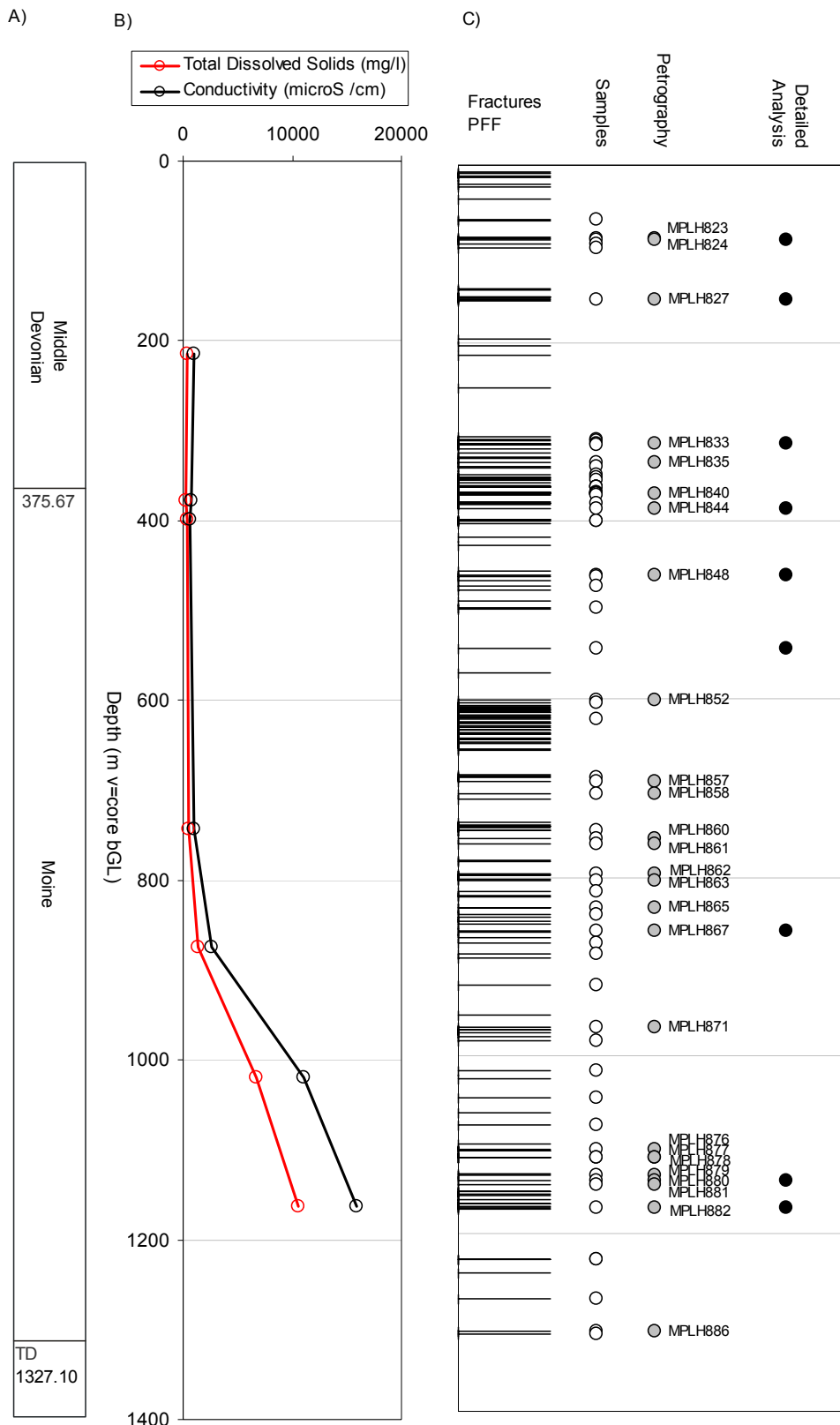
Figure 3-50. Down hole plots illustrating (a) stratigraphy, (b) variation in total salinity (Discrete Extraction Test data from Nirex 1994a), and (c) PFF and mineralogical sample positions in borehole NDN-1.

A total of 70 samples were recovered from the borehole. Polished thin-sections and/or SEM stubs were prepared from 26 of these samples, and following preliminary petrographical observations, a number of these were selected for more detailed microchemical analyses.

This sampling strategy provided reasonable overall coverage of the calcite cements as they occur within the borehole. However, there were a number of intervals that contained relatively few fractures and/or calcite-cement (Figure 3-50).

Table 3-11. List of samples studied from the Dounreay site (borehole NDN1) with analytical schedule.

Sample ID	Top Depth (m core bRT)	Bottom Depth (m core bRT)	Petrography	SEM	CL	Fluid Inclusion Microthermometry	Fluid Inclusion Micro-chemistry by Laser Ablation	EPMA Maps	EPMA Point Analyses	IPMA Trace Element Data	IPMA Stable isotope Analysis	LAMP-ICP-MS Trace Element Data	LACE-He Stable isotope Data
MPLH823	82.91	83.09	Y		Y								
MPLH824	83.60	83.75	Y	Y	Y			Y	Y	Y	Y	Y	Y
MPLH827	151.64	151.79	Y	Y	Y	Y		Y	Y				
MPLH833	313.36	313.51	Y	Y	Y	Y	Y						
MPLH835	334.56	334.65	Y	Y	Y								
MPLH840	369.25	369.46		Y									
MPLH844	386.03	386.17	Y		Y	Y	Y						
MPLH848	460.57	461.00		Y	Y	Y	Y	Y	Y	Y	Y	Y	Y
MPLH851	542.74	542.85	Y		Y	-		Y	Y				
MPLH852	603.16	603.41	Y	Y	Y								
MPLH857	692.25	692.35		Y									
MPLH858	706.29	706.46	Y	Y	Y								
MPLH860	756.71	756.86	Y		Y								
MPLH861	762.34	762.49	Y	Y									
MPLH862	796.30	796.50	Y		Y								
MPLH863	803.81	803.99	Y	Y	Y								
MPLH865	833.42	833.60		Y									
MPLH867	859.59	859.76	Y	Y	Y	Y		-	-				
MPLH871	969.33	969.53	Y	Y	Y								
MPLH876	1105.11	1105.50	Y	Y									
MPLH877	1114.75	1114.99	Y		Y								
MPLH878	1114.95	1115.29	Y		Y								
MPLH879	1135.00	1135.37	Y	Y	Y								
MPLH880	1141.46	1141.81			Y	Y		Y	Y				
MPLH881	1145.18	1145.41	Y	Y	Y								
MPLH882	1171.99	1172.16	Y	Y	Y	Y	Y	Y	Y	Y	Y	Y	Y
MPLH886	1309.32	1309.53	Y	Y	Y								
TOTAL			22	19	22	7	4	6	6	3	3	3	3

3.4.2 Fracture mineralogy and paragenesis

Several authors have described various aspects of the fracture mineralization in the Dounreay area previously. However, the observations have never been integrated to produce a paragenetic framework of fracturing history and fracture mineralization. A limited study of the fracture mineralization in the basement rocks was carried out by the BGS from 1978 to 1981 as part of the UK Department of the Environment research programme into the feasibility of the disposal of radioactive wastes in crystalline rocks. This study investigated fracture mineralization and associated alteration in the Strath Halladale Granite at the Altnabreac site, about 30 km south of Dounreay (Storey & Lintern, 1981). The fracture mineralization in the Strath Halladale Granite was re-investigated by Basham (2000) as part of the Nirex Safety Assessment Research Programme, with the focus on evaluating the distribution and re-mobilization of uranium in fractured crystalline rock. Both of these early studies identified a wide range of mineralization,

from early high-temperature hydrothermal mineralization to late-stage, low-temperature mineralization associated with the formation of calcite and montmorillonite. Basham (2000) found that calcite was the most abundant fracture-filling phase, forming over 60 % of all filled fractures. Neither of these studies evaluated the paragenesis of the fracture mineralization. Milodowski et al. (1989) described the fracture mineralization in the Middle Old Red Sandstone (MORS) Caithness Flagstone Group (Middle Devonian) at Broubster, 7 km southeast of Dounreay, as part of a natural analogue study of uranium migration and retardation. More comprehensive investigations of the fracturing and associated mineralization have subsequently been carried out on the Caithness Flagstone Group (Milodowski et al., 2000b), Moine (Precambrian) basement rocks (Milodowski et al., 2000a) and across the unconformity between the Moine and the Devonian (Hyslop and Milodowski, 2000) in the Dounreay area, within the Nirex Safety Assessment Research Programme. These authors placed age constraints on the mineralization on the basis of paragenetic/mineralogical correlations across the basement-Devonian unconformity, and relationships between the fracture mineralization and burial diagenetic fabrics and cements in the Middle Devonian sedimentary strata. The fracture and diagenetic mineralization in Dounreay borehole NDN1 was also examined as part of the Nirex site investigation programme at Dounreay (Hyslop & Milodowski, 1994a,b), although the data were not evaluated following the cessation of the site investigation programme at Dounreay in 1991. The results from these earlier studies have been reviewed during the PADAMOT project and a summary of the fracturing history and mineralization paragenesis has been compiled, and is presented in Table 3-12. This excludes the phases of metamorphic deformation, and migmatitic and granitic veining that have been recognised within the Moine and that predate the brittle fracturing (McCourt, 1980).

The Moine (Precambrian) crystalline basement and Devonian sedimentary cover rocks of the Dounreay area have been affected by a long history of tectonic fracturing and hydrothermal mineralization (Table 3-10). At least 18 fracturing and associated mineralization events (FE's) can be differentiated on the basis of fracture/mineral cross-cutting relationships, mineralogy and fluid characteristics. These can be grouped into five broad categories, which are briefly described below.

3.4.2.1 EARLY PRE-DEVONIAN HYDROTHERMAL MINERALIZATION

This corresponds to FE1 to FE4. It is restricted to the Precambrian basement rocks, and is truncated by the Devonian unconformity, and is therefore pre-Devonian.

Hydrothermal veins of quartz, often accompanied by chlorite and adularia, predominantly represent the mineralization. Multiple generations of quartz mineralization are evident. Assemblages containing titanite (sphene), biotite, epidote, garnet, apatite, sulphide minerals and rare scheelite (calcium tungstate) are sometimes present, and indicate mineralization from high-temperature hydrothermal fluids. The later pre-Devonian fracture mineralization was principally quartz and colloform hematite. This appears to be associated with repeated brecciation and mineralization, with up to 19 generations of quartz and hematite being observed in some fractures in basement rocks at Red Point 6 km west of Dounreay (Milodowski et al., 2000a).

Early fracture mineralization utilized pre-existing discontinuities such as foliated basic dykes. The pre-existing dyke assemblages were retrogressively altered to chlorite-quartz-sericite-calcite.

Table 3-12. Summary of the paragenesis, principal mineral assemblages and stratigraphical range of fracture mineralization in the Dounreay area

Fracture Event	Description
EARLY PRE-DEVONIAN FRACTURING AND MINERALIZATION (Basement rocks only)	
1	Quartz ±biotite ±adularia ±scheelite
2	Dissolution of early hydrothermal silicate vein minerals (?)
3	Quartz ±chlorite ±titanite ±epidote ±garnet ±sulphides ±apatite
4	Quartz-hematite. At least three-brecciation event recognised, and up to 19 generations of quartz and hematite can be recognized in some fractures.
POST-CALEDONIAN UPLIFT, EROSION AND DEVELOPMENT OF DEVONIAN UNCONFORMITY	
MINERALIZATION ASSOCIATED WITH EARLY DIAGENESIS OF THE DEVONIAN STRATA	
5	Smectite-chlorite + framboidal pyrite (Basement). Authigenic overgrowths on quartz and feldspars in the fracture weak in basement rocks at the MORS unconformity, coincident with authigenic overgrowths on similar detrital minerals in the MORS. Formation of calcrete fissure coatings and early, strongly-zoned freshwater-type calcite in fractures (MORS and Basement rocks).
MINERALIZATION ASSOCIATED WITH LATE BURIAL OF DEVONIAN STRATA AND HYDROCARBON MIGRATION	
6	Ankerite-dolomite ±pyrite ±sphalerite ±galena (MORS and Basement rocks). Major fracturing/faulting.
7	Post diagenetic calcite ±titanite ±hematite ±galena ±barite (MORS and Basement rocks) - possibly several generations.
8	Major fault brecciation (MORS and Basement rocks).
9	Silicification of fault rocks and fractured limestones (MORS). Galena alteration to secondary lead oxides and lead carbonates may have occurred at this time (Basement rocks). Pressure solution of calcite fracture mineralization (Basement rocks).
10	Hydrocarbon emplacement in fault rocks and porous sandstones (MORS).
11	Hydrocarbon degradation and U-Si-Ti mineralization (MORS).
12	Calcite ±pyrite ±barite mineralization (MORS and Basement), with possibly up to three generations.
13	Hydrocarbon emplacement (MORS).
14	Hydrocarbon degradation and bituminisation (MORS).
LATE-STAGE MINERALIZATION (POST-TECTONIC)	
15	Precipitation of euhedral crystals of harmotome (barium zeolite) in open fractures.
16	Precipitation of late-stage calcite as euhedral crystals on open fracture surfaces (MORS and basement). Fine euhedral crystals of pyrite or marcasite may also be present and a minor or trace component, resting on fracture surfaces, coating calcite or occurring as inclusions in the calcite
17	Late emplacement of light oil (observed in the MORS only).
WEATHERING	
18	Near-surface dissolution of carbonate minerals and oxidation of sulphides in fractures and matrix, and precipitation of secondary iron and manganese oxyhydroxides, and traces of barite. Precipitation of calcite. (deeper, below weathered zone).

3.4.2.2 MINERALIZATION ASSOCIATED WITH EARLY DIAGENESIS OF THE DEVONIAN STRATA

This mineralization corresponds to FE5 and is observed in fractures in the basement rocks immediately (0-5 m) beneath the Devonian unconformity. FE5 exploited early basement fractures that were opened up by the Devonian erosion.

The most common features are grey micritic calcite coatings on fissure walls and fissure fillings (calcrete). These are typically laminated and extend downwards from the unconformity surface for up to 3 m. They are particularly well developed in exposures of basement rocks at Red Point and to the west. Slightly deeper below the unconformity the fractures may be mineralized by colourless early sparry calcite. These sometimes contain scattered sub-millimetre-scale micronodular calcrete. These concretions are overgrown by equant euhedral calcite with distinctive alternating concentric growth zones of strongly luminescent and non-luminescent calcite. This type of calcite is very reminiscent of the freshwater-type late ME9 calcite from Sellafield, and may be indicative of an early precipitate within the shallow Devonian fresh groundwater system. Smectite clay coatings may also be present beneath later calcite vein mineralization close to the unconformity. These are occasionally associated with minor framboidal pyrite, which is often indicative of low-temperature biogenic iron reduction processes.

3.4.2.3 FRACTURING AND MINERALIZATION ASSOCIATED WITH LATE BURIAL OF THE DEVONIAN STRATA AND HYDROCARBON MIGRATION

FE6 to FE14 represent a complex sequence of fracture mineralization associated with major fault movement that affected both the basement rocks and the overlying Devonian strata. In the basement rocks, the faulting and mineralization reactivated older fault and fracture structures, including basic dykes (Milodowski et al., 2000a).

The fracture mineralization is dominated by carbonate minerals, with minor to trace amounts of sulphide minerals (galena, pyrite, sphalerite), barite, baritocelestite, and strontianite. Minor hematite may be associated with the carbonate veining in the basement rocks. Minor dolomite, ferroan dolomite and ankerite were observed as an early stage (FE6) of the carbonate-dominated mineralization in Dounreay borehole NDN1 but ferromanganoan calcite dominates the vein mineralization. FE6 and FE7 fracture carbonate mineralization can be broadly correlated with mesodiagenetic (post-compactional) cements in the matrix of siltstones, sandstones, and limestones of the Caithness Flagstone Group rocks. FE7 appears to be post-dated by major fault brecciation (FE8), which affected both the basement and Devonian strata. In Dounreay borehole NDN1 thin limestones affected by faulting and brecciation were locally silicified (FE9). This tectonic deformation also caused brecciation, pressure-solution and stylolitization within the earlier FE7 calcite mineralization. FE7 galena mineralization was also locally brecciated and partially altered to lead oxides and cerussite, possibly during this stage.

Subsequent fracturing and mineralization (FE10-FE14) was accompanied by hydrocarbon migration and emplacement within porous fault rocks and in adjacent porous sandstones. The calcite mineralization carries hydrocarbon fluid inclusions indicating a close association between hydrocarbon-bearing fluids and the mineralization. In Dounreay borehole NDN1 hydrocarbon accumulation is only present in the Devonian strata and is not found in the basement rocks. This suggests that the basement rocks remained below the water-oil contact during hydrocarbon migration. At least two episodes of hydrocarbon flooding occurred (FE10, FE13), separated by episodes when the hydrocarbons were degraded and bituminized (FE11, FE14). Hydrocarbon-bearing calcite-galena vein mineralization was observed (Milodowski et al., 2000a,b) to cut late Permian (249-268 Ma) camptonite-monchiquite dykes (Baxter & Mitchell, 1984) intruded into the Caithness Flagstone Group at Castletown 25 km to the east of Dounreay. This implies that the vein mineralization and hydrocarbon migration is, at least in part, of late- or post-Permian age. However, hydrocarbon migration may have begun much earlier since the Devonian

sequence reached its maximum burial depth, and passed through the oil window, by the end of the Devonian (Marshall et al., 1985; Parnell, 1985).

The earliest of the hydrocarbon degradation events was accompanied by the accumulation of uranium mineralization (uraninite, uranium silicate and uranium-titanium oxides). Hydrocarbon degradation may be the result of meteoric invasion – invading oxidizing groundwater would have leached uranium from the overlying strata and then re-deposited the uranium at the redox front developed at the interface with the hydrocarbon. This may have occurred following Permian uplift and erosion.

3.4.2.4 LATE-STAGE POST-TECTONIC MINERALIZATION AND FLUID MOVEMENT

FE15 to FE17 appear to post-date fracture/fault deformation effects.

Rare harmotome (barium zeolite) was observed as a late-stage fracture mineral (referred to here tentatively as FE15) lining some open fractures in both basement and Devonian cover rocks of Dounreay borehole NDN1. The harmotome forms euhedral barrel-shaped and 'Maltese-cross' twinned crystals, and as with FE16, shows no evidence of deformation due to later fracture movement. The petrographical relationship between harmotome and late-calcite mineralization (FE16) could not be seen. The FE15 harmotome is very similar to that seen in the Laxemar site and Simpevarp peninsula (Section 3.2), which was attributed to mineralization deposited from warm brine. It may also be the product of late-stage warm hydrothermal mineralization in the Dounreay area.

FE16 is characterized by euhedral calcite mineralization lining open fractures (PFFs) in Dounreay borehole NDN1. The calcite forms overgrowths on older vein calcite substrates, and also coats fresh wallrock directly. It shows no evidence of damage or deformation due to tectonic movement. These open fractures coincide with groundwater flow in Dounreay borehole NDN1. The PADAMOT studies in the Dounreay site have focussed on this late-stage calcite mineralization. Fine grained euhedral pyrite or marcasite is occasionally present in association with late calcite (Figure 3-56). It occurs as scattered crystals resting on fracture surfaces, or as dusty coatings on calcite, or as inclusions within the calcite.

Light oil has migrated at a late stage into some fractures in some horizons in the Devonian rocks of Dounreay borehole NDN1. This oil coats or encloses what appears to be the late calcite in these fractures, possibly arresting any further calcite growth. This event is referred to as FE17.

3.4.2.5 WEATHERING AND OXIDATIVE NEAR SURFACE GROUNDWATER ALTERATION

FE18 is characterized by late-stage oxidation of pyrite to goethite, and the dissolution of carbonate vein fills and host-rock cements associated with the formation of films, mottles and dendritic coatings of fine-grained goethite and manganese oxyhydroxide. These are evident at outcrop and in the upper 60 m or so of Dounreay borehole NDN1, and increase in development towards the present surface. FE18 is interpreted to relate to recent oxidative weathering and groundwater alteration. In outcrop, some localised tufa deposition can be observed in fissures below the weathering zone.

3.4.3 Distribution and morphological characteristics of late calcite mineralization

The distribution and variation in crystal morphology of late-stage (FE16) calcite in Dounreay borehole NDN1 is summarised in Figure 3-51. Morphological characterization of the calcite mineralization is based on observations from a combination of visual inspection (aided by binocular microscope) of fracture surfaces during the logging of PFFs (Section 3.4.1) and more detailed measurement of crystallographic axial ratios during SEM observation of selected samples.
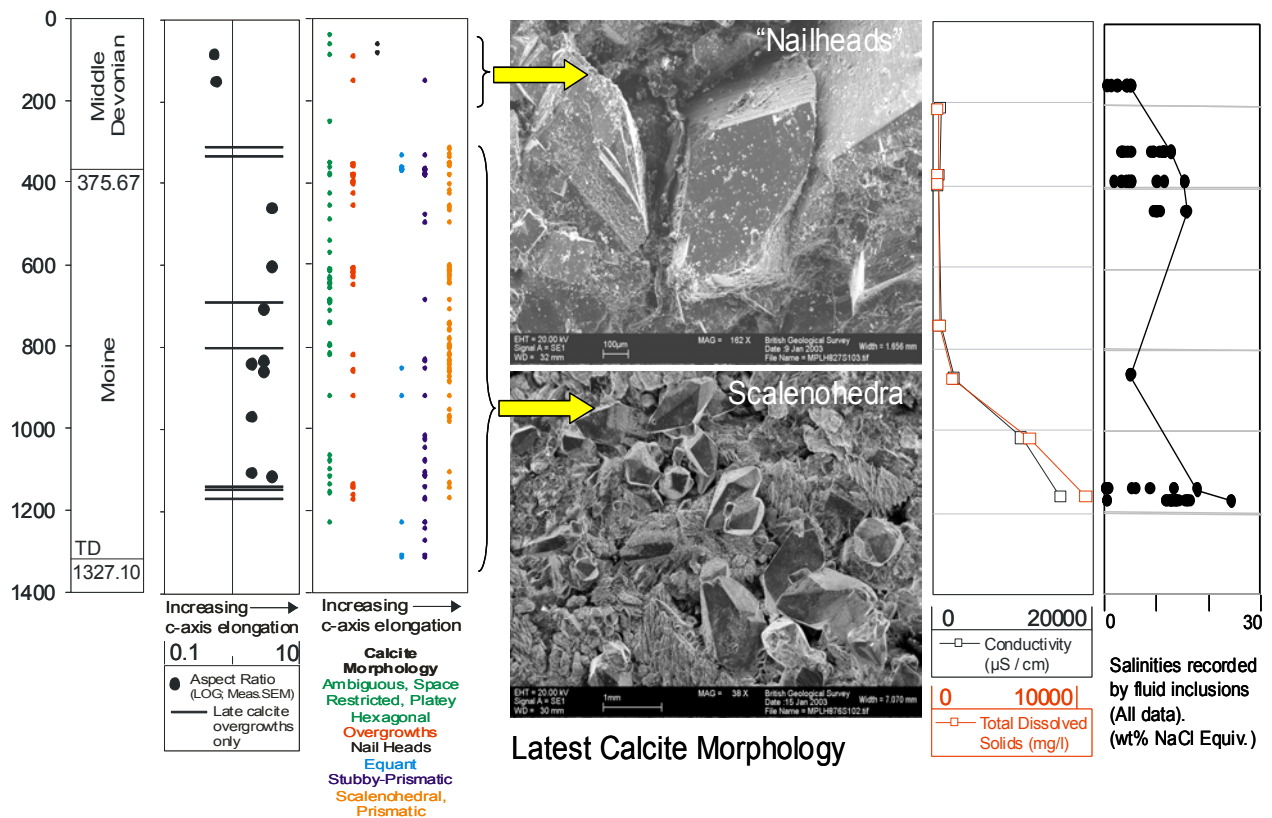
Figure 3-51. **Variation in crystal morphology of late-stage calcite in fractures from Dounreay borehole NDN1. Left:** *c:a* **crystallographic axial ratio determined by SEM and descriptive morphology from core logging. Centre: SEM images of examples of end-member calcite forms. Right: depth variation in salinity in groundwater (DET data) and in calcite-hosted fluid inclusions.**

Euhedral late-stage calcite crystals vary in size from a few tens of microns up to 25 mm, with a range of morphologies from nailhead (short *c*-axis), through equant to scalenohedral (*c*-axis elongated) forms. In addition, a number of other crystal forms were very locally encountered (hexagonal blocky, and hexagonal platy being two particularly distinctive types). Determination of the morphology for the latest calcite cement generation was in many places limited by the presence of coarsely-crystalline earlier calcite, upon which the last calcite had developed. The late-stage calcite overgrowths 'inherit' the crystal morphology of the older 'seed' calcite, masking its growth morphology. All of the coarser (>5 mm) euhedral calcite displays *c*-axis elongated crystal forms, and the bulk of this calcite is probably old (probably equivalent to FE7-12) hydrothermal mineralization. This is confirmed by detailed CL petrography and fluid inclusion studies. Evaluation of the morphological variation in the late calcite is also hindered by the fact that many of the PFFs contain calcite formed as scaly films within hairline fractures, where crystal growth was restricted by very limited fracture apertures (Figure 3-51). Because the calcite has not been able to grow unhindered, its morphological characteristics are ambiguous or unclear.

Despite these difficulties, there does appear to be an overall trend in morphology from predominantly short *c*-axis 'nailhead' type calcite in the upper part of the borehole, to predominantly *c*-axis elongated 'scalenohedral' calcite with depth (Figure 3-51). Nailhead morphology calcite was only observed above 152 m. More equant crystals predominantly occur above the unconformity at 375.67 m but are locally present in some PFFs in the underlying basement rocks. Elongate *c*-axis calcite is the predominant crystal form below about 380 m (i.e. from just above the Devonian-Moine unconformity).

138

Unfortunately, observations within the interval over which the main morphological transition from short c-axis to elongate c-axis takes places are poorly represented because this part of the sequence is relatively lightly fractured. Furthermore, some of the fractures within this interval are coated or saturated with light, late-migrated oil (FE18), which appears to have locally inhibited calcite precipitation. The late calcite morphological variations are similar to those seen in the Sellafield boreholes but the transition between different morphological types is not as well-defined in the Dounreay site. The sporadic occurrence of equant calcite (which characterizes the freshwater zone in the Sellafield boreholes) throughout the sequence, and even at depth in the basement, is similar to observations in the Laxemar KLX01 borehole (Section 3.2). It may be indicative of zones of localised freshwater penetration or flow.

Only limited data are available on the groundwater chemistry at Dounreay (Nirex, 1994a.b). The general depth-versus total salinity variations (based on the analysis of groundwaters from discrete extraction tests, DETs) are illustrated for comparison with the late calcite morphology trend in Figure 3-51. The salinities are relatively low at depths shallower than about 750 m core bRT, but below this, salinities progressively increase to about 10000 mg l^{-1} TDS at c.1150 m core bRT. From this data it can be seen that the morphological transition from nailhead to scalenohedral calcite forms does not coincide with the present day transition from fresh to brackish/saline groundwater.

3.4.4 Petrographical and growth zoning characteristics of the late calcite mineralization

CL-petrography, coupled with SEM observations, and EPMA microchemical mapping and point analyses (Figure 3-52 and Figure 3-53) indicate that the samples from the Devonian interval contain late-stage calcite of different character and composition to that seen at greater depth within the Moine basement rocks. Therefore, two separate calcite cement stratigraphical schemes have been constructed, one for above the Devonian-Moine contact (375.67 m core bRT), and one for below. The interval containing the transition between the two calcite types is, unfortunately, rather poorly represented within the sample set due to a general scarcity of late-calcite-mineralized fractures in the core between c.150-300 m core bRT.

3.4.4.1 LATE CALCITE FROM ABOVE THE DEVONIAN-MOINE CONTACT

A total of 4 calcite generations are recognised in the samples from this interval. All these generations are chemically distinct from the calcite observed below the Devonian-Moine contact, being characterised by relatively high Mg-contents (Figure 3-52 and Figure 3-53). The following generations are identified:

A0   An apparently relatively early generation of moderately orange-luminescent calcite, which typically has a brecciated vein-filling morphology and a relatively high Mg-content ((Figure 3-52 and Figure 3-53)). This is probably earlier hydrothermal calcite.

A1   A0 is overlain by three generations of euhedral calcite. The earliest (A1) is bright-orange to yellow luminescent, with concentric zoning (Figure 3-54). This only occurs as a relatively finely crystalline coating in one sample (MPLH827). Microchemical mapping indicates the calcite has relatively high Mn-contents.

A2   This is more coarsely crystalline than A1, and forms large, orange-luminescent euhedral overgrowths. It has a relatively low Mn-content.

A3   This generation is orange- to orange-yellow luminescent, with well-developed growth zoning, defined by variations in Mn-content (4 specific zones are recognised). Overall Mn-contents are relatively high. This, youngest generation of calcite, has a well-defined nailhead (c-axis flattened) morphology; Figure 3-55).
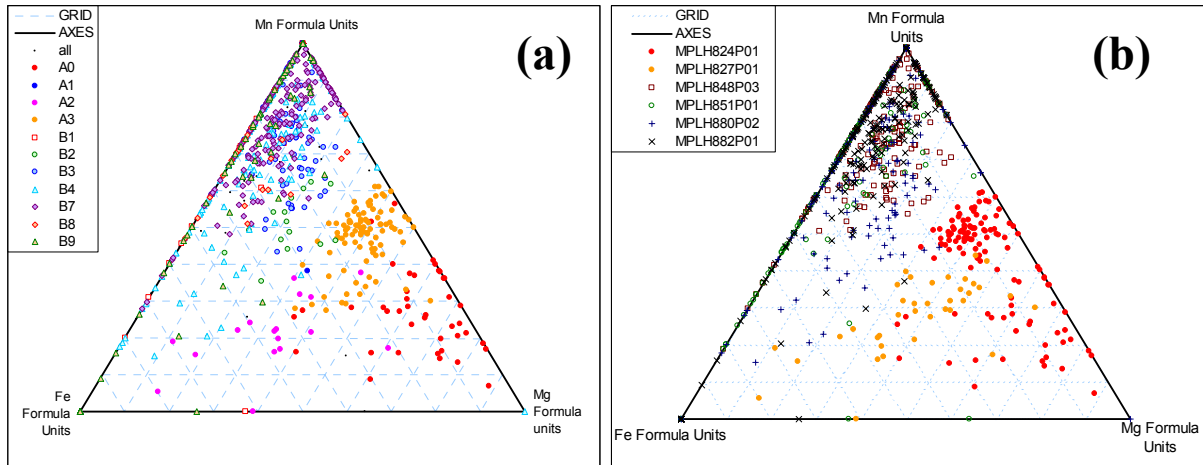
Figure 3-52. Triplots showing variations in minor and trace element chemistry of calcite from borehole NDN-1 (EPMA data corrected to formula units assuming 1 cation, prior to plotting). (a) Points coloured by sample: The two samples from the Devonian (MPLH824 and MPLH827) contain notably higher proportions of substituted Mg, than the samples from the Moine. (b) Points coloured by calcite generation. This illustrates some consistency in the composition of equivalent calcite generations in the samples from the Devonian. However, the compositional fields for individual calcite generations overlap almost completely in the Moine.
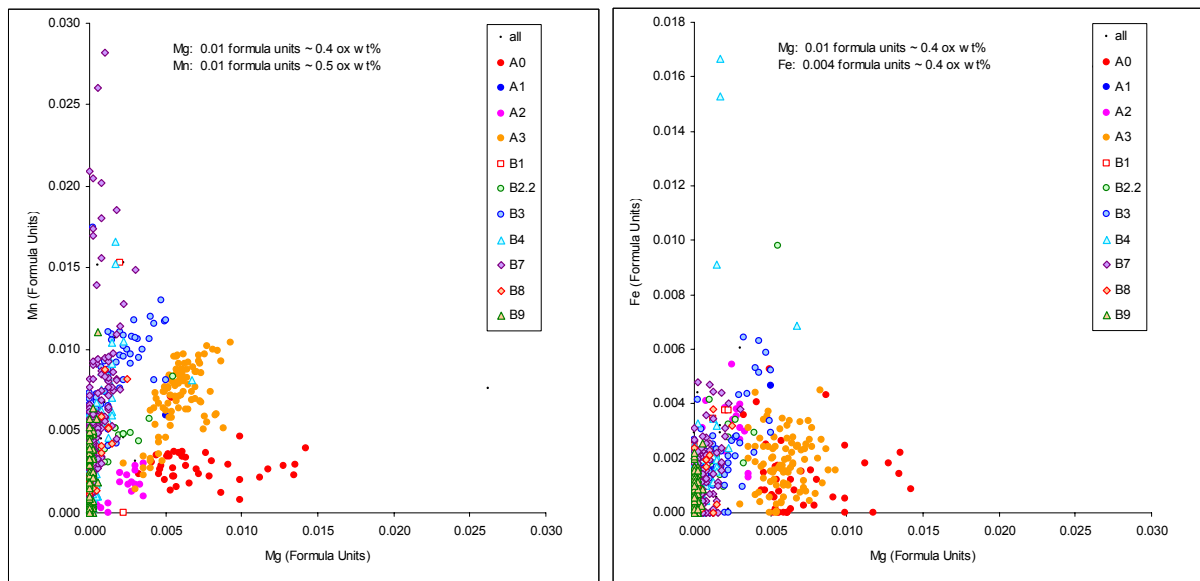
Figure 3-53. Cross plots of minor element chemistry in calcite from borehole NDN-1. Analyses are colour-coded by calcite cement generation, and normalised to one cation.
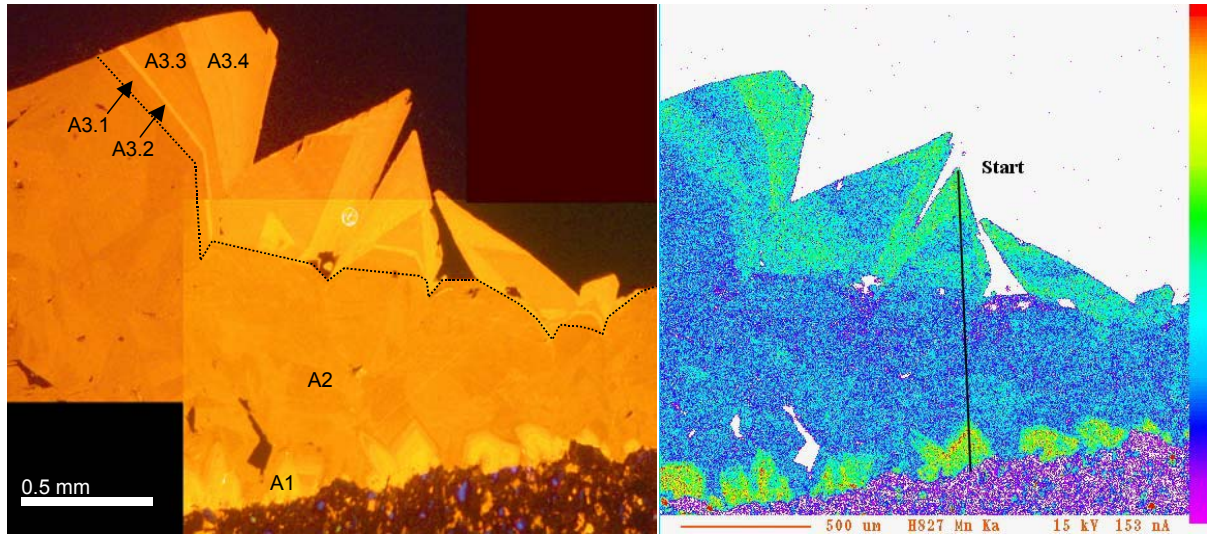
Figure 3-54. (a) Cathodoluminescence and (b) microchemical map (Mn) of calcite cement generations A1 to A3, from above 153 m core bRT (sample MPLH827).
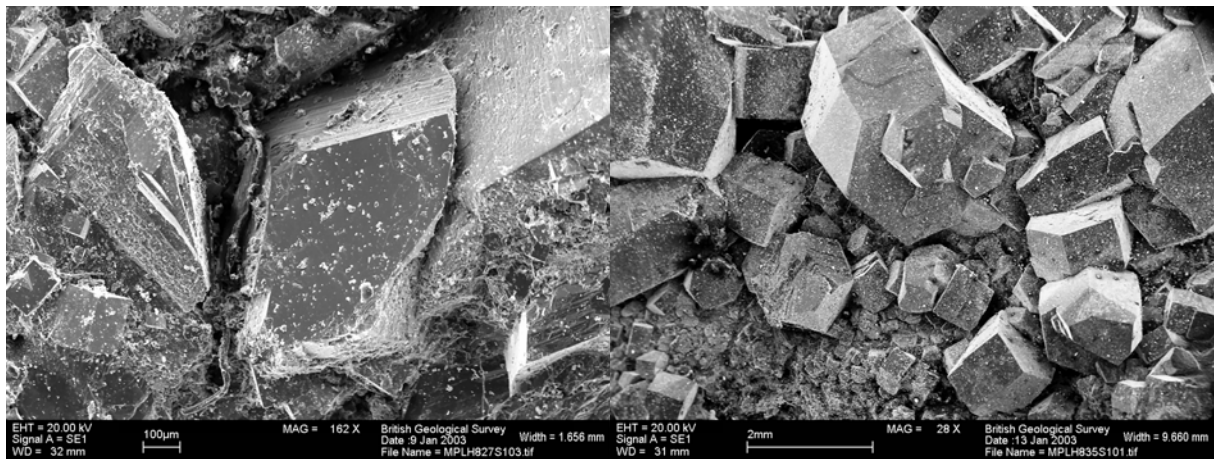
Figure 3-55. SEM image showing calcite morphologies above the Devonian-Moine contact. (a) Nailhead (*c*-axis-flattened) morphology (sample MPLH827), (b) Hexagonal-blocky or barrel-shaped crystals near the Devonian-Moine contact (sample MPLH835).

3.4.4.2 LATE CALCITE FROM BELOW THE DEVONIAN-MOINE CONTACT

Below the Devonian-Moine contact, the late calcite cement stratigraphy is markedly different from that described above. A larger number of cement generations are observed, and identification of equivalent generations in different samples (and in some cases even within different polished thin-sections from the same sample) is locally very difficult. In most samples from below the Devonian-Moine contact, the calcite has a scalenohedral (*c*-axis elongated) morphology (Figure 3-56), but some anomalies are also locally encountered. A total of 9 calcite generations are recognised (illustrated in Figure 3-57 to Figure 3-59), as follows:

B1   This is the earliest generation recognised below the Devonian-Moine contact, and is only locally observed/preserved (samples MPLH844, MPLH851 and MPLH852). It is highly distinctive, being characterised by an early core of bright-yellow-orange luminescent calcite, overgrown by successive bands of oscillatory-zoned, but progressively duller-luminescent calcite (Figure 3-57)

B2 This generation is widely developed and can be recognised in some form or another in most samples from below the Devonian-Moine contact. Locally it can be further subdivided into 2 (or more) discrete generations of subtly different character. It typically has relatively dull- to moderate -orange luminescence, and has a somewhat 'granulated fabric', which locally shows evidence for dissolution with the development of intra-crystalline pores which may be lined by successive generations of later calcite cements. This probably represents a core of earlier hydrothermal calcite that has been tectonically deformed to some extent.

B3 This generation typically forms relatively thin overgrowths on the earlier calcite, but is locally well-developed. Within a given sample, generation B3 is marginally more brightly-luminescent than generation B2, reflecting typically higher Mn-concentrations.

B4 This generation has marginally duller luminescence than B3, and is widely developed. It locally shows evidence for corrosion (Figure 3-57).

B5 Generation B5 is relatively brightly luminescent (brighter than B4). Within a given sample, it is almost identical in appearance and composition to generation B7, and can only be differentiated by the localised development of the very-dully luminescent generation B6 that separates them (Figure 3-58).

B6 This is only locally developed, and has a distinctive non- or very dully-luminescent character (Figure 3-58), reflecting a low Mn-content.

B7 As noted above, this generation is almost indistinguishable from generation B5. In samples where generation B6 is not recognised, all calcite of this character has been defined as this generation. It is relatively brightly luminescent and locally has corroded margins prior to overgrowth by generation B8.

B8 This generation is relatively dully-luminescent, and forms a typically thin overgrowth on the older calcites.

B9 This generation is only developed within a restricted interval near the base of the borehole (Samples MPLH877, MPLH880, MPLH882), and only in small amounts. It occurs as incipient, initially moderately luminescent (B9.1) fading to non-luminescent (B9.2) overgrowths (Figure 3-66).
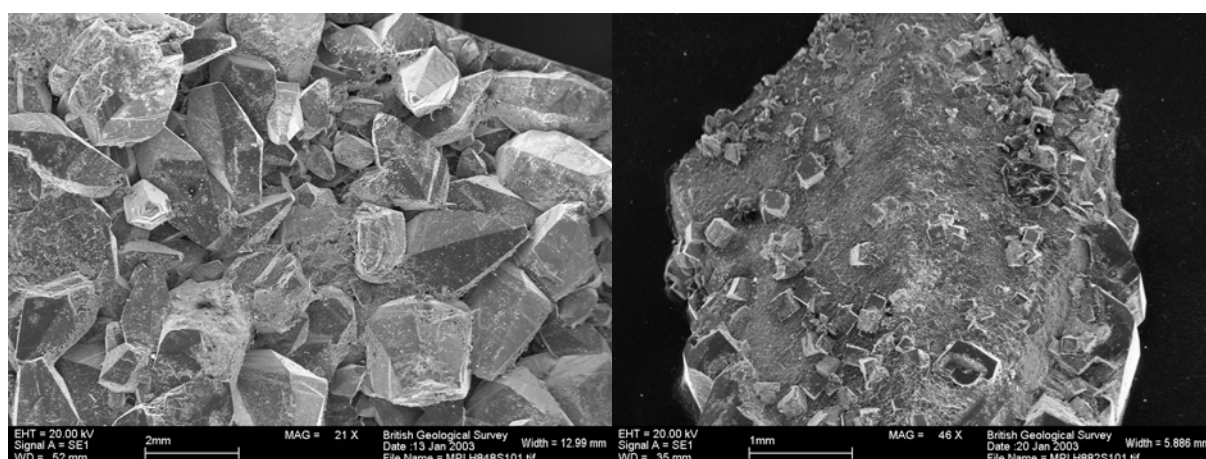
Figure 3-56. BSEM images of calcite crystals from the Moine. (a) Well-developed scalenohedral crystals (sample MPLH848). (b) Fragment of very coarse calcite crystal, with surface coating of euhedral (cubic) pyrite. At the right hand side of the image, this is seen to be engulfed by calcite overgrowths (probably generation B9; sample MPLH880).
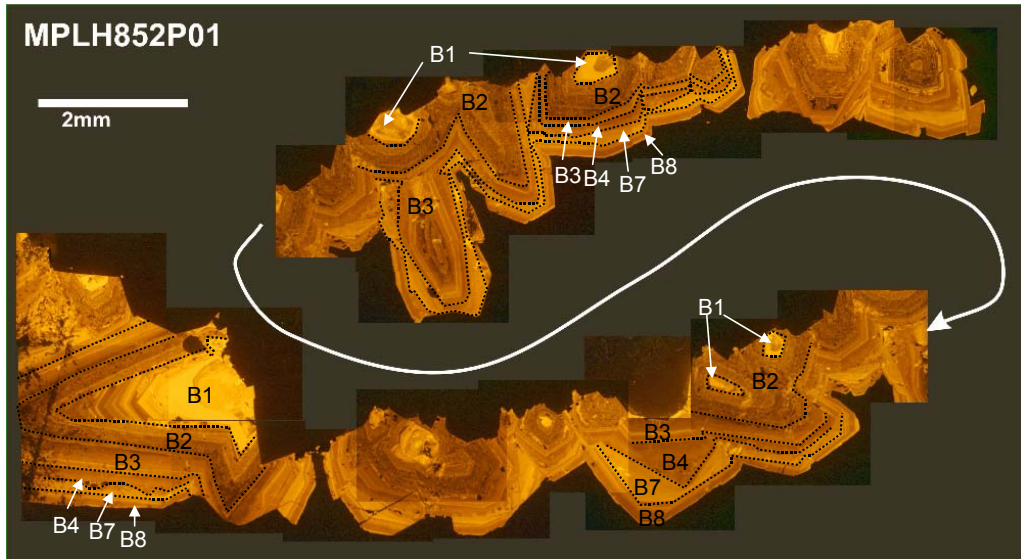
Figure 3-57. CL image montage showing well-developed calcite lining fracture from below the Devonian-Moine contact. This sample preserves almost the entire range of calcite generations, which are recognised (sample MPLH852).
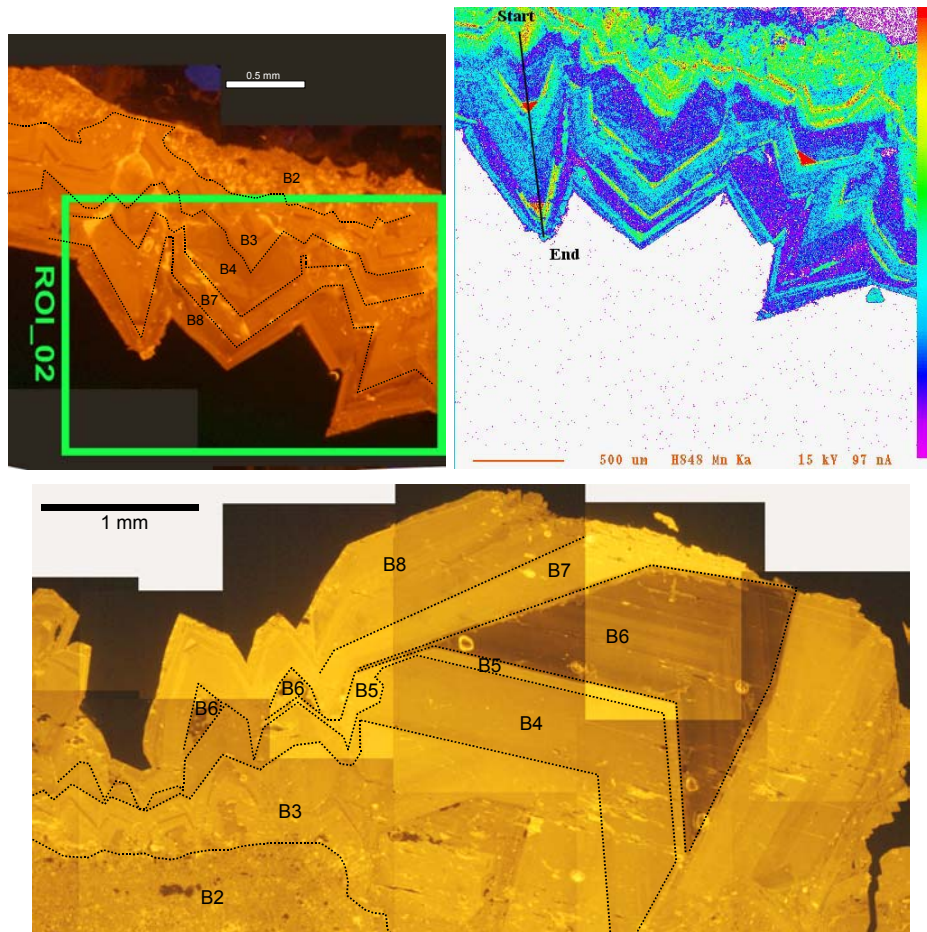
Figure 3-58. Calcite generations B5 and B6 are only locally developed, but generation B6 is highly distinctive with its very dull luminescence. In (a) and (b) relatively finely-crystalline fracture lining calcite shows well-developed concentric growth zonation (primarily defined by small variations in Mn-content). Generations B5 and B6 are not developed. In (c) the fracture-lining calcite has locally developed very coarsely-crystalline overgrowths of non-luminescent calcite B6. Calcite generations B7 and B8 occur as overgrowths throughout the sample. Sample MPLH848.

143
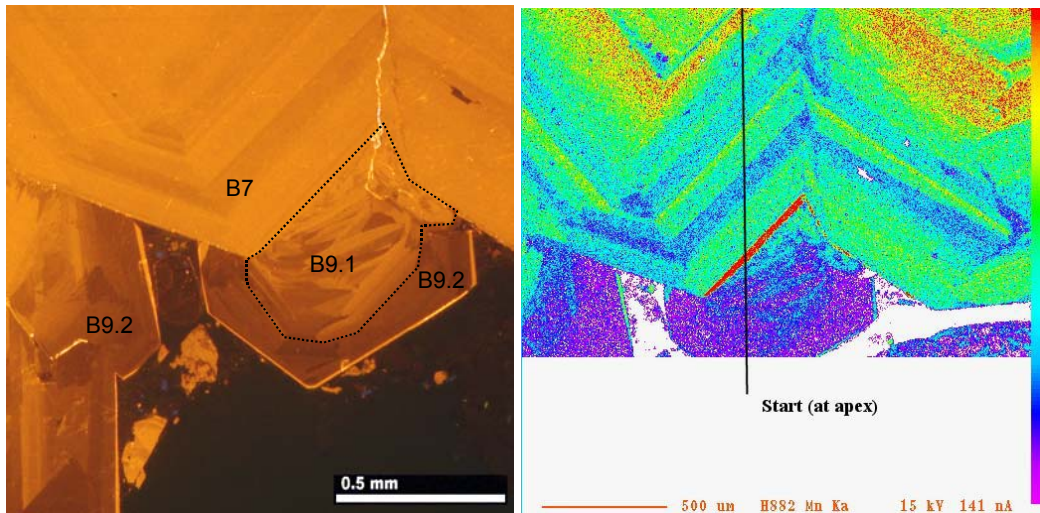
Figure 3-59. Calcite generation B9, showing its occurrence as incipient overgrowths on older calcite. Left - CL image; Right - EPMA map of Mn distribution (sample MPLH882).

3.4.5 Trace element characteristics of the late calcite mineralization

Trace element data were obtained for the Dounreay late-stage calcites using both the ion microprobe (Edinburgh University) and LAMP-ICP-MS (at BGS) techniques. Three samples were examined, which were selected to span between different types of calcite morphology: from shallow nailhead to deep *c*-axis elongated crystal forms. The objective was to examine trace element variation during calcite crystal growth that might reflect the evolution of the palaeogroundwater system.

The sub-samples examined by LAMP-ICP-MS were all prepared as polished blocks mounted in M70 low-melting point (70 °C) Bi-Pb-Sn alloy, in order that the same samples might also be analysed for oxygen and carbon stable isotope ($\delta^{18}O$ and $\delta^{13}C$) composition using He-LACE microsampling (Section 3.4.7). Although these blocks provided a sample mount that did not contribute $\delta^{18}O$ and $\delta^{13}C$ contamination artefacts during He-LACE, unfortunately these blocks could not be produced with as high quality of polished finish as more conventional polished sections prepared using epoxy-resin impregnation. The consequence of this was that the CL images obtained from the samples were poor and precise correlation of the analysis points with the calcite zone stratigraphy was very difficult. In contrast, the ion microprobe data were obtained from conventional polished thin sections and provide a more detailed (and finer resolution) insight into the chemical variations associated with the growth zoning of the calcites that could be more closely correlated with the calcite growth zoning observed under CL. However, the LAMP-ICP-MS data still provide broadly similar results that corroborate the ion microprobe data, and are tabulated in Appendix 7. The trace element variation, determined by ion microprobe, within the zoned late calcite mineralization is summarized in Figure 3-60, Figure 3-61 and Figure 3-62.

As shown by the EPMA point analysis and X-ray mapping (Section 3.4.4), the principal control on the luminescence variations and zoning observed under CL is the variation in Fe and Mn. High Mn:Fe calcite has bright luminescence, whereas low Mn:Fe calcite has duller luminescence.

In contrast to the shallow calcites observed at Sellafield, the late-stage calcite in the upper two Dounreay samples (152 and 461 m bRT) are both generally luminescent, and they lack the negative Ce-anomaly that characterizes the non-luminescent calcite of the strikingly-zoned Sellafield freshwater calcite. Overall, the ion microprobe and LAMP-ICP-MS data indicate only

144

small variations in minor and trace element chemistry during the growth of the late-stage calcites at these depths, consistent with the detailed petrographical observations in Section 3.4.4.

The late-stage calcite in the deepest Dounreay sample, MPLH882 (1172 m bRT), comprises finely alternating non-luminescent and luminescent calcite of generation B9 (labelled bands III – V in Figure 3-62) forming overgrowths on generally moderately to brightly luminescent calcite mainly of generation B7 (labelled bands I-II in Figure 3-62). The B9 calcite shows similar minor and trace element chemistry (e.g. Mn:Fe, Mg, Sr) to that seen in the freshwater (above STZ-type) calcite at Sellafield. However, a notable difference is the absence of any negative Ce-anomaly in the Dounreay calcite. Despite the lack of a negative Ce-anomaly, the strongly varying luminescence of the latest B9 generation of calcite, and associated fluctuations in trace element concentrations and normalized REE values points to significant fluctuations in groundwater composition during the growth of late stage calcite at depth (>1000 m) at Dounreay.
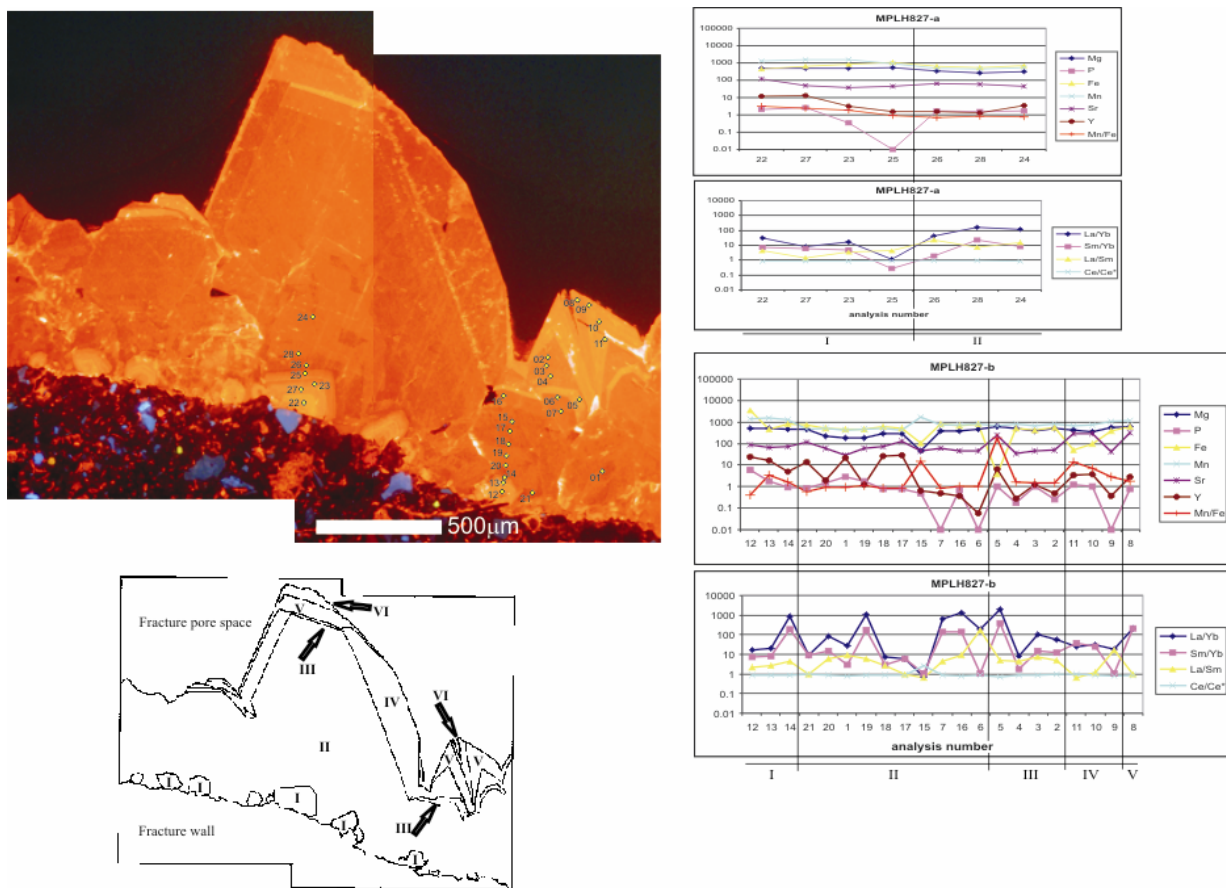
Figure 3-60. Cathodoluminescence characteristics, ion microprobe analysis locations, and compositional characteristics of late-stage calcite in sample MPLH827, Dounreay.

145
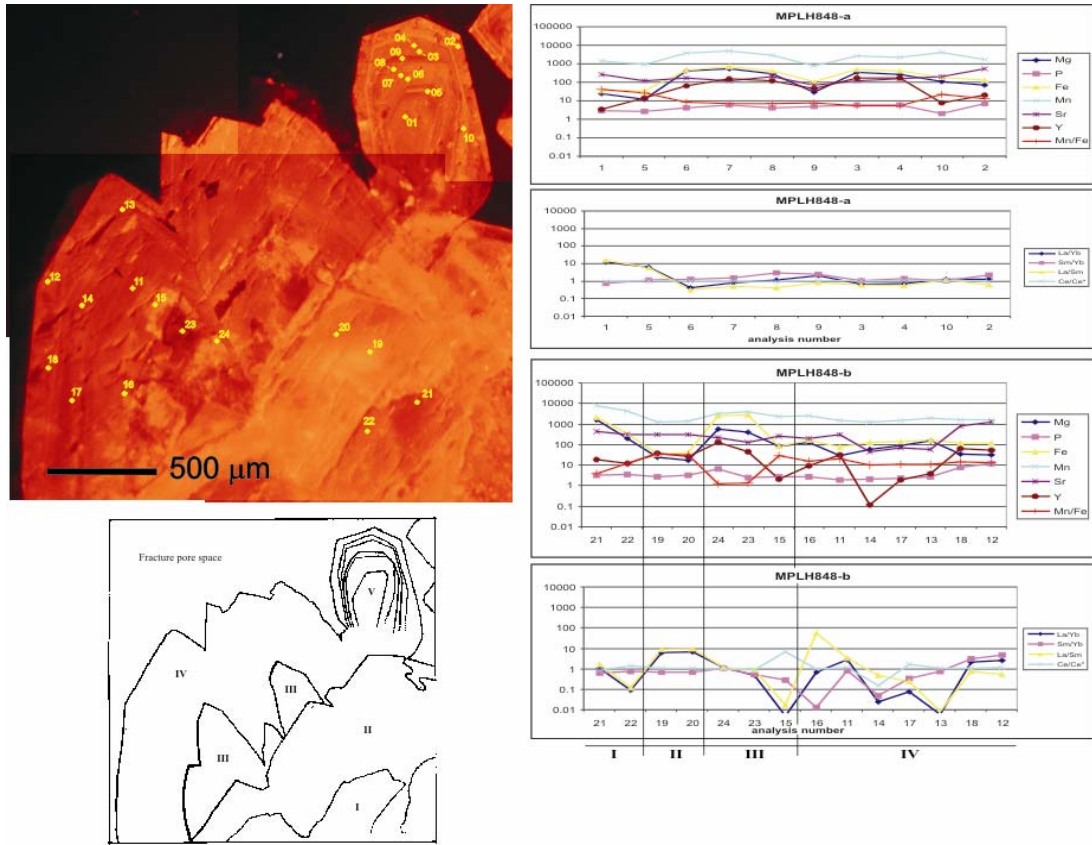
Figure 3-61. Cathodoluminescence characteristics, ion microprobe analysis locations, and compositional characteristics of late-stage calcite in sample MPLH848, Dounreay.
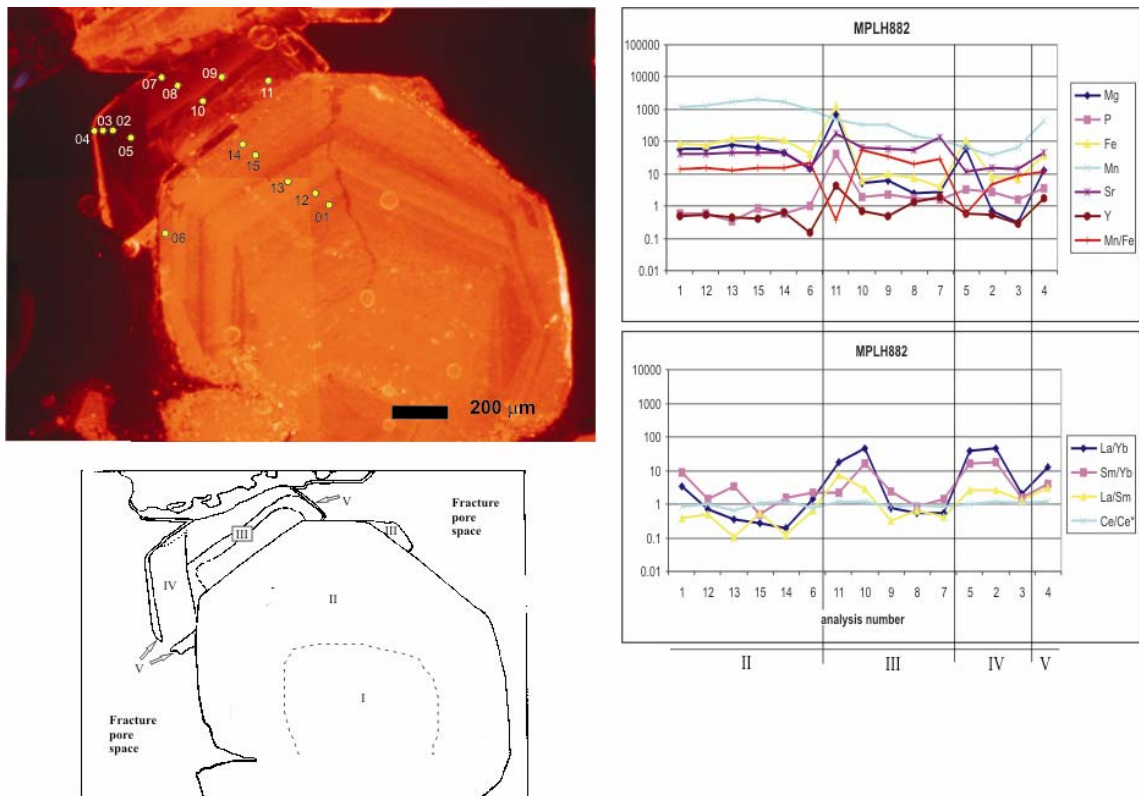
Figure 3-62. Cathodoluminescence characteristics, ion microprobe analysis locations, and compositional characteristics of late-stage calcite in sample MPLH882, Dounreay. Zones III-V are the same as zone B9.

146

3.4.6 Fluid inclusion studies

Fluid inclusion studies attempted to focus on the late stage calcite mineralization. Samples were analysed using conventional microthermometric techniques at the BGS and by BGS staff using laser ablation inductively coupled plasma mass spectrometry (LA-ICP-MS) at the Department of Earth Sciences, University of Leeds. Details of the samples analysed are given in Table 3-11.

3.4.6.1 Conventional microthermometry

Data were acquired from a total of 103 inclusions in 7 samples. This enables an assessment of the nature of the fluids present during and after calcite precipitation, and of any changes that may have occurred over time. CL was used following the microthermometric analysis to assess the cement generation within which each analysed inclusion occurred. The microthermometric dataset was coded accordingly. In addition 'legacy data' from the earlier Nirex Dounreay Site Investigation Programme (n = 156) were also compiled for comparative purposes. However, these could not be cross-correlated with the calcite cement generations distinguished during PADAMOT.

Figure 3-63 and Figure 3-64 show histograms of fluid inclusion salinity and homogenisation temperature (T_h) for inclusions in calcite from Dounreay. Data acquired in the course of the PADAMOT project are plotted by calcite cement generation in Figure 3-63, and by sample in Figure 3-64. Legacy data derived from the Nirex site investigations are also plotted for comparison in Figure 3-63.

The majority of the analysed inclusions are monophase (i.e. contain a liquid phase only). Whilst no precise information about likely trapping temperatures can be inferred from such inclusions, monophase inclusions are usually indicative of relatively cool conditions during mineral precipitation (although this interpretation is not always valid; Roedder 1984 and see also Section 3.2.4.3). Where inclusions contain both a liquid and a vapour phase, homogenisation temperatures (T_h) are widely variable (47.5-132.5 °C) and no clear maxima is observed within this range. Total salinities are highly variable (0.0-19.6 wt%) and there are two (possibly three) populations: a relatively high salinity component (c. >9 wt%); a moderate salinity component (c. 2-9 wt%); and a relatively fresh component (c. <2 wt%). First melting temperature data (T_{fm}) are very scarce, particularly for the low-salinity inclusions, however, two distinct populations of inclusion are evident: those with T_{fm} ~ -20 °C, and those with T_{fm} <-35 (and typically c. –50 °C). These T_{fm} data are consistent with the eutectic temperatures of NaCl- and mixed $NaCl$-$CaCl_2$-bearing fluids respectively. Fluid inclusion salinities are also variable (0.0-19.6 wt% total salt).

There are no strong patterns of variation in T_h, salinity, or dissolved components between calcite of different generations and/or from different samples (Figure 3-63 and Figure 3-64, Table 3-13). This is not particularly surprising given the long history of cementation in the area. However, in spite of these difficulties, the following observations and conclusions can be derived from the data:

- The euhedral calcites lining open fractures (PFFs) in the Dounreay borehole contain evidence of a wide range of palaeofluid salinity from dilute groundwaters (<2 wt% total salt) to brines (up to 20 wt% total salt). Most of the fluid inclusions are more saline than seawater, and are between 10-20 times more saline than any groundwater now present at depth in Dounreay borehole NDN1 (Figure 3-51). This type of fluid is indicative of deep basinal brines, and may be geologically very old. Most of the inclusion data is derived from the early 'core-zones' (generations A2, and B2-B3) of the calcite. At least part of this calcite probably represents cores of old hydrothermal calcite (e.g. FE7, FE12) that has acted as seeds for the nucleation of the younger calcite.
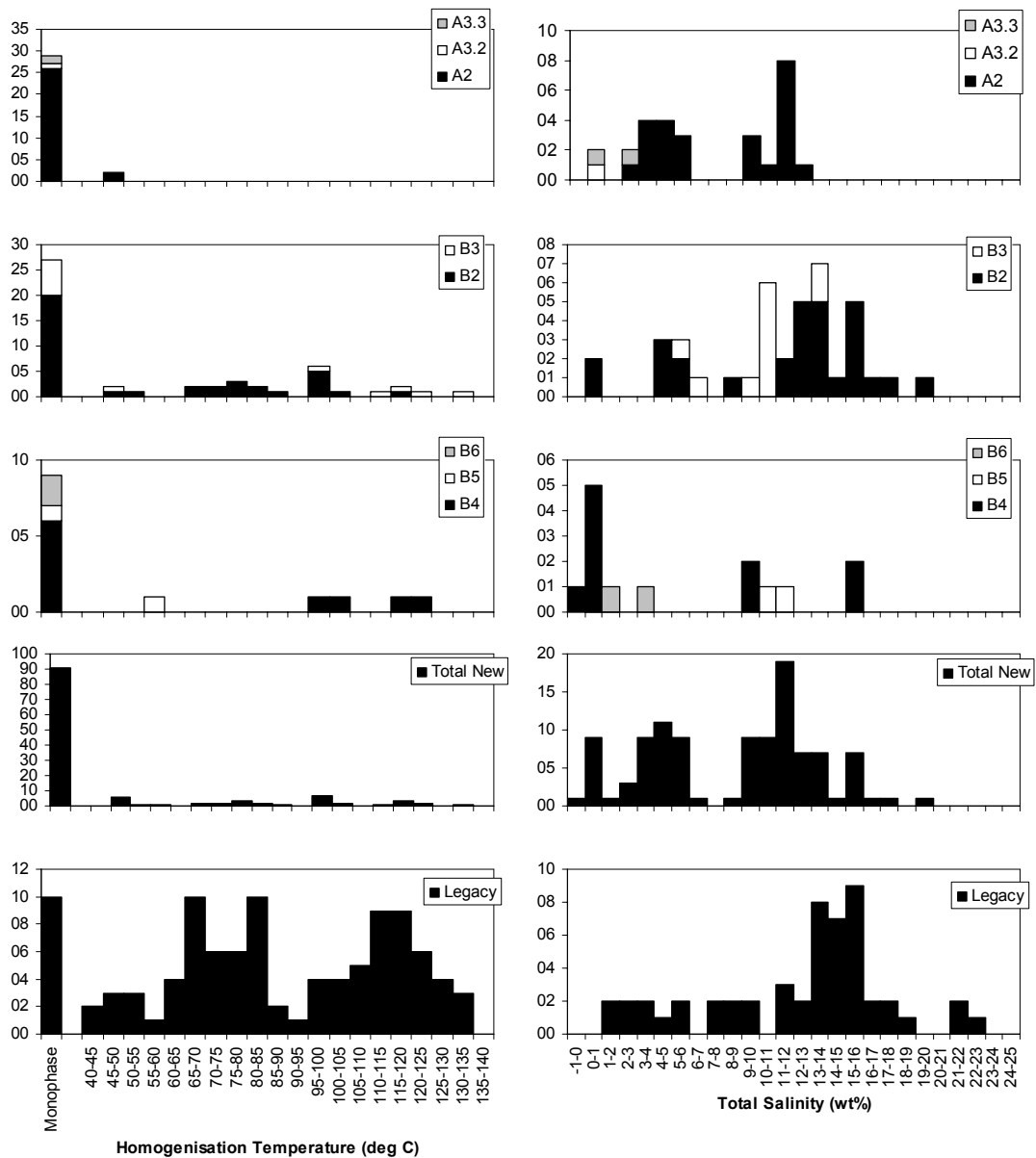
Figure 3-63. Histograms showing variations in homogenisation temperature and total salinity, by sample, for fluid inclusions from borehole NDN-1.

- Relatively high-salinity inclusions (i.e. >9 wt% total salt) occur in late calcite mineralization throughout the borehole, except for the shallowest (nailhead-type) calcite sample that was studied (MPLH827; 151.64 m core bRT). The fact that relatively high salinity fluids occur trapped in fluid inclusions at depths well above the present day transition zone between fresh and more saline fluids implies that the palaeogroundwater must have been very different at some time in the geological past, with a much shallower contact between the fresh and more saline groundwaters.

- Moderate-salinity inclusions (i.e. 2-9 wt% total salt) occur throughout the borehole.

- Relatively low-salinity inclusions (i.e. <2 wt% total salt) are only observed within the shallowest sample (MPLH827; 151.64m core BRT), and within two relatively deep samples (MPLH880 and MPLH882; 1141.46 and 1171.99 m core bRT respectively). The presence of these fluids at great depth within the borehole indicates that relatively fresh water has penetrated to depths far greater than its present limit. However, the apparent absence of relatively fresh water-bearing inclusions in the interval c.200-1100 m

148

bRT, suggests that this may be a more localised fluid event, not necessarily representing a shift in the contact between fresh and more saline fluids. This interpretation is further supported by the observation that the relatively fresh inclusions only occur in the samples that contain distinctive dully-luminescence calcite of generation B9 (see above) that is only observed in this part of the borehole. These two features suggest this may be a localised flow zone of some description.

- Although there is relatively little data to confidently assert this, calcite generation A3, in the shallow part of the borehole, appears to be dominated by low salinity (i.e. <2 wt%) fluids.

- Calcite generations B5 and B3 do not appear to bear inclusions containing the relatively low salinity fluid.
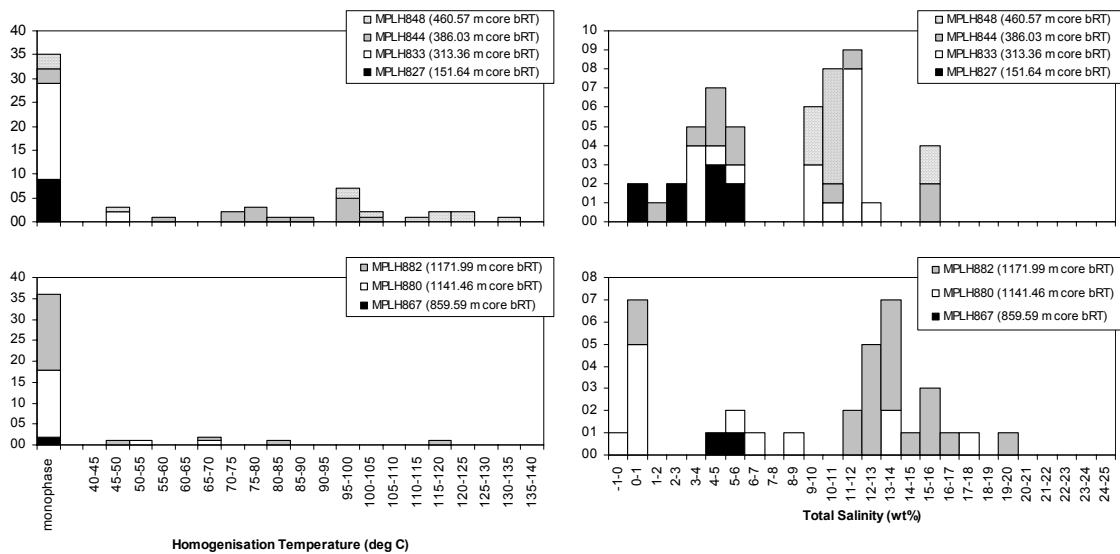
Figure 3-64. Histograms showing variations in homogenisation temperature and total salinity, by sample, for fluid inclusions from borehole NDN-1.

Table 3-13. Summary of the distribution of the different fluid types within inclusions in borehole NDN-1, by sample and calcite cement generation. Each "X" represents a single analysed fluid inclusion. Individual "inclusions" are coloured according to groupings in total salinity: Blue <2 wt%, green 2-9 wt %, red >9 wt%.

Sample	Top Depth (m core bRT)	Calcite Cement Generation						
		A2	A3	B2	B3	B4	B5	B6
MPLH827	151.64	XXXXX	XXX					
MPLH833	313.36	XXXXXX XXXXXX XXXXXX X						
MPLH844	386.03			XXXXXX X			XXX	XX
MPLH848	460.57				XXXXXX X	XXXX		
MPLH880	1141.46			XX	XXXX	XXXXX		
MPLH882	1171.99			XXXXX XXXXX XXXXX XX				

149

Six carbonate samples were selected for detailed microchemical fluid inclusion analysis by LAMP-ICP-MS (Table 3-11). From these, 54 inclusions were analysed, 22 of which yielded data for one or more of the following elements: Li, Na, Mg, Cl, K, Ca, Mn, Fe, Sr (Appendix 7). Petrographical observations made during microthermometric analysis shows that most of the fluid inclusions are likely to be hosted in the older core zones of the calcite crystals.

Na, K and Cl were unequivocally detected in 80% of the inclusions analysed. Li was generally below detection. Sr and Mg were present in significant amounts in 50% of the inclusions and, where reported, have been corrected for matrix interference. From the distribution of Na/Cl mole ratios, two general palaeofluid types can be recognised. One has an excess of Cl, the second has an excess of Na. Given that the eutectic temperatures for the 'Cl excess' inclusions are very low and indicative of Ca-Na-Cl fluids, it is reasonable to suppose that the cation deficiency is due to Ca and/or Mg ions. Since Mg-rich fluids are confined to very alkaline environments, the most likely parent fluid is a typical basinal brine of the Ca-Na-Cl type. The 'Na excess' inclusions are more diverse. Na/Cl mole ratios close to 1 suggest an affinity with marine ocean water (or an early evaporitic marine brine) or the influence of halite dissolution. Those with Na/Cl mole ratios >1.2 are thought to be shallow groundwaters of the Na-Ca-Cl-HCO_3-SO_4 type; the anion deficiency being attributed to bicarbonate and/or sulphate ions. Neither S nor C can be analysed by LAMP-ICP-MS. The range of Na/K mole ratios (12-179) is exceptionally large for low temperature fluids. Using simple Na-K and Na-K-Ca geothermometers (Fournier and Truesdell, 1973), inclusions with Na/K ratios <100 yield improbably high temperatures compared to measured or inferred homogenisation temperatures. This strongly suggests that the fluids have undergone varying degrees of low temperature modification by ion exchange or interaction with clays and feldspars.

Calcite matrix analyses show a significant enrichment in Sr in samples immediately below the Devonian/Basement unconformity suggesting some degree of vertical heterogeneity in the chemistry of the groundwaters at the time of carbonate deposition. This is also reflected, albeit less strongly, in the variation in Na/K ratios. The fluid inclusions in the shallow samples associated with Sr-poor calcite have Na/K mole ratios >60 whereas the fluid inclusions in deeper samples are more K-enriched, with ratios typically <60. Similar variations in Na/K can also be observed with respect to Mg. Thus, independent of local differences in cement chronology as illustrated by changes in CL (for late stage calcites), the palaeofluids preserved in the fluid inclusions appear to be vertically stratified.

3.4.7   Stable isotope (δ^{18}O and δ^{13}C) characteristics of late calcite mineralization

Three samples of late calcite were examined for oxygen (δ^{18}O) stable isotope composition using the ion microprobe at Edinburgh University (Table 3-11). The samples were selected to span between different types of calcite morphology, from shallow nailhead to deep *c*-axis elongated crystal forms. The objective was to use the ion microprobe to examine the variation in the δ^{18}O signature across calcite crystals that might reflect the evolution of the palaeogroundwater. In addition, one sample (MPLH848) was analysed by conventional mass spectrometry for both δ^{18}O and δ^{13}C, using a micro drill to subsample the calcite and extract small amounts of material from the same polished block sections of calcite that were being studied by ion microprobe. This sample shows generally similar results to Sellafield (Figure 3-49), but in detail, no C/O co-variation exists. In this case it is possible that temperature changes had more effect, which changed ^{18}O fractionation but without changing ^{13}C fractionation. Data points obtained for δ^{18}O from different analytical periods, with different techniques overlap very well, with no sign of sampling or analytical artefacts more than 0.1 ‰. Reproducibility between the methods was therefore good, and well within the range of natural variation.

Figure 3-65 displays the δ^{18}O isotope results obtained by micro drilling and ion microprobe from Dounreay. The data points are shown, and superimposed are model lines to show effects of

present–day water, glacial water influx, or of cooling. A similar modelling approach has been used as that carried out for the Sellafield site (Section 3.3.), and the groundwater and temperature values used in the model are also based on those for Sellafield (Section 3.3), being fairly typical of the present UK (cf. Darling et al., 2003).

The $\delta^{18}O$ data from the shallow (nailhead) calcite at -152 m show a bimodal distribution, with the most depleted values found in the sharply-defined outermost parts of the crystals (late calcite zone A3). This would be consistent with a period of glacial water influx, between 50 – 65 % volume (assumed $\delta^{18}O$ -20 ‰). Preceding this was a distinct period of glacial influx up to 30 % by volume, mixing with waters identical to the present-day, or slightly cooler (essentially corresponding to calcite zone A2).

At -461 m calcites can be modelled to have grown from 50 % volume glacial water, gradually mixing back to 25 % volume glacial water. There is no isotopic evidence of calcite growth from the present-day water.

At -1172 m, the spread of $\delta^{18}O$ analyses suggest a markedly different process, where calcite could have grown from a water of $\delta^{18}O_{SMOW}$ -1.5 to -1.8 ‰. This water is close to marine values (1.2 ‰$_{SMOW}$), or could have been meteoric or glacial mixed with a water expelled from the deep sediment basin (+4 ‰$_{SMOW}$) by ice loading. The spread of $\delta^{18}O$ data shows that this mixed to compositions consistent with present-day meteoric water values. This mirrors the petrological and fluid inclusion observations, which indicate: earlier growth stages of calcite (late calcite zones B2-B4) associated with crystallization from a very saline fluid similar to that which might be expected for a deep basinal brine-type fluid; followed by very late calcite, which by analogy with Sellafield (Section 3.3) and Cloud Hill (Section 3.5), has chemical, CL and morphological characteristics expected for freshwater calcite mineralization.
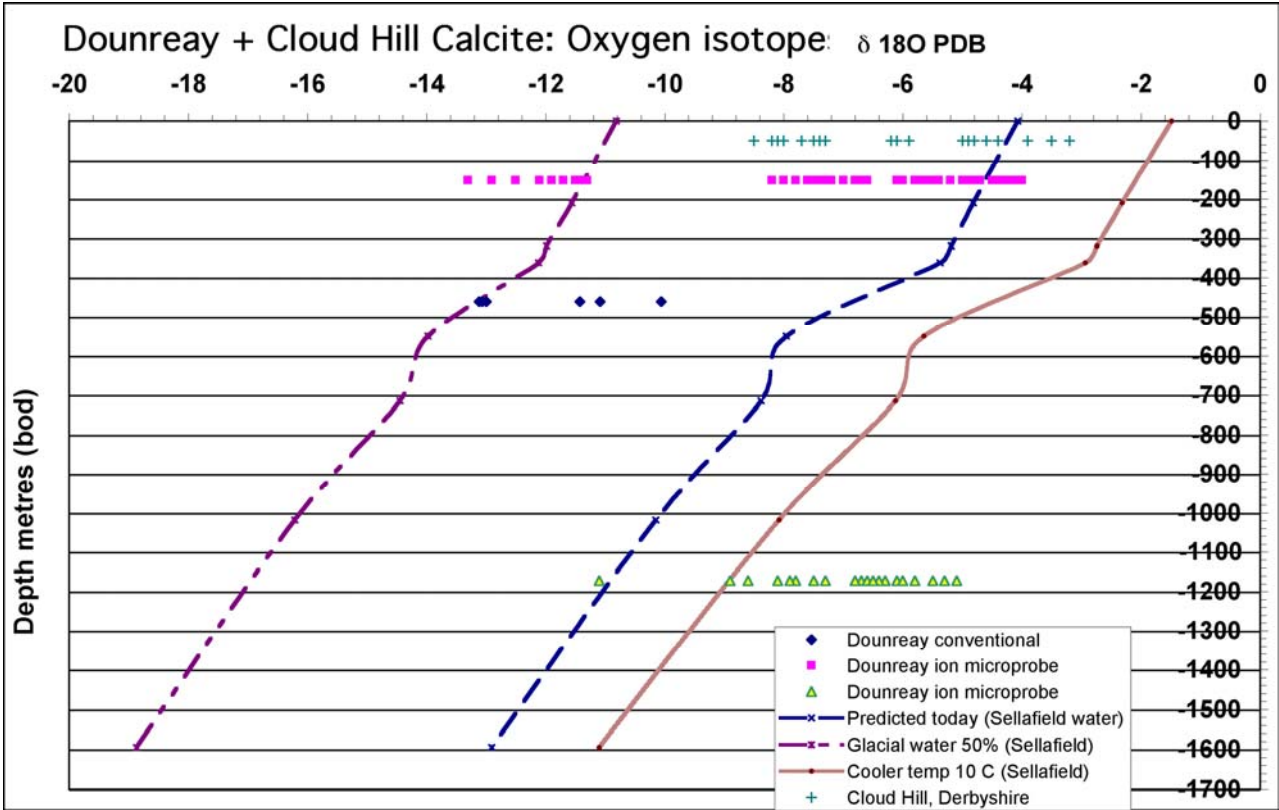
Figure 3-65. Oxygen isotope data from Dounreay (conventional and ion microprobe) and from Cloud Hill (Derbyshire, Central England).

151

Stable isotope analyses were obtained from the same three samples using the He-LACE microsampling technique at the BGS (Appendix 8). The data are much more limited and good CL images, required to enable the analyses points to be located precisely within the established calcite cement stratigraphy framework, could not be obtained from the M70 alloy mounts used for He-LACE analysis. Furthermore, the He-LACE ablation pit size was much larger than that produced by the ion microprobe, and may have sampled more than one zone. Because of this it also proved impossible to specifically sample the latest generations of calcite that are present only as fine overgrowths. Consequently, there is significant uncertainty in reliably attributing the He-LACE data to a particular growth zone of the late calcite. In most cases, the data probably represent the older (volumetrically larger) core regions of the calcites. Despite these problems, the He-LACE data suggest similar (although somewhat wider) ranges for $\delta^{18}O$ to those obtained by the ion microprobe. The more depleted $\delta^{18}O$ values obtained by He-LACE may represent old hydrothermal cores in the calcite.

In summary, the stable isotope data for late calcite at Dounreay shows a similar process to Sellafield down to 400m, with potential evidence for a large influx of glacially–derived water. Deeper than this, a distinct source of water was present – with a $\delta^{18}O$ isotopic signature that could be interpreted to be similar to marine, or possibly representing a glacial water mixed with a deep sedimentary basinal brine.

3.4.8   Biomarker studies

Six samples of late-stage calcite from the Dounreay borehole NDN1 were analysed by GC-MS by the Universidad Politecnica de Madrid for the presence of organic biomarker compounds during the course of the PADAMOT project (listed in Table 3-14). Only one sample (MPLH848, 460.79 m bRT) furnished any evidence of trace organic compounds within the late-stage calcite. This sample yielded only octadecanoic acid, and the origin of this compound cannot be interpreted definitively. It could indicate the input of organic matter of plant origin but it could also be formed in situ by bacterial activity.

Table 3-14. Abundances of the different biomarkers found in late-stage calcites from the Dounreay borehole NDN1.

Sample No.	Depth (m bRT)	Sample wt. (mg)	Cyclo-pentane	Hexadeca-noic acid	Octadeca-noic acid	1, 2 benzenedi-carboxilic acid	Isoquino-line	Pyrrolo [3,2-a] dibenzo-furan
MPLH827	151.72	116.3	nd	nd	nd	nd	nd	nd
MPLH833	313.44	110.9	nd	nd	nd	nd	nd	nd
MPLH848	460.79	75.0	nd	nd	1441455	nd	nd	nd
MPLH867	859.68	84.3	nd	nd	nd	nd	nd	nd
MPLH880	1141.64	132.4	nd	nd	nd	nd	nd	nd
MPLH882	1172.08	113.7	nd	nd	nd	nd	nd	nd

Notes:
1. nd = not detected
2. Relative concentrations of organic compounds shown as total GC-MS peak counts.

3.4.9   Conclusions

3.4.9.1 GENERAL CONCLUSIONS ON THE SAMPLING AND ANALYTICAL METHODOLOGY

3.4.9.1.1 *Core preservation and sampling*

Core preservation and sampling issues are similar to those that have already been discussed for the Sellafield and Swedish sites. Dounreay borehole NDN1 was drilled in 1990 with similar technology to that at Sellafield, using triple-barrel tubing providing large diameter core (95 mm).

A large proportion of the late calcite at Dounreay occurs only as very thin or limited coatings, or as fine overgrowths on much older (hydrothermal) calcite. As in the case of Laxemar, the limited amount of material available restricts the range of analytical techniques that can be applied to a given sample.

3.4.9.1.2 Calcite morphology

Observations from Dounreay have identified a similar range of crystal morphological variations in the late stage calcite to those observed previously at Sellafield during the EQUIP project (Bath et al. 2000). As at Sellafield, short *c*-axis calcite ('nailhead') crystal forms occur at shallow depth, and there is a general trend towards *c*-axis elongated ('scalenohedral') crystal forms with depth. However, the MTZ in Dounreay borehole NDN1 is not as clearly defined as at Sellafield. There are a number of reasons that may explain this:

- The interval over which the crystal morphology changes from short *c*-axis to long *c*-axis calcite has a relatively low population of open fractures or potentially flowing features (PFFs). Consequently, this limits the number of observations that can be made on calcite fracture mineralization;

- PFFs within the MTZ have been heavily sampled and surfaces damaged by core handling for earlier studies, which significantly restricts the availability of suitable material observation;

- There is a low abundance of late calcite on PFF surfaces in the upper part of the borehole and within the MTZ. In part, this may be due to the presence of late-migrated oil in the fractures and rock matrix, which may have caused calcite growth to cease or restricted subsequent calcite growth by inhibiting nucleation on fracture walls and older calcite surfaces;

- Much of the late calcite that is present in this interval is present as fine scaly films within hairline PFFs. The calcite has grown into confined pore space, which restricted the development of well-defined crystal forms that could be readily recognised during core logging. More extensive detailed observations using high-resolution microscopy (e.g. SEM) may help define the crystal morphology more clearly in any future investigations;

- Much of the late calcite in the borehole is also developed as thin overgrowths seeded onto geologically old calcite. Because the late calcite is volumetrically small, its morphology is dominated by that inherited from the earlier calcite substrate. This makes defining the actual morphology attributable specifically to the late calcite much more difficult. Again, a much more extensive detailed survey using high-resolution microscopic observations (e.g. SEM) may resolve this in any future study.

Despite these difficulties, the observations from this site confirm a similar trend in calcite morphological variations to those observed initially in Sellafield and, subsequently, in Äspö and Laxemar. This shows that calcite crystal morphology variation has application as a palaeohydrogeological indicator to a wide range of sites.

3.4.9.1.3 Fluid inclusion studies

As for Sellafield (Section 3.3.9), there are a number of factors that limit the use of fluid inclusions for reconstructing the chemistry of palaeogroundwaters at Dounreay by microthermometry and laser LAMP-ICP-MS:

- Size of inclusion;

- TDS of inclusion fluid;

- Analytical detection limits.

153

Again as at Sellafield, within the youngest generations of calcite (which is of most relevance to palaeohydrogeology) fluid inclusions are generally sparse and are typically very small (<5 μm), Their small sizes make measurements of the more subtle phase changes such as temperatures of first melting (T_{fm}), hydrate melting (T_{hyd}) and ice melting (T_{ice}), very difficult to determine.

With respect to LAMP-ICP-MS analysis, the very small inclusion size severely limits the amount of analyte available for analysis (typically less than 10-12 ng), and many elements fall well below the instrumental detection limit for transient signals. [N.B. Detection limits as calculated for conventional solution analysis do not apply to transient signals]. This problem is exacerbated where the amount of analyte is further reduced in the case of low salinity inclusions. Consequently this method of analysis carried a high failure rate per inclusion.

Another factor constraining reconstruction is the difficulty in obtaining microthermometric and chemical data for the same inclusion. The majority of inclusions analysed in the Dounreay site were monophase (i.e. low temperature groundwaters). This causes additional complications in the microthermometric determination of melting temperature as the inclusion has to be stretched, or caused to leak slightly during testing, before these phase changes can be measured. The unfortunate side effect of this process is that inclusions within the analysed portion of the sample may leak or completely decrepitate, making successive analysis by LAMP-ICP-MS impossible. Since laser ablation is also destructive, it is not possible to calculate the absolute concentrations of solutes (e.g. K ppm) and TDS for the same inclusion. Likewise, detection limits expressed as ppm or mole % cannot be estimated. At best, reference must be made to inclusions in the same growth zone.

There was a major problem in correlating inclusion data with cathodoluminescence zonation. CL images of carbonates cannot be acquired in advance of microthermometric analysis because the CL excitation process destroys low temperature inclusions. This limits the selection of inclusions based on CL zones for determining high-resolution changes in groundwater chemistry. Duplicate samples must be used.

Owing to the scarcity of inclusions, in some cases it proved impossible to confidently differentiate between primary inclusions (i.e. those formed during precipitation of the host mineral) and secondary inclusions (i.e. those formed, typically along healed microfractures, at some time after mineral precipitation). In other cases, it proved necessary to analyse secondary inclusions in order to acquire data at all. This places limitations on the interpretation of the data – as inclusions may represent any fluid of contemporaneous or younger age than the surrounding mineral.

In addition to the analytical problems outlined above, most of the fluid inclusions observed in the Dounreay calcites occur within the earlier 'core' growth zones of the calcite crystal (calcite generations A2, and B2-B3). The salinity of these inclusions is much higher than is now seen in the modern groundwaters, and more characteristic of basinal brines. At least part of the calcite hosting these inclusions is probably geologically old hydrothermal calcite. The use of fluid inclusions for palaeohydrogeological studies on the present groundwater system at Dounreay is severely limited by the lack of inclusions within the most recent generations of calcite. A similar problem was also encountered in the previous fluid inclusion studies at Sellafield (Bath et al., 2000) and in the recent studies at the Cloud Hill site (Section 3.5).

3.4.9.1.4 *He-LACE and LAMP-ICP-MS versus ion microprobe techniques*

He-LACE, LAMP-ICP-MS and ion microprobe techniques have been used to try to micro-sample and analyse discrete growth zones within individual crystals of late-calcite mineralization at Dounreay, in order to evaluate the variation in trace element and stable isotope ($\delta^{18}O$ and $\delta^{13}C$) compositions at different stages of crystal growth. Several advantages and disadvantages in the use of these techniques were encountered, similar to those discussed previously in their application at the Sellafield site (Section 3.3.9.1).

He-LACE studies required sample mounts prepared using M70 low melting point Bi-Pb-Sn alloy (see Sections 3.3.5 and 3.3.7). In the case of the Dounreay samples, it proved difficult to separate the calcite crystals from the wall rock without causing damage to the calcite. Therefore, calcite was mounted with fragments of wallrock still attached. Unfortunately, this made polishing the M70 blocks very difficult because of a combination of the low adhesion between the sample and the M70 alloy, and because of the very large hardness contrast between the soft metal mounting medium and the silicate rock (this was not such a problem at Sellafield, where the greater abundance and coarser grain size of the calcite allowed individual crystals to be mounted relatively easily). As a result, the quality of surface finish of the polished mounts was generally poor, and this had a major impact on the quality of CL images that could be obtained from the mounts. In contrast, the ion microprobe employed polished thin sections prepared from material mounted conventionally in epoxy-resin. The advantages of this are discussed in Section 3.3.9.1. As for Sellafield, for efficiency and budget constraints, the same M70 mounts were used at the BGS for both He-LACE and LAMP-ICP-MS, although future LAMP-ICP-MS studies would be improved by the use of polished thin sections.

Despite the differences and problems, the ion microprobe and the laser techniques provided corroborative results for the Dounreay site.

3.4.9.1.5 Biomarker studies

Evidence of biomarkers in the late calcite from this site is extremely limited, restricted to only octadecanoic acid found in only one sample, and its presence cannot be interpreted definitively. Because these trace organic compounds have a very low concentration in the calcite, the very small amount of late-calcite available on the fracture surfaces was a major problem for the analysis of biomarkers. The limited material that could be provided for analysis from fractures in Dounreay NDN1 was at the working limits of the current technique.

3.4.9.2 PALAEOHYDROGEOLOGICAL INTERPRETATION

The Dounreay site was studied because it potentially provided an example of a coastal discharge area with upward groundwater flow (Section 2.3.3.2) analogous to the coastal discharge area inferred to occur in the west of the Sellafield site. The mineralogical characteristics of this part of the flow system could not be studied at the Sellafield site because of the lack of cored boreholes in this area of interest.

As discussed above, there is an overall change in morphology of the late calcite with depth, from short *c*-axis to *c*-axis elongated crystal forms, similar to that observed at Sellafield. By analogy with the Sellafield observations, the morphological studies indicate Dounreay late calcite grew from palaeogroundwater that increased in salinity with depth. However, the position of the calcite MTZ (152-376 m bRT) does not coincide with the present-day STZ from fresh to brackish/saline water at Dounreay, the top of which starts at about 750 m bRT. This implies that the late calcite MTZ at Dounreay represents the position of an older STZ, and that the overall position of the STZ must have moved significantly downwards over time. This is also supported to some extent by the fluid inclusion data, which show the presence of much more saline inclusion fluids than the present groundwater, however, a high proportion of the fluid inclusion information is derived from geologically old core zones of the calcite.

The pattern of late calcite morphological variation is not as clearly defined as at Sellafield. Sporadic occurrences of equant calcite, more characteristic of calcite from the freshwater zone, are found in some fractures within the saline groundwater zone in the basement. This may imply penetration of freshwater to considerable depth along isolated or localized fracture zones in the past. An analogous situation is concluded from observations at the Laxemar and Äspö sites (Section 3.2.5.2).

In contrast to the Sellafield site, the late-stage calcites from the freshwater zone at Dounreay are dominantly manganoan and magnesian. They lack both the striking zoning pattern of alternations of non-luminescent, non-ferroan, non-manganoan calcite and brightly-luminescent manganoan calcite, and a marked Ce-depletion seen in the above 'MTZ type' ME9 calcite at Sellafield. This may indicate that, unlike Sellafield, the freshwater zone has not been strongly oxidizing (except at very shallow levels affected by recent weathering, and associated with pyrite and ferroan carbonate dissolution and oxidation) within most of the sequence in Dounreay borehole NDN1. The absence of strongly oxidising conditions in the freshwater zone at the Dounreay site may be related to:

- Effective redox buffering of the groundwater by interaction with the hydrocarbon/organic-rich and pyritic Devonian cover rocks;

- Dominantly upward or lateral flow of groundwater, rather than downwards flow of oxidising meteoric water.

The deepest sample of late-stage calcite studied in borehole NDN1 (1172 m bRT) displayed the development of overgrowths of freshwater-type calcite (generation B9) on earlier saline groundwater type calcite (generation B7). The CL characteristics of the Dounreay B9 overgrowths were very similar to those seen in the 'above-MTZ type' ME9 calcite from Sellafield. However, this lacks any evidence of the Ce depletion that is observed in calcites from the near-surface aquifer at Sellafield. Thus, while this may indicate relatively recent penetration to depth by dilute groundwater along localised fracture flow paths, the oxidation conditions observed in the shallow-level at Sellafield (as indicated by the CeIII/CeIV redox couple) are not evident.

This preliminary result is supported by modelling of limited oxygen isotope ($\delta^{18}O$) data obtained by ion probe and He-LACE from the late calcite. The data also indicate that there has potentially been a significant input in the past of a glacial groundwater component (30-65 % by volume) in the palaeogroundwaters above 500 m. However, at greater depth, (1172 m bRT) the $\delta^{18}O$ data from the late calcite are consistent with precipitation from a marine groundwater source, or from a meteoric or glacial water mixed with water expelled from the deep sedimentary basin (perhaps by ice loading). The Dounreay site lies on the coast and may have undergone significant isostatic depression during the Quaternary (in line with loading of the adjacent land mass at least). This would have allowed ingress of greater fluxes of marine water post-glaciation but prior to the last stages of uplift. The spread of $\delta^{18}O$ values shows that this groundwater component mixed to compositions consistent with present-day meteoric waters. There is no mineralogical or geochemical evidence to suggest that oxidizing conditions were developed in association with this potential recharge by a component of glacially-derived groundwater.

The extent to which the Dounreay site was glaciated during the Devensian is unclear. The tills occupying the Dounreay area are considered by some authors to have been deposited by the earlier 'Wolstonian' ice (Sutherland, 1984). On the contrary, Hall and Whittington (1989) argue that these deposits are Late Devensian. If indeed the tills in the Dounreay area are Wolstonian, then their preservation suggests that Dounreay may not have experienced significant ice cover during the Devensian. Therefore, the isotopic signature of a glacial component in the palaeogroundwaters that is preserved in the late calcite at Dounreay may reflect flushing by older (i.e. pre-Devensian) glacial recharge than that recorded by late calcite at Sellafield.

3.5 CLOUD HILL

3.5.1 Sample selection criteria

Cloud Hill fracture mineralization was sampled from exposures in the bottom of the deep quarry workings at Cloud Hill (-10 m aOD). The site is extensively fractured, and groundwater can be

seen to be locally discharging from these fractures. Within a particularly fractured and mineralised part of the site, where groundwater was seen to be freely flowing at the time of sampling (January 2001), calcite in fractures has developed finely crystalline dentate overgrowths. These correspond to calcite generation FC4, described below, which may relate to the modern groundwater system. In addition, similar late calcite fracture mineralization was also examined from a cored borehole (Ticknall BH1) drilled about 5 km to the northeast of Cloud Hill. The samples of this late calcite mineralization that were examined from south Derbyshire for the PADAMOT study are listed in Table 3-15.

Table 3-15. List of samples studied from the Cloud Hill area, south Derbyshire with analytical schedule.

Location	Sample ID	Top Depth (m bGL)	Bottom Depth (m bGL)	Fluid Inclusion Micro-thermometry	EPMA maps	EPMA point analyses	IPMA trace element data	IPMA stable isotope analysis	LAMP-ICP-MS trace element data	LACE-He stable isotope data
Cloud Hill	MPLG285			Y	Y	Y				
Ticknall BH1	MPLG522	17.2	17.26	Y	Y	Y				
Cloud Hill	MPLK174						1	1	1	1
TOTAL				*2*	*2*	*2*	*1*	*1*	*1*	*1*

The key features of this late-stage calcite that suggested it was potentially useful for examining the palaeohydrogeology of the groundwater system were:

- Its occurrence lining demonstrably porous or open fractures;
- Its association with present-day groundwaters discharge (Cloud Hill Quarry);
- It represents the latest mineralization.

A major issue with the late-stage calcite from this site is that it is largely developed as thin overgrowths on top of older calcite. This impacts on the application of mineral palaeohydrogeological indicators in several ways, which must be taken into account in interpretation of the observations:

- The morphology of the crystals is dominated by the morphology of the older substrate calcite crystals because there is often insufficient late calcite for it to display its own morphological characteristics.

- Because of the very fine grain size of the late calcite crystals and overgrowths it is often extremely difficult to uniquely sub-sample the latest generation of calcite for chemical or isotopic characterization, even when using microsampling techniques such as LAMP-ICP-MS or He-LACE.

- It is also very difficult to make observations on fluid inclusions within the late calcite because of its fine grain size and very limited presence of inclusions.

However, the preservation of the delicate calcite mineralization is very good because it has not suffered any damage due to drilling.

3.5.2 Fracture mineralogy and paragenesis

The fracture mineralization of the Cloud Hill site has been described in detail by Bouch et al. (2004), and a generalized paragenesis is summarised in Figure 3-66. The majority of the mineralization is considered to represent precipitation from diagenetic basinal brines derived from the adjacent mudstone-filled basin in the Widmerpool Gulf (Figure 2-11).

			TIME ——→
Early marine/meteoric Reducing (?)	MC1	Micrite neomorphism	
		Non-luminescent intercrystalline calcite	
		Luminescent intercrystalline calcite	
Dolomitisation	MD1	Nodular, luminescent dolomite (pedogenic?)	
	MD2	Rhombic, non-/patchily luminescent dolomite	
Fracturing		Fracturing	
		Generation of significant intercrystalline porosity (saccharoidal dolostone)	
		Internal Sediment	
Fracture-filling dolomite	FD1	Non-ferroan, dully-luminescent dolomite	
	FD2	Non-ferroan, brightly-luminescent dolomite	
	Oxidation		
	FD3	Ferroan, non-luminescent dolomite	
Mineralisation		Sulphides	
		Barite	
		Fluorite	
		Dolomite corrosion	??▬??
Saline Fluid Calcite	FC1	Weakly ferroan, brightly-luminescent calcite	
	FC2	Strongly ferroan, dully-luminescent calcite	
Fresh-water calcite	FC3	Brightly luminescent calcite, with high heavy metal concentrations	
	FC4	Non-luminescent calcite, with luminescent bands	

Figure 3-66. Summary paragenetic scheme for the mineralization in the Cloud Hill and Ticknall area, south Derbyshire (modified from Bouch et al. 2004)

Dolomitization of the host limestones largely predates fracturing, and two principal generations of matrix dolomite are recognised (MD1 and MD2). The earliest (MD1) is only locally developed, it is non-ferroan and non- or only dull-luminescent, and has an irregular nodular habit. It is interpreted as dolocrete associated with the development of palaeosols (Bouch et al., 2004). MD2 dolomite is also non-ferroan and comprises interlocking idiomorphic rhombs with weakly red-luminescent cores charged with inclusions and clear non-luminescent rims.

The earliest fractures are associated with dolomite mineralization. Three generations of fracture dolomite can be distinguished (FD1-FD3):

- FD1 – non-ferroan dolomite with dull luminescence. This replaces dolomite in the wallrock adjacent to fractures and forms overgrowths on corroded dolomite in saccharoidal dolostones;

- FD2 – bright orange luminescent manganoan, non-ferroan dolomite occurring as fracture fillings and forming thin overgrowths on dolomite lining mouldic pores (dissolution cavities) in the dolostone matrix away from fractures;

- FD3 – ferroan, non-luminescent dolomite forming coatings up to 1 mm thick on fracture surfaces. It also occurs as overgrowths on dolomite rhombs in saccharoidal dolostones, and lines vuggy and mouldic pores in the host dolostones. Dolomite FD3 typically displays slightly curved crystal faces ('saddle-rhomb' crystal morphology) – a common feature of ferroan dolomite and ankerite. FD3 is volumetrically the most significant dolomite fracture mineralization.

Oxidizing fluid conditions prevailed for a period between FD2 and FD3, as recorded by the localised formation of bands of iron oxides. These impart a red or orange colouration to some of the fracture lining dolomite. The possibility that these iron oxides represent oxidized sulphide minerals cannot be discounted entirely, however no clear evidence of sulphide mineralization was found before the later stages of FD3. The later stages of dolomite FD3 mineralization were accompanied by the precipitation of a minor amount of sulphide mineralization, including pyrite, chalcopyrite, sphalerite and galena.

158

Fluid inclusion data from the FD1-FD3 dolomite shows that all three generations of dolomite mineralization precipitated from saline (20-24 wt% NaCl eq.) $NaCl-CaCl_2-H_2O$ brines, with homogenization (T_h) temperatures providing minimum estimates for precipitation temperatures of 70-100 °C.

Following FD3, some dolomite dissolution occurred, evidenced by the corrosion of dolomite crystals and the formation of secondary Mn oxide that is engulfed by the subsequent calcite mineralization. Barite mineralization occurred in the period between FD3 and the succeeding calcite mineralization. Although not observed in Cloud Hill quarry, fluorite also accompanies the barite mineralization in the nearby Ticknall borehole (Bouch et al., 2004).

Dolomite mineralization is succeeded by calcite fracture mineralization. Four generations of calcite mineralization (FC1-FC4) are recognised:

- FC1 – weakly ferroan calcite with orange-yellow luminescence that highlights a complex pattern of irregular growth zoning. This calcite is the most volumetrically significant generation and occurs both as a fracture filling cement and as a replacement of earlier dolomite;

- FC2 – ferroan calcite (more ferroan than FC1) with dull-orange luminescence that displays concentric and sector zoning;

- FC3 – brightly luminescent calcite forming a discontinuous thin layer of overgrowths on FC2. This calcite is characterized by lower Fe and higher Mg than earlier calcite. In addition, this generation also contains micron-scale Cd- and/or Pb-rich growth zones with up to 0.7 wt% CdO or PbO.

- FC4 – non-ferroan, relatively Mg-rich calcite forming localised euhedral overgrowths on earlier calcites.

Thin bands of inclusions of pyrite and chalcopyrite are present locally along the crystal growth zone boundaries in FC1 and FC2 calcites.

Fluid inclusion data show that FC1 and FC2 calcite was deposited from warm (T_h = 70-100 °C) $NaCl-CaCl_2-H_2O$ dominated brines that were marginally lower salinity (18-22 wt% NaCl eq.) than those associated with the preceding dolomite mineralization (Bouch et al., 2004). The salinity and temperature, and association with base-metal ore minerals, are consistent with the mineralization from fluids expelled from compacting Lower Carboniferous mudstones and shales in the Widmerpool Gulf.

Bouch et al. (2004) originally included FC3 with the geologically older FC1-FC3 mineralization. However, this has been re-evaluated as a result of the PADAMOT investigations, and FC3 is now considered to represent an early stage of the alteration and mineralization associated with the modern groundwater system.

3.5.3 Distribution and morphological characteristics of late calcite mineralization

Late-stage (FC3 and FC4) calcite mineralization is the youngest mineralization observed at the Cloud Hill site. Characteristically this occurs as euhedral crystals lining open fractures and vuggy porosity in the adjacent wallrock. Present-day groundwater is observed to discharge from these open fractures and from zones of porous dolostone at the base of the Cloud Hill Quarry.

FC3 and FC4 calcite are primarily developed as overgrowths seeded on earlier FC1 and FC2 calcites. The morphology of the two earlier generations of calcite is characterized by euhedral, *c*-axis elongated (scalenohedral), crystals. This morphology is consistent with the growth of this calcite from a saline mineralizing fluid, as has been observed in studies on calcite crystal growth from experimental and natural diagenetic systems (Folk 1974; Lahann, 1978; Given & Wilkinson, 1985; Braithwaite & Heath, 1989; Gonzalez et al., 1992) and as seen in the deep groundwater system at Sellafield (cf. Section 3.3), and this is confirmed by the fluid inclusion

observations (Section 3.5.2 and Bouch et al., 2004).

Because the FC3 and FC4 calcites are generally developed only as thin, syntaxial overgrowths, the external morphology of the 'composite' FC1-FC4 calcite crystals is dominated by the volumetrically much greater FC1-FC2 calcite host substrate and assumes an overall *c*-axis elongate habit. However, the late calcite does form some very small isolated crystals that are scattered on dolomite host rock surfaces. These are relatively rare, however they exhibit a doubly-terminated, equant to *c*-axis flattened crystal morphology. This morphology is characteristic of low-temperature calcite grown from fresh water (cf. Folk 1974; Lahann, 1978; Given & Wilkinson, 1985; Braithwaite & Heath, 1989; Gonzalez et al., 1992), and is similar to that seen in late (ME9) calcites from the shallow freshwater aquifer system at Sellafield (cf. Section 3.3). More detailed CL petrographical observations show that the FC3 and FC4 overgrowths do not simply mimic the *c*-axis elongated growth pattern of the older calcite substrates. Rather, the two later calcite generations appear to show preferential deposition on calcite on faces parallel or sub-parallel to the *c*-axis that would eventually lead to the development of less-elongated crystal forms (Figure 3-67). An equant or short *c*-axis crystal morphology would be expected for calcite that precipitated from the present groundwater encountered at Cloud Hill Quarry.

3.5.4 Petrographical and growth zoning characteristics of the late calcite mineralization

CL petrography, BSEM-EDXA and EPMA microchemical X-ray mapping shows that FC3 and FC4 calcite are both very finely growth zoned with micron-scale concentric oscillatory growth zones (Figure 3-67).

FC3 is Mg-rich and Fe-poor relative to earlier calcite mineralization, and characteristically displays alternations of very brightly yellow-luminescent Mn-rich and dull-luminescent Mn-poor calcite. Some brightly-luminescent growth zones are also Cd- and Pb-rich, with up to 0.7 wt% CdO or PbO, respectively. There is also some evidence for minor corrosion or dissolution of the older calcite substrate immediately beneath FC3.

FC4 is Mg-rich, Mn-poor and non-ferroan, and dominantly non-luminescent, with very fine brightly luminescent bands. It very closely resembles the shallow 'fresh water-type' calcite that is characteristic of late-stage (ME9) calcite from above the 'morphological transition zone' (MTZ) in the freshwater zone at Sellafield. FC4 locally engulfs patches of copper oxide (after chalcopyrite) and iron oxyhydroxide (after pyrite) indicating that sulphide alteration had at least been initiated prior to the onset of FC4 mineralization.

FC3 and FC4 calcite generations may both be late and related to relatively recent supergene fresh groundwater processes. FC3 may represent calcite formed during the early stages of fresh groundwater invasion. The Mg content of the late calcites is most probably derived from dissolution of the dolomite host rock and older dolomite-ankerite mineralization. Invasion by oxidizing groundwaters would result in the oxidation of the sulphide minerals (galena, chalcopyrite, pyrite, sphalerite) present as minor phases in the conductive fractures. The high Cd and Pb content of this calcite can be explained by the release of these metals to the groundwater from sulphide oxidation, and their incorporation by co-precipitation with calcite during the early stages of oxidative groundwater alteration. As the very limited primary sulphide source of base metals was depleted, the later (FC4) generation of calcite precipitating from the groundwater would not have been enriched in Cd and Pb. This would be consistent with the observation that FC4 calcite engulfs earlier-formed copper oxide and iron oxyhydroxide alteration products of sulphides. The minor corrosion of older calcite mineralization that is evident beneath the FC3 and FC4 layers, may reflect dissolution in response to an initial lowering of pH (sulphuric acid formation) during sulphide oxidation.
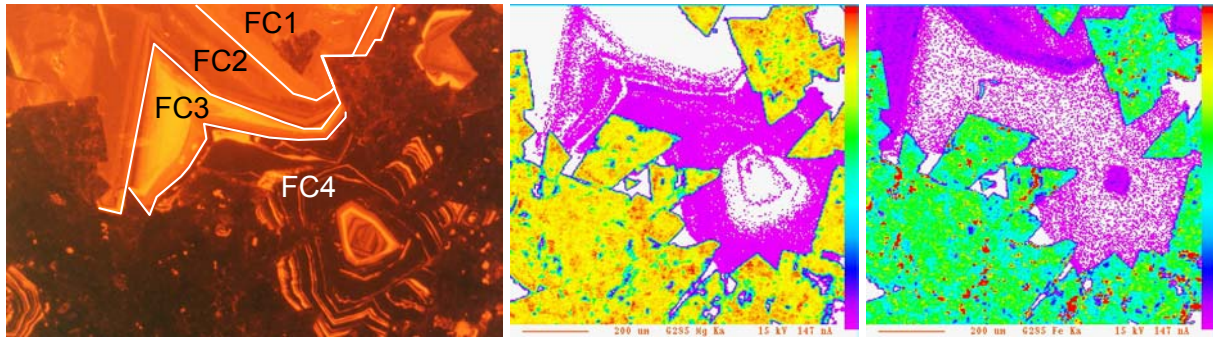
Figure 3-67. Chemical variations in fracture-related calcites from Cloud Hill. (a) CL photomicrograph of variably luminescent calcite filling intercrystalline porosity in a saccharoidal dolostone (dolomite is non-luminescent) with calcite of generations FC1 to FC4 labelled (field of view 1.35 mm). (b) and (c) EPMA microchemical maps of part of the area shown in (a), showing variations in Mg and Fe contents respectively. FC1 and FC2 are characterised by moderate Fe-, moderate Mn- and low Mg contents. In contrast FC3 and FC4 are relatively Mg-rich, Fe-poor, and Mn-poor, with thin Mn-rich, and Pb-rich zones (sample MPLG285; Milldale Limestone; Cloud Hill Quarry).

Calculations using the PHREEQC code (with the WATEQ4F.DAT database) (Parkhurst and Appelo, 2001) show the present groundwaters at Cloud Hill are supersaturated with respect to calcite and dolomite (Table 3-16). Therefore, it is realistic to expect that calcite could be precipitating in the groundwater system at the present-day. There is no evidence for late neoformed dolomite mineralization. However, this might not be expected since kinetic factors inhibit the formation of dolomite at low temperatures and CO_2 pressures, and that most natural waters then lie in the stability field of calcite (Langmuir, 1997).

Table 3-16. Saturation index for carbonate minerals in Cloud Hill groundwaters (calculated using PHREEQC Interactive code (version 2.10) with the WATEQ4F.DAT database, Parkhurst and Appelo, 2001)

Groundwater Sample	Calcite saturation index	Dolomite saturation index
CH1	0.92	1.6
CH2	0.95	1.6
CH3	0.92	1.7

3.5.5 Trace element characteristics of the late calcite mineralization

An attempt was made to characterize the REE chemistry of the late-stage calcite from Cloud Hill using LAMP-ICP-MS at the BGS. In general, it was found that the size of LAMP-ICP-MS laser ablation pits (50-80 μm diameter), coupled with the limitations of the optical targeting of the laser, was too coarse to specifically sample individual growth zones in the calcite, particularly in the case of the very thin bright luminescent zones in FC4 calcite. Consequently, the data obtained may represent an 'average' of two or more zones, and it is therefore difficult to correlate the fine detail of the growth zoning patterns observed under CL with variations in REE geochemistry.

Chondrite-normalised REE distribution patterns for the calcite analyses are illustrated in Figure 3-68. Analyses 1-8 and 9-16 (Figure 3-68) represent traverses taken progressively from the overgrowth rim into the core of two crystals of calcite. Overall, the late calcite displays two types of REE distribution pattern that clearly differentiate between the old (FC1/FC2) and young (FC3/FC4) calcites:

161

- Calcite displaying an inclined distribution pattern with a markedly enhanced concentration of LREEs relative to HREEs (Figure 3-68 - analyses 6-8 and 13-16). These analyses correspond to the old hydrothermal calcites FC1 and FC2;

- Calcite with a marked depletion in LREEs, and relatively 'flat' distribution of MREEs and HREEs (Figure 3-68 – analyses 1-5 and 9-12). These analyses correspond to the late-stage calcites FC3 and FC4

The LREE enriched distribution patterns for FC1/FC2 are similar to those observed in typical siliciclastic sedimentary rocks (McLennan, 1989; Fleet, 1984). This suggests that the REE signature of the early mineralization may be inherited from the deeply-buried Carboniferous shales and mudstones in Widmerpool Basin, which would have been the source rocks of the mineralizing fluid. Marine limestones often show a marked Ce depletion, reflecting the depletion of Ce in seawater (McLennan, 1989). However, this is not always the case (e.g. the Carboniferous Limestone at Sellafield (Kemp & Strong, 1997; Strong & Kemp, 1997)), and derivation of the REE signature of FC1/FC2 through interaction with the host limestones and dolostones cannot be ruled out.

The LREEs depleted signature of FC3/FC4 mineralization might reflect weathering processes. The limestones and dolostones will be weathered in the near-surface by rain water percolating through the soil zone, which will have a relatively low pH as a result of the uptake of CO_2 and the dissolution of organic acids, and through the oxidation of sulphide minerals. This acidic groundwater will leach REEs from the host rock in the weathering zone. Because MREEs and HREEs preferentially form more stable (more soluble) complexes (relative to the LREEs) with carbonate and organic ligands, they will be more readily transported in groundwater percolating through the weathering zone (Girin et al., 1970; Humphris, 1984; Fleet, 1984). As the groundwater percolates deeper through the fracture system the pH of the groundwater will rise as it becomes buffered by reaction with carbonate minerals, and the relatively soluble REEs will be adsorbed or co-precipitated in secondary minerals such as calcite. This calcite would be depleted in LREE, particularly where relatively high water-rock ratios prevail as might be expected within a fracture flow system. The REE distribution in FC3/FC4 calcite could be explained by this process. This pattern is also observed in the brightly luminescent bands in shallow 'above-STZ' (freshwater)-type late (ME9) calcite at Sellafield.

Despite the similarity in the CL characteristics between the non-ferroan/non-manganoan late calcites found in Cloud Hill and the ME9 calcite in the shallow freshwater zone at the Sellafield site, there is no evidence in the Cloud Hill calcite of the marked depletion in Ce (negative Ce anomaly) that is observed in the non-luminescent zones of the shallow Sellafield ME9 calcite mineralization (Section 3.3.6). This may indicate that although oxidizing with respect to the Fe(II)/Fe(III) and Mn(II)/Mn(IV) redox couples, the palaeogroundwaters at Cloud Hill were less oxidizing with respect to the Ce(III)/Ce(IV) couple than in shallow Sellafield groundwater system. The redox of the groundwater at Cloud Hill may be buffered to some extent by the oxidation of sulphide minerals, which are present as a minor component within the fracture flow system. In contrast, sulphides are essentially absent (except for very rare examples – cf. Milodowski et al., 2002) in the freshwater Permo-Triassic aquifer at Sellafield). This may help explain the differences in the redox signatures recorded by the REE patterns of the otherwise very similar calcites from the two sites.

An attempt was made to use the ion microprobe to obtain trace element data from the Cloud Hill site. However, the polished section that was prepared for this purpose proved to be too thin and ion microprobe data could not be obtained successfully.
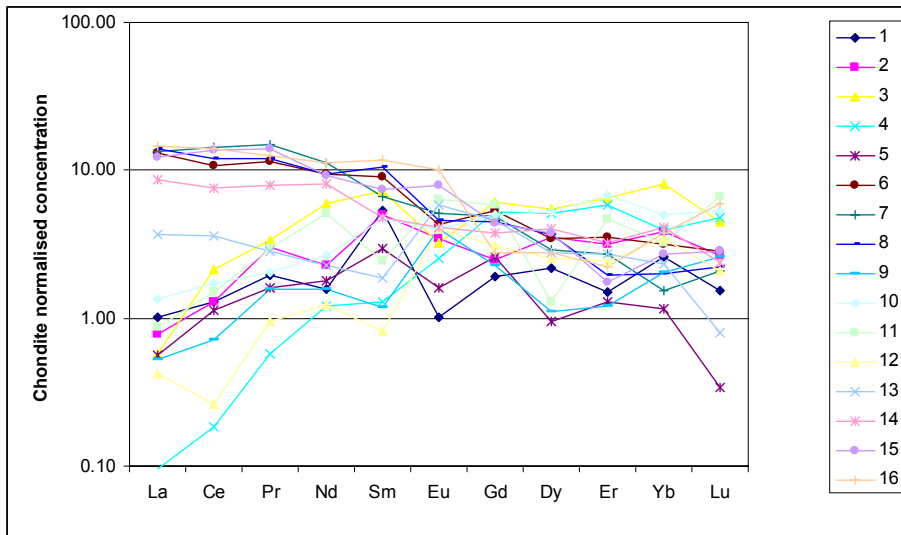
Figure 3-68. Chondrite-normalised REE distribution patterns (determined by LAMP-ICP-MS) for late calcite from Cloud Hill.

3.5.6 Fluid inclusion studies

Samples from Cloud Hill quarry and the Ticknall Borehole were analysed by conventional microthermometric techniques at the BGS. Details of the analyses undertaken are given in Table 3-15, and the fluid inclusion results are provided in Appendix 9.

Attempts were made to acquire fluid inclusion data from the latest generations of calcite only, however, because CL analysis has to be conducted after fluid inclusion microthermometric analysis, the microthermometry was effectively conducted "blind". Retrospective CL analysis of the analysed portions of the samples, revealed that all the analysed inclusions occur within calcite of generation FC1. The analysed inclusions were either monophase or two-phase. The two-phase inclusions had relatively low homogenisation temperatures (T_h range 67-93 °C). Data on temperatures of first melting (T_{fm}) indicates low eutectics (c. -60 to -50 °C) consistent with mixed $NaCl$-$CaCl_2$-brines. Salinities are relatively high with total salinities typically in the range 19-23 °C. These fluids are similar in character to those described by Bouch et al. (2004) for the main geologically-old basinal fluid-related mineralization in the area, and are clearly unrelated to the modern groundwater system.

A characteristic feature of the late calcites is that they are water-clear, reflecting the very low abundance of inclusions in the calcite. Any inclusions that were present were too small to make realistic observations on and no workable inclusions for analysis could be located within the later calcite generations (FC3 and FC4).

3.5.7 Stable isotope ($\delta^{18}O$ and $\delta^{13}C$) characteristics of late calcite mineralization

Only 2 stable isotope analyses were obtained from one sample (MPLK174) of the late (FC3 and FC4) calcite from Cloud Hill using He-LACE microsampling at the BGS. As in the case of LAMP-ICP-MS, the size of the laser ablation pits (c. 80-100 μm diameter), coupled with the limited resolution of the optical laser targeting system, was too coarse to sub-sample individual growth zones. Subsequent petrographical observations showed that the He-LACE isotope data represent bulk values for the late calcite generations. The isotopic composition was found to be $\delta^{13}C_{PDB}$ = -0.85 ‰ and $\delta^{18}O_{PDB}$ = -2.96 ‰, and $\delta^{13}C_{PDB}$ = -7.49 ‰ and $\delta^{18}O_{PDB}$ = -8.15 ‰, for FC3 and FC4, respectively. The isotopic composition of the late calcite appears to be markedly heavier with respect to $\delta^{18}O$ than the older FC1 and FC2 hydrothermal calcite ($\delta^{13}C_{PDB}$ = -3.9 to -6.9 ‰, $\delta^{18}O_{PDB}$ = -12.8 to -16.2 ‰).

163

Further oxygen isotope data were obtained from the same sample using the ion microprobe at the University of Edinburgh. The ion microprobe was able to sample the FC3/FC4 (undifferentiated) calcite with much finer spatial resolution (20 μm diameter), and the isotopic composition was found to vary from -8.5 to -3.2 ‰ $\delta^{18}O_{PDB}$. These data are consistent with the coarser He-LACE results, which fall within this range. The ion microprobe data are included in Figure 3-65 for comparison with late calcites from Dounreay.

The present groundwater (Table 2-3) discharges from the late-calcite-mineralized fractures at about 10 °C, and has a mean composition of -7.86 ‰ $\delta^{18}O_{SMOW}$. Calcite in equilibrium with this groundwater should have a theoretical composition of -6.5 ‰ $\delta^{18}O_{PDB}$ (calculated using Hays and Grossman's (1991) 'fit' of O'Neil et al.'s (1969) experimental data). This lies in the middle of the compositional range determined by ion microprobe, and it is therefore conceivable that part of the late calcite at Cloud Hill could have precipitated from groundwater similar to that of the present-day. As at Sellafield and Dounreay (cf. Sections 3.3 and 3.4) the more depleted $\delta^{18}O$ values might be explained by calcite precipitation from groundwater containing a significant component of glacial melt water (c. 30% volume glacial influx, mixing back to present-day meteoric values). The least depleted $\delta^{18}O$ values in the range (-3.0 to -4.0 ‰) could be modelled by precipitation under conditions that were colder than at the present-day, and/or from water that was isotopically slightly heavier. The geographical location of Cloud Hill in the centre of England makes it unlikely that there is any influence from late marine incursion (in contrast to Äspö/Laxemar [Section 3.2], or potentially at Sellafield or Dounreay [Sections 3.3 and 3.4]). However, evaporation can also produce groundwaters with heavier $\delta^{18}O$ (e.g. Salomons et al., 1978; Bath et al., 1987). There is evidence from the British Quaternary record that arid conditions existed in northern and southern England, with the development of calcreted soil profiles under periglacial climate states during both the Late Devensian and Anglian stages (Strong et al., 1992; Candy, 2002; BGS CASQUE Project unpublished data). Shallow groundwaters could have become enriched in [18]O as a result of this evaporation process.

3.5.8 Biomarker studies

A single sample (MPLK174) of late calcite from Cloud Hill was analysed by GC-MS by the Universidad Politecnica de Madrid for the presence of organic biomarker compounds. No evidence of biomarkers was detected.

3.5.9 Conclusions

3.5.9.1 GENERAL CONCLUSIONS ON ANALYTICAL METHODOLOGY

3.5.9.1.1 Calcite morphology

Only a few samples were analysed and depth variation in late-stage (FC3/FC4) calcite could not be studied at this site. However, the short *c*-axis/equant morphology of the late calcite found in the fractures that conduct dilute (fresh) groundwater at the present-day at this site, is consistent with late-stage (ME9) calcite morphologies observed in the freshwater zone at Sellafield. This lends further support to the generic applicability of calcite crystal morphology as a palaeohydrogeological indicator.

3.5.9.1.2 Trace element chemistry of fracture fillings

LAMP-ICP-MS did not have the resolution to be confident about analysing individual growth zones in late-stage calcite, so REE variations cannot be attributed to specific zones. However distinct REE distribution patterns differentiate older hydrothermal (FC1/FC2) and younger 'meteoric' (FC3/FC4) calcites. The latter are characterised especially by depleted LREEs which

is thought to be related to weathering processes. There is no negative Ce anomaly in these calcites despite the apparent oxidising character of the present-day groundwater.

3.5.9.1.3 Biomarker studies

No evidence was found for the presence of biomarkers within the late calcite at Cloud Hill. However, it should be noted that only one sample of mineralization was examined. Furthermore, the late calcite (FC3/FC4) was largely present as thin overgrowths on cores of older (FC1/FC2) calcite. The volumetrically more significant old calcite would have significantly diluted any biomarkers that may have been present in the late calcite.

3.6 MELECHOV MASSIF

3.6.1 Sample selection criteria

The petrological, mineralogical and geochemical characterization of the Melechov Massif fracture mineralization is based entirely on observations of samples from borehole PDM-1. The borehole was situated at the southeastern foot of the Melechov Hill, and is described in Section 2.4. The drill core from borehole PDM-1 contained very few open fractures, and minerals unambiguously precipitated from recent groundwater flow were also missing. Therefore, the investigations at the Melechov site have focussed on a detailed geochemical and mineralogical study of fractures dominated by clay minerals and Fe-Mn oxyhydroxides. Some of these fracture fillings reach up to 5 mm in thickness. These fractures are widely present throughout the whole sequence penetrated by the borehole. Even though there is no evidence about the absolute age of these fillings, no other possibly younger fillings were encountered in the site. Because these fractures contain late-stage or low-temperature mineral assemblages, they were studied in the hope that they might provide information on the most recent rock-water interaction processes. Magmatic dykes and hydrothermal veins were excluded from this study.

In contrast to the other PADAMOT study sites at Los Ratones in Spain (Section 3.1), Äspö and Laxemar in Sweden (Section 3.2), and Sellafield, Dounreay and Cloud Hill in the United Kingdom (Section 3.3), no carbonate mineralization was identified at this locality, neither in the fractures (as groundwater precipitates), nor in the host-rocks (older hydrothermal alterations).

Partly open fractures were found rarely but most of these were also filled with clay minerals and Fe-Mn oxyhydroxides. Some of these open fractures were lined by relatively coarse quartz crystals several millimetres in size, which are most probably of late hydrothermal origin.

Correlation of the studied mineral fillings with groundwater flow is suggested on indirect evidence only:

- Firstly, these low-temperature oxidative mineral assemblages are most likely to owe their origin to chemical/physical weathering;

- Secondly, a relationship with groundwater movement can partly be inferred from the correlation of some trace element data with the present groundwater flows (indicated by hydrogeological well logging).

3.6.2 Host rock mineralogy

The host granite encountered in the PDM-1 drill core consists of the two-mica Lipnice Granite. Primary magmatic minerals are relatively fresh and not affected by deuteric alteration or weathering processes. The modal composition of various granitic rocks from the Melechov Massif, as given in the literature, is summarised in Table 1 in Appendix 10. Estimated modal composition of the PDM-1 granite samples is given in Table 2 in Appendix 10.

K-feldspar is fresh, with a significant Na component ($Or_{90}Ab_{10}$). Magmatic growth zoning is

manifested by variations in Ba content.

Plagioclase is less abundant than K-feldspar. Usually it represents the most altered mineral present, and is intensively altered to a cloudy mixture of micron-sized white-mica products (sericite). Magmatic growth zoning is also present, but less frequent than is observed in K-feldspar. Composition of the plagioclase grains varied between An_{10} to An_{16}. Less frequently, thin rims or small grains of almost pure albite (An_{1-2}) were present. The plagioclase usually contains less than 1 mol. % orthoclase component (Or_1) in solid-solution.

Biotite is present in all samples, but is generally less abundant than muscovite. Locally biotite is partly altered to a chlorite. Microprobe analyses did not yield fully stoichiometric formulae (with respect to K). The $Fe^{II}_{tot}/(Fe^{II}_{tot} + Mg)$ ratio of the biotite varies from 0.45 to 0.63. The analysed biotites approximate to a binary mixture of phlogopite and annite (in a ratio of approximately 1:1).

Muscovite is abundant and unaltered. There are probably two generations present: an older one (Mu-I) comprising large flakes, isolated or intergrown with biotite; and a younger one (Mu-II): consisting of fine grained (up to 10 μm) mica, which together with apatite-II and quartz-II rims the coarse-grained granite matrix. No significant differences in the chemistry between the Mu-I and Mu-II muscovite generations were found.

Radial aggregates of muscovite resembling Mu-II were also found as the overgrowths on the walls of a thin fracture, and are of hydrothermal origin. The fracture was filled mostly with rounded quartz grains (of variable size) and with an ultrafine granite-mylonite matrix. Using the muscovite composition geothermometer (Cathelineau, 1988), this late hydrothermal muscovite formed at about 250 °C.

Chlorite is a minor to accessory component. Only chlorite that replaces biotite was identified in the rock. No hydrothermal chlorite is associated with the brittle fractures, or with the brittle-ductile deformation zones in the granite. The chlorite is a tri-octahedral chlorite of the clinochlore–chamosite series, with a $Fe^{II}_{tot}/(Fe^{II}_{tot} + Mg)$ ratio ranging from 0.68 to 0.72. Its chemistry indicates formation temperatures from 200 to 280 °C.

Apatite is a frequent accessory mineral. It is probably present in two or three generations: (1) early magmatic apatite (up to 0.5 mm large euhedral grains, locally zoned); (2) late magmatic apatite (up to 0.5 mm large anhedral grains, that fills "triple" junctions between the grains of quartz, feldspars and micas); and (3) post-magmatic apatite (fine grained, up to 10 μm; associated with ductile to brittle-ductile deformation zones, where it occurs with quartz and muscovite-II).

Monazite and zircon are present in the granite as accessory minerals.

3.6.3 Classification of fracture types

Fractures filled with low-temperature minerals at the PDM-1 site can be classified under three categories according to the nature of their mineral fillings and their morphological characteristics:

1. Dominated by clay minerals;

2. Dominated by clay minerals, but with significant admixtures of Fe and Mn oxyhydroxides;

3. Open fractures lined by coarse quartz crystals (several millimetres in size), and filled by later clay minerals and iron oxyhydroxides.

Most of the fracture fillings are powdery and microcrystalline. Compact, sheared clay-rich fillings with tectonic slickensides were observed in the lower part of the borehole. Rarely, more complex fillings consisting of a 'triple-layer' of clay-rich material were found. These comprise a core-layer (youngest) of powdery clay, enclosed within two layers of compact and sheared clays

166

(older). The younger filling was identified by FTIR as a mixture of montmorillonite and chlorite (montmorillonite > chlorite); and the older compacted clay was identified as a mixture of nontronite and chlorite (nontronite > chlorite).

Two subtypes of iron oxyhydroxide-rich fillings can also be macroscopically distinguished:

- Fractures, several millimetres wide, filled with a powdery clay-FeO.OH mixture;

- Fracture fillings up to 1 mm thick comprising close-packed fractures with FeO.OH phases only.

The first subtype of iron oxyhydroxide mineralization is not associated with any wallrock alteration (colouring). However, the later sub-type is commonly associated with brownish envelopes of wallrock alteration, up to 3 cm thick, caused by the intimate impregnation of the rock by fine-grained FeO.OH. The first subtype of iron oxyhydroxide mineralization is most probably of low-temperature origin. However, the origin of the second subtype is uncertain, and a hydrothermal alteration origin cannot be excluded.

In addition to the fractures described above, thin mylonitic zones in the granite were also recognized. These have narrow muscovitic (monominerallic) zones that line the host-rock-contacts. These zones of muscovite mineralization have a late hydrothermal-tectonic origin. Chlorite and muscovite composition geothermometry indicates mineralization temperatures of about 300 to 200 °C.

3.6.4   Fracture mineralogy

About 16 to 18 mineral phases were identified in the fractures from borehole PDM-1 (Table 3-17). They most probably represent products either of mechanical weathering/disintegration, or of chemical weathering of the host-granite. The later group includes both in-situ neoformed weathering products as well as neoformed phases that precipitated after some (short?) transport in groundwater. Minerals of supposed late hydrothermal origin are rare.

Table 3-17. List of minerals identified in the latest fillings of the fractures from borehole PDM-1. Minerals were identified by XRD or by FTIR (italics).

Origin	Mineral assemblage
Mechanical weathering related phases (detrital phases)	Quartz, plagioclase, K-feldspar and fluorapatite
Chemical weathering related phases (neoformed phases)	Smectite, kaolinite, goethite and Mn-oxides (cryptomelane, todorokite, pyrochroite?) *montmorillonite, nontronite, quartz, chlorite*
Phases of ambiguous origin	Relatively frequent dioctahedral micas in the XRD pattern may represent either detrital muscovite, or neoformed illite. These two minerals could not be differentiated by XRD.
Late hydrothermal phases • Crystals in open fractures: • Mylonitic zones:	 Quartz Quartz, trioctahedral chlorite, apatite-II, muscovite-II

The presence of smectites was confirmed by glycolation of XRD samples and by FTIR analyses that also enabled identification of individual smectites: montmorillonite (frequent, younger) and nontronite (sparse, older). Neither the microscopic techniques (binocular, optical microscope, cold-stage CL, BSEM), nor the analytical techniques (XRD, FTIR) could detect the presence of any carbonate minerals.

3.6.5   Relative mineral abundances in different types of fracture fillings

Initially, attempts were made to use XRD analyses to estimate the mineral abundances in fracture

fillings but this proved impossible because the diffraction intensities of the different minerals could not be calibrated. Consequently, attempts were made to calculate normative mineral proportions from the trace and major element chemistry data. These were then corrected to provide volumetric proportions by taking account of the specific densities for the 'ideal' mineral.

Two estimates of mineral abundance were made:

- On the basis of total Fe and Mn contents, neglecting other phases (assuming average density of other phases to be 2.68 g/cm^3);

- By progressive recalculation by (i) assigning all Mg to be present as chlorite, with Fe/Mg chlorite ratio equal to one; (ii) assigning most of the K to illite; (iii) assigning all Ca and Na to montmorillonite (having the same Na/Ca ratio as plagioclases of the granite); (iv) assigning the remaining Fe to goethite; (v) assigning all Mn into Mn-oxides; and (vi) assigning all Zr into zircon.

Some fracture fillings yielded sums of the major oxides approaching 100 wt. % in a simple one-step procedure. However, in other cases, it was necessary to modify the calculations by attributing part of the content of K, Na, and Ca to primary magmatic phases (feldspars, muscovite).

The calculated mineral abundances are summarised in Figure 3-69. The estimation of Fe- and Mn-oxyhydroxide abundances can be considered to be relatively precise (± 5 %). The abundances of illite and montmorillonite are, however, less precise (±10-15 %) and should be regarded more cautiously. Figure 3-69 shows that iron and manganese oxyhydroxides and montmorillonite fracture fillings tend to be more abundant towards the surface, while chlorite and illite more or less gradually increase downwards. This would be consistent with a weathering related origin for these fracture minerals.
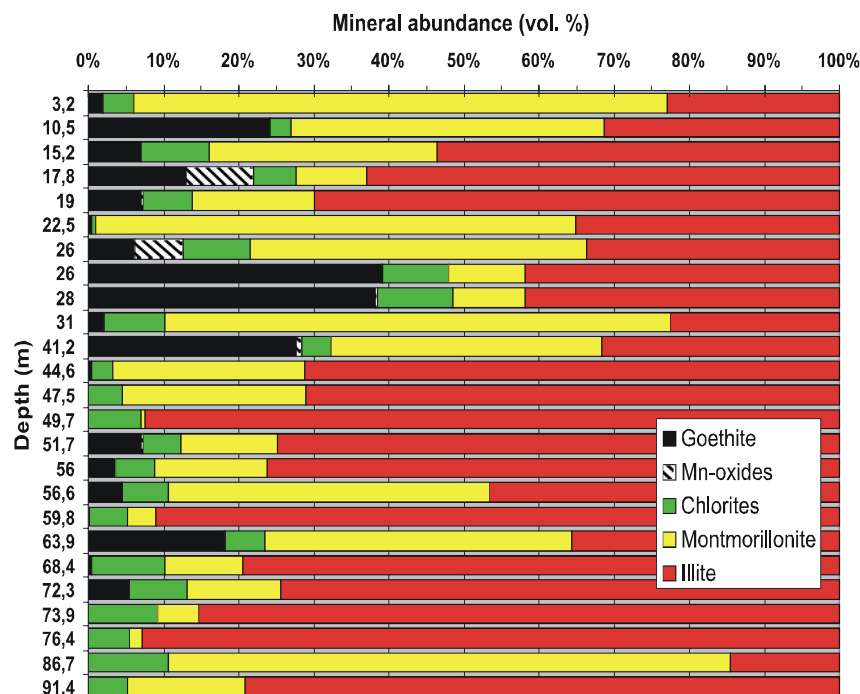
Figure 3-69. Volume fractions of major minerals found in late-stage fracture-fillings from borehole PDM-1.

3.6.6 Geochemistry of fracture fillings

A total of 40 minor and trace elements (Tables 4-5 in Appendix 2) were analysed from 25 samples of fracture fillings, 5 samples of fresh granite, and 1 sample of paragneiss. Five high-

purity mineral separates (4 apatites, 1 montmorillonite) were analysed for U, Th, Pb concentration and for lead isotopes measurements. Major oxides were determined by wet chemical analysis, but only the rock-samples were analysed since the quantity of fracture fill material was too low for the standard wet chemical analyses techniques employed.

3.6.6.1 MAJOR AND MINOR ELEMENTS

The highest elemental contents were found for Fe (29.5 wt. %), and occasionally also Mn (5.9 wt. %) and K (5.3 wt. %). Other metals Na, Ca, Mg are present in amounts less than 1.9 wt. % each.

3.6.6.2 TRACE ELEMENTS

Analytical results are summarised in Appendix 10. Variations in trace element chemistry relative to the average PDM-1 granite (i.e. element enrichment/element depletion factors) are more informative of alteration behaviour than the absolute elemental concentrations. Specific trace element data were found to provide useful indicators of:

- Weathering of a hydrothermal mineralization (Zn, Cu);

- Chemical weathering of alkali feldspars (Li, Ba, Rb) and muscovite (Li, Rb);

- The presence of residual resistate ('detrital') phases – zircon (Zr), monazite (La, Ce, Nd, Sm).

3.6.6.3 CORRELATION BETWEEN THE DEPTH AND ELEMENT ENRICHMENT FACTORS

The elemental enrichment and depletion effects are mostly strongly observed towards the surface (Table 3-18, and Figures. 1-2 in Appendix 10). However, individual data are usually broadly scattered and there is often a poor correlation in this relationship. Elements such as Mg, Mn, Fe, REE, Zr, Y, U, Th, Pb, V, Ni, Co, Cu, Sr, and Be and to a lesser extent, Ca, Hf, and Rb are generally enriched towards the surface. Sr and K (and possibly Rb and Tl) tend to exhibit the opposite trend (i.e. downward enrichment). Of all the data, the Sr shows the best correlation of the relative enrichment factor with depth (Figure 3-70).

Table 3-18. Summary of element mobility with respect to the parent granite

General trend	Element
Mostly depleted	K, Na, Ta, Nb, Ba, Cr, Li
Both moderately depleted and enriched	Ca, Hf, Rb, Tl
Mostly enriched (upward enrichment)	Mg, Mn, Fe, REE, Zr, Y, U, Th, Pb, V, Ni, Co, Cu, Sr, Be
Negative correlation with depth (downward enrichment)	Sr, Rb, Tl
Specific depth of extreme enrichment (m)	**Element**
17.8 and 26.0 m	Li, Ba, Ni, Co, V, Mn
19.0 and 68.4 m (73.9m)	Fe, REE, Zr, Y, U, Th, Pb, V, Ni, Co, Cu, Sr, Be
44.6 m	Nb, Ta, Be, Mn
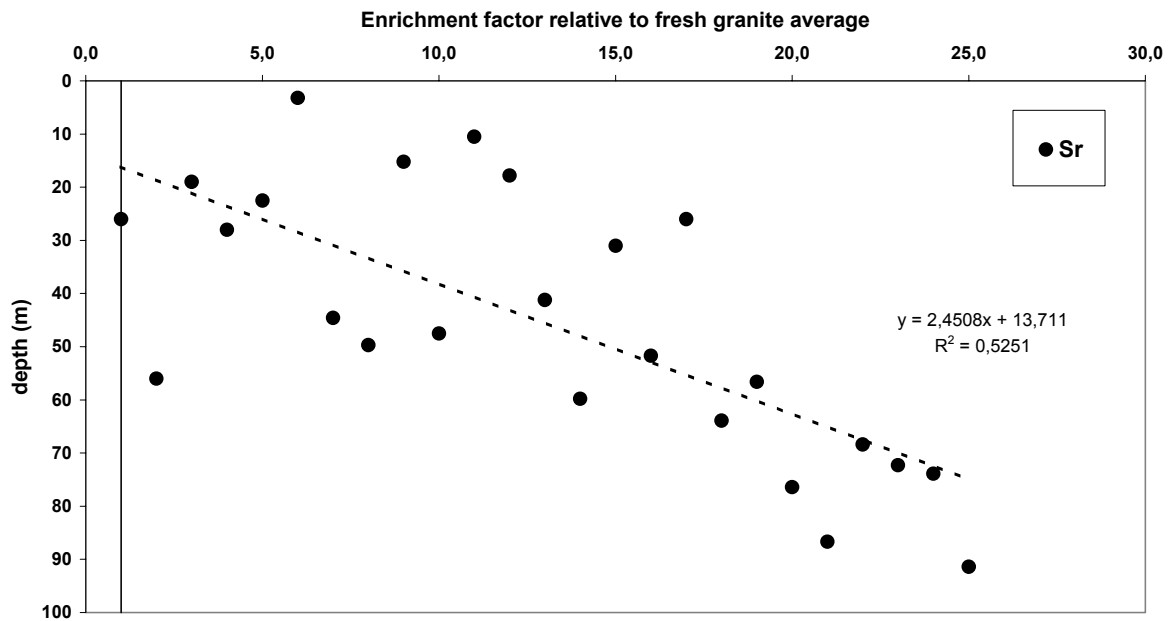
Figure 3-70. Correlation between the strontium enrichment in fracture fillings and sample depth. The variation is roughly linear, and strontium is likely adsorbed on clay minerals.
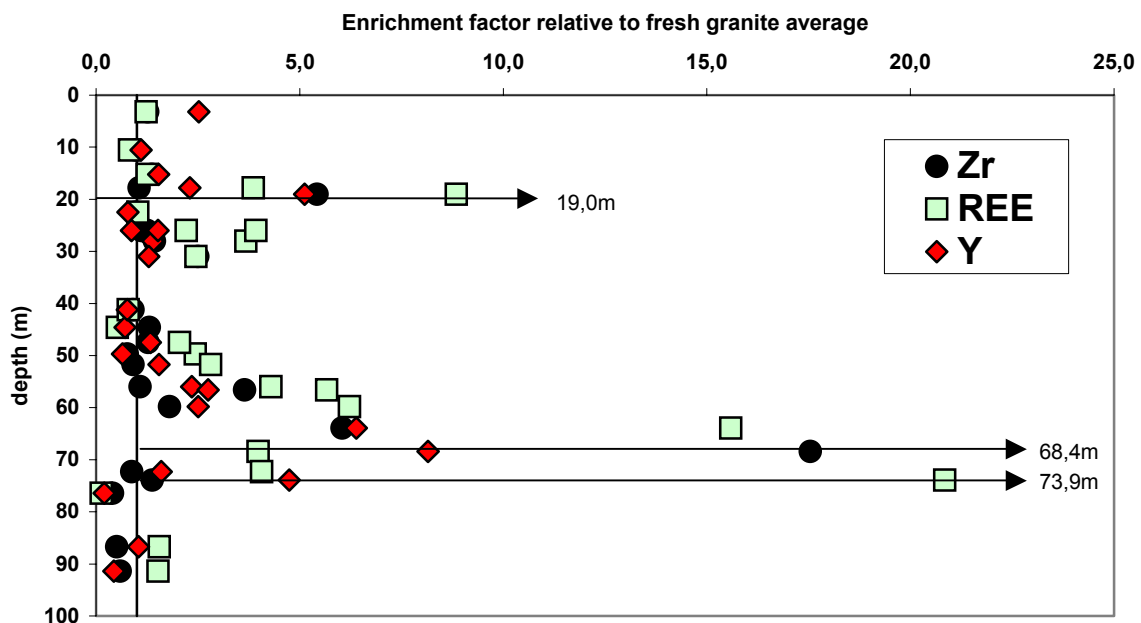
Figure 3-71. Relative enrichment in fracture fillings of trace elements characteristic of resistate ('detrital') magmatic-accessory minerals. High enrichment of Zr, REE and Y is inferred to result from concentration of fine grained heavy minerals that are gravitationally sorted during transport in groundwater flow at the indicated depths.

In addition to a general trend, some of the studied elements displayed high enrichment at specific depths (Figure 3-71). The observed enrichment of Zr, REE and Y, which are typically associated with resistate (or 'refractory') heavy accessory minerals in the granite (zircon, monazite, apatite and xenotime), is interpreted to reflect concentration of these accessory

170

magmatic minerals as they are liberated during the weathering of the parent granite. They are considered to be gravity-concentrated as a 'detrital phase' by the groundwater flow, and to a limited extent they may also represent in-situ enrichment in residual weathering-resistate phases (i.e. significant transport by groundwater is missing).

Present-day measured groundwater outflows inside the PDM-1 borehole were recorded at the following depths: 17.7-18.2m; 34.6-37.0m; 50.5-51.0m; 69.0-69.5m; 73.5-74.5m; and 94.5-96.5m.

3.6.7 Lead isotope studies

Lead isotopes (^{208}Pb, ^{207}Pb, ^{206}Pb, ^{204}Pb) were measured on fresh rocks and fracture fillings. All the analysed samples have lead isotope ratios higher than present-day crustal lead. They also differ from the composition of anthropogenic lead contamination (i.e. lead in gasoline).

The fresh granite displays only a small variation of the Pb-isotope data. However, a small gradual change in the Pb-isotope ratios can be observed with respect to the depth (Figure 3-72).

The fracture-fillings display a much larger scatter of data than that of the fresh granite. Most of the fracture fillings form a quasi-linear trend on lead-isotope cross ratio plots (Figure 3-73 and Figure 3-74, and Figures 6 and 7 in Appendix 10). Only a few fracture fills deviate slightly from this trend. Two of these are enriched in ^{208}Pb (^{208}Pb /^{204}Pb), while the other two are slightly depleted in the ^{207}Pb (^{207}Pb/^{204}Pb).
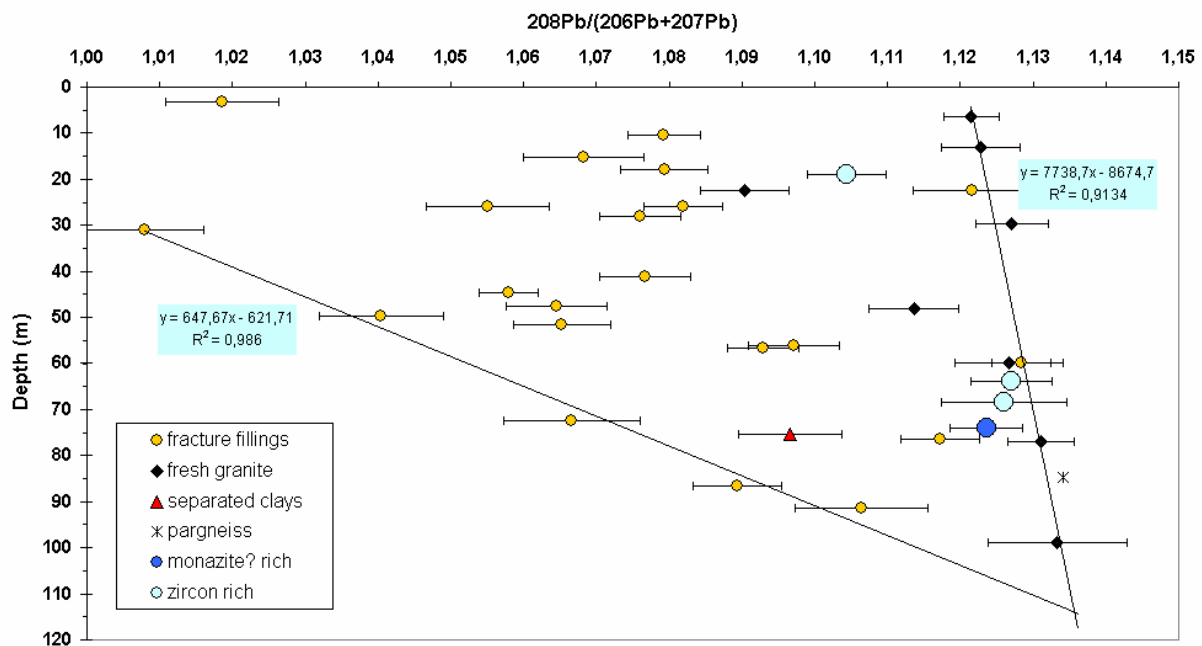
Figure 3-72. The ^{208}Pb/(^{207}Pb+^{206}Pb) ratio variations with depth. Analytical uncertainty at 1 sigma level is indicated by error bars.

In contrast to the quasi-linear mutual correlation of most of the lead isotope ratios, there are generally no obvious correlations between the trace and minor element chemistry, and the lead isotope ratios. However, the most Pb-, U-, Zr-, REE-rich samples are usually less evolved with respect to their Pb-isotope ratios. This clearly indicates that zircon, monazite, apatite or other REE-bearing phases do not represent major sources of the observed lead isotope quasi-linear variations.

Primary or secondary minerals may either retain their original isotope characteristics, or they may be enriched in radiogenic lead as a result of the high- or low-temperature alteration of U/Th-bearing minerals.

The absence of any obvious correlation between the trace element chemistry (in particular, Zr, Th, U, Pb, REE, Sr, P_2O_5; Figure 3-74), and the lead isotope composition suggests that the observed lead isotope trends do not result from a simple residual (or 'detrital') enrichment of the fracture filling assemblages in resistate U-/Th-rich accessory minerals, and it is proposed that the pattern probably also includes enrichment in radiogenic lead (especially uranogenic lead) transported by groundwaters.

Table 3-19 summarises theoretical minimum and maximum "contamination" by external, mostly uranogenic, lead sources that would be able to produce similar trends by mixing with the fresh PDM-1 granite (Figure 3-73). In this model calculation reference apatite concentrates from the Melechov Massif have been used in conjunction with published uraninite data from vein/zone-type uranium deposits in the Bohemian Massif (Pribram and Rozna deposits).

Table 3-19. Calculated amount of external radiogenic lead needed to produce variations similar to those observed in the fracture fillings of the PDM-1 bore-core.

	PDM-1		Rozna U deposit		Melechov Massif		Pribram U deposit	
	Granite	Fracture filling	Uraninite most-rich	Uraninite most-poor	Apatite most-rich	Apatite most-poor	Uraninite most-poor	Uraninite most-rich
Pb-isotope data used in the estimation								
$^{206}Pb/^{204}Pb$	18.86	22.89	4676.50	481.88	553.96	37.08	37.64	185.41
$^{207}Pb/^{204}Pb$	15.65	15.86	288.50	45.34	44.10	16.86	16.92	24.04
$^{208}Pb/^{204}Pb$	39.03	39.05	35.00	39.83	56.21	42.16	38.33	37.72
Maximum and minimum amount of the external radiogenic lead needed for the generation of Pb-isotope signature of the most outlying PDM-1 fillings data								
Contamination (relative %):			Min: 0.07	Max: 0.87	Min: 0.75	Max: 21.9	Max: 21.4	Min: 2.4
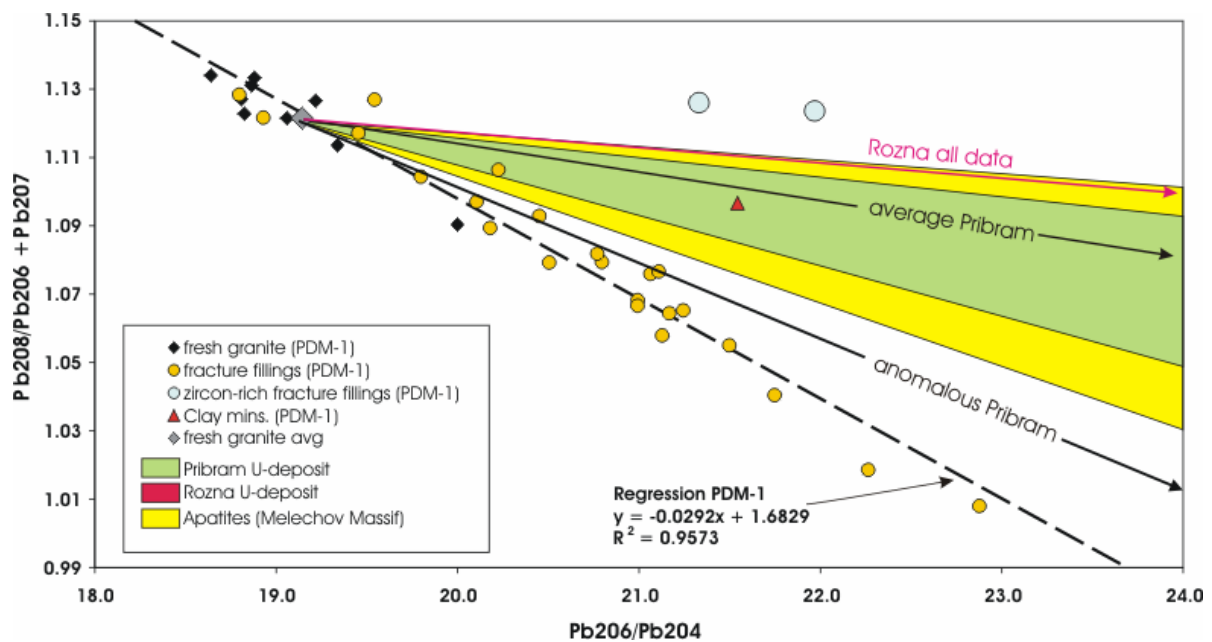
Figure 3-73. Lead isotope ratio diagram where possible "contamination" trends are highlighted. Most of the studied fracture fillings are located outside the hypothetical contamination mixing lines.
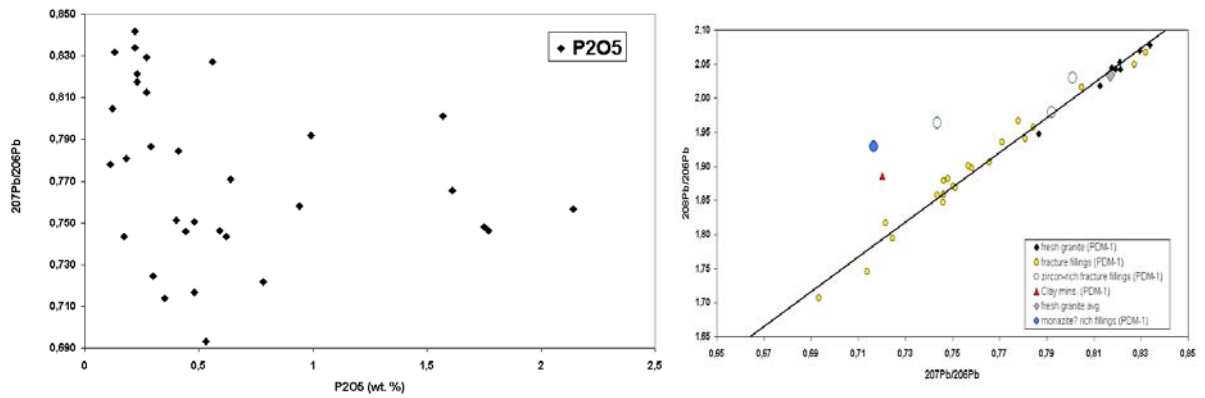
Figure 3-74. Poor correlation of the total P$_2$O$_5$ content (left) with the measured ^{207}Pb/^{206}Pb isotopic ratio, in contrast with linear trend on the Pb-isotope plot (right). This fact clearly demonstrates that the observed linear isotopic trends were not produced in simple mechanical enrichment in apatite, or in other accessory mineral, but that the mobilisation of radiogenic lead during weathering processes played a major role.

3.6.8 Fluid inclusion studies

The clays and iron oxyhydroxides forming the mineral assemblages of the late-stage fracture-fillings in the Melechov granite in the sequence encountered in borehole PDM-1, were unsuitable for fluid inclusion studies. However, two of the examined fractures that were partially open were also lined by coarse euhedral quartz crystals (up to several millimetres in size) growing perpendicularly from the wallrock contact.
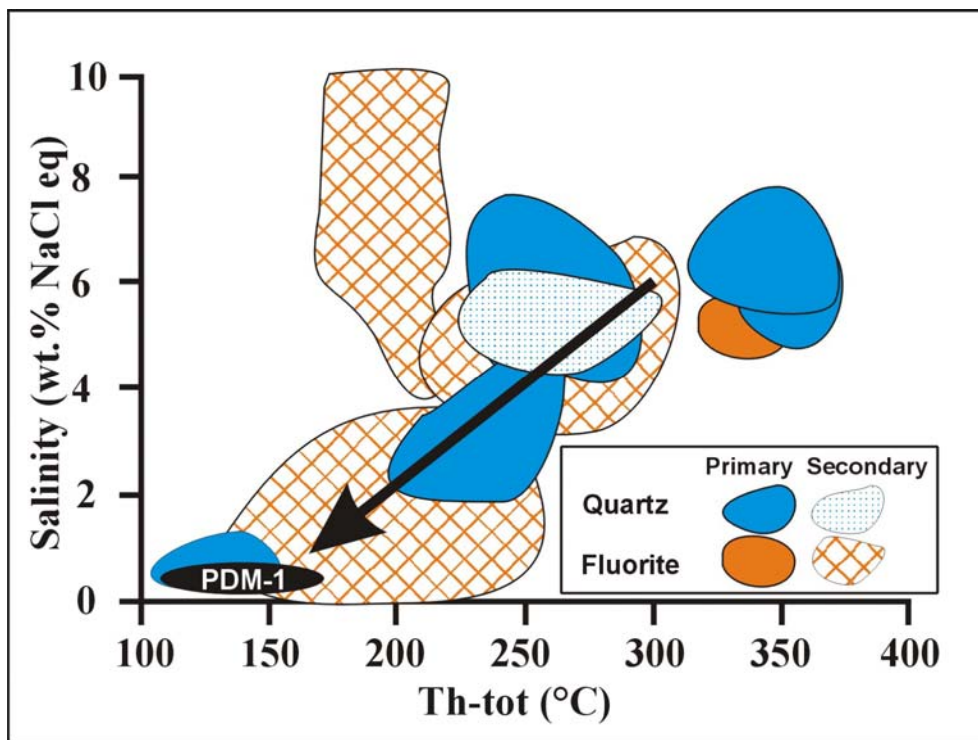
Figure 3-75. Summary of fluid inclusion data for the Melechov massif area (after Dobeš, 1995). Data for the two-phase liquid-rich fluid inclusions from the PDM-1 site are shown by the black ellipse.

173

Fluid inclusions in the quartz are predominantly single-phase liquid inclusions. Only rarely were two-phase liquid-rich inclusions found in the cores of the quartz crystals. The two-phase inclusions indicate that early stages of quartz mineralization was formed from a hot hydrothermal fluid (T_h = 130-160 °C), of low salinity with 0-0.6 wt. % equivalent NaCl (T_{ice} = -0.3 to 0 °C). Hydrate melting characteristics suggest that the aqueous fluid is dominated by Na-Fe-Mg chlorides (T_{fm}: -38 °C). Single phase liquid inclusions exhibit similar salinities, but were most probably trapped at temperatures lower than about ~50-70 °C. However, it was difficult to determine whether inclusions in the quartz were of primary or secondary origin.

Compared with published fluid inclusion data from the whole area of the Melechov Massif (Dobeš, 1995), the fluid inclusions observed in the quartz mineralization from borehole PDM-1 most probably represent the waning stages of the latest regional hydrothermal event (Figure 3-75).

3.6.9 Conclusions

3.6.9.1 LATE STAGE FRACTURE MINERALS FORMED AT SHALLOW DEPTHS.

In contrast to the deep (0-2000 m) drill core studies at Äspö and Laxemar (Sweden), Los Ratones (Spain), and Sellafield and Dounreay (United Kingdom), the PADAMOT investigations at the Melechov site were limited to observations of fracture mineralization from relatively shallow depths (0-100 m), determined by the maximum depth of the PDM-1 borehole. The late-stage fracture mineralization within this depth range in PDM-1 is dominated by iron and manganese oxyhydroxides, clay minerals (montmorillonite, nontronite, and chlorites) and microcrystalline quartz.

The abundance of iron and manganese oxyhydroxides and montmorillonite, gradually increases toward the present surface. These minerals formed as a result of low-temperature oxidative (chemical) weathering of the host (Lipnice type) granite in the shallow groundwater system. Their variation in abundance reflects the degree of weathering (i.e. weathering decreases with depth from the surface).

Other neoformed clay minerals such as chlorite and illite display an opposing trend, increasing in abundance with depth. Their origin is, however, ambiguous. The same mineral phases studied in the granite thin sections are clearly of hydrothermal origin and formed at about 250 °C (based on Cathelineau (1988) chlorite and illite geothermometers).

No carbonate minerals were identified in the fracture mineralization at this depth. Possible explanations for this might be:

- Calcium carbonate mineralization originally might not have been present because the primary Ca-content of the granite was too low to provide sufficient Ca for mineralization by alteration of primary minerals, and that any of the released Ca is fixed in other secondary phases (chlorites, smectites).

- If calcite (or carbonate) vein mineralization had originally been present, then it may have been leached by weathering. Weathering and dissolution of carbonate fracture mineralization is observed in the upper parts of the groundwater systems at Sellafield and Dounreay, and the precipitation of oxidative late-stage iron and manganese alteration products is observed as deep as 660 m in certain fracture zones at Sellafield.

Other minerals such as zircon, apatite, quartz, and feldspars are also found within the late-stage fracture fillings. Unlike iron and manganese oxyhydroxides and clay minerals, which are the products of chemical weathering, these minerals are resistate residual minerals derived from the host rock. It is considered that they may have been liberated from the host granite by weathering, and have been deposited in the fractures after being transported some distance in

groundwater. However, it is possible that they may also in part reflect residual concentration in-situ of resistate minerals during granite weathering.

3.6.9.2 CHEMISTRY OF FRACTURE FILLINGS

Major and trace element data for whole-filling samples show changes in concentration for most of the analysed elements, with either gradual enrichment or depletion from about 100 m depth towards the present surface. Elements including; Mg, Mn, Fe, REE, Zr, Y, U, Th, Pb, V, Ni, Co, Cu, Sr, Be typically show the greatest enrichment towards the surface. Ca, Hf, Rb and Tl are more variable, in distribution. K, Na, Ta, Nb, Ba, Cr, Li are generally depleted towards the surface. Below 100 m there is little evidence for either elemental enrichment or depletion in the major or trace element chemistry. This indicates that the recognizable depth of fracture-related weathering in the Melechov site is limited to about 100 m below the present surface.

Strong enrichment of specific elements (Zr, REE, P) is observed in some fracture fillings, and clearly indicates anomalous concentration of 'detrital' (resistate) magmatic accessory phases at these levels. Some of these depths indicated by anomalous trace element concentration correspond to elevated present-day groundwater flows. It is suggested that this secondary enrichment in accessory phases may be due to gravity sorting during sedimentation of minerals physically transported by groundwater flow within the fracture system. However, they may also partially be due to a residual deposit from weathering in situ.

3.6.9.3 LEAD ISOTOPE STUDIES

Whole-fracture-filling lead isotope data indicate linear inter-Pb-isotope-ratio mixing trends, and the isotopic signatures are anomalous with respect to the present-day crustal lead reservoir. In addition to the effect of the presence of detrital magmatic-accessory phases, we have recognized a dominant role of the mobilization, transport, and precipitation(?) or adsorption(?) of uranogenic and thorogenic lead from an external source(s), although this is probably relatively local.

3.7 CÚLLAR-BAZA BASIN AND PADUL PEAT BOG

3.7.1 Palaeoclimatic history

3.7.1.1 CÚLLAR-BAZA BASIN

The palaeoclimatic history of the Cúllar-Baza Basin has been established by studying the variations in isotopic signature (C and O) of calcitic valves of the ostracod (Cyprideis torosa). The $\delta^{13}C$ values vary between -9.68 ‰ and -2.0 ‰ and the $\delta^{18}O$ values range from -11.08 ‰ to +4.9 ‰.

Palaeoenvironmental analysis from $\delta^{18}O$ and $\delta^{13}C$ values was based not only on the interpretation of relative through-time variations, but also on regression analysis of the analytical data. The correlation coefficient between $\delta^{18}O$ and $\delta^{13}C$ values is significant (r=0.50; p=0.000). This indicates that the ostracods grew in an endorheic basin whose hydrogeology behaviour may have gradually changed during the Middle Pleistocene. The samples recovered in the lower 255 metres of the section (Lower Pleistocene) have a higher correlation coefficient (0.70), which is considered to be typical of carbonates that have normally precipitated from a closed basin (Talbot, 1990).

In general, $\delta^{18}O$ changes are interpreted to vary (although differently) with changes in salinity and water temperature. However, in lacustrine systems the $\delta^{18}O$ oscillations are due mainly to evaporation/infill (E/I) ratio changes. $\delta^{18}O$ is higher when E/I is higher and, therefore, when

there is an increase in the salinity and a decline in the water level. When residence time is long the $\delta^{18}O$ values also increase.

In order to understand the effect of global temperature changes in the southern part of the Iberian Peninsula, the theoretical $\delta^{18}O$ variation was estimated and compared with the measured $\delta^{18}O$ variation (16 ‰) of Cúllar-Baza Basin. Some findings from previous work must be considered when interpreting the relationship between $\delta^{18}O$ and $\delta^{13}C$ and climatic variations:

- During glacial periods the $\delta^{18}O$ of sea water became enriched by 1.5 ‰ (cf. Shackleton, 1995), or even by as much as 4 ‰;

- Because it is estimated that 65 % of the ocean evaporation originated in low latitudes, between 30º S and 30º N (Rozanski et al., 1993), and because the water temperature difference between cold and warm periods in those seas is very low: 5-6 ºC (Guilderson et al., 1994), any temperature effect on the composition of the rain (which is mainly produced by evaporation of sea water) at low latitudes would be largely disguised due to the fact that sea temperature in these latitudes had almost no variation.

In summary, because there is more ^{18}O in the ocean water during a cold period, atmospheric water vapour (produced by seawater evaporation) and subsequent rainfall would also be more enriched in $\delta^{18}O$ than during warm episodes. However, mean air temperature changed more widely than sea water temperature. A mean temperature variation of 12 ºC has been reported in La Grand Pile and Les Echets peat bog (France) records since the Last Glacial Maximum (Guiot, et al., 1989).

In order to estimate the theoretical $\delta^{18}O$ variation of rainwater and compare it with the measured $\delta^{18}O$ variation of Cúllar-Baza Basin we must consider the effect of temperature variation in $\delta^{18}O$ rainwater for the Iberian Peninsula, which is 0.4 ‰ per 1 ºC (Delgado, et al., 1991). The calculated theoretical variation in $\delta^{18}O$ in the atmospheric water vapour from cold to warm periods, using the maximum temperature difference (12 ºC) estimated throughout the whole of the Pleistocene in Europe, is 4.8 ‰ (i.e. 0.40 ‰/ºC x 12 ºC). This means that the rainwater $\delta^{18}O$ would be 4.8 ‰ lighter during cold periods. However, because seawater was enriched in $\delta^{18}O$ during these cold periods the actual atmospheric variation in $\delta^{18}O$ would have been slightly less. This difference ($\leq$4.8 ‰) is small when compared to the actual range of $\delta^{18}O$ values (16 ‰) observed in ostracods from the Cúllar-Baza Basin, which corroborates other studies that have found very large $\delta^{18}O$ differences between glacial and interglacial periods in continental environments.

In order to calculate the theoretical $\delta^{18}O$ in water it is necessary to consider that $\delta^{18}O$ is inversely proportional to the temperature of calcite formation, and decreases by 0.26 ‰ per degree Celsius (Craig, 1965). For the Cúllar-Baza Basin, which has an estimated maximum temperature difference of 12 ºC, this translates into a value of -3.12 ‰ (12 ºC x -0.26 ‰/ ºC) for the water composition.

Taking into account both temperature and its linked effects with calcification over the $\delta^{18}O$ variation in water, the basic theoretical $\delta^{18}O$ variation between cold and warm episodes in the Cúllar-Baza Basin would be 1.68 ‰ (4.8 ‰ -3.12 ‰). However, this differs markedly from the observed variation (16 ‰), and suggests that neither the increase of $\delta^{18}O$ in seawater during a glacial period, nor the global differences in the isotopic composition of rainwater that are linked to temperature variations, would have been reflected in the hydrogeochemistry of lacustrine water bodies of Cúllar-Baza Basin.

However, in this study we consider that the global temperature oscillations, together with other factors such as moisture, will have markedly affected evaporation rates from the water bodies of the area. If high moisture and relatively cold conditions are coeval, precipitation will be significant with a decrease in $\delta^{18}O$ in the rainfall, which would also be reflected in the water bodies. When warm and arid conditions coincide then the rainfall would be expected to have heavier $\delta^{18}O$ (Rozanski et al.,1993), and again this would be reflected in enhanced ^{18}O in the

water bodies. The effect of evaporation will also reinforce the enrichment of ^{18}O in the lakes. This is confirmed by the presence of intrasedimentary gypsum crystals (evaporite mineralization) in beds where ostracod δ^{18}O values are high.

Low δ^{13}C values could be explained as a consequence of scarce evaporation, high humidity and/or important input of carbon from vegetation, with higher C_3 plants content, which characteristically have lower δ^{13}C values, ranging from -31 to -23 ‰. In contrast, during warm and arid episodes the δ^{13}C can reach high values due to the effect of evaporation and less carbon input from more restricted plant biomass. Likewise, C_4 plants (with δ^{13}C comprised between -16 and -9 ‰), which are better adapted to arid climates, would contribute with less negative δ^{13}C values.

Cluster analysis of δ^{18}O and δ^{13}C data was undertaken (employing complete linkage and euclidean distance approaches) and shows that the data cluster into three groups:

- Group 1 with low δ^{18}O and δ^{13}C values;

- Group 2 with high δ^{18}O and δ^{13}C values;

- Group 3 with intermediate δ^{18}O and δ^{13}C values.

These groups are also distinguished in the linear regression plot between δ^{18}O and δ^{13}C (Figure 3-76), and can be matched with three different climatological scenarios, based on the interpretations detailed above.

$$\delta^{18}O = 1.30004 + 0.58482 \times \delta^{13}C$$

$$r = 0.50$$
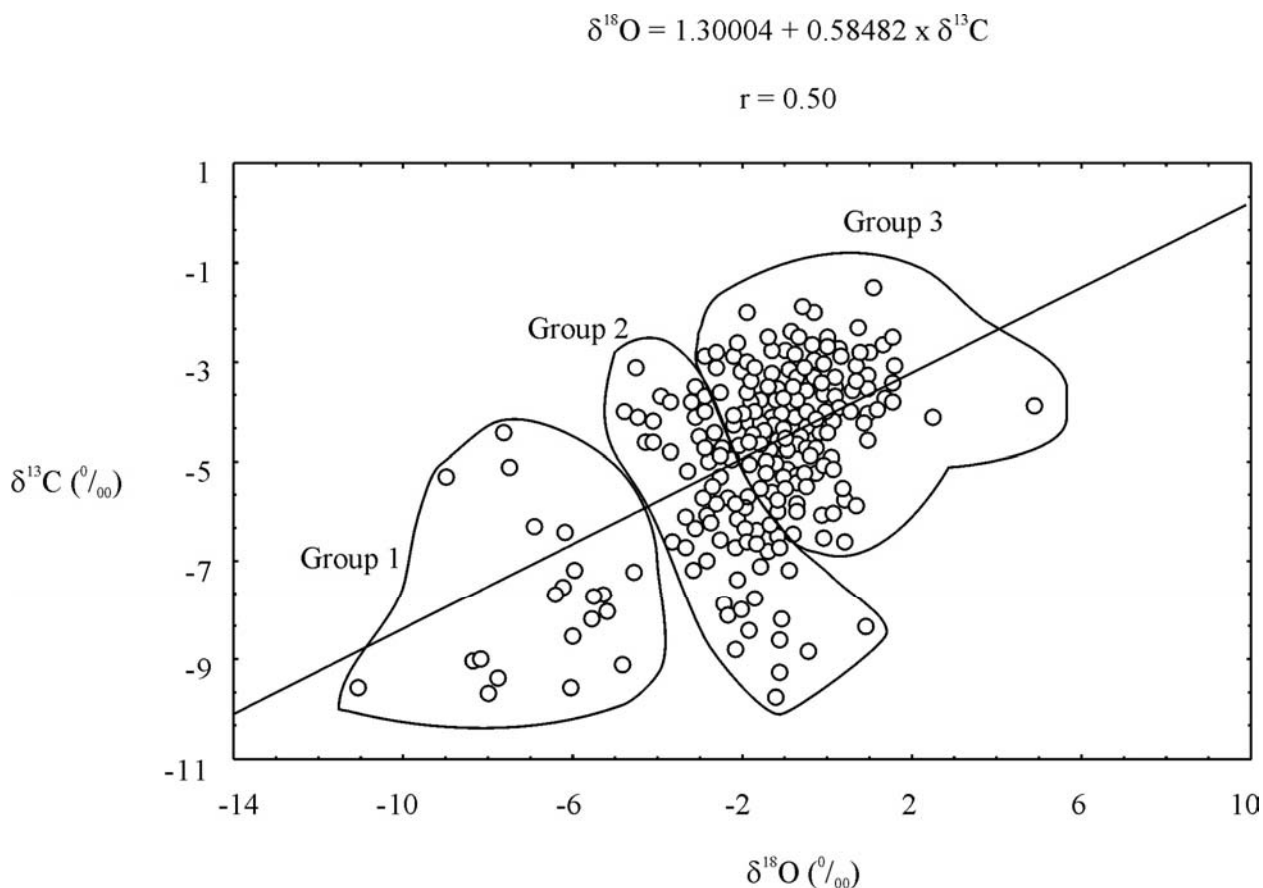
Figure 3-76. Regression analysis between the δ^{13}C and δ^{18}O values obtained in Cyprideis torosa (Jones) ostracods from Cúllar-Baza Basin.

Group 1 (low $\delta^{18}O$ and $\delta^{13}C$) corresponds to a 'Humid and Cold Period' scenario. The cold conditions and the greater rainfall would result in lake waters with more negative $\delta^{18}O$. Low evaporation rates should also maintain low $\delta^{18}O$ values. The $\delta^{13}C$ would also be low as a result of the humid conditions, low evaporation rates, and the presence of C_3 plants.

Group 2 (intermediate $\delta^{18}O$ and $\delta^{13}C$ values) corresponds to an Intermediate climate scenario.

Group 3 (high $\delta^{18}O$ and $\delta^{13}C$) corresponds to an 'Arid and Warm Period' scenario. High $\delta^{18}O$ and $\delta^{13}C$ values were produced as a consequence of higher temperatures and evaporation rates from the lake waters. Algae and macrophyte development would also produce an increase in $\delta^{13}C$. Vegetation cover would comprise mainly C_4 plants, which characteristically have less negative $\delta^{13}C$.

Figure 3-77 shows the stratigraphical variation of $\delta^{18}O$ in ostracod (Cyprideis torosa (Jones)) tests for the composite type-section for the Cúllar-Baza Basin. The data have been smoothed to remove the effects of outliers. Stratigraphical variation in $\delta^{13}C$ is not shown because these values are largely dependent on other palaeoenvironmental factors, such as biomass. The variation in $\delta^{18}O$ in Figure 3-77 can be interpreted in terms of a scenario with four 'Cold and Humid Great Periods', alternating with four 'Warm and Arid Great Periods'.
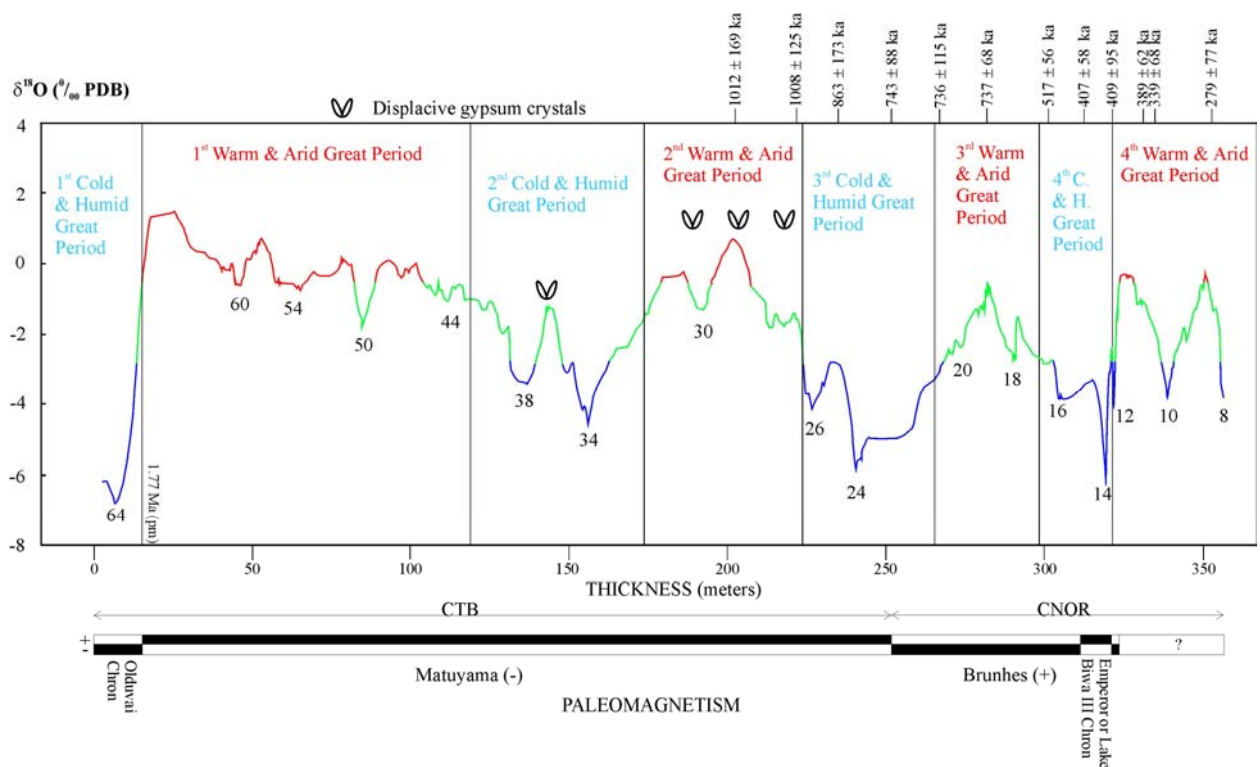
Figure 3-77. Smoothed curve of the $\delta^{18}O$ values obtained in Cyprideis torosa (Jones) ostracods from Cúllar-Baza Basin, together with the identified palaeoenvironmental periods and the standard oxygen isotope stages (OIS) (data smoothing based in linear regression of five nearest neighbours). The position of displacive gypsum crystals is also shown.

The occurrence of intra-sedimentary displacive gypsum during the 2nd Warm and Arid Great Period corresponds to the highest $\delta^{18}O$ (and $\delta^{13}C$) ostracod values. Gypsum occurrence also coincides with the samples that mark the $\delta^{18}O$ maximum during the 2nd Cúllar-Baza Basin Cold and Humid Great Period. This shows that high $\delta^{18}O$ ostracod values are not only linked to warm conditions but also to arid conditions. According to Rosen (1994) the presence of displacive

178

evaporite minerals in sedimentary horizons is the result of high aridity with a marked negative water balance of the lacustrine system.

No displacive gypsum has been found in the lower part of the composite-stratigraphical type section, interpreted as the 1st Warm and Arid Great Period. Nor does it occur in the top of the section (3rd and 4th Warm and Arid Great Periods). This is interpreted to be a reflection of the palaeogeographical environment, located at the foot of an alluvial fan near the margin of the lacustrine environment.
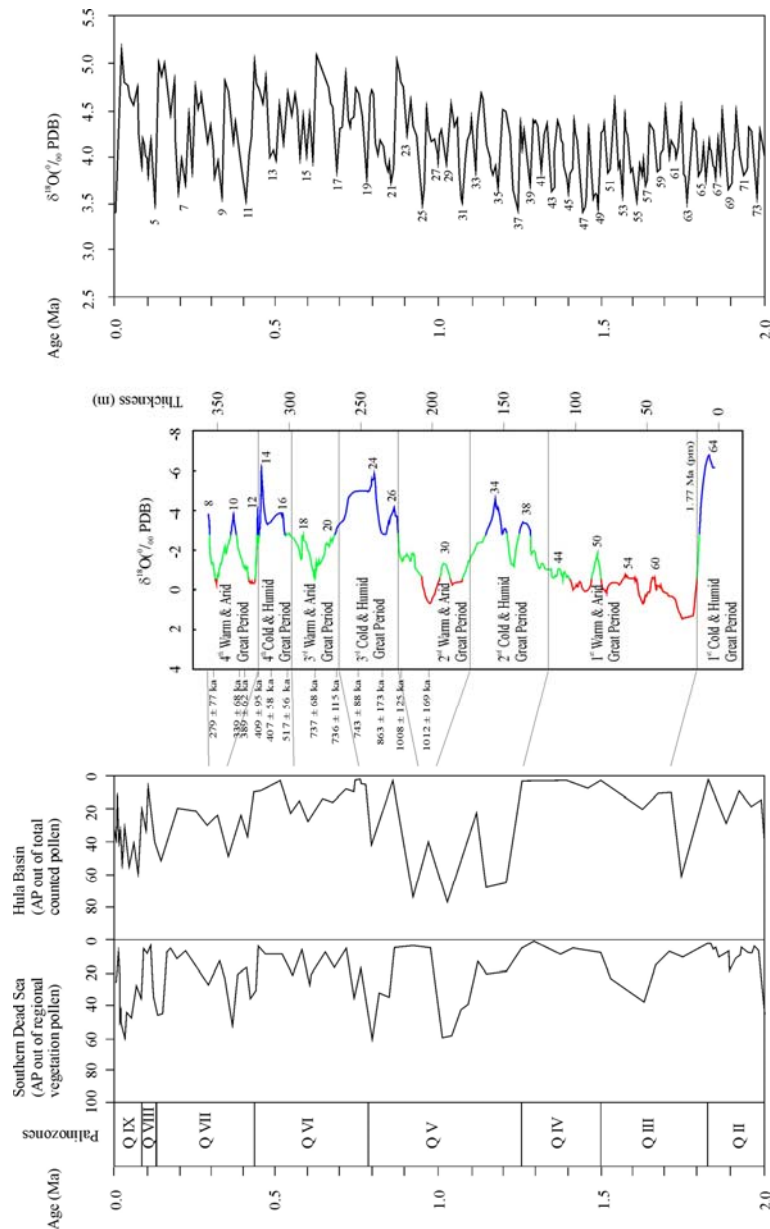
Figure 3-78. Correlation of the palaeoenvironmental sequence (smoothed δ18O obtained in Cyprideis torosa ostracods) from Cúllar-Baza Basin, the pollen sequences (percentage of arboreal pollen) obtained in the Southern Dead Sea region and the Hula Basin (Horowitz, 1987, 1989), both in Israel, and the marine oxygen isotopic record (Shackleton, 1995)[1].

---

[1] The curve for the Hula Basin is mainly based on a pollen diagram from Notera 3 borehole. The curve for the southern Dead Sea is mainly based on the pollen distribution for Amazyahu 1 borehole, with additions from Melekh Sdom 1, Ami´az 1, Sdom 2 and Har Sedom 1. The percentage of arboreal pollen is interpreted as an increase in humidity. The data of the marine oxygen isotope record derive from the SPECMAP stack for the interval 0-0.62 Ma and OPD site 677 for the interval 0.62-2.0 Ma.

179

Attempts were made to compare the correspondence between oxygen isotope stages obtained in marine records and the peaks observed in the smoothed ostracod $\delta^{18}O$ curve for the Cúllar-Baza Basin. Tentative correlations can be made on the basis of results from the PADAMOT study. Assuming that the magnetic reversal at the base of the section (18 m depth) corresponds to the end of the Olduvai Chron (Plio-Pleistocene boundary), and that the Plio-Pleistocene boundary corresponds to the 64th OIS, the correlation between the palaeoclimatic periods established in Cúllar-Baza Basin and the marine oxygen isotope stages, is shown in Figure 3-78. This shows that there are good correlations between both the age and the characteristics of the marine oxygen isotope curves and stages of Shackleton (1995) and those identified in the Cúllar-Baza Basin smoothed ostracod $\delta^{18}O$ curve.

Elsewhere in the Mediterranean Area a similar palaeoenvironmental evolution is found in the Hula Basin (northern Israel). Horowitz (1987, 1989) studied a large pollen sequence in Hula Basin covering the Pleistocene and most of the Upper Pliocene. He correlated the Günz, Mindel and Riss Glaciations to periods where humidity predominated, whereas during interglacial episodes (Günz/Mindel, Mindel/Riss and Riss/Würm) the palaeoclimatic conditions corresponded to increased aridity. A similar correlation was also found with a pollen sequence obtained from southern Israel (southern Dead Sea region). These sequences can also be correlated with those established by the PADAMOT studies in the Cúllar-Baza Basin (Figure 3-78). The 1st Cold and Humid Period of Cúllar-Baza Basin corresponds to an increase of the percentage of arboreal pollen (higher humidity) in the Hula Basin, whereas the 1st Warm and Arid Period of Cúllar-Baza Basin coincides with low percentages of arboreal pollen in the Hula Basin. In the southern Dead Sea the increase of arboreal pollen occurs between 1.65 and 1.5 Ma, a bit later than in the Hula Basin and the Cúllar-Baza Basin. Similarly, there is a good correspondence between the 2nd, 3rd and 4th Cold and Humid Periods of Cúllar-Baza Basin and high percentages of the arboreal pollen recorded in both the southern Dead Sea region and the Hula Basin. Likewise, the 2nd, 3rd and 4th Warm and Arid Periods of Cúllar-Baza Basin are well-correlated with low percentages of arboreal pollen of the two sequences from Israel.

Similar palaeoenvironmental models have been found in the pluvial lakes developed in the "Basin and Range" area of United States of America, such as Owens Lake in southeast California (Smith and Bischoff, 1997). In this area conditions of less evaporation and higher water availability prevailed during cold periods (glacial), while during warm episodes the climate was arid and promoted the development of playa-lakes

3.7.1.2 PADUL PEAT BOG

In the Padul Bog site, the concentration of organic carbon (% TOC), H/C and C/N ratios, $\delta^{13}C$ values, the carbon preference index (CPI) and the *n*-alkane predominant chain were studied as palaeoenvironmental proxies. Logs showing the variations in these parameters through the sequence of the Padul borehole are shown in Figure 3-79.

Concentration of total organic carbon (% TOC)

% TOC represents the organic matter that escaped mineralization during sedimentation, and is influenced by both the initial production of biomass and subsequent degree of degradation. It therefore integrates organic matter of different origins.

Low concentrations of organic carbon, less than 0.5 %, were found in sediments from several horizons in the bottom of the Padul borehole (Figure 3-79). This provides evidence of periods of greater water depth in the sedimentary environment. A sudden increase in the concentration of organic carbon above 70 m marks a dramatic change in the sedimentary record. However, there are some minima in the % TOC curve correlated with horizons consisting of marls (36.0 to 33.4 m) or sands (7 to 4.5 m).

The correspondence between the concentration of organic carbon and lithology can be interpreted in terms of palaeohydrogeological behaviour. During the first third of the record (107 to 70 m) there was a relatively deep-water body (lacustrine conditions) in the Padul Basin, probably associated with some run-off. In contrast, in the uppermost 70 metres the depositional environment changed to palustrine conditions (peat bog).
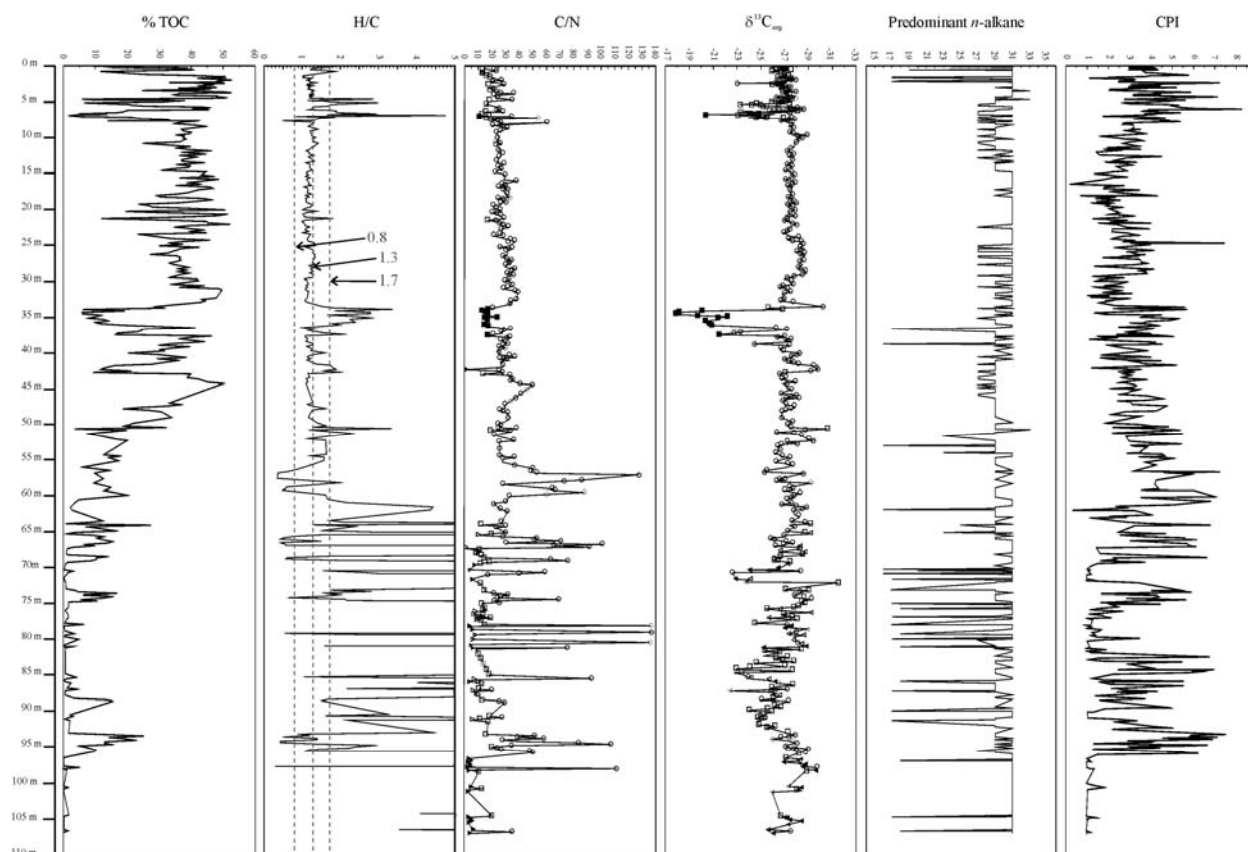
Figure 3-79. Concentration of organic carbon (%TOC), H/C, C/N, δ^{13}C, CPI and predominant *n*-alkane chain logs. H/C ratios are represented up to 5, although there are some greater values, especially at the bottom of the core (in some cases >100). We have preferred to use a smaller scale (0 to 5) in order to show the cut-off values of different groups (0.8; 1.3 and 1.7). When H/C values are greater than 5, they are beyond the scale upper limit. In the δ^{13}C and C/N logs, samples have been identified according to the groups differentiated in figure 3.7.5 with distinctive symbols (Group 1: triangles, Group 2: squares, Group 3: full-squares, Group 4: circles). Full triangles represent samples with low %TOC values.

Organic matter H/C ratios

The atomic H/C ratio can be used to determine the origin of organic matter and indicate changes in lake level (i.e. oxic-anoxic conditions). Algal and amorphous remains have H/C ratios higher than 1.7 (Talbot and Livingstone, 1989). Herbaceous remains have H/C values between 1.3 and 1.7, while woody material is dominated by polycyclic aromatic compounds that are even less hydrogen-rich with H/C ratios between 0.8 and 1.3. At the other extreme, altered or oxidized plant material (coaly) has H/C values lower than 0.8.

The log of the variation in atomic H/C ratio for the Padul borehole is shown in Figure 3-79. The cut-off values of the different organic groups (0.8; 1.3 and 1.7) that can be distinguished have been highlighted using a scale ranging from 0 to 5. The H/C variation plot (Figure 3-79), from 107 to 60 m indicates a dominance of organic matter derived from phytoplankton (values higher

181

than 1.7), with some spikes in the profile with H/C ratios characteristic of land plants. The high H/C values obtained from the bottom of the core are indicative of the good preservation of organic matter within an oxygen-poor (lacustrine) environment. In some places in the profile the H/C ratio decreases below 0.8, which indicates oxidation or alteration of the organic matter and usually corresponds to gravel horizons.

The character of the Padul basin changed radically in the uppermost 60 m. The H/C ratio at this point marks a predominance in the inputs of organic matter from terrestrial plants (values between 0.8 and 1.7), suggesting the existence of low-water episodes (palustrine). There are, however, eight episodes that indicate a rise of the water level, shown in the H/C curve.

Organic matter C/N ratios and carbon stable isotopic composition

The C/N ratio is an indicator of the protein content:

- Benthic organisms and bacteria have C/N ratios around 4.2 and 4.1, whereas planktonic organisms the C/N ratio can vary between 4 and 7;

- Fresh organic matter from lake algae has C/N values ranging between 4 and 10, whereas vascular land plants usually have C/N ratios of 20 and greater (Hedges et al., 1986);

- C/N ratios between 30 and 40 are characteristic of cellulosic plants, whereas C/N values of 12-17 suggest a mixture of algal and vascular plants.

The carbon isotope ratio of organic carbon can often be used, together with C/N values, to answer questions concerning the sources and composition of organic matter:

- Freshwater phytoplankton typically has $\delta^{13}C$ values between -20 and -30 ‰ (Galimov, 1985);

- The common range for $\delta^{13}C$ values of C_3 land-plants (trees, shrubs and cold climate grasses) is -23 to -31 ‰ O´Leary, 1981);

- On the other hand, land plants that use the C_4 (Hatch-Slack) photosynthetic pathway (i.e. grasses and sedges) have $\delta^{13}C$ values between -9 and -17 ‰.

The atomic C/N ratios and the $\delta^{13}C_{org}$ values are compared in Figure 3-80. Four groups can be distinguished according to the inferred major sources of organic matter:

- Group 1 (algae-increasing water input);

- Group 2 (mixed origin: algae and C_3 plants-less wet conditions);

- Group 3 (algae, and C_3 and C_4 land plants- warm and dry conditions);

- Group 4 (C_3 land plants).

Samples of each group were identified with distinctive symbols in the C/N and $\delta^{13}C_{org}$ logs (Figure 3-79).

Figure 3-79 shows that at the bottom of the core (below 65 m) algae were a major organic-matter source (predominance of samples belonging to Group 1). This suggests that the water was deeper at this point in time than in the middle and upper part of the record, when palustrine conditions probably predominated. However, samples belonging to Group 1 with low concentrations of organic carbon (data shown by full triangles in Figure 3-79) cannot be interpreted as being derived from phytoplankton. These results are consistent with variations shown by lithology, % TOC and H/C ratio, although there is a lag of about 5 m between these properties at the top of this part of the sequence (65-60 m). Likewise, some episodes with land-derived organic matter are also important in this part of the core. These correlate extremely well with the decrease in the H/C ratio (Figure 3-79).
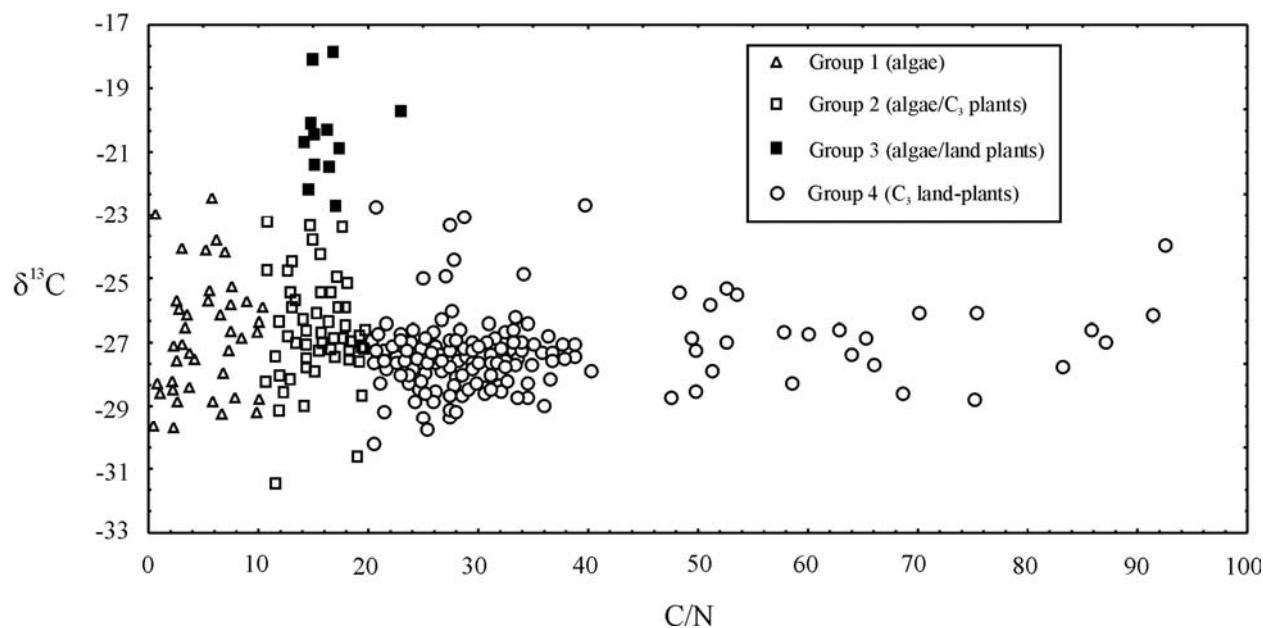
Figure 3-80. $\delta^{13}C_{org}$ vs. C/N plot. Four groups have been distinguished: Group 1 (algae), Group 2 (algae/C₃ plants), Group 3 (algae/land plants), and Group 4 (C₃ land-plants). C/N ratios are represented up to 100. Samples (7) with C/N values higher than 100, have $\delta^{13}C_{org}$ values between -28.5 and -27.1 ‰, being included within group 4.

Between 60.0 and 36.0 m (ca. 400-180 ka B.P.), most of the samples fall within Group 4, with some phases of major phytoplankton and algae development - as can be interpreted from the H/C ratio (see discussion above). Most of the information derived from interpretation of the atomic H/C ratio indicates alternations of grass-dominated and tree-dominated episodes.

There is also close correlation between the oscillations observed in the H/C plot, and the C/N and $\delta^{13}C_{org}$ values in the rest of the core. The rise in water level recorded in samples of Group 3 (36.0-33.6 and 6.7 m) is also recorded in the H/C log (Figure 3-79).

The global climatic changes occurring from ca. 170 to 25 ka B.P. (33.6 to 7 m) did not strongly affect the palaeoenvironmental proxies in the Padul Bog; i.e., H/C and C/N ratios and $\delta^{13}C_{org}$ values vary little, except at 21.2 m where C/N and $\delta^{13}C_{org}$ values fall into Group 2, the H/C ratio increases and the concentration of organic carbon decreases. This is interpreted to correspond to a rise in the peat bog water level.

Many samples in the uppermost part of the core (approximately the top 7 m), belong to Group 2 (mixed organic sources from algae and C3 plants) alternating with samples belonging to Group 4 (C₃ land plant dominated organic sources). There is a marked variation in (-23.3 to -28.3 ‰). the $\delta^{13}C_{org}$ curve between 6.7 and 4.5 m, with a maximum difference of about 5 ‰ (Figure 3-79). These differences are undoubtedly related to important vegetation changes linked to the Last Glacial Maximum and the beginning of the Holocene, although the organic signature is always dominated by organic input dominated from sources within the range of plants following the C₃ photosynthetic pathway. The samples with lower $\delta^{13}C_{org}$ values, that are included in Group 4, coincide with atomic H/C ratios common to grasses (1.3<H/C<1.7) and contain predominantly *n*-alkane chains with 31 carbon atoms typical of grasses (Cranwell, 1973). Although the $\delta^{13}C_{org}$ remains almost constant, the palaeoenvironmental proxies show that some changes occurred during the Holocene and we interpret intervals characterised by Group 2 and Group 4 samples to reflect alternations of wet and dry episodes, respectively.

183

Biomarker molecule proxies (n-alkanes)

There are three principal sources of biotic hydrocarbons in lake sediments that produce different *n*-alkane profiles:

- Algae;

- Aquatic macrophytes;

- Vascular plants that live around a lake.

The hydrocarbon compositions of phytoplankton and algae are dominated by low molecular weight *n*-alkanes, with a maximum at C_{17} *n*-alkane. The submerged/floating macrophytes have maxima at C_{21}, C_{23} and C_{25} (Cranwell, 1984). Emergent macrophytes have *n*-alkane distributions similar to terrestrial plants, that is with maxima at C_{27} and C_{29}. Vascular plants on land or around edges of lakes contain large proportions of higher molecular weight *n*-alkanes (C_{27}, C_{29} and C_{31}) in their epicuticular waxy coatings (Eglinton and Hamilton, 1963), and the abundance of these wax hydrocarbons reflects the amount of organic matter transported to lakes from the surrounding land.

The carbon preference index (CPI) can be used as a proxy of the preservation potential of the organic matter when there is a clear predominance of superior plant waxes. CPI values are high in living plants and surface sediments but decrease (towards a final value of 1) with increasing organic maturity. In general, young (modern) vascular plants have CPI values around 7 but due to diagenetic processes their CPI gradually decreases down to 1 (Hedges and Prahl, 1993). However, this index cannot be used uniquely as a preservation potential proxy in all cases because a CPI of 1 may also indicate immature organic matter with low higher plants influence.

The log of the predominant *n*-alkane chain is shown in Figure 3-79. This is interpreted to be an indicator of the origin of the organic debris input (algae, aquatic macrophytes or land plants) (Cranwell et al., 1987), and of variations over time of the water-body depth. The predominance of *n*-alkanes of low molecular weight at the bottom of the core (below 70 m) indicates that algae and bacteria are important organic matter sources (Gelpi et al., 1970). This, together with the variation shown by the other palaeoenvironmental proxies, suggests that the water body in the Padul Bog would have had some depth. There is also an important number of samples with a predominance of C_{27} to C_{31} *n*-alkanes that indicate other organic sources (land plants or aquatic macrophytes). Organic matter inputs in these were smaller than in the upper part of the core (cf. % TOC).

With the aid of the predominant *n*-alkane chain proxy, samples of a more doubtful origin (e.g. those with low concentrations of organic carbon) can also be classified. Thus, samples with predominantly lower-molecular-weight *n*-alkanes are considered to derive their organic matter from phytoplankton (104.6; 96.8; 85.6; 80.9; 71.4; 70.1), whereas in the remaining samples the organic matter came from other sources (macrophytes or land plants).

Between 70 and 65 m depth, the C_{31} *n*-alkane predominates, suggesting input from grasses, with three episodes in which the C_{29} *n*-alkane is abundant. In is considered to indicate the existence of dry conditions, which caused the recession of trees and the expansion of grasses.

In the lower and middle parts of the core, the predominance of C_{27}, C_{29} and C_{31} *n*-alkanes might be related to palustrine conditions with important organic matter inputs from trees or grasses. However, this signature may also indicate periods of high water level phases, as emergent macrophytes usually have *n*-alkanes with maxima at these molecular weights (Ficken et al., 2000). There are some exceptions, such as between metres 36.0 and 33.6 m, where low molecular weight *n*-alkanes typical of phytoplankton are predominant. This corroborates the information provided by the other proxies (as discussed above).
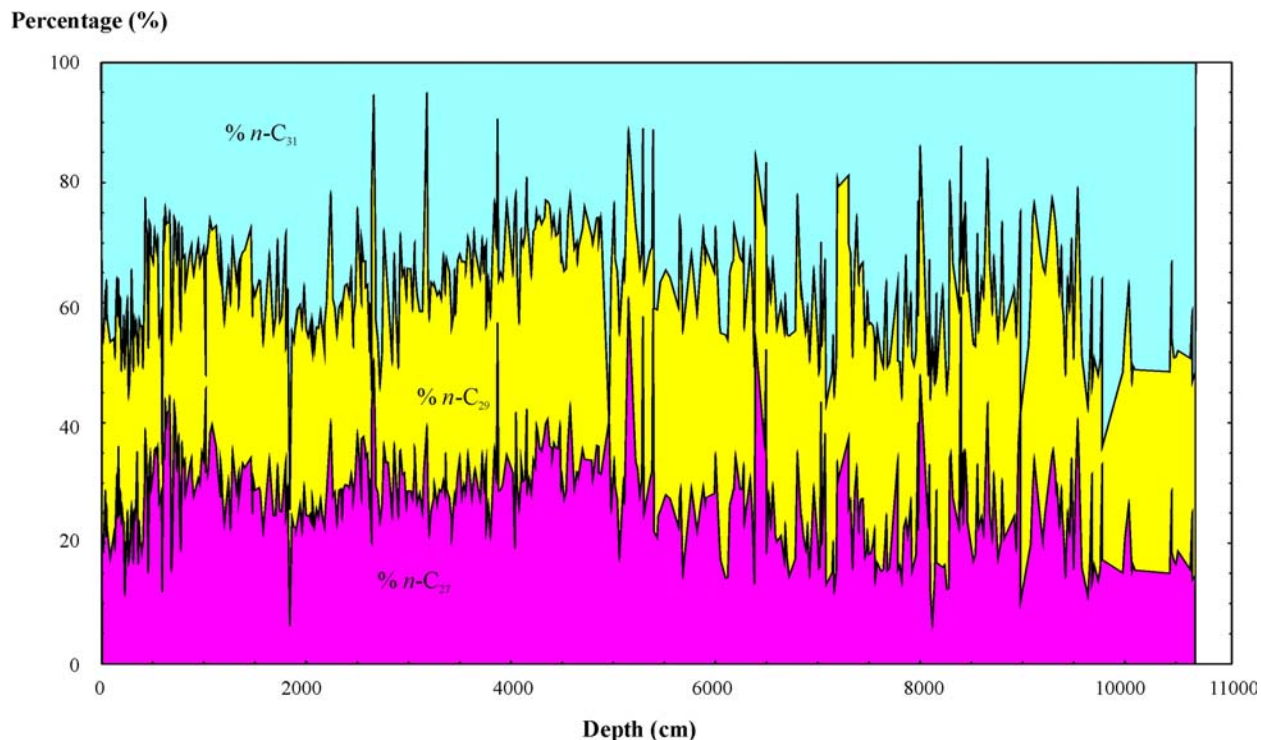
Figure 3-81. Depth variation in *n*-alkane composition in the Padul borehole, shown as percentages of the C_{27}, C_{29}, and C_{31} isomers with respect to the sum C_{27} + C_{29} + C_{31}.
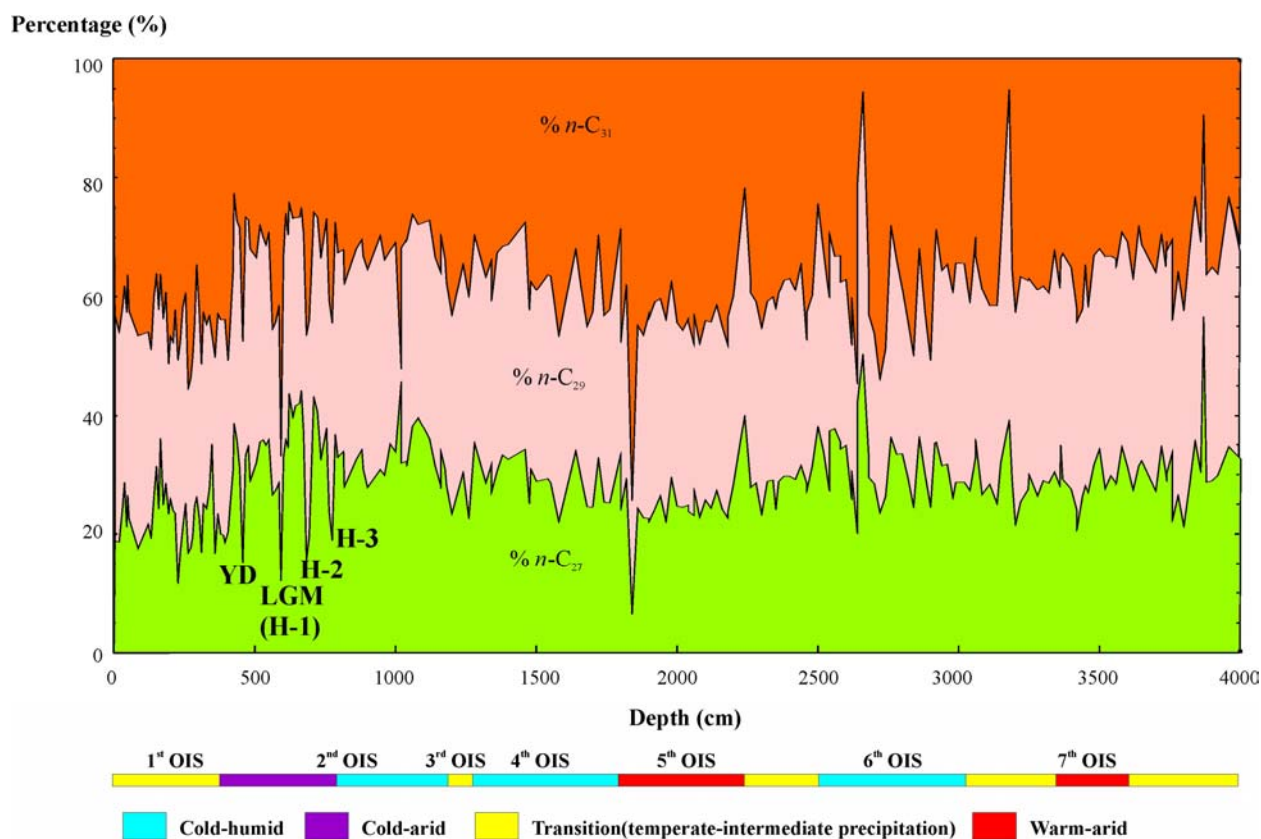
Figure 3-82. Depth variation in *n*-alkane composition in the upper 40 m of the Padul borehole, shown as percentages of C_{27}, C_{29}, and C_{31} isomers with respect to the sum C_{27} + C_{29} + C_{31}, and palaeoenvironmental interpretation compared with the OIS record.

185

The n-alkane profile, represented as percentages of C_{27}, C_{29}, and C_{31} isomers with respect to the sum $C_{27} + C_{29} + C_{31}$, is shown for Padul borehole core in Figure 3-81. A more detailed log of the relative percentages of the C_{27}, C_{29} and C_{31} n-alkanes of the upper 40 m (corresponding to approximately 235 ka B.P.) is also included (Figure 3-82). Grasses are documented to have a C_{31} maximum in the n-alkane distribution, while C_{27} n-alkane is more abundant in deciduous trees, and pines are enriched in C_{29} n-alkane (Cranwell, 1973; Ortiz et al., 2004b). Therefore, the increasing contribution of n-C_{29} alkanes can be attributed to the increased development in conifers (Schwark et al., 2002). Likewise, the enrichment in C_{27} n-alkane can be attributed to the colonization by many species of deciduous trees and, thus, the existence of more humid and temperate conditions. High amounts of n-C_{31} can be associated with dry phases (cold or warm) with the development of an important grass-vegetation cover and/or the development of cold-climate pines. This is confirmed by the high negative correlation coefficient obtained between the percentages of n-C_{27} and n-C_{31} n-alkanes along Padul peat bog core, which, in our opinion, is related with wet/dry phases. As observed, C_{29} n-alkane can behave independently with respect to C_{27} n-alkane, and it displays a less negative correlation with C_{31} n-alkane. These results suggest that contribution of n-C_{29} alkanes can be attributed only to variations of the density of conifers in the neighbourhood of the basin, but not to the establishment of more or less diverse deciduous tree assemblages.

Implications for rainfall and recharge history

Cúllar-Baza Basin

The variation in $\delta^{18}O$ signature obtained in the ostracod *Cyprideis torosa* (Jones) valves from Cúllar-Baza Basin, reflects the global climatic variations from 2 Ma to the upper part of Middle Pleistocene (279 ± 77 ka). The $\delta^{18}O$ variation resulted from changes of the evaporation/infill ratio in the water bodies and in the rain amount.

Periods with high $\delta^{13}C$ and $\delta^{18}O$ values have been associated with warm and arid palaeoenvironmental conditions, while low $\delta^{13}C$ and $\delta^{18}O$ values have been correlated with cold and humid episodes. Also, the signature of four Cold and Humid Great Periods alternating with four Warm and Arid Great Periods can be recognised from the ostracod smoothed $\delta^{18}O$ curve. This interpretation is supported by other geochemical signals including the presence of displacive gypsum crystals which developed under episodes of high salinity and aridity, mostly during the 2nd Warm and Arid Great Period.

This pattern of alternating "warm-arid "and "cold-humid" episodes is the inverse to the palaeoclimatological record of Northern Europe. The Cúllar-Baza Basin is located in the Mediterranean area where glacial periods did not produce permafrost and the scarcity of liquid water that was experienced in Northern Europe. In the northern latitudes higher precipitation rates would have occurred during interglacial episodes.

A good correlation between Cúllar-Baza Basin and the deep-sea oxygen-isotope stage (OIS) record (Shackleton, 1995) has been obtained. There is also a good correspondence of palaeoclimate proxies with other Quaternary basins in the Mediterranean area (Horowitz, 1987, 1989). Similar palaeoenvironmental models have been found in North America pluvial lakes. This indicates that climate recorded in the Cúllar-Baza Basin was responding to global climatic changes.

Padul Peat Bog

In the Padul Peat Bog, the concentration of organic carbon, the atomic H/C and C/N ratios, the $\delta^{13}C_{org}$ and CPI values and the distribution of the predominant n-alkane chain organics, proved to be excellent palaeoenvironmental proxies for the study of the palaeoclimatological and

palaeohydrological evolution. The atomic H/C ratios and CPI values indicate that little alteration and diagenesis occurred during transport and after deposition in the basin.

These proxies provide evidence of two markedly different hydrogeological scenarios in the Padul Basin. From the bottom of the sequence (ca. 1 Ma B.P.) to 60 m (ca. 400 ka B.P.), a period of significant run-off recharge made the water-body much deeper than during the rest of the record. From 60 m depth to the uppermost part (ca. 400-4.5 ka B.P.) of the sequence, the Padul Basin became a peat bog (sensu stricto), with the main water input derived by groundwater inflow.

Samples with low C/N ratios and intermediate-low $\delta^{13}C_{org}$ values (Group 1) as well as with high values of H/C and abundance of low molecular weight n-alkanes, are interpreted as deriving from phytoplankton. These signatures are predominant in the lower part of the core (ca. 1Ma-400 ka B.P.) and can be related to wet episodes, which caused the water-body level to rise.

From ca. 400 ka to ca. 180 ka B.P. (60 to 36.0 m), alternating episodes linked to wet/dry phases with dominancy of grasses or trees and aquatic macrophytes, respectively, have been identified by the atomic H/C ratio.

Two important warm-wet episodes, interpreted from low C/N and high $\delta^{13}Corg$ values (Group 3), occurred at ca. 180 to 170 ka B.P. (36-33.6 m) and at ca. 20 ka B.P. (6.7 m). The former can be correlated with the marine isotopic stage (OIS) 7a; and the latter with the climatic optimum published by Florschütz et al. (1971). The 20 ka B.P. climatic optimum was also identified in Padul in an earlier study by Valle et al. (2003).

The global climatic changes occurring from ca. 170 to 25 ka B.P. (33.6 to 7 m) are not recorded by some proxies. During this period, H/C and C/N ratios and $\delta^{13}C_{org}$ values varied little, although significant variations occurred in the pollen log and in the relative percentages of C27, C29 and C31 n-alkanes. However, important changes linked to the Last Glacial Maximum and the beginning of the Holocene were detected (metres 7-4.5). Samples with lower $\delta^{13}C_{org}$ values, coinciding with high atomic C/N ratios, atomic H/C ratios between 1.3 and 1.7 and with a predominance of n-alkane chains of 31 carbon atoms, represent cold-dry phases. This caused the recession of temperate forests and the extension of grasses. After these periods, both temperature and precipitation recovered, causing the expansion of temperate forests and a rise in water level of lakes, which is associated with a major production of lacustrine algae. These latter episodes are characterized by samples with intermediate C/N ratios and $\delta^{13}C_{org}$ values, as well as by H/C ratios characteristic of phytoplankton or trees, and C_{27} or C_{29} predominant n-alkanes.

Few changes during the Holocene (uppermost 4.5 metres) were recorded in the palaeoenvironmental proxies, though there are indications that there were alternating wet and dry episodes.

The predominant n-alkane chain provides evidence of organic matter origin and, in general, is consistent with the interpretation made from the other proxies.

4 Summary and Implications for Palaeohydrogeology

4.1 INTRODUCTION

Mineralogical and geochemical studies have been carried out on fracture-flow groundwater systems at six European sites in the PADAMOT project. These include:

- Melechov Hill, in the Bohemian Massif of the Czech Republic: a shallow (0-100 m) dilute groundwater flow system within the near-surface weathering zone in fractured granitic rocks;

- Cloud Hill, in the English Midlands: a (~100 m) shallow dilute groundwater flow system in fractured and dolomitized Carboniferous limestone;

- Los Ratones, in southwest Spain: an intermediate depth (0-500 m) dilute groundwater flow system in fractured granitic rocks;

- Laxemar, in southeast Sweden: a deep (0-1000 m) groundwater flow system in fractured granitic rocks

- Sellafield, northwest England: a deep (0-2000 m) groundwater flow system in fractured Ordovician low-grade metamorphosed volcaniclastic rocks and discontinuous Carboniferous Limestone, overlain by a Permo-Triassic sedimentary sequence with fracture and matrix porosity;

- Dounreay, northeast Scotland: a deep (0-1400 m) groundwater flow system in fractured Precambrian crystalline basement overlain by fractured Devonian sedimentary rocks.

The project aimed to develop and evaluate methods for obtaining information about past groundwater evolution during the Quaternary (about the last 2 million years) by examining the late-stage mineralization that might record mineralogical, petrographical and geochemical evidence of how the groundwater system may have responded to past geological and climatological changes.

In addition, a study has been made of two Quaternary sequences in Andalusia in southeastern Spain to provide a basis of estimating the palaeoclimatic history of the region that could be used in any reconstruction of the palaeoclimatic history at the Los Ratones site. The Cúllar-Baza lacustrine sequence records information about precipitation and palaeotemperature regimes, based largely on the analysis of the stable isotope (δ^{18}O and δ^{13}C) signatures from biogenic calcite (ostracod shells). The Padul Peat Bog site study derived information on past vegetation cover and palaeogroundwater inputs based on the study of fossil pollen and biomarkers as proxies for past climate change.

In the case of the Los Ratones site, late-stage mineralization is either absent or extremely scarce, and both the quantity and fine crystal size of any late-stage fracture mineralization relevant to Quaternary palaeohydrogeological investigations is difficult to work with. The results from the material investigated during the PADAMOT studies indicate that quartz and carbonate fracture fillings are related to hydrothermal activity, and so do not have direct relevance as Quaternary indicators. Neoformed calcite has not been found at this site at the present depth of the investigations. Furthermore, the HCO_3^- concentration in all the Los Ratones groundwaters is mainly controlled by complex carbonate dissolution. The carbonate mineral saturation indices do not indicate precipitation conditions, and this is consistent with the fact that neoformed calcite, ankerite or dolomite have not been observed petrographically.

4.2 MINERALOGICAL INDICATORS OF PALAEOSALINITY IN FRACTURE MINERALIZATION

4.2.1 Fluid inclusion studies

Fluid inclusions preserve a 'snap-shot' sample of past groundwaters, and provide the only direct means of quantitatively determining salinity and confirming the presence of conservative elements such as chlorine in palaeogroundwaters. Furthermore, short residence times and lack of mineral-fluid equilibrium at low temperatures for some elements introduces large uncertainties into solute concentration estimates based solely on thermodynamic calculations. It has been shown that it is possible to obtain salinity and microchemical data for palaeogroundwaters from fluid inclusions in the late-stage calcites. This has been achieved successfully at Sellafield, Dounreay and Laxemar during the PADAMOT and earlier studies. However, a number of factors constrain the use of fluid inclusions for palaeohydrogeological reconstruction:

- Size of inclusions;

- TDS of inclusion fluids;

- Analytical detection limits

Late-stage calcite contains a very low abundance of fluid inclusions in all of the sites where it has been observed (Sellafield, Dounreay, Cloud Hill, Laxemar and Äspö). This is a typical feature of low-temperature calcite mineralization, where crystals often grow slowly with less likelihood of conditions favourable for trapping fluid inclusions on nucleating mineral surfaces. Most inclusions that are observed are located within the early cores of calcite crystal, often concentrated along the interface between the corroded older mineralization that has acted as a 'seed' crystal. Inclusions within later, outer growth zones of the calcite are generally absent or, at best, very rare. This means that fluid inclusions cannot realistically be used to study the more recent evolution of the groundwater systems at these four sites. Furthermore, inclusions that are present are typically very small (<5 μm), making it very difficult to make microthermometric observation and measurements of subtle phase changes required to determine salinity characteristics. The small size of the inclusions also severely restricts the ability to undertake microchemical analysis using LAMP-ICP-MS techniques because the inclusions furnish very low mass of materials, which is often below detection limits.

The detection limit for fluid inclusion salinity determination places significant constraints on the application of the technique to reliably differentiate between freshwater and brackish water. Salinity determination is limited by the precision of the measurement of temperature. Modern fluid inclusion analysis equipment can measure temperatures to a limit of precision of ±0.1 °C. This translates into a precision of 0.2 wt. % NaCl eq. (i.e. 2000 ppm NaCl eq.). Therefore, for dilute palaeofluids, this places an effective detection limit for fluid inclusion analysis at 0 ±0.1 °C which equates to a salinity of 2000 ppm NaCl eq. (or 1213 ppm Cl eq.). This makes it very difficult to distinguish between brackish water and freshwater in the upper part of the STZ at sites like Sellafield and Dounreay, or to differentiate the different episodes of fresh and brackish recharge at sites such as Laxemar and Äspö. In this respect, calcite crystal morphology may provide a better and more sensitive indication of palaeosalinity changes in low-salinity groundwater systems.

In order to overcome the above practical limitations with inclusion abundance, future palaeofluid geochemical studies need to allocate considerably more time and resources to this approach. Even using the Dounreay or Sellafield sites (as examples where late-stage calcites are particularly well-developed), to unequivocally identify the principal palaeofluids involved, their spatial distribution and evolution with time would probably necessitate at least a 10-fold increase in effort. This obviously has significant cost implications for any palaeohydrogeological investigation.

Fine-grained fracture cements and aluminosilicate minerals currently remain outside the scope of integrated mineralogical-fluid inclusion studies, but given the development of millimetric, crystalline, fracture cements, there is no theoretical reason why this approach cannot be applied to most quartz-carbonate-sulphate mineral assemblages.

4.2.2   Studies of the distribution and morphology of late-stage calcite

As a result of the PADAMOT studies calcite morphology has now been studied at several study sites (Sellafield, Dounreay, Äspö, Laxemar and Cloud Hill). At Sellafield, Dounreay and Cloud Hill, is has been shown that there is a relationship between the crystal morphology of late-stage calcite mineralization and either present groundwater composition or palaeogroundwater composition, as demonstrated by fluid inclusion studies. This confirms observations from previous studies at the Sellafield site, which demonstrated that the crystal morphology of the late-stage calcite mineralization varied systematically with groundwater salinity (Milodowski et al., 1995; 1997, 1998a, 2002; Bath et al., 2000). Limited studies at Äspö during the EQUIP project also indicated that there was a relationship between calcite morphology and groundwater salinity (1998b). However, this relationship is not so clear at the Laxemar site, although at this site the variations in calcite morphology can be interpreted in terms of palaeo-variations in salinity, principally because of fluid inclusion evidence and by analogy with Sellafield. However, the relationship with present groundwater chemistry is unclear. It was also found that the occurrence and distribution of late calcite in fractures in drill cores can be used to identify and predict the location of potential flowing features in the boreholes at all of these sites.

Calcite precipitated in freshwater characteristically forms short c-axis crystals ('nailhead' calcite), whereas in saline groundwaters the calcite morphology is characterized by c-axis elongated crystal forms ('dog-tooth' or 'scalenohedral' calcite). Examination of calcite growth zoning using CL or microchemical mapping provides a means of following the morphological changes during the growth of the calcite, thereby proving a proxy for the evolution of the salinity of the groundwater system.

In the case of Sellafield, the morphological variation is very well-defined, and the interval over which the crystal morphology changes - the 'Morphological Transition Zone' (MTZ) - occurs just above the modern Saline Transition Zone (STZ) between the shallow freshwater zone and the deeper saline groundwater (arbitrarily defined on the basis of electrical logs at approximately 3500 to 6000 mg/L chloride). Comparison with the salinity of the modern groundwater shows that the base of the MTZ, marked by the transition from equant to c-axis elongated calcite, occurs between 1000-2000 mg/L chloride. The top of the MTZ, marked by the transition from short c-axis to equant calcite, is less well defined but appears to occur at salinities >300 mg/L chloride. Calcite morphology therefore provides a sensitive indicator of changes in palaeosalinity in dilute groundwater systems, and can be used to differentiate fresh from brackish or saline groundwaters. In this respect, it has potential advantages over the use of fluid inclusion studies (Section 4.4.1) where this salinity differentiation is severely limited. However, the change from brackish to very saline groundwaters or brines is not marked by any obvious morphological change. Fluid inclusions studies provide a better means of monitoring changes within this higher salinity range.

Calcite morphology and observations of crystal growth fabric at the Sellafield site suggest that the location of the interface between the shallow fresh groundwater and the deeper saline groundwater (STZ) has changed with time. In general across the site, the morphology and growth fabrics of ME9 calcite within the MTZ, revealed by CL, show that later freshwater-type (c-axis flattened crystal forms) calcite has grown on earlier cores of more saline-type (c-axis elongated crystal forms) calcite within the MTZ, indicating an overall progressive downward movement (between 50 to 150 m) of the MTZ/STZ during the more recent palaeohydrogeological history of the Sellafield site. However, there is some evidence for the palaeo-position of the STZ having moved in the opposite direction along a few localised

fractures or fracture zones. Rare observations of saline-morphology calcite nucleated on top of (i.e. younger than) freshwater-morphology ME9 calcite in the east of the site (borehole BH9A – PRZ/RCF area) suggest deeper penetration of freshwater in the past, and that this saline water-freshwater interface may have been depressed by between 100-200 m and may have occurred along a very localised fractures or fracture zones. This might reflect 'fingering' of freshwater along a small number of more conductive, fracture flow paths that perhaps responded more rapidly than the bulk of the flow system, to short-lived enhanced freshwater flushing events in the past. Similarly, the distribution and relationships of ME8 and ME9 mineralization also suggest locally deeper penetration of more oxidizing palaeo-waters than at present. ME8 iron and manganese oxyhydroxides occur to maximum depths, which increase from east to west. The maximum depth of ME8 oxide mineralization coincides closely with the top of the MTZ in the PRZ/RCF area and further east but extends virtually to the base of the MTZ in the Fleming Hall Fault Zone area. ME9 calcite rests on, and contains inclusions of, this ME8 mineralization, with 'below-MTZ type' ferromanganoan calcite (containing reduced iron and manganese) now present above these depths. The greater depth of development of ME8 mineralization in the Fleming Hall Fault Zone may be a result of this fault zone being locally more conductive, and having facilitated deeper penetration by fresh, oxidizing palaeogroundwater. However, limited isotopic age dating suggests that some of the ME8 mineralization may be late Miocene, and therefore may represent deep Tertiary weathering following regional uplift at that time, rather than deep Quaternary meteoric groundwater invasion.

At Dounreay, the position of the calcite MTZ (152-376 m bRT) does not coincide with the present-day STZ from fresh to brackish/saline water, the top of which starts at about 750 m bRT. This implies that the late calcite MTZ at Dounreay reflects the position of an older STZ, and that the overall position of the STZ must have moved significantly downwards over time. This implies, as at Sellafield, a deeper influx of modern freshwater, compared to shallower palaeowaters, which were more saline at shallow depth. This is also supported to some extent by the fluid inclusion data, which show the presence of much more saline inclusion fluids than the present groundwater. However, a high proportion of the fluid inclusion information is derived from geologically old core zones of the calcite, so this evidence may not be relevant to palaeohydrogeology in the timescale of interest. A novel feature of Dounreay is the possibility that modern low-salinity water has penetrated along one flowing fracture zone, to depths (1172 m bRT) well below the present STZ. This suggests that ancient flushing of waters may have been mediated by a suite of individual inputs rather than through a uniform flow front.

At Laxemar, the calcite morphology is variable and complex. There is an overall change in calcite morphology consistent with an increase in salinity from shallow freshwater to more saline groundwater with depth in the upper 200 m. Below this depth calcite reverts to short *c*-axis and equant forms, implying more dilute water in the past. Despite the complexity of the downhole variation, characterization of the calcite crystal morphology, integrated together with stable isotope, strontium isotope, and trace element geochemical characteristics, has proved very useful for differentiating calcites precipitated from different groundwaters and provides a possible method to identify "end member" calcite types. Based on morphological studies, freshwater-type late calcite mineralization has been identified in fractures at ~1000 m bgl at this site. This is consistent with concepts that dilute groundwater may have penetrated to significant depths, along localized fracture flow paths at Laxemar.

Overall, at the four sites where it has been studied (Laxemar, Sellafield, Dounreay and Cloud Hill), crystal morphology and growth fabric information from late calcite have been shown to be a potentially powerful tool for following the evolution of palaeogroundwater salinity. It can successfully be used to map palaeo- fresh-saline groundwater interfaces and to study the movement of these interfaces over time. Anomalous calcite morphology (i.e. freshwater-type calcite occurring within a volume of rock mass dominated by saline-type calcite or vice-versa) might identify zones or 'fingering' of locally-enhanced conductivity (or 'fast flow paths'), which have reacted more rapidly than the surrounding rock mass to past palaeohydrogeological events.

It might also provide a useful insight into the interconnectivity or compartmentalization of groundwater flow paths.

A problem encountered at both the Laxemar and Dounreay sites was the limited extent of late-stage calcite growth. Volumetrically, late-stage calcite forms a very small proportion of the calcite vein mineralization, compounded by its presence often only as very thin overgrowths on older calcite. Where this happens the late-calcite superficially inherits the morphology of the older calcite substrate and may lead to erroneous interpretation. This is not a problem in fractures where the late calcite is more extensive in development, and has been able to develop its own morphological identity. Care must be taken in using calcite morphological observations to assess the characteristics of the overgrowths in relation to the 'seeding' carbonate substrate. This would normally require that cathodoluminescence petrography is carried out to check growth-zoning fabrics for evidence of subtle changes in preferential crystal face development.

Very narrow veins also present a problem because they provide only restricted space for crystal growth. Consequently, only partial crystal face development may be possible in such confined space and as a result the crystal form is difficult to distinguish from visual core inspection or SEM observations. Detailed optical petrographical analysis, coupled with CL petrography, may be required to identify crystallographic orientations and faces in these situations.

4.2.3 Analysis of halogens in calcite by ion microprobe

Ion-microprobe technology was successfully used to investigate trace Cl and Br variations in late calcite from the Sellafield site. The high spatial resolution of the ion-microprobe enabled variation in trace elements such as Br and Cl to be determined for the first time in the individual fine-scale growth zones in the calcite revealed by CL. The ability to record other trace elements and oxygen isotope information from the same calcite zone, using ion microprobe technology, presents the opportunity to examine co-variations between isotopic composition, chemistry and salinity variations.

Data were obtained from two calcite samples: one from the shallow fresh groundwater above the MTZ and one from below the STZ. Variations in Cl and Br were observed in the calcites that suggest varying cycles of salinity. In the calcite from the shallow groundwater, two cycles of salinity appear to be recorded from inner bright CL zones, to outer dark CL zones. In contrast the calcite sample in the deep saline groundwater zone (1527m) shows less varying salinity, with much higher Br suggestive of a more continuous history of the basement water regime.

The ion microprobe data obtained from these two samples appears to show the potential signatures of ancient groundwater salinity. The Br:Cl ratio can potentially be used to track water origins, and compare directly with modern water analyses. However the ratio values from either sample are unlike those from present-day waters at Sellafield reported by Bath et al (1996), implying that a selective fractionation may have occurred.

4.3 MINERALOGICAL INDICATORS OF REDOX CHANGES IN FRACTURE MINERALIZATION

4.3.1 General

LAMP-ICP-MS and ion microprobe techniques have been successfully used to obtain trace element data from late-stage calcite mineralization. Both techniques have comparable sensitivity for trace element analysis of calcites. LAMP-ICP-MS has an advantage of being able to provide a greater number of analyses more rapidly than the ion microprobe, and cost of the LAMP-ICP-MS equipment is substantially less than for ion microprobe facilities. However, the ion microprobe has the advantage of better spatial resolution and more controllable sample ablation. The LAMP-ICP-MS laser can be reduced to a spot size of about 5 μm, which provides a

resolution similar to the ion microprobe but analytical sensitivity is reduced. Thermal shock and rapid thermal expansion of the calcite under the laser probe can sometimes cause the calcite crystals to shatter, particularly near the edges of crystals. However, advances in laser technology and ICP-MS development are likely to result in better micro-sampling resolution and analytical sensitivity in the future.

4.3.2   Iron and manganese variations in late-stage calcite

Late-stage calcites from Laxemar, Sellafield, Dounreay and Cloud Hill all display fine scale growth zone variations in Fe and Mn, which can be potentially attributed to factors influencing redox. These are reflected in variations in the CL characteristics of the calcite.

Shallow, freshwater-zone calcites from Sellafield and Cloud Hill are characterized by very sharp oscillatory zones of brightly luminescent and non-luminescent bands. These correspond to luminescent manganoan calcite, and non-luminescent non-ferroan/non-manganoan calcite, respectively. Their distribution is closely associated with that of iron and manganese oxyhydroxide mineralization, suggesting growth in dominantly oxic groundwaters, with episodic periods of mildly reducing conditions with respect to the MnII/MnIII (or MnIV) couple.

In the deeper parts of the freshwater zone, and below the STZ at Sellafield, all of the late-stage calcite is ferromanganoan. CL banding reflects variations in Fe:Mn, with low ratios corresponding to periods when iron was probably being preferentially incorporated into co-precipitating pyrite or marcasite – i.e. corresponding to periods of sulphate reduction. This suggests that reducing conditions have prevailed below the STZ at Sellafield, although the value of Eh cannot be directly determined by this method. The Fe:Mn variations in the calcites might be explained by fluctuations in microbial activity associated with the low-temperature reduction of sulphate to sulphide.

In contrast to the Sellafield site, the late-stage calcites from the freshwater zone at Dounreay are dominantly manganoan and magnesian. They lack both the striking zoning pattern of alternations of non-luminescent, non-ferroan, non-manganoan calcite and brightly luminescent manganoan calcite, and the marked Ce-depletion that characterizes the 'above-MTZ type' ME9 calcite at Sellafield. This may indicate that, unlike Sellafield, the freshwater zone has, in general, never been strongly oxidizing throughout most of the sequence in Dounreay borehole NDN1 (except at very shallow levels affected by recent weathering, and associated with pyrite and ferroan carbonate dissolution and oxidation). The absence of strongly oxidising conditions in the freshwater zone may be related to:

- Effective redox buffering of the groundwater by interaction with the hydrocarbon/organic rich and pyritic Devonian cover rocks;

- Dominantly upward or lateral flow of groundwater, rather than downwards flow of oxidizing meteoric water.

However, significant redox variations may be influenced by localised fracture flow paths. The deepest sample of late-stage calcite studied below the STZ in borehole NDN1 (1172 m bRT) displayed overgrowths of freshwater-type calcite on earlier saline water-type calcite. The CL characteristics of the calcite overgrowths are similar to that seen in the 'above-MTZ type' ME9 calcite from Sellafield, displaying well-developed oscillatory zoning of manganoan and non-manganoan calcite. This may indicate relatively recent penetration to significant depths by dilute and possibly oxidizing groundwater along localised fracture flow paths. This is similar to observations in the Laxemar site, where oxidizing groundwaters in localised flow paths may account for a similar freshwater-type calcite found in isolated fractures at depth.

4.3.3 REE geochemistry of late-stage calcite

Ion microprobe and LAMP-ICP-MS have been used to examine fine-scale variations in REE chemistry of the late stage calcites from Sellafield, Dounreay and Cloud Hill. At Sellafield, a marked negative Ce anomaly is observed in the non-luminescent non-ferroan/non-manganoan calcite growth bands of the above MTZ-type calcite, indicative of formation under oxidizing conditions, and confirming conclusions based on consideration of the Fe and Mn content. In contrast, the alternating brightly luminescent manganoan calcite bands show no Ce anomaly, which implies that they formed under less strongly oxidizing conditions. Deeper in the freshwater zone, and below the STZ, there is no evidence for a marked Ce anomaly in calcites, suggesting that oxidizing groundwaters have not penetrated deep into this part of the groundwater system in the recent past (Quaternary).

Late stage calcites from Dounreay and from Cloud Hill also lack any evidence of Ce anomalies. This implies that these two groundwater systems, even at shallow depth or along the deeper localised flow paths, have not experienced conditions as strongly oxidizing as has the shallow system at Sellafield.

At Sellafield, the Ce anomaly occurs in the latest growth zones of the calcite. However, this does not coincide with the depleted $\delta^{18}O$ values in calcite that were detected by ion microprobe, and which might be attributed to glacial groundwater. Therefore, it appears that the most oxidizing groundwaters from which the late calcite grew are not obviously linked to a glacial origin. Furthermore, the Mn and Fe contents or the REE characteristics of the late calcite suggest that there is no evidence for oxidizing conditions at depth associated with groundwaters of potentially glacial origin. This is similar to the conclusions from the Laxemar site, where observations also suggest that although waters of potentially glacial origin can be identified (on the basis of groundwater $\delta^{18}O$ values) at depths of 1000 m there is no evidence that invasion by glacially-recharged water produced oxidizing conditions.

4.4 MINERALOGICAL INDICATORS OF GROUNDWATER ORIGIN AND PALAEOENVIRONMENTAL IMPACTS

4.4.1 Bulk geochemical characteristics of calcite fracture mineralization

At the Laxemar and Äspö sites, integration of stable carbon and oxygen isotope and Sr isotope data and trace element (REE, Sr, Ba, Mn) data obtained on bulk samples of late calcite fracture mineralization, together with observations on calcite morphology and fluid inclusion data, enabled the differentiation of six different types of calcite that might be related to different palaeohydrogeological regimes:

- Type 1, with characteristics interpreted to represent low-temperature calcite precipitated from water similar to present-day meteoric;

- Type 2, with characteristics interpreted to represent low-temperature calcite precipitated from groundwater recharged by a Baltic Sea water composition during conditions of high biogenic activity;

- Type 3, with characteristics interpreted to represent low-temperature calcite precipitated from groundwater recharged by a more oceanic water composition;

- Type 4, with characteristics interpreted to represent precipitation from a cold climate meteoric water (glacial component?);

- Type 5, with characteristics interpreted to represent old calcite mineralization deposited by a warm hydrothermal brine;

- Type 6, with characteristics interpreted to represent old high temperature hydrothermal mineralization.

Using this approach, low-temperature calcite, of possible brackish to marine groundwater origin (Type 2 and 3), is found down to depths of 200 m in Laxemar and 500 m in Äspö. In contrast, low-temperature calcite of dilute meteoric origin (Type 1) is found over a wide depth range from the surface to at least 950 m, indicating a deeper penetration of fresh groundwater in the past. Calcite possibly precipitated from recharged glacial meltwater (Type 4) has previously been distinguished in the Äspö area. However, no evidence of Type 4 calcite has been found during this study at Laxemar. Although some fresh water calcites from Laxemar have an isotopic composition that indicates precipitation from a water slightly lighter in $\delta^{18}O$ than the present groundwater, these calcites are not clearly differentiated from the Type 1 calcites, and are therefore included in this group. Present-day groundwater with various proportions of a glacial meltwater component (isotopically-determined) has however been identified at depth from 100 to 1100 m in the Laxemar area. Two possible explanations for this are:

- The intrusion of glacial meltwater did not result in any calcite production, or;

- The amount of glacial meltwater component in the present groundwaters is small, and has not been identified so far.

4.4.2 High spatial resolution studies of growth zone variations in $\delta^{18}O$ and $\delta^{13}C$ in late-stage calcite

He-LACE, LAMP-ICP-MS and ion microprobe techniques have been successfully used to micro-sample and analyse individual growth zones in crystals of late-calcite mineralization at Sellafield, in order to evaluate the variation in trace element and stable isotope ($\delta^{18}O$ and $\delta^{13}C$) compositions at different stages of crystal growth. Several advantages and disadvantages of these techniques were encountered.

4.4.2.1 IMPACT OF SAMPLE PREPARATION

The sample preparation methodology used for the different techniques had a significant impact on their application.

Initial trials at the BGS showed that conventional epoxy-resin-impregnated polished thin sections or polished epoxy-resin blocks could not be used for He-LACE studies. This is because the epoxy-resin decomposes and evolves some CO_2 as it gets hot during laser ablation. Consequently, attempts were made to prepare samples for He-LACE analysis by embedding the calcite crystals in blocks of Plaster of Paris, and then cutting and polishing their surfaces. This overcame the problem of isotopic contamination but the surfaces were too poorly polished for CL characterization. The BGS subsequently developed a method of mounting the calcite in a low melting point Bi-Pb-Sn alloy (M70 alloy). Where individual calcite crystals could be readily separated and mounted (e.g. Sellafield site), reasonably good quality polished sections could be produced. However, when samples had to be prepared with calcite crystals still attached to fragments of wallrock, the differential hardness between the silicate wallrock, and the M70 alloy and calcite made a good polished surface difficult to achieve (e.g. Dounreay, Laxemar, Los Ratones). The quality of the polished surface has a major impact on the quality of CL images that could be obtained from the mounts, and which were essential for relating the analysis points to the crystal growth fabric.

In contrast, the ion microprobe at the University of Edinburgh employed polished thin sections prepared from material mounted conventionally in epoxy-resin. The sections were prepared slightly thicker than for standard polished thin sections to facilitate ion-beam ablation. This enabled a high-quality surface polish, and thus allowed high-quality CL images to be acquired from the samples. Furthermore, the use of polished thin sections has a major advantage in that

the samples can be examined and analysis points located using optical transmitted light microscopy, as well as by use of SEM with element mapping. Optical transmitted light microscopy is not possible using the M70 polished metal blocks.

For reasons of efficiency and budgetary constraints, the BGS LAMP-ICP-MS studies utilised the same M70 mount prepared for He-LACE analysis. However, M70 mounts are not a requirement for LAMP-ICP-MS analysis, and the application of this analytical method would be much improved in any future study by the use of the same type of polished sections as used for ion microprobe studies during PADAMOT.

4.4.2.2 COMPARISON OF ION-MICROPROBE AND LASER MICROBEAM RESULTS

The ion microprobe was found to have a much better spatial resolution than the two laser micro-sampling techniques. This enabled the very fine overgrowths and fine-scale growth zoning to be precisely sampled for both trace element and $\delta^{18}O$ isotope analyses. In contrast, the two laser-based techniques produced much coarser-scale sampling. In particular, the current BGS He-LACE laser system was not able to provide the very fine spatial resolution needed to sub-sample some of the ME9 calcite zones, particularly the later growth zones. Thermal shock and rapid thermal expansion of the calcite under the laser probe can sometimes cause the calcite crystals to shatter, particularly near the edges of crystals. However, advances in laser technology and mass spectrometry development are likely to result in better micro-sampling resolution and analytical sensitivity in the future.

For stable isotope studies, He-LACE analysis has an advantage over the ion microprobe by being able to provide both $\delta^{18}O$ and $\delta^{13}C$ data simultaneously, whereas the ion microprobe is set up to determine the isotopic composition of only one element ($\delta^{18}O$ in this case) at a time. To provide $\delta^{13}C$ data is feasible if adequate analytical standards for the local instrument are developed. The cost of the He-LACE equipment is also substantially lower than ion microprobe facilities. However, the ion microprobe has much better spatial resolution and more controllable sample ablation, whereas with the coarser micro-sampling by He-LACE it proved much more difficult to relate the analytical data to specific growth zones in the calcite

Despite these differences and problems the ion microprobe and the laser techniques provided corroborative results on the samples studied. Oxygen isotope data obtained by ion microprobe and He-LACE data both identified strongly depleted $\delta^{18}O$ values in calcites from both Sellafield and Dounreay, which provide potential evidence for a significant (30-100 %) component of glacially-recharged groundwater at depth in the past.

4.4.3 Biomarkers in late-stage calcite in deep groundwater systems

Biomarkers have been studied in late-stage mineralization from five of the investigation sites (Sellafield, Dounreay, Laxemar, Los Ratones and Cloud Hill). Potentially, biomarkers might provide information on the origin of the groundwater (via identification of the source of the biomarker) and on palaeoclimatic/palaeoenvironmental conditions in the recharge area (i.e. organics derived from the soil zone processes and different types of plants). Although only a limited number of samples have been analysed during the PADAMOT project, the study found evidence at three sites (Sellafield, Dounreay and Laxemar) that biomarkers can be preserved in late calcite mineralization. Unfortunately, the biomarkers are only present in low abundance, and because the amount of fracture calcite that is available for analysis is typically very small, analysis was very close to analytical detection limits of the GC-MS technique used. In this study, only a few organic compounds were detected, many of which have ambiguous origins. In a few cases, biomarkers indicative of possible plant origins were detected (Sellafield, Laxemar), which may have been derived during recharge of the groundwater through the soil zone. Unfortunately, the dataset is too small to make any reliable interpretation. Nevertheless, the work completed in PADAMOT has demonstrated the feasibility of finding biomarkers in the late

calcite. As analytical methods improve in sensitivity the study of biomarkers may allow the development of this application in future palaeohydrogeological studies.

The carbonate fracture mineralization analysed from the Los Ratones site does not have biomarkers, which supports the argument that the carbonate mineralization is geologically old.

4.5 PALAEOCLIMATE RECONSTRUCTION

Palaeoclimatic reconstructions have been successfully carried out for the Cúllar-Baza Basin and the Padul Basin in southern Spain in order to provide a regional understanding of climate change and recharge variations during the Quaternary.

In the Cúllar-Baza Basin study, it was found that the $\delta^{18}O$ signature of ostracod shells provided a good proxy for global climatic variations from 2 Ma to the upper part of the Middle Pleistocene (279 ± 77 ka). The variation in $\delta^{18}O$ reflected changes in the evaporation/inflow ratio of the water bodies and the amount of rainfall. A good correlation was found between the ostracod $\delta^{18}O$ variation and the deep-sea oxygen isotope (OIS) record, and with palaeoclimate proxies in other Quaternary basins in the Mediterranean area.

In the Padul Basin study, it has been shown that the concentration of organic carbon, the atomic H/C and C/N ratios, the $\delta^{13}C_{org}$ and CPI values, and the distribution of organic biomarkers (*n*-alkanes) proved to be excellent palaeoenvironmental proxies for evaluating palaeoclimatological and palaeohydrogeological evolution. Used together, these measurements can be used to provide information on the nature of plant cover, which can be used to infer the palaeoclimatic conditions within the basin region. This in turn can be used in modelling past recharge and water balances.

4.6 EVOLUTION OF GROUNDWATER FLOW PATHS AND FLOW PROPERTIES

Although secondary porosity has long been recognised as an important factor in controlling the hydrogeological properties of hydrocarbon reservoirs (Schmidt and McDonald, 1979), it is seldom considered in evaluating the long-term evolution of fracture-controlled groundwater systems in repository PA. In most cases, the distribution of fracture porosity is considered to be tectonically- or structurally-controlled. However, petrological investigations on core samples from the Sellafield site, and to some extent on samples from the Dounreay site and the Äspö-Simpevarp-Laxemar area (cf. earlier EQUIP study observations by Milodowski et al, 1998b) show that secondary porosity is an important component of the porosity of both shallow and deep groundwater systems at these sites. In the case of Sellafield, most of the present-day fracture porosity in the shallow and deep groundwater system and a large proportion of the matrix porosity in the shallow sandstone aquifer are the results of dissolution of minerals, primarily anhydrite, gypsum, dolomite-ankerite and, in the near-surface, calcite. Consequently, the shallow and deep groundwater flow paths, and their porosity and permeability distributions, have evolved over time since uplift, weathering and erosion introduced recharge of meteoric water at Sellafield during the Tertiary period.

Dissolution of those pre-existing fracture-filling and matrix minerals would have been a major contributor to saturated compositions of groundwaters from which new generations of secondary minerals were precipitated. Solutes derived from dissolution of ankerite and ferroan dolomite would have contributed to ME8 Mn and Fe oxide and dissolved calcium from anhydrite/gypsum would have stimulated precipitation of ME9 calcite. Therefore permeability on a regional scale has been affected over time by both dissolution and precipitation, with the general pattern being that precipitation would have taken place down-gradient of dissolution. The mass transfer involved in the overall process, and therefore the effect on permeability, decreases with depth because of smaller water fluxes and more equilibrated compositions. Mass transfer via groundwater flux through the system suggests that cumulative dissolution should be slightly

greater than precipitation, and this is certainly the case in the shallow system, but it is uncertain for the deeper system as also is the local spatial variability of the processes.

At present, PA models do not generally account for the progressive evolution of site characteristics such as porosity, permeability, and water chemistry, and define these as fixed properties. This limitation follows from the requirement for simulations to be carried out in reasonably short times, particularly where large numbers of realisations are undertaken to explore uncertainties/ranges in parameter values. Thus, it is probably not feasible to incorporate the observed progressive evolution of porosity such as identified at Sellafield into PA simulations directly. Instead, the observations made during PADAMOT and EQUIP are presently more relevant for specifying conceptual models and scenarios on which the PA simulations are based.

The potential limitation of PA models in their inability to consider the evolution of porosity and permeability, and changes in flow paths due to mineral dissolution (which will also affect factors such as matrix diffusion and changes in surface with which radionuclides transported in the groundwater will interact) may need to be examined more closely in future.

References

ACKHURST, M.C., CHADWICK, R.A., HOLLIDAY, D.W., McCORMAC, M., McMILLAN, A.A., MILLWARD, D AND YOUNG, B. 1997. *Geology of the West Cumbria District.* British Geological Survey Memoir, England and Wales, Sheets 28, 37 and 47. Keyworth, Nottingham.

ÅHÄLL, K.-I. 2001. Åldersbestämning av svårdaterade bergarter i sydöstra Sverige. *Swedish Nuclear Waste and Fuel Management Co (SKB) Progress Report*, **R-01-60**, 28 pp.

ALLAN ET AL. 2005 (in prep.) Validation of LA-ICP-MS fluid inclusion analysis with synthetic fluid inclusions.

AMBROSE, K. AND CARNEY, J.N. 1997a. Geology of the Calke Abbey Area, 1:10 000 Sheet SK32SE: Part of 1:50 000 Sheet 141 (Loughborough). *British Geological Survey, Technical Report,* **WA/97/17**.

AMBROSE, K. AND CARNEY, J.N. 1997b. Geology of the Breedon-on-the-Hill Area, 1:10 000 Sheet SK42SW: Part of 1:50 000 Sheet 141 (Loughborough). *British Geological Survey, Technical Report,* **WA/97/42**.

ANDERS, E., AND GREVASSE, N. 1989. Abundances of the elements: meteoritic and solar. *Geochimica et Cosmochimica Acta*, **53**, 197-214.

ANDRA. 2002. *BIOCLIM Deliverable D2: Site-specific and Palaeo-environmental Data,*. Agence Nationale pour la Gestion des Déchets Radioactifs, Parc de la Croix Blanche, 1/7, rue Jean-Monnet, 92298 Châtenay-Malabry, France.

ARRIBAS, A. 1962. Mineralogía y metalogenia de los yacimientos españoles de uranio. "Los Ratones", Albalá (Cáceres). *Estudios Geológicos*, **XVII**, 117-131.

ARRIBAS, A. 1975. Caracteres geológicos de los yacimientos españoles de uranio. *Studia Geológica*, **IX**, 7-63.

BAILEY, D.E. (compiler). 2002. Constraining the timing of movements on faults in the Sellafield area. *British Geological Survey Technical Report*, **WG/97/36**.

BARCLAY, W.J., GLOVER, B.W., HIGHTON, A.J. AND ROBERTSON, S. 1992. The geology of Dounreay Number 1 borehole. *United Kingdom Nirex Limited Report*, **185**. United Kingdom Nirex Limited, Harwell.

BARR, D., HOLDSWORTH, R.E. AND ROBERTS, A.M. 1986. Caledonian ductile thrusting in a Precambrian metamorphic complex: the Moine of northwestern Scotland. *Geological Society of America Bulletin*, **97**, 754-764.

BASHAM, I.R. 2000. Microfractures and uranium distributions in specimens from basement lithologies in Caithness, northern Scotland. *British Geological Survey Technical Report*, **WG/90/19**.

BATH, A.H., MILODOWSKI, A.E. AND SPIRO, B. 1987. Diagenesis of carbonate cements in Permo-Triassic sandstones in the Wessex and East Yorkshire-Lincolnshire Basins, UK: a stable isotope study. In: MARSHALL, J.D. (EDITOR). *Diagenesis of Sedimentary Sequences.* Geological Society Special Publication, **36**, 173-190.

BATH, A.H., McCARTNEY, R.A., RICHARDS, H.G., METCALFE, R. AND CRAWFORD, M.B. 1996. Groundwater chemistry in the Sellafield area: preliminary interpretation. *Quarterly Journal of Engineering Geology*, **29**, S39-S58.

BATH, A. MILODOWSKI, A.E. RUOTSALAINEN, P. TULLBORG, E.-L. CORTÉS RUIZ, A. AND ARANYOSSY, J.-F. 2000. Evidence from mineralogy and geochemistry for the evolution of groundwater systems during the Quaternary for use in radioactive waste repository safety assessment (EQUIP project). **EUR 19613 EN**, European Commission, Nuclear Science and Technology.

BATH, A.H., RICHARDS, H., METCALFE, R., MCCARTNEY, R., DEGNAN, P. AND LITTLEBOY, A. 2005 (in press). Geochemical indicators of deep groundwater movements at Sellafield.. In: PEYAUD, J-B, DE PUTTER, T AND MCKINLEY, I. (guest editors) *Geochemical Aspects of Radioactive Waste Disposal*, Journal of Geochemical Exploration, Special Volume.

BAXTER, A.N. AND MITCHELL, J.G. 1984. Camptonite-monchiquite dyke swarms of northern Scotland; age relationships and their implications. *Scottish Journal of Geology, 20*, 297-308.

BIELY, A., et al. 1966. *Geological map of Czechoslovakia, 1:1000000*. – Ústřední Ústav Geologický, Praha (Czech Geological Survey).

BISCHOFF, J.L. AND FITZPATRICK, J.A., 1991. U-series dating of impure carbonates: an isochron technique using total-sample dissolution. *Geochimica et Cosmochimica* Acta, **55**, 543-554.

BLACK, J.H. AND BRIGHTMAN, M.A. 1996. Conceptual model of the palaeohydrogeology of Sellafield. *Quarterly Journal of Engineering Geology*, **29**, S83-S94.

BORISENKO, A S. 1977. Study of the salt composition of solutions in gas-liquid inclusions in minerals by the cryogenic method. *Soviet Geology and Geophysics,* Vol. 18, 11-19.

BOUCH, J.E. 2004. Cathodoluminescence petrography and fluid inclusion microthermometry of vein calcites from Laxemar borehole KLX-01, Sweden. *British Geological Survey, Commissioned Report*, **CR/04/161**.

BOUCH, J.E., MILODOWSKI, A.E. AND AMBROSE, K. 2004. Contrasting patterns of pore-system modification due to dolomitization and fracturing in Dinantian basin-margin carbonates from the UK. In: BRAITHWAITE, C.J.R., RIZZI, G. AND DARKE, G. (editors). *The Geometry and Petrogenesis of Dolomite Hydrocarbon Reservoirs.* Geological Society, London, Special Publication, **235**, 325-348.

BOUÉ-BIGNE, F., MASTERS, B.J., CRIGHTON, J.S. AND SHARP, B.L. 1999. A calibration strategy for LA-ICP-MS analysis employing aqueous standards having modified absorption coefficients. *Journal of Analytical and Atomic Spectrometry, 14*, 1665-1672.

BOWEN D.Q. 1999. *A Revised Correlation of Quaternary Deposits in the British Isles*. Geological Society Special Report No. 23, The Geological Society Publishing House, Bath.

BRAITHWAITE, C.J.R. AND HEATH, R.A. 1989. Inhibition, distortion and dissolution of overgrowth cements on pelmatazoan fragments. *Journal of Sedimentary Petrology*, **59**, 267-271.

BRAUN, J-J., PAGEL, M., MULLER, J-P., BILONG, P., MICHARD, A., AND GUILLET, B., 1990. Cerium anomalies in lateritic profiles. *Geochimica et Cosmochimica Acta*, **54**, 781-795.

BROOKINS, D.G. 1989. Aqueous geochemistry of rare earth elements. In: LIPIN, B.R. AND MCKAY, G.A. (editors). *Geochemistry and Mineralogy of Rare Earth Elements.* Mineralogical Society of America, Reviews in Mineralogy, **21**, 201-225

BUIL, B. 2002. Caracterización petrológica, mineralógica y geoquímica y evaluación del comportamiento geoquímico de las REE en la fase sólida (granitoides y rellenos fisurales) del sistema de interacción agua-roca del entorno de la Mina Ratones. *Publicación Técnica Enresa* **07/2002** ISSN1134-380X, 155 pp.

BUIL, B. 2004. Estudio comparativo del comportamiento geoquímico de las tierras raras en los procesos de interacción agua-roca desarrollados en sistemas geotermales del Pirineo Central (Lérida) y en el sistema geológico del entorno de Mina Ratones (Cáceres). *Colección Documentos CIEMAT*; ISBN: 84-7834-439-X. NIPO: 402-03-014-2. Eds CIEMAT, 424 pp.

CAÑADA, P. 1984. *Estudio hidrogeológico preliminar y de drenaje de las explotaciones a cielo abierto de lignito de Arenas del Rey y de turba de Padul*. MSc. Thesis, Granada University. 189 pp.

CANDY, I. 2002. Formation of rhizogenic calcrete during glacial stage (Oxygen Isotope Stage 12): its palaeoenvironmental and stratigraphical significance. *Proceedings of the Geologists Association*, **113**, 259-270.

CARBONELL, R, MARTÍ, D., y TRYGVASON, A. 1999b. Estudios Geológico-Estructurales y Geofísicos en Mina Ratones. Informe Final: Geofísica. *Enresa* **10-CJA-IF-02**.

CARNEY, J.N., AMBROSE, K. AND BRANDON, A. 2001a. *Geology of the Loughborough District – A brief Explanation of the Geological Map Sheet 141 (Loughborough)*. Sheet Explanation of the British Geological Survey, 1:50 000 Series Sheet 141 Loughborough (England and Wales). British Geological Survey, Keyworth, Nottingham.

CARNEY, J.N., AMBROSE, K. AND BRANDON, A. 2001b. *Geology of the Country Between Loughborough, Burton and Derby: Sheet Description of the 1:50 000 Series Sheet 141 Loughborough (England and Wales).* British Geological Survey, Keyworth, Nottingham.

CARNEY, J.N., AMBROSE, K. AND BRANDON, A. 2002a. *Geology of the Melton Mowbray District – A brief Explanation of the Geological Map Sheet 142 (Melton Mowbray).* Sheet Explanation of the British Geological Survey, 1:50 000 Series Sheet 142 Melton Mowbray (England and Wales). British Geological Survey, Keyworth, Nottingham.

CARNEY, J.N., AMBROSE, K. AND BRANDON, A. 2002b. *Geology of the Country Around Melton Mowbray: Sheet Description of the 1:50 000 Series Sheet 142 Melton Mowbray (England and Wales).* British Geological Survey, Keyworth, Nottingham.

CATHELINEAU., M.. 1988. Cation site occupancy in chlorites and illites as a function of temperature. *Clay minerals*, **23**, 471-485.

CHENERY, S. AND COOK, J.M. 1993. Determination of Rare Earth Elements in single mineral grains by laser ablation microprobe-inductively coupled plasma mass spectrometry. *Journal of Analytical Atomic Spectroscopy*, **8**, 299-303.

CHLUPÁČ, I., BRZOBOHATÝ, R., KOVANDA, J., STRÁNÍK, Z. 2002. *Geologická minulost České republiky.* – Academia, Praha, 436 p. (Geological past of the Czech Republic).

CRAIG, H. 1961. Isotopic variations in meteoric waters. *Science*, **133**, 1702-1703.

CRAIG, H. 1965. The measurement of oxygen isotope paleotemperatures. In: TONGIORGI, E. (editor), *Stable Isotopes in Oceanographic Studies and Paleotemperatures*. Proceedings of the Spoleto Conference. Consiglio Nazionale delle Ricerche, Pisa: 3-24.

CRANWELL P.A. 1973. Chain-length distribution of n-alkanes from lake sediments in relation to postglacial environmental change. *Freshwater Biology*, **3**, 259-265.

CRANWELL P.A. 1984. Lipid geochemistry of sediments from Upton Broad, a small productive lake. *Organic Geochemistry*, **7**, 25-37.

CRANWELL P.A., EGLINTON, G. AND ROBINSON, N., 1987. Lipids of aquatic organisms as potential contributors to lacustrine sediments-II. Organic Geochemistry 11, 513-527.

DANSGAARD, W. 1964 Stable isotopes in precipitation. *Tellus,* **16**: 436-468.

DARLING, W.G., BATH, A.H. AND TALBOT, J.C. 2003. The O & H stable isotope composition of fresh waters in the British Isles. 2. Surface waters and groundwater. *Hydrology and Earth System Sciences*, **7**, 183-195.

DAWSON, J.B. AND HINTON, R. W. 2003. Trace-element content and partitioning in calcite, dolomite and apatite in carbonatite, Phalaborwa, South Africa. *Mineralogical Magazine*, **67**, 921-930.

DELGADO, A., NÚÑEZ, R., CABALLERO, E., JIMÉNEZ DE CISNEROS, C. AND REYES, E. 1991. *Composición isotópica del agua de lluvia en Granada.* IV Congreso Geoquímica España, **1**, 350-358.

DENNISTON, R.F., SHEARE, C.K., LAYNE, G.D. AND VANIMAN, D.T. 1997. SIMS analysis of minor and trace element distributions in fracture calcite from Yucca Mountain, Nevada, USA. *Geochimica et Cosmochimica Acta*, **61**, 1803-1818.

DOBEŠ, P. 1995. Fluid inclusion study of hydrothermal mineralization of the Melechov Massif (in Czech). In: Jelínek E. (editor), *Geochemical Interactions in Geological Repositories of Highly Radioactive Nuclear Waste*. Unpublished research report, Faculty of Science, Charles University, Prague.

DRAKE, H AND TULLBORG E-L 2004. Fracture mineralogy and wall rock alteration. results from drill core KSH01A+B. Oskarshamn site investigation. *SKB Report*, **SKB P-04-250**.

DUDEK, A., FROLÍKOVÁ, I., NEKOVAŘÍK, Č. 1991. Depth of the intrusion of the Hercynian granitoid plutons in the Bohemian Massif (in Czech). *Acta Universitatis Carolinae – Geologica*, **3-4***, 249-256, Praha.

EGLINTON, G. AND HAMILTON, R.J. 1963. The distribution of n-alkanes. In: SWAIN, T. (editor.), *Chemical Plant Taxonomy*. Academic Press. pp. 87-217.GREEN, P.F., THOMSON, K AND HUDSON, J.D. 2001. Recognition of tectonic events in undeformed regions: contrasting results from the Midland Platform and East midlands Shelf. *Journal of the Geological Society, London*, **158**, 59-73.

ENRESA. 1996. Memoria cartográfica, geológica y estructural. rocas plutónicas, albalá (g111). *ENRESA Internal Report*, **94-G111-IF**. Madrid, Vol. II, 249 PP.

ESCUDER VIRUETE, J., Y PÉREZ ESTAÚN, A. 1998. Fracturación en Mina Ratones. Informe Final 1: Estructura. Instituto de Ciencias de la Tierra. *Enresa* **10-CJA-IF-01**, 33 pp.

ESCUDER VIRUETE, J. 1999. Estudios Geológico-Estructurales y Geofísicos en Mina Ratones. Informe Final: Estructura. *Enresa* **10-CJA-IF-01**, 134 pp.

FICKEN, K. J., LI, B., SWAIN, D.L. AND EGLINTON, G. 2000. An n-alkane proxy for the sedimentary input of submerged/floating freshwater aquatic macrophytes. *Organic Geochemistry*, **31**, 745-749.

FLEET, A.J. 1984. Aqueous and sedimentary geochemistry of the rare earth elements. In: HENDERSON, P. (editor). *Rare Earth Element Geochemistry,* Developments in Geochemistry Series, **2**, Elsevier, Amsterdam, 343-373

FLORSCHÜTZ, F., MENÉNDEZ AMOR, J. AND WIJMSTRA, T.A. 1971. Palynology of a thick Quaternary succession in southern Spain. *Palaeogeography, Palaeoclimatology, Palaeoecology*, **10**, 233-264.

FOLK, R.L. 1974. The natural history of crystalline calcium carbonate: effect of magnesium content and salinity. *Journal of Sedimentary Petrology*, **44**, 40-53.

FOURNIER, R. O. AND TRUESDELL, A. H. 1973. An empirical Na-K-Ca geothermometer for natural waters. *Geochimica et Cosmochimica Acta*, **37**, 1255-1275

FRIEDMAN, I., AND O'NEIL, J.R., 1977, Compilation of stable isotope fractionation factors of geochemical interest: *U.S. Geological Survey, Professional Paper,* **440-KK**, p. KK1-KK12.

GALIMOV, E.M. 1985. *The biological fractionation of isotopes.* Academic Press, Orlando.

GELPI, E., SCHEIDER, H., MANN, J. AND ORO, J., 1970. Hydrocarbons of geochemical significance in microscopic algae. *Phytochemistry*, **9**, 603-612.

GHAZI, A.M. AND SHUTTLEWORTH, S. 2000. Trace element determination of single fluid inclusions by laser ablation ICP-MS: applications for halites from sedimentary basins. Analyst, 125 (1), 205-210.

GIRIN, Y.P., BALASHOV, Y.A. AND BRATISHKO, R.K. 1970. Redistribution of the rare earths during diagenesis of humid sediments. *Geochemistry International*, **7**, 438-452.

GIVEN, R.K. AND WILKINSON, B.H. 1985. Kinetic control on morphology, composition and mineralogy of abiotic sedimentary carbonates. *Journal of Sedimentary Petrology*, **55**, 109-119.

GOLDSTEIN, R H, and REYNOLDS, T J. 1995. Systematics of fluid inclusions in diagenetic minerals. *Society of Economic Paleontologists and Mineralogists Short Course,* Vol.31. Tulsa, USA.

GÓMEZ, P., GARRALÓN, A. TURRERO, M.J., SÁNCHEZ, L., MELÓN, A., RUIZ, B. Y FERNÁNDEZ, F. 1999. *Impacto medioambiental de la restauración de la Mina Ratones en las aguas subterráneas. Modelo hidrogeoquímico*. 10-CIE-IF-21-99. CIEAMT/DIAE/54211/7/99.

GÓMEZ, P., GARRALÓN, A. TURRERO, M.J., SÁNCHEZ, L. Y RUIZ, B. 2001. *Actualización de la información aportada por el muestreo de Marzo de 2001 al modelo de funcionamiento hidrogeoquímico de la Mina Ratones (Albalá, Cáceres).* CIEMAT/DIAE/54440/1/01.

GÓMEZ, P. 2002. Impacto de la Mina Ratones (Albalá, Cáceres) sobre las aguas superficiales y subterráneas: Modelación Hidrogeoquímica. *Publicación Técnica de ENRESA* **06/2002**, ISSN: 1134-380X, 303pp.

GONZALEZ, L.A., CARPENTER, S.C. AND LOMANN, K.C. 1992. Inorganic calcite morphology: roles of fluid chemistry and fluid flow. *Journal of Sedimentary Petrology*, **62**, 382-399.

GOODFRIEND, G.A. 1991. Patterns of racemization and epimerization of amino acids in land snail shells over the course of the Holocene. *Geochimica et Cosmochimica Acta*, **55**, 293-302.

GUILDERSON, T., FAIRBANKS, R.G. AND RUBENSTONES, J.L. 1994. Tropical temperature variations since 20,000 years ago: modulating interhemispheric climate change. *Science*, **263**, 663-665.

GUIOT, J., PONS, A., BEAULIEU, J.-L. AND REILLE, M. 1989. A 140,000 year continental climate reconstruction from two European pollen records. *Nature*, **338**, 309-313.

GUNTHER, D., FRISCHKNECHT, R., HEINRICH, C.A. AND KAHLERT, H.-J. 1997a. Capabilities of an argon fluoride 193nm Excimer Laser for laser ablation inductively coupled plasma mass spectrometry microanalysis of geological materials. *Journal of .Analytical and Atomic Spectrometry*, **12**, 939-944.

GUNTHER, D., FRISCHKNECHT, R., MÜSCHENBORN, H.-J. AND HEINRICH, C.A. 1997b. Direct liquid ablation: a new calibration strategy for laser ablation ICP-MS microanalysis of solids and liquids. *Fres.Journal of.Analytical Chemistry*, **359**, 390-393.

HALL, A.M. AND WHITTINGTON, G. 1989. Late Devensian Glaciation of southern Caithness. *Scottish Journal of Geology*, **25**, 307-324.

HAYS, P.D. AND GROSSMAN, E.L. 1991. Oxygen isotopes in meteoric calcite cements as indicators of continental paleoclimate. *Geology*, **19**, 441-444.

HEATHCOTE, J.A., GOMME, J.W., MCMILLAN, A.A., MILODOWSKI, A.E. AND PINE, R.J. 2000. Quaternary conditions in the Sellafield area relevant to hydrogeological modelling. *United Kingdom Nirex Report*, **SA/97/047**. United Kingdom Nirex Limited, Harwell.

HEDGES, J.I. AND PRAHL, F.G. 1993. Early diagenesis: consequences for applications of molecular biomarkers. In: ENGEL, M.H. AND MACKO, S.A. (editors.), *Organic Geochemistry. Principles and Applications*. Plenum Press, New York. pp. 237-253.

HEDGES, J.I., CLARK, W.A., QUAY, P.D., RICHEY, J.E., DEVL, A.H. AND DE SANTOS, U. 1986. Compositions and fluxes of particulate organic material in the Amazon River. *Limnology and* Oceanography, 31, 717-738.

HOLDSWORTH, R.E. 1989. The geology and structural evolution of a Caledonian fold and ductile thrust zone, Kyle of Tongue region, Sutherland, northern Scotland. *Journal of the Geological Society, London*, **146**, 809-823.

HOROWITZ, A., 1987. Subsurface Palynostratigraphy and Paleoclimates of the Quaternary Jordan Rift Valley Fill, Israel. *Israel Journal of Earth Sciences*, **36**, 31-44.

HOROWITZ, A., 1989. Continuous pollen diagrams from the last 3.5 m.y. from Israel: vegetation, climate and correlation with the oxygen isotope record. *Palaeogeography, Palaeoclimatology, Palaeoecology*, **72** (1-2), 63-78.

HUMPHRIS. S.E. 1984. The mobility of the rare earth elements in the crust. In: HENDERSON, P. (editor). *Rare Earth Element Geochemistry,* Developments in Geochemistry Series, **2**, Elsevier, Amsterdam, 317-342

HYSLOP, E.K. AND MILODOWSKI, A.E. 1994a. Petrography of fracture samples from the Devonian rocks of Dounreay BH1. *Nirex Core Characterization Programme, British Geological Survey Report*, **CC94D/412/IF-A-C**.

HYSLOP, E.K. AND MILODOWSKI, A.E. 1994b. Off-site core characterisation programme: the mineralogy , petrology and geochemistry of the Devonian and Moine Rocks of Dounreay Borehole No.1. *UK Nirex Limited Report*, **639**.

HYSLOP, E.K. AND MILODOWSKI, A.E. 2000. The mineralogy and petrography of altered rocks from the ORS unconformity in the Caithness District of northern Scotland. *British Geological Survey Technical Report*, **WG/92/4**.

IWATSUKI, T., SATAKE, H., METALFE, R., YOSHIDA, H. AND HAMA, K. 2002. Isotopic and morphological features of fracture calcite from granitic rocks of the Tono area, Japan: a promising palaeohydrogeological tool. *Applied Geochemistry*, **17**, 1241-1257.

JULIVERT, M., FONTBOTE, J.M., RIBEIRO, A. AND CONDE, L. 1972. *Mapa Tectónico de la Península Ibérica y Baleares E. 1:1.000.000*. Instituto Geológico y Minero de España, Madrid.

KEMP, S.J AND STRONG, G.E. 1997. The petrographical, mineralogical and lithogeochemical characteristics of Permo-Triassic and Carboniferous rocks from Sellafield BH7A and 7B. *Nirex Report*, **536**.

KIMBELL, T.N. AND HUMPHREY, J.D. 1994. Geochemistry and crystal morphology of aragonite cements of mixing-zone origin, Barbados, West Indies. *Journal of Sedimentary Research*, **A64**, 604-614.

KÖRNFALT, K.A., PERSSON, P.O. AND WIKMAN, H. 1997. Granitoids from the Äspö area, SE Sweden – Geochemical and geochronological data. *Geologiska Föreningens i Stockholm Förhandlingar*, **119**, 109-114.

LAAKSOHARJU, M., TULLBORG, E.-L., WIKBERG, P., WALLIN B. AND SMELLIE. J.A.T. 1999. Hydrogeochemical conditions and evolution at the Äspö HRL, Sweden. *Applied Geochemistry*, **14**, 835-859.

LAHANN, R.W. 1978. A chemical model for calcite crystal growth and morphology control. *Journal of Sedimentary Petrology*, **48**, 337-344.

LANDSTRÖM, O. AND TULLBORG, E.-L. 1995. Interactions of trace elements with fracture filling minerals from the Äspö Hard Rock Laboratory. *SKB Technical Report No.* **SKB TR-95-13**. ISSN 0284-3757. SKB, Stockholm.

LANGMUIR, O. *Aqueous Environmental Geochemistry*. Prentice Hall, New Jersey, pp208-211.

LARSON, S.Å., TULLBORG, E-L., CEDERBOM, C. AND STIBERG, J-P. 2000. Sveconorwegian and Caledonian foreland basins in the Baltic Shield revealed by fission track thermochronology. *Terra Nova*, **11**, 210-215.

LEE, J.R., ROSE, J., HAMBLIN, J.O. AND MOORLOCK, B.S.P. 2004. Dating the earliest lowland glaciation of eastern England: a pre-MIS 12 early Middle Pleistocene Happisburgh glaciation. *Quaternary Science Reviews,* **23**, 1551-1566.

LEYBOURNE, M.I., GOODFELLOW, W.D., BOYLE, D.R. AND HALL, G.M. 2000. Rapid development of negative Ce anomalies in surface waters and contrasting REE patterns in groundwaters associated with Zn-Pb massive sulphide deposits. *Applied Geochemistry*,**15**, 695-723.

LIDMAR-BERGSTRÖM K, 1995: Relief and saprolites through time on the Baltic Shield, *Geomorphology,* **12**, 45-61.

LOUVAT D.1, MICHELOT J.L. AND ARANYOSSY J.F. 1999. Origin and residence time of salinity in the Aspo groundwater system. *Applied Geochemistry*, **14**, 917-925.

LOWE I.J., AMMANN B., BIRKS H.H., BJÖRCK S., COOPE G.R., CWYNAR L., DE BEAULIEU J-L., MOTT R.J., PETEET D.M. AND WALKER M.J.C. 1994. Climatic changes in areas adjacent to the North Atlantic during the last glacial-interglacial transition (14-9 ka BP): a contribution to IGCP-253. *Journal of Quaternary Science*, **9**, 185-198.

LUCINI, M., TORRES, T., LLAMAS, J.F., CANOIRA, L., ORTIZ, J.E. AND GARCÍA DE LA MORENA, M.A. 2000. Geoquímica orgánica de las lutitas lacustres de las cuencas cenozoicas del Duero y Ebro. *Geogaceta*, **28**, 93-96.

MARSHALL, J.D. 1988. *Cathodoluminescence of Geological Materials*. Allen & Unwin Inc., USA.

MARSHALL, J.E.A., BROWN, J.F. AND HINDMARSH, S. 1985. Hydrocarbon source rock potential of the Devonian rocks of the Orcadian Basin. *Scottish Journal of Geology*, **21**, 301-320.

MARTÍ D., CARBONELL R., TRYGVASON A., ESCUDER VIRUETE J., AND PÉREZ-ESTAÚN A. 2002. Mapping brittle fracture zones in 3-dimensions: high resolution travel time seismic tomography in a granitic plutón. *Geophysical Journal International*, **149**, 95-105.

MCCOURT, W.J. 1980. The geology of the Strath Halladale-Altnabreac district. *British Geological Survey Technical Report*, **ENPU 80-1**.

MCLENNAN, S.M. 1989. Chapter 7. Rare earth elements in sedimentary rocks: influence of provenance and sedimentary processes. In: LIPIN, B.R. AND MCKAY, G.A. (editors). *Geochemistry and Mineralogy of Rare Earth Elements*. Reviews in Mineralogy, 21, 169-200, Mineralogical Society of America, Washington, D.C.

MICHIE, U.MCL. 1996. The geological framework of the Sellafield area and its relationship to hydrogeology. *Quarterly Journal of Engineering Geology*, **29**, 513-527.

MICHIE, U.MCL. AND BOWDEN, R.A. 1994. UK NIREX geological investigations at Sellafield. *Proceedings of the Yorkshire Geological Society*, **50**, 5-9.

MILODOWSKI, A.E., BASHAM, I.R., HYSLOP, E.K. AND PEARCE, J.M. 1989. The uranium source-term mineralogy and geochemistry at the Broubster Natural Analogue Site, Caithness. *British Geological Survey Technical Report*, **WG/89/50**.

MILODOWSKI, A.E., GILLESPIE, M.R., SHAW, R.P., AND BAILEY, D.E. 1995. Flow-zone characterisation: mineralogical and fracture orientation characteristics in the PRZ and Fleming Hall Fault Zone area boreholes, Sellafield. *Nirex Report*, **SA/95/001**.

MILODOWSKI, A.E., GILLESPIE, M.R. AND METCALFE, R. 1997. Relationship between mineralogical transformations and groundwater chemistry at Sellafield, NW England: a tool for studying Quaternary palaeohydrogeology. In: HENDRY, J., CAREY, P., PARNELL, J., RUFFELL, A. AND WORDEN, R. (editors), *GEOFLUIDS II '97: Contributions to the Second International Conference on Fluid Evolution, Migration and Interaction in Sedimentary Basins and Orogenic Belts (Belfast, Northern Ireland, March 10th – 14th, 1997)*. Queens University, Belfast, 30-33.

MILODOWSKI, A.E., GILLESPIE, M.R., NADEN, J., FORTEY, N.J., SHEPHERD, T.J., PEARCE, J.M. AND METCALFE, R. 1998a. The petrology and paragenesis of fracture mineralization in the Sellafield area, west Cumbria. *Proceedings of the Yorkshire Geological Society*, **52**, 215-241.

MILODOWSKI, A. E. GILLESPIE, M. R. PEARCE, J. M. AND METCALFE. R. 1998b. Collaboration with the SKB 'EQUIP' programme: Petrographical characterization of calcites from Äspö and Laxemar deep boreholes by scanning electron microscopy, electron microprobe and cathodoluminescence petrography. *British Geological Survey Technical Report*, **WG/98/45C**, British Geological Survey, Keyworth, Nottingham.

MILODOWSKI, A.E., HYSLOP, E.K., SPIRO, B. AND PEARCE, J.M. 2000a. The characterization, mineralogy and petrology of fractures and other discontinuities in basement lithologies in the Dounreay area, northern Scotland. *British Geological Survey Technical Report*, **WG/90/35**.

MILODOWSKI, A.E., PEARCE, J.M. AND BASHAM, I.R. 2000b. The characterization, mineralogy and petrology of fractures and associated alteration in the Caithness Flagstone Group, Middle Old Red Sandstone, Caithness, northern Scotland. *British Geological Survey Technical Report*, **WE/89/96**.

MILODOWSKI, A.E., FORTEY, N.J., GILLESPIE, M.R., PEARCE, J.M. AND HYSLOP, E.K. 2002. Synthesis report on the mineralogical characteristics of fractures from the Nirex boreholes in the Sellafield area. *British Geological Survey, Technical Report*, **WG/98/8**.

MILODOWSKI, A.E. TULLBORG, E.-L., BUIL, B., GÓMEZ, P., TURRERO, M.-J., HASZELDINE, S., ENGLAND, G., GILLESPIE, M.R., TORRES, T., ORTIZ, J.E., ZACHARIÁŠ, SILAR, J., CHVÁTAL, M., STRNAD, L., ŠEBEK, O. BOUCH, JESR CHENERY1, C CHENERY, C., SHEPHERD, T.J. 2005. Application of Mineralogical, Petrological and Geochemical tools for Evaluating the Palaeohydrogeological Evolution of the PADAMOT Study Sites. *PADAMOT Project Technical Report* WP2.

MITCHELL G.F., PENNY L.F., SHOTTON F.W. AND WEST R.G. 1973. *A Correlation of Quaternary Deposits in the British Isles*, Geological Society Special Report No. 4, The Geological Society Publishing House, Bath.

MLČOCH, B., BREITER, K., SCHULMANNOVÁ, B. 2000. Výzkum melechovského granitového masivu. *Zprávy o geologických výzkumech v roce 1999*, 91-93, Praha (Investigation of the Melechov granite massif).

MOORHOUSE, V.E. AND MOORHOUSE, S.J. 1979. The Moine amphibolite suites of central and northern Sutherland, Scotland. *Mineralogical Magazine*, **43**, 211-225.

MYERS, W.J., 1991. Calcite cement stratigraphy: an overview. In: BARKER, C.E. AND KOPP, O.C. (editors), *Luminescence Microscopy: Quantitative and Qualitative Aspects*, SEPM (Society for Sedimentary Geology) Short Course **25**, 133-149.

MYKURA, W. 1983. Old Red Sandstone. In: CRAIG, G.Y. (editor). *Geology of Scotland.* Chapter 8, 205-251. Scottish Academic Press, Edinburgh.

NADEN, J. 1996. CalcicBrine 1.5: a Microsoft Excel 5.0 Add-in for calculating salinities from microthermometric data in the system NaCl-CaCl2-H2O. *PACROFI VI Abstracts*, University of Wisconsin.

NESBITT, H.W. 1979. Mobility and fractionation of rare earth elements during weathering of a granodiorite. *Nature*, **279**, 206-210.

NIREX. 1993. The geology and hydrogeology of the Sellafield area, interim assessment, December 1993. *UK Nirex Limited Report*, **524**.

NIREX. 1994a. Dounreay geological investigations: hydrogeology. *UK Nirex Limited Report*, **660**.

NIREX. 1994b. The geology and hydrogeology of Dounreay. Executive Summary. *UK Nirex Limited Report*, **653**.

NIREX. 1997. The hydrochemistry of Sellafield, 1997 Update. *UK Nirex Limited Report*, **SA/97/089**.

NORTON, M.G., McCLAY, K.R. AND WAY, N.A. 1987. Tectonic evolution of Devonian basins in northern Scotland and southern Norway. *Norsk Geologisk Tidsskrift*, **67**, 323-338.

OAKES, C S, BODNAR, R J, and SIMONSON, J M. 1990. The system NaCl-CaCl2-H2O: I. The ice liquidus at 1 atm total pressure. *Geochimica et Cosmochimica Acta,* Vol.54, 603-610.

O´LEARY, M.H. 1981. Carbon isotopic fractionation in plants. *Phytochemistry*, **20**, 553-567.

O'NEIL, J.R., CLAYTON, R.N. AND MAYEDA, T.K. 1969. Oxygen isotope fractionation in divalent metal carbonates. *Journal of Chemical Physics*, **51**, 5547-5558.

ORTIZ, J.E., TORRES, T., JULIÀ, R., DELGADO, A., LLAMAS, F.J., SOLER, V AND DELGADO, J. 2004. Numerical dating algorithms of amino acid racemization ratios from continental ostracodes. Application to the Cúllar-Baza Basin (southern Spain). *Quaternary Science Reviews 23(5-6), 717-730.*

ORTIZ J.E., TORRES, T., DELGADO, A., JULIÀ, R., LUCINI, M., LLAMAS, F.J., REYES, E., SOLER, V. AND VALLE, M. 2004. The palaeoenvironmental and palaeohydrological evolution of Padul Peat Bog (Granada, Spain) over one million years, from elemental, isotopic, and molecular organic geochemical proxies. *Organic Geochemistry*, **35**(11-12), 1243-1260.

ORTUÑO, F., FLORÍA, E., CARRETERO G. y SUSO, J. 1999. *Caracterización hidráulica de Mina Ratones*. AITEMIN. 10-AIT-IA-04.

PARKHURST, D L AND APPELO, C A J. 2001. *PHREEQC-2 - version 2.4.2.* US Geological Survey Denver, Colorado, USA.

PARNELL, J. 1985. Hydrocarbon source rocks, reservoir rocks and migration in the Orcadian Basin. *Scottish Journal of Geology*, **21**, 321-336.

PEARSON, M.J., HENDRY, J.P., TAYLOR, C.W. AND RUSSELL, M.A. 2005. Fatty acids in sparry calcite fracture fills and microsparite cement of septarian diagenetic concretions. *Geochimica et Cosmochimica Acta*, **69**, 1773-1786.

PEDERSEN, K., EKENDAHL, S., TULLBORG,, E-H., FURNES, H., THORSETH, I-G. AND TUMYR. O. 1997. Evidence of ancient life at 207 m depth in a granitic aquifer. *Geology.* **25,** 827-830.

PÉREZ ESTAÚN, A. 1999. Estudios Geológico-estructurales y geofísicos en Mina Ratones. 10-CJA-IF-03. Tomo VI.

PÉREZ ESTAÚN A., MARTÍNEZ CATALÁN J.R. AND BASTIDA F. 1991. Crustal thickening and deformation séquense in the footwall to the suture of the Variscan Belt of Northwest Spain. *Tectonophysics*, **191**, 243-253.

PETERMAN, Z.E. AND WALLIN. B. 1999. Synopsis of strontium isotope variations in groundwater at Äspö , southern Sweden. *Applied Geochemistry.* **14**, 939-952.

PETRÁNEK, J. 1966. Geology of Czechoslovakia. – In: BIELY, A., et al. *Geological Map of Czechoslovakia, 1:1000000.* Ústřední ústav geologický, Praha.

PIERSON, B.J. 1981. The control of cathodoluminescence in dolomite by iron and manganese. *Sedimentology*, **28**, 601-610.

PONS, A. AND REILLE, M. 1988. The Holocene and upper Pleistocene pollen record from Padul (Granada, Spain): a new study. *Palaeogeography, Palaeoclimatology, Palaeoecology*, **66**, 243-263.

REGUILÓN, R., ARRIBAS, A., MARTÍN-IZARD, A., Y MANGAS, J. 1996. Las mineralizaciones de Uranio de la Carretona y Casas del Gallo en el granito de Albalá (Cáceres). *Geogaceta*, **20**, 1598-1600.

ROEDDER, E. 1984. Fluid Inclusions. *Mineralogical Society of America, Reviews in Mineralogy,* Vol.12, ISBN 0-939950-16-2.

ROSEN, M.R. 1994. The importance of groundwater in playas: a review of playa classifications and the sedimentology and hydrology of playas. In ROSEN, M.R. (editor), *Paleoclimate and Basin Evolution of Playa Systems*. Geological Society of America, Special Paper, **289**, 1-8.

ROZANSKI, K., ARAGUAS-ARAGUAS, L. AND GONFIATINI, R. 1993. Isotopic patterns in modern global precipitation. In: SMART, P.K., LOHMANN, K.C., MCKENZIE, J. AND SAVIN, S. (editors), *Climate Change in Continental Isotopic Records*. Geophysical Monograph. American Geophysical Union **78**, 1-36.

SALOMONS, W., GOODIE, A. AND MOOK, W.G. 1978. Isotopic composition of calcrete deposits from Europe, Africa and India. *Earth Surface Processes,* **3**, 43-57.

SCHMIDT, V. AND MCDONALD, D.A. 1979. The role of secondary porosity in the coarse of sandstone diagenesis. In: SCHOLLE, P.A. AND SCHLUGER, P.R. (editors). *Aspects of Diagenesis.* Society of Economic Palaeontologists and Mineralogists, Special Publication, **26**, 175-207.

SCHWARK, L., ZINK, K. AND LECHTERBECK, J. 2002. Reconstruction of postglacial to early Holocene vegetation history in terrestrial Central Europe via cuticular lipid biomarkers and pollen records from lake sediments. *Geology* **30**(5), 463-466.

SHACKLETON, N.J. 1995. New data on the evolution of Pliocene climatic variability. In: VRBA, E.S., DENTON, G.H., PARTIDGE, T.C., BURCKLE, L.H. (editors): *Palaeoclimate and Evolution with Emphasis on Human Origins*. Yale University Press, New Haven, pp. 242-248.

SHEPHERD, T J, RANKIN, A H, and ALDERTON, D H M. 1985. A Practical Guide to Fluid Inclusion Studies. (*Blackie, Glasgow and London*) ISBN 0-412-00601-4.

SHEPHERD, T.J., NADEN, J., CHENERY, S.R., MILODOWSKI, A.E. AND GILLESPIE, M.R. 2000. Chemical analysis of palaeogroundwaters: a new frontier for fluid inclusion research. *Journal of Geochemical Exploration*, **69-70**, 415-418.

SKB. 2004. Hydrogeochemical evaluation for the Simpevarp model version 1.2. Preliminary site description of the Simpevarp area. *Swedish Nuclear Waste and Fuel Management Co (SKB) Report*, **R-04-74**.

SMELLIE, J.A.T., LAAKSOHARJU, M. AND WIKBERG. P. 1995. Äspö*,* SE Sweden: a natural groundwater flow model derived from hydrogeological observations. *Journal of Hydrology*. **172**, 147-169.

SMITH, G.I. AND BISCHOFF, J.L. 1997. An 800,000-year Paleoclimatic record from Core OL-92, Owens Lake, Southeast California. *Geological Society of America, Special paper*, **317**, 165 pp.

SPINK, K. 1965. Coalfield geology of Leicestershire and South Derbyshire: The exposed coalfields. *Transactions of the Leicester Literary and Philosophical Society*, **59**, 41-98.

STANLEY, C.J. AND VAUGHAN, D.J. 1982. Copper, lead, zinc and cobalt mineralization in the English Lake District: classification, conditions of formation and genesis. *Journal of the Geological Society, London*, **139**, 569-579.

STERNER, S M, HALL, D L, and BODNAR, R J. 1988. Synthetic fluid inclusions: V. Solubility relations in the system NaCl-KCl-H2O under vapour saturated conditions. *Geochimica et Cosmochimica Acta,* Vol.52, 989-1005.

STRONG, G.E., MILODOWSKI, A.E., PEARCE, J.M., KEMP, S.J., PRIOR, S.V. AND MORTON, A.C. 1994. The petrology and diagenesis of Permo-Triassic rocks of the Sellafield area, Cumbria. *Proceedings of the Yorkshire Geological Society*, **50**, 77-89.

STRONG, G.E. AND KEMP, S.J. 1997. The petrographical, mineralogical and lithogeochemical characteristics of Permo-Triassic and Carboniferous rocks from Sellafield Borehole 10A. *Nirex Report*, **735**.

STRONG, G.E., GILES, G.E., WRIGHT, V.P. 1992. A Holocene calcrete from North Yorkshire, England: implications for interpreting palaeoclimates using calcretes. *Sedimentology*, **39**, 333-347.

STOREY, B.C. AND LINTERN, B.C. 1981. Alteration, fracture infills and weathering of the Strath Halladale Granite. *British Geological Survey Report*, **ENPU 81-13**.

STUART, A.J. AND LISTER, A.M. 2001. The mammalian faunas of Pakefield, Kessingland and Corton, Suffolk, UK: evidence for a new temperate episode in the British early Middle Pleistocene. *Quaternary Science Reviews*, **20**, 1677-1692.

SUTHERLAND, D.G. 1984. The Quaternary deposits and landforms of Scotland and the neighbouring shelves: a review. *Quaternary Science Reviews*, **3**, 157-254.

TALBOT, M.R. 1990. A review of the palaeohydrological interpretation of carbon and oxygen isotopic ratios in primary lacustrine carbonates. *Chemical Geology*, **80**, 261-279.

TALBOT, M.R. AND LIVINGSTONE, D.A. 1989. Hydrogen index and carbon isotopes of lacustrine organic matter as lake level indicators. *Palaeogeography, Palaeoclimatology, Palaeoecology*, **70**, 121-137.

TORRES, T., ORTIZ, J.E., SOLER, V., REYES, E., DELGADO, A., VALLE, M., COBO, R., JULIÀ, R., BADAL, E., GARCÍA DE LA MORENA, M.A., GARCÍA-MARTÍNEZ, M.J., FERNÁNDEZ-GIANOTTI, J., CALVO, J.P. AND CORTÉS, A. 2003a. Pleistocene lacustrine basin of the east domain of Guadix-Baza basin (Granada, Spain): sedimentology, chronostratigraphy and palaeoenvironment. In: VALERO-GARCÉS, B. (editor). *Limnogeología en España: un tributo a Kerry Kelts*. Consejo Superior de Investigaciones Científicas, Madrid, pp. 151-185.

TULLBORG, E-L. 1995. Mineralogical and chemical data on rocks and fracture mineralization from Äspö. SKB *Swedish Hard rock Laboratory, Progress report*, **25-90-01**.

TULLBORG, E-L., LARSON, S.Å. AND STIBERG, J-P. 1996. Subsidence and uplift of the present land surface in the southeastern part of the Fennoscandian Shield. *Geologiska Föreningen i Stokholms Förhandlingar*, **118**, 126-128.

TULLBORG, E.-L. 1997. *Recognition of low-temperature processes in the Fennoscandinavian shield.* PhD Thesis Geoscience Center A17, Göteborg University, ISSN 1400-3813

TULLBORG, E.-L., LANDSTRÖM, O. AND WALLIN, B. 1999. Low-temperature trace element mobility influenced by microbial activity – inclusions from fracture calcite and pyrite in crystalline basement. *Chemical Geology*, 157, 199-218.

VALLE, M., RIVAS, M.R., LUCINI, M., ORTIZ, J.E. AND TORRES, T. 2003. Interpretación paleoecológica y paleoclimática del tramo superior de la turbera de Padul (Granada, España) a partir de datos palinológicos. *Pollen* **13**, 85-95.

VANIMAN, D.T. AND CHIPERA, S.J. 1996. Palaeotransport of lanthanides and strontium recorded in calcite compositions from tuffs at Yucca Mountain, Nevada, USA. *Geochimica et Cosmochimica Acta*, **60**, 4417-4433.

VANKO, D A, BADNAR, R J, and STERNER, S M. 1988. Synthetic fluid inclusions: VIII. Vapour saturated halite solubility in part of the system $NaCl$-$CaCl_2$-H_2O, with application to fluid inclusions from oceanic hydrothermal systems. *Geochimica et Cosmochimica Acta,* Vol. 52, 2451-2456.

VASCONCELOS, P.M., RENNE, P.R., BRIMHALL, G.H. AND BECKER, T.A. 1994. Direct dating of weathering phenomena by 40Ar/39Ar and K-Ar analysis of supergene K-Mn oxides. *Geochimica et Cosmochimica Acta*, **58**, 1635-1665.

VOGEL, J.C. AND KRONFELD, J., 1980. A new method for dating peat. *South African Journal of Science*, **76**, 557-558.

WALKER, G., ABUMERE, O.E. AND KAMALUDDIN, B. 1989. Luminscence spectroscopy of Mn^{2+} centres in rock-forming carbonates. *Mineralogical Magazine*, **53**, 201-211.

WALLIN, B. AND PETERMAN, Z. E. 1999. Calcite fracture fillings as indicators of palaeohydrogeology at Laxemar and the Äspö Hard Rock Laboratory, southern Sweden. *Applied Geochemistry*, **14**, 953-962.